frontiers | Research Topics

Brain stimulation mechanisms and therapeutic effects in neural circuits

Edited by
Kevin A. Caulfield, Joshua C. Brown and Lisa McTeague

Published in
Frontiers in Neural Circuits
Frontiers in Human Neuroscience

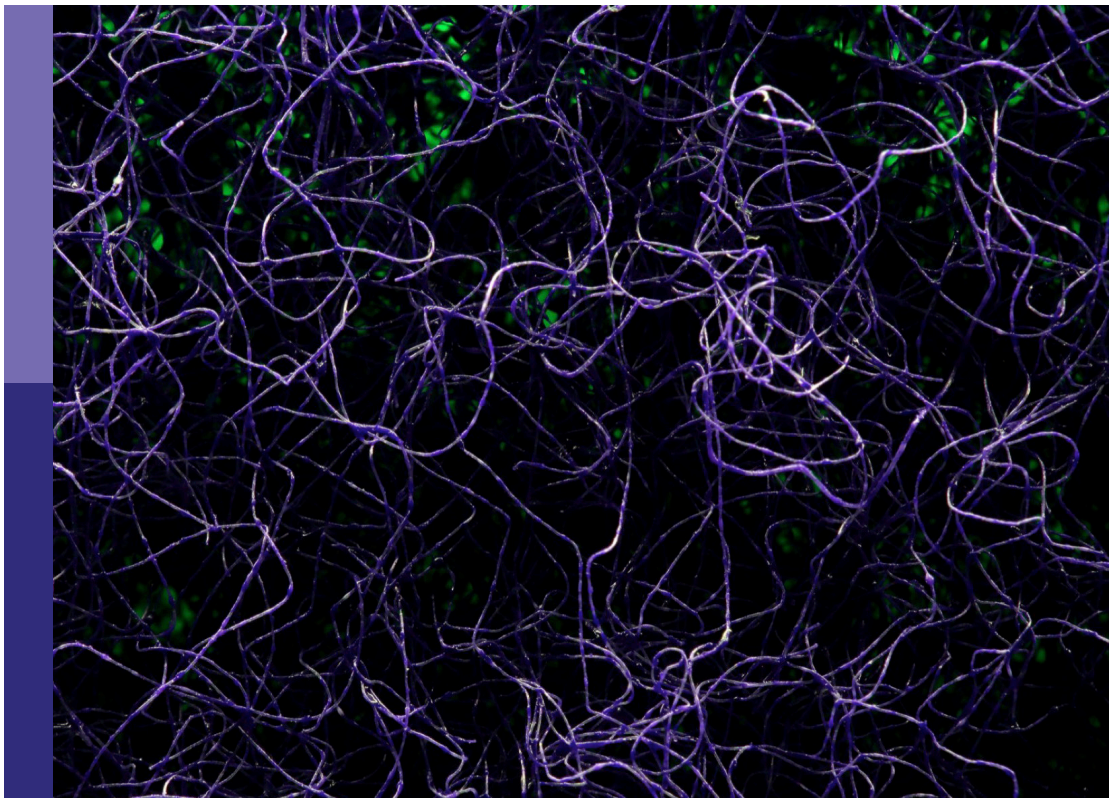

ISSN 1664-8714
ISBN 978-2-8325-4107-4
DOI 10.3389/978-2-8325-4107-4

About Frontiers

Frontiers is more than just an open access publisher of scholarly articles: it is a pioneering approach to the world of academia, radically improving the way scholarly research is managed. The grand vision of Frontiers is a world where all people have an equal opportunity to seek, share and generate knowledge. Frontiers provides immediate and permanent online open access to all its publications, but this alone is not enough to realize our grand goals.

Frontiers journal series

The Frontiers journal series is a multi-tier and interdisciplinary set of open-access, online journals, promising a paradigm shift from the current review, selection and dissemination processes in academic publishing. All Frontiers journals are driven by researchers for researchers; therefore, they constitute a service to the scholarly community. At the same time, the *Frontiers journal series* operates on a revolutionary invention, the tiered publishing system, initially addressing specific communities of scholars, and gradually climbing up to broader public understanding, thus serving the interests of the lay society, too.

Dedication to quality

Each Frontiers article is a landmark of the highest quality, thanks to genuinely collaborative interactions between authors and review editors, who include some of the world's best academicians. Research must be certified by peers before entering a stream of knowledge that may eventually reach the public - and shape society; therefore, Frontiers only applies the most rigorous and unbiased reviews. Frontiers revolutionizes research publishing by freely delivering the most outstanding research, evaluated with no bias from both the academic and social point of view. By applying the most advanced information technologies, Frontiers is catapulting scholarly publishing into a new generation.

What are Frontiers Research Topics?

Frontiers Research Topics are very popular trademarks of the *Frontiers journals series*: they are collections of at least ten articles, all centered on a particular subject. With their unique mix of varied contributions from Original Research to Review Articles, Frontiers Research Topics unify the most influential researchers, the latest key findings and historical advances in a hot research area.

Find out more on how to host your own Frontiers Research Topic or contribute to one as an author by contacting the Frontiers editorial office: frontiersin.org/about/contact

Brain stimulation mechanisms and therapeutic effects in neural circuits

Topic editors

Kevin A. Caulfield — Medical University of South Carolina, United States
Joshua C. Brown — Harvard Medical School, United States
Lisa McTeague — Medical University of South Carolina, United States

Citation

Caulfield, K. A., Brown, J. C., McTeague, L., eds. (2023). *Brain stimulation mechanisms and therapeutic effects in neural circuits*. Lausanne: Frontiers Media SA. doi: 10.3389/978-2-8325-4107-4

Table of contents

frontiers in Neural Circuits

ORIGINAL RESEARCH
published: 29 September 2020
doi: 10.3389/fncir.2020.585624

Continuous Theta-Burst Stimulation Intensity Dependently Facilitates Motor-Evoked Potentials Following Focal Electrical Stimulation of the Rat Motor Cortex

Minoru Fujiki, Yukari Kawasaki and Hirotaka Fudaba*

Department of Neurosurgery, School of Medicine, Oita University, Oita, Japan

Although theta-burst stimulation (TBS) is known to differentially modify motor cortical excitability according to stimulus conditions in humans, whether similar effects can be seen in animals, in particular rats, remains to be defined. Given the importance of experimental rat models for humans, this study explored this stimulation paradigm in rats. Specifically, this study aimed to explore corticospinal excitability after TBS in anesthetized animals to confirm its comparability with human results. Both inhibition-facilitation configurations using paired electrical stimulation protocols and the effects of the TBS paradigm on motor-evoked potentials (MEPs) in rat descending motor pathways were assessed. Paired-stimulation MEPs showed inhibition [interstimulus interval (ISI): 3 ms] and facilitation (11 ms) patterns under medetomidine/midazolam/butorphanol (MMB) anesthesia. Furthermore, while ketamine and xylazine (K/X) anesthesia completely blocked facilitation at 11-ms ISI, inhibition at a 3-ms ISI was preserved. Continuous and intermittent TBS strongly facilitated MEPs depending on stimulus intensity, persisting for up to 25 min under both MMB and K/X anesthesia. These findings are similar to the intracortical inhibition and facilitation observed in the human motor cortex using paired-pulse magnetic stimulation, particularly the glutamate-mediated facilitation phase. However, different TBS facilitatory mechanisms occur in the rat motor cortex. These different TBS facilitatory mechanisms affect the comparability and interpretations of TBS between rat and human models.

Keywords: corticospinal tract, electrical stimulation, motor-evoked potentials, intracortical inhibition, intracortical facilitation, theta burst stimulation

OPEN ACCESS

Edited by:
Heiko J. Luhmann,
Johannes Gutenberg University Mainz, Germany

Reviewed by:
Rune W. Berg,
University of Copenhagen, Denmark
Yoshikazu Isomura,
Tokyo Medical and Dental University, Japan

****Correspondence:***
Minoru Fujiki
fujiki@oita-u.ac.jp

Received: *21 July 2020*
Accepted: *31 August 2020*
Published: *29 September 2020*

Citation:
Fujiki M, Kawasaki Y and Fudaba H (2020) Continuous Theta-Burst Stimulation Intensity Dependently Facilitates Motor-Evoked Potentials Following Focal Electrical Stimulation of the Rat Motor Cortex. Front. Neural Circuits 14:585624. doi: 10.3389/fncir.2020.585624

INTRODUCTION

The non-invasive neuromodulation method can potentially be used as an adjuvant strategy in the rehabilitation of motor and cognitive deficits caused by neurological disorders (Müller-Dahlhaus and Vlachos, 2013; Rodger and Sherrard, 2015). The effect of stimulation depends on the stimulus parameters, such as location, intensity, polarity, and frequency mode of the stimulation (Gamboa et al., 2010; Hamada et al., 2013; Nakamura et al., 2016;

Shirota et al., 2017; Sasaki et al., 2018). Theta-burst stimulation (TBS) of the motor cortex (3–5 pulses at 100 Hz repeated at 5 Hz), which was originally reported in animal studies in the hippocampus of cats and rats (Hess and Donoghue, 1996), has been successfully translated in the awake human motor cortex as either intermittent and facilitatory or continuous and inhibitory TBS paradigms for motor-evoked potentials (MEPs) with repetitive transcranial magnetic stimulation (rTMS; Huang et al., 2005). Comparability, i.e., whether similar effects would be seen particularly in the descending motor system of rats, and underlying functional validations are yet to be determined. With the widespread application of TBS as a tool to modify the excitability of the human motor cortex, the present study explored corticospinal excitability after TBS using two different standard anesthetics on freely behaving animals to replicate human findings. Recent TMS-TBS protocols and MEP recording methods in animal models have been useful for translation purposes and for understanding the mechanisms underlying human results (Vahabzadeh-Hagh et al., 2011; Hsieh et al., 2012, 2015; Sykes et al., 2016). In contrast, a single pulse stimulation-MEP, such as TMS-MEP, causes activation of both the motor cortex and subcortical structures (Mishra et al., 2017); thus, focal short-burst triple-pulses for MEP have been proposed in rat models (Carmel et al., 2010; Mishra et al., 2017). Electrical motor cortical stimulation would enable focal stimulation protocols with greater specificity and accuracy for basic MEP recording, intracortical inhibition-facilitation exploration, and TBS modulation in rat models.

Therefore, we focused on electrically-induced MEPs, continuous TBS (cTBS), and intermittent TBS (iTBS), as previous work has predominantly employed TMS-MEP and TMS-TBS (Hsieh et al., 2015; Sykes et al., 2016) in rats based on the original human paradigm, but few reports have employed more focal and stable motor cortical electrical stimulation (Barry et al., 2014). This study aimed to establish an animal model that allowed for the study of factors possibly affecting MEP amplitudes, and thus cortical excitability, under a more standardized condition and with additional focal stimulation than that achieved with conventional TMS. Configuration of the induced current flow (polarity, location, and monophasic or biphasic) *via* epidural electrodes was preliminarily tested to assess whether it is compatible with TMS-induced electric fields relative to monopolar direct electrical stimulation of the motor cortex. This is important, as determining the stability of the protocol under anesthesia is required before future repeated experiments can be conducted, e.g., exploring the effects on the central nervous system (CNS) of drugs, wakefulness, and free-moving conditions. Indeed, drug effects in human results (Kujirai et al., 1993; Rothwell, 1997) and acute changes in TMS measures of motor excitability after a single-dose application (Ziemann et al., 2015) require confirmation under experimental settings.

The present results provide animal platforms in conditioned laboratory settings for pharmacological and various pathophysiological evaluations, as well as an understanding of previous human results.

MATERIALS AND METHODS

Animals

All experimental protocols were approved by the Ethical Committee of the School of Medicine, Oita University (protocol number 192301). Experiments were conducted on 48 adult male Sprague–Dawley rats (body weight, 290–375 g; purchased from Charles River Laboratories, Japan) housed at controlled room temperature (24 ± 1°C) with a 12/12 h light/dark cycle. The room was maintained at 24°C with constant humidity. Rat food pellets and tap water were provided *ad libitum* between experimental procedures. This study constituted six separate experimental conditions involving 48 animals [time course for no TBS (n = 7), cTBS (n = 7) and iTBS (n = 7) under medetomidine/midazolam/butorphanol (MMB) anesthesia; same procedures under ketamine and xylazine (K/X) anesthesia (n = 21); and preliminary studies (n = 6); see **Figure 1** for details]. We used "one animal" for "two sessions" for animals used twice (see also "Paired Motor Cortex Electrical Stimulation: SICI and ICF" section for detail).

Preliminary studies were undertaken to test three different configurations of the induced current flow (i.e., polarity, location, and monophasic or biphasic) *via* epidural electrodes delivering electrical pulses at 1.2 times the resting motor threshold (RMT) of the MEPs (for which a separate set of six rats were prepared). For this study, rats (n = 3) were anesthetized and placed in a stereotactic frame (**Figure 1**). Recording methods were similar to those described elsewhere (Hsieh et al., 2012; Sykes et al., 2016). For comparison, additional rats (n = 3) were prepared similarly and received direct electrical stimulation of the motor cortex. Briefly, a craniectomy of 9 × 5 mm^2, i.e., drilling above the forelimb and hindlimb regions of the sensorimotor cortex (coordinates relative to bregma: 4.5 mm caudal, 4.5 mm rostral, and 0.5–5.5 mm lateral) to expose the to-be-stimulated cortex, was performed over the motor cortex where single electrodes were positioned at different locations. Electrical stimulation consisted of 3–10 500-μs biphasic pulses (cathode first) delivered at 500 Hz, and the maximum stimulator output (MSO) was adjusted to 1.0 mA; 808 ± 33 Ω impedance. Such stimulation yielded MEPs from the forelimb biceps brachii (BB) muscle when the motor cortex was stimulated 2 mm anterior and 2–3 mm lateral to the bregma (Takemi et al., 2017). A set of two epidural electrodes placed over the rat's motor cortex can be systematically adjusted to the best position for eliciting MEPs *via* the motor cortex (Fujiki et al., 2020). Epidural stimulating configurations were determined based on the comparison of these procedures.

Motor Cortex Stimulation and Recording of Motor-Evoked Potentials

The basic procedures of electrical stimulation and MEP recordings were based on methods previously described by Mishra et al. (2017). Briefly, epidural cortical stimulating electrodes [Plastics One with 1.19 mm diameter with a flat tip on two locations: 1.0 mm rostral and 2.0 mm lateral (1R, 2L) and 3.0 mm rostral and 4.0 mm lateral from bregma (3R, 4L); orange circles in **Figure 1B**] were placed 7 days before testing under

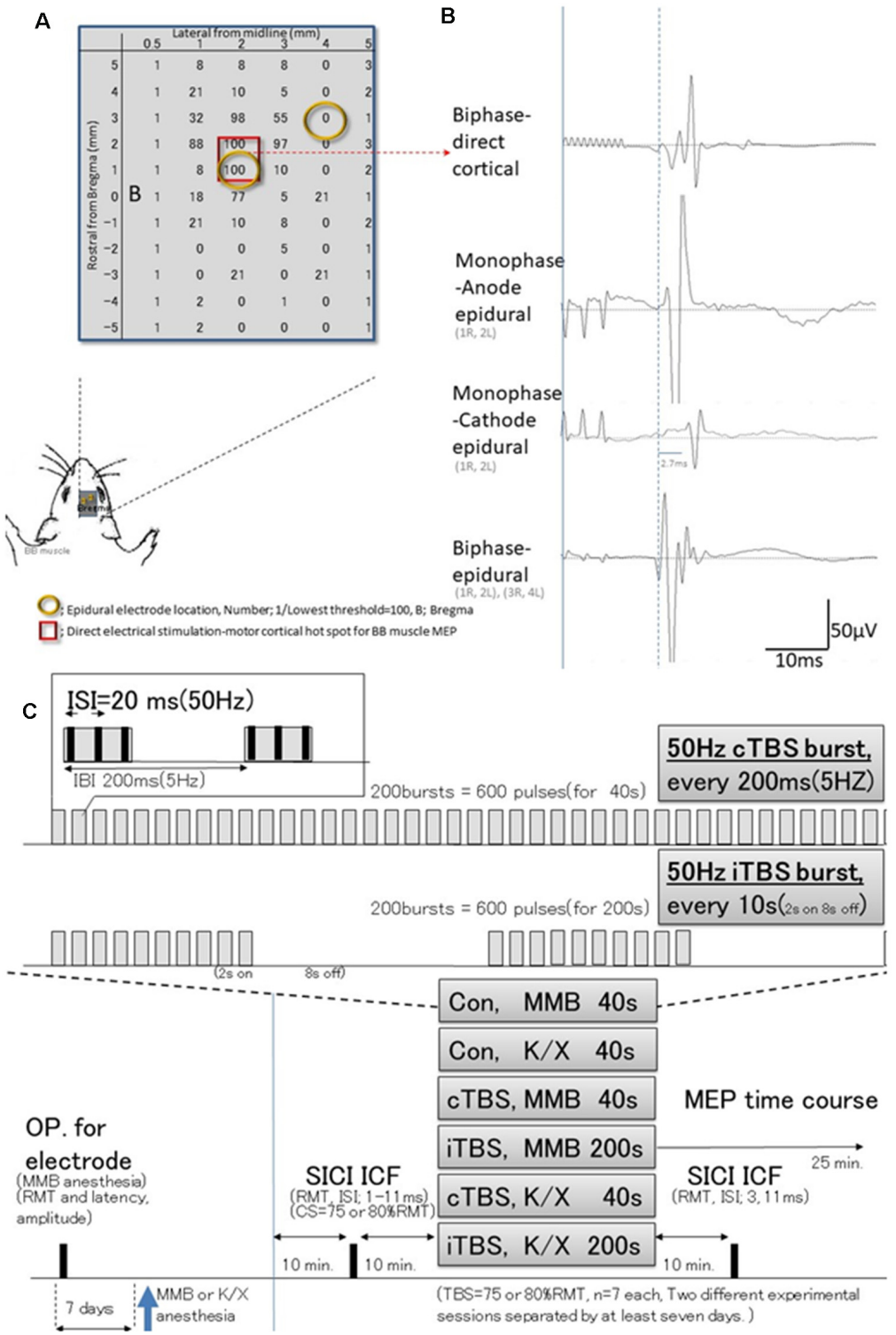

FIGURE 1 | Schematic illustration of experiments; stimulus-accuracy validation and timeline; comparisons between direct motor cortical electrical stimulation induced-motor-evoked potentials (MEPs) and epidural stimulation MEPs (different configuration of the induced current flow; polarity, location, and monophasic or biphasic). **(A)** The results of cortical motor mapping (2 mm anterior and 2–3 mm lateral to the bregma) were following previous work comparing intracortical electrical stimulation and epidural stimulation (Takemi et al., 2017). Hot spot mapping for the biceps brachii muscle was identified; locations were defined as [1/(lowest threshold (mA) of direct motor cortical stimulation induced-MEPs)] 100 (red square identifies two locations). Before a full craniotomy, the location of two epidural electrodes placed over the rat's motor cortex was systematically changed to identify the best area for eliciting MEPs *via* the motor cortex. **(B)** MEP latencies after

(*Continued*)

FIGURE 1 | Continued
direct motor cortical electrical stimulation corresponded with those after monophase-anode (1R, 2L) epidural stimulation and biphase-epidural stimulation [(1R, 2L) and (3R, 4L)], whereas MEPs after monophase-cathode (1R, 2L) epidural stimulation exhibited a 2.7 ms delay in latency, and lower amplitudes than other modalities. Thus, the biphasic epidural stimulation electrode was located on the motor cortical hot spot for BB muscle, inducing a horizontally oriented electric field across forelimb representation confirmed compatibility those with MEPs identified by direct cortical electrical stimulation. **(C)** Epidural electrodes were placed 7 days before testing under MMB anesthesia. The SICI and ICF were evaluated after 10 min. Base recording, cTBS, iTBS, and no-theta-burst stimulation (TBS)- were performed under MMB or K/X anesthesia at 10 min. Base recording (n = 7, each group). Full ISIs, as well as ISIs of 3 and 11 ms, were tested 10 min after TBS. MMB, medetomidine/midazolam/butorphanol anesthesia; K/X, ketamine and xylazine anesthesia; SICI, short-latency intracortical inhibition; ICF, intracortical facilitation; cTBS, iTBS; continuous or intermittent theta burst stimulation; ISI, inter-stimulus interval; IBI, inter-burst interval; RMT, resting motor threshold.

MMB anesthesia. The screw electrodes were attached in advance to a head connector (Plastics One) such that they were secured with skull screws and dental acryl for repeated measurements (Mishra et al., 2017). To assay the descending motor systems, we stimulated the motor cortex and measured MEPs from the contralateral BB muscle. For motor cortex stimulation, a train of three biphasic square wave pulses was delivered with an isolated pulse stimulator (A-M Systems, Model 2100, Sequim, WA, USA) to achieve temporal summation for selective activation of the motor cortex (0.2 ms per pulse for each polarity; interstimulus interval of 3 ms; **Figure 2A**). Also, we compared latencies with three pulses to those with single pulses delivered over the motor cortex. For testing, trains of stimuli were delivered every 5 s to allow for the recovery of responses (Carmel et al., 2010).

Paired Motor Cortex Electrical Stimulation: SICI and ICF

The RMT was determined by first decreasing the stimulator output by 0.1 mA until MEPs disappeared and then increasing the output in 0.1-mA increments until six MEPs of 50 μV (peak-to-peak) were elicited out of every 12 trains of 3-ms interval three biphasic square wave pulses. We recorded 20 min of baseline MEPs every 5 s (0.2 Hz) at 120% of RMT. Two isolated electrical stimulators connected to a single stimulus electrode with custom-made switching systems were used. Parameters were controlled for appropriate stimulus intervals and intensity like that for paired TMS (Kujirai et al., 1993; Vahabzadeh-Hagh et al., 2011; Hsieh et al., 2012). Intracortical inhibitions or facilitations [corresponding to short-latency intracortical inhibition (SICI) and intracortical facilitation (ICF) in human motor cortex using paired-pulse TMS] were tested using a paired electrical and subthreshold conditioning stimulus (CS) preceding a suprathreshold test stimulus (TS; Kujirai et al., 1993; Rothwell, 1997). Subthreshold CS was set at 70, 75, and 80% RMT, while the intensity of TS was adjusted to evoke an MEP of approximately 300 μV (peak-to-peak) in the left BB muscle. Interstimulus intervals (ISIs) of 1, 2, 3, 5, 7, 11, 13, and 15 ms were utilized to test intracortical inhibitions or facilitation. Full ISIs were tested 10 min before TBS, while ISIs of 3 ms and 11 ms were tested 10 min after TBS. Two different experimental sessions separated by at least 7 days were conducted, while one of two TBS intensity protocols were used in each session in a pseudo-randomized order.

Motor Cortex Electrical Stimulation: cTBS and iTBS

Either a continuous or intermittent TBS (cTBS or iTBS under MMB or K/X; n = 7 each) or an absent (no-) TBS- (MMB or K/X; n = 7 each) was applied for a total duration of 40 s or 200 s, respectively. cTBS consists of a burst of three pulses at 50 Hz, repeated at 5 Hz, and delivered for 40 s continuously (600 pulses). In contrast, iTBS involves the same burst, delivered for 2 s with an 8 s off-period, consisting of 600 pulses based on original reports of rTMS of the human motor cortex by Huang et al. (2005). At the end of the data collection, rats were sacrificed humanely by an anesthetic overdose (350 mg/kg pentobarbital sodium, Henry Schein) before decapitation. Finally, extracted brains were fixed in paraformaldehyde and sectioned for the histological verification of electrode positioning.

TBS was delivered at 75 and 80% of the RMT [approximately 0.5–1.2 mA, corresponding to previous reports (Yang et al., 2019)] for 600 pulses. Also, a final 25-min MEPs post-stimulation was recorded at 0.2 Hz at 120% RMT. No-TBS- was instead delivered by unplugging the electrodes at the stimulator while the cTBS or iTBS protocol was conducted.

MEP Acquisition

MEPs were measured *via* a stainless-steel braided wire (Cooner Wire, catalog number AS 634, Chatsworth, CA, USA) inserted into the left BB muscle. Successively, they were pre-amplified and stored (Neuropack 8, Nihon-Kohden Co. Limited, Tokyo, Japan and Brain Vision Recorder, Brain Products, Germany, with 5–3,000 Hz bandpass at a sampling rate of 5,000 Hz and 100-ms analysis time). We acquired the first 100 ms of electromyography (EMG) data after the stimulation for quantification. The EMG response diminished to baseline within this period after the presentation of the conditioning stimulus followed by a TS (see below). For motor threshold determination, recordings were obtained at regular intervals from a low cortical stimulus intensity that did not produce any motor response (subthreshold: 0.5 mA) to high intensity (3.0 mA) that saturated the MEPs.

Rats were deeply anesthetized with either a combination of MMB anesthesia (0.15/2.0/5.0 mg/kg, respectively; intraperitoneally) or a combination of ketamine (90 mg/kg) and xylazine (10 mg/kg), which was used to preserve motor responses. Anesthesia depth was monitored periodically using the pedal withdrawal (''toe-pinch'') reflex at the same relative timing and frequency in all animals. The absence of such reflex indicated that a standardized depth of anesthesia and analgesia was achieved, and this was maintained throughout electrode implantation and recording. We used a temperature-controlled heating pad to maintain the body temperature at 37°C intraoperatively both during the post-surgical recovery and the recording period. Rats were placed in a grounded stereotaxic frame (Narishige, Japan) and electrically isolated from metal ear bars using parafilm.

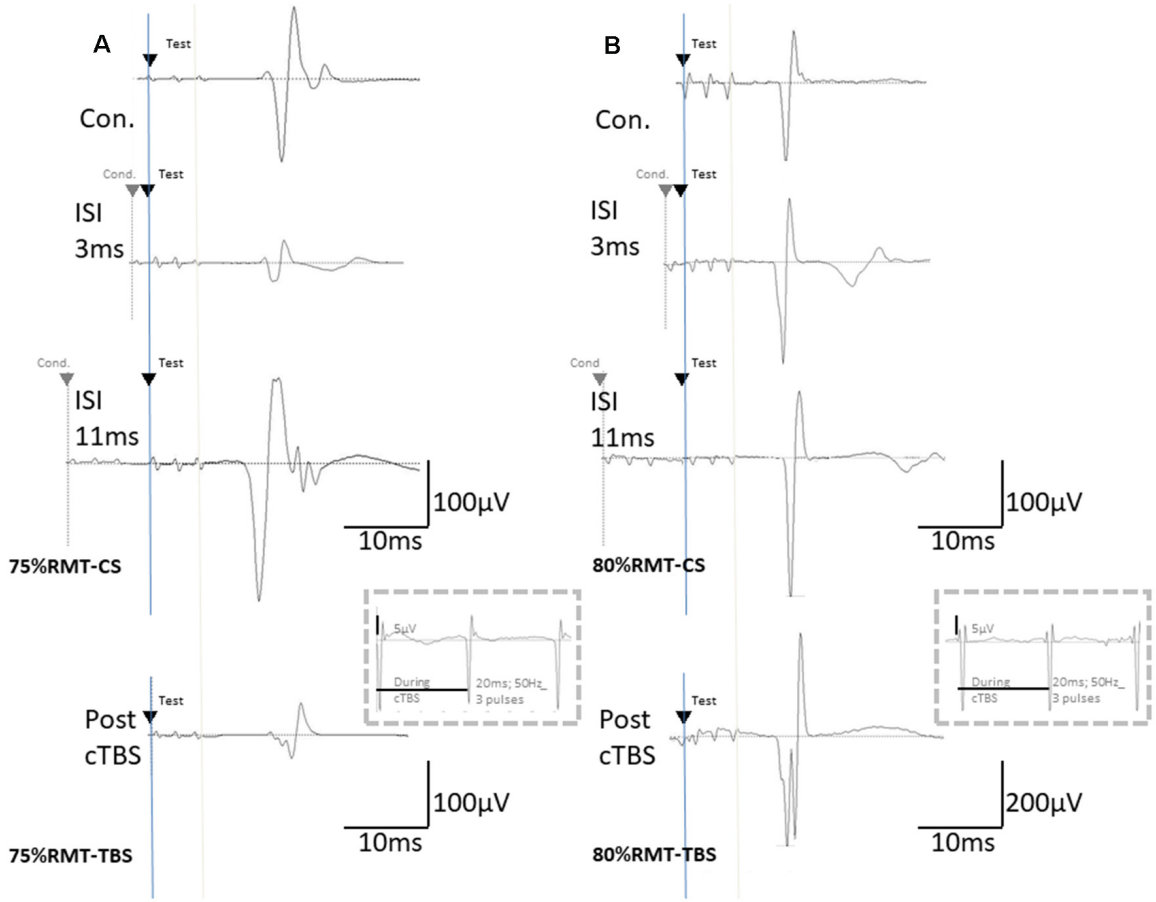

FIGURE 2 | The basic waveform of MEPs recorded from the biceps is composed of short-latency (approximately 14 ms) biphasic waves. **(A)** Inhibition and facilitation of MEPs at ISIs of 1, 3, and 11 ms under MMB anesthesia at 75% RMT-CS. This phenomenon is reminiscent of the short-latency intracortical inhibition (SICI) and ICF in the human motor cortex observed when using paired-pulse TMS. MEPs at pre- and post-cTBS (top and bottom, respectively), at ISIs of 3 (second) and 11 (third) ms, and EMG recordings during cTBS (fourth trace). **(B)** Inhibition and facilitation of MEPs at ISIs of 1, 3, and 11 ms under MMB anesthesia at 80% RMT-CS. MEPs at pre- and post-cTBS (top and bottom, respectively), at ISIs of 3 (second) and 11 (third) ms, and post-cTBS (bottom), and EMG recordings during cTBS (fourth trace). Note that recordings during cTBS (fourth trace, inside dashed line boxes) show small electrical stimulation artifacts (50 Hz), three 20-ms pulses, and an absence of evoked MEPs during cTBS (**A,B**; 5 μV of amplitude calibration in the fourth trace, inside dashed line-boxes). MEPs were inhibited after cortical motor cTBS at 75% of the RMT, while they were strongly facilitated immediately after cortical motor cTBS at 80% RMT (Note: 200 μV of amplitude calibration in the bottom trace, right **B**).

Data Analysis

All MEP data were analyzed offline using Brain Vision Analyzer2 (Brain Products, Germany), as also reported by Sykes et al. (2016). Peak-to-peak MEP amplitudes were measured (at 120% RMT intensity, composed of 12 individual sweeps in each minute run). Successively, normalized amplitudes to the final 5 min of baseline amplitude were expressed as a percentage change, allowing for between-subject comparisons, and were grouped into 2-min bins and a final 3-min bin.

All data are presented as mean ± standard error of the mean (SEM). Different groups of animals were compared using a one-way (two-way for time course) analysis of variance (ANOVA) with a Student-Newman–Keul *post hoc* analysis (SPSS, Cary, NC, USA). Experiments with three or more groups were analyzed with a two-way ANOVA followed by a *post hoc* Bonferroni-Dunn test. For TBS effects, the statistical significance of group differences was analyzed with an ANOVA with time (TIME) as a within-subject factor and group (GROUP) as a between-subjects factor. This was followed by a *post hoc* Holm test. To investigate whether the time effect differed among groups, we confirmed the TIME × GROUP interaction. Differences were considered significant at $P \leq 0.05$.

RESULTS

MEP Basic Waveforms

Direct motor cortical and epidural stimulation-induced MEPs were compared for accuracy verification (different methodological configurations of the induced current flow; polarity, location, and monophasic or biphasic, see **Figure 1** for detail). Quantitative differences in the final 5 min of MEP baseline parameters between the two anesthetic conditions

were not observed (RMT: 1.04 ± 0.03 vs. 1.03 ± 0.03 mA; latency: 13.9 ± 0.29 vs. 13.6 ± 0.25 ms; amplitude: 286 ± 7.4 vs. 302 ± 14.8 μV; under MMB and K/X anesthesia, respectively). In addition, an absence of statistically significant effects of anesthetic combinations on RMT ($t_{(40)} = 0.17$; $P > 0.05$), latency ($t_{(40)} = 0.94$; $P > 0.05$), or amplitude ($t_{(40)} = 0.96$; $P > 0.05$) was found.

Similarly, statistically significant effects of previous TBS sessions on RMT ($t_{(40)} = 1.56$; $P > 0.05$, $t_{(40)} = 1.59$; $P > 0.05$), latency ($t_{(40)} = 0.15$; $P > 0.05$, $t_{(40)} = 0.2$; $P > 0.05$), or amplitude (t = $_{(40)} = 0.24$; $P > 0.05$, $t_{(40)} = 1.38$; $P > 0.05$, MMB and K/X anesthesia respectively) were not seen.

Following previous methodological standards (Mishra et al., 2017), motor cortical electrical stimulation elicited a clear short-latency MEP (14.1 ms in latency, not including waveforms with latencies <5 ms), as illustrated in **Figure 1B**. We analyzed electrophysiological changes in MEPs based on the effects of anesthetic combinations, GABA-A agonist midazolam-based MMB, and non-specific NMDA receptor blocker, ketamine-based K/X, with or without cTBS or iTBS.

Inhibition and Facilitation Patterns of Paired-Stimulation MEPs

CS at 75% of the RMT preceding TS-MEPs showed inhibition (ISI, 3 ms) and facilitation (ISI, 11 ms) patterns under MMB anesthesia (**Figures 2A**, **3A**). While K/X anesthesia completely blocked facilitation at an ISI of 11 ms, inhibition at an ISI of 3 ms was preserved ($P < 0.05$; **Figure 3A**). A one-way ANOVA revealed a significant difference at an ISI of 9 ($F_{(1,26)}$: 5.52, $P < 0.05$), 11 ($F_{(1,26)}$: 26.89, $P < 0.001$) and 13 ($F_{(1,26)}$: 4.41, $P < 0.05$) ms, respectively.

CS at 80% of the RMT preceding TS-MEPs showed inhibition (ISI, 1 ms) and facilitation (ISI, 3 ms, and 11 ms) patterns under MMB anesthesia (**Figures 2B**, **3B**). While K/X anesthesia completely blocked facilitation at an ISI of 11 ms, inhibition at an ISI of 1 ms and facilitation at an ISI of 3 ms were preserved ($P < 0.05$; **Figure 3B**). A one-way ANOVA revealed a significant difference at an ISI of 7 ($F_{(1,26)}$: 5.23, $P < 0.05$), 9 ($F_{(1,26)}$: 9.72, $P < 0.0005$), 11 ($F_{(1,26)}$: 19.2, $P < 0.0005$) and 13 ($F_{(1,26)}$: 6.01. $P < 0.05$) ms, respectively. Therefore, the intracortical inhibition and facilitation profiles of a CS intensity at 75% of the RMT are reminiscent of the SICI and ICF in the human motor cortex using paired-pulse TMS. In contrast, such profiles of a CS intensity at 80% of the RMT were not entirely comparable to those seen in the human motor cortex using paired-pulse TMS.

Overall, given that CS at 70% of the RMT preceding the TS-MEPs revealed non-identical patterns under both conditions of anesthesia (data not shown), we chose CS intensities of 75 and 80% for the TBS procedures in the present study.

TBS Effects on Rat MEPs

MEPs were inhibited after motor cortical cTBS at 75% of the RMT, lasting up to 25 min under both MMB and K/X anesthesia ($P < 0.05$; **Figure 2A**, bottom trace, and **Figure 4A** red, pink line). In contrast, iTBS at 75% of the RMT facilitated MEPs, lasting up to 25 min under both MMB and K/X anesthesia ($P < 0.05$; **Figure 4A** green and blue line). Finally, both cTBS and iTBS at 75% of the RMT lead to MEP inhibition, while facilitation profiles were identical to those obtained using biphasic TMS at 80% of the active motor threshold (AMT) of the human motor cortex.

An ANOVA revealed a significant main effect of group on MEP, whereby the effects of the stimulation differed among the six groups (main effect of GROUP, $F_{(5,83)} = 180.3$, $P < 0.001$; main effect of TIME, $F_{(13,502)} = 3.385$, $P < 0.001$; interaction of GROUP × TIME, $F_{(65,502)} = 3.315$, $P < 0.001$).

A *post hoc* analysis indicated that the MEP amplitudes after stimulation in the 75% RMT-cTBS under both the MMB and K/X groups were significantly decreased compared with those in the no-TBS group ($P < 0.001$). In contrast, the MEP amplitudes were significantly increased in the iTBS groups compared to the no-TBS group ($P < 0.001$, respectively).

MEPs were strongly facilitated immediately after motor cortical cTBS at 80% of the RMT (**Figure 2B**), lasting up to 25 min under both the MMB and K/X anesthesia ($P < 0.05$; **Figure 2B**, bottom trace and **4B** red, pink line). Similarly, iTBS also facilitated MEPs, lasting up to 25 min under both anesthetic conditions ($P < 0.05$; **Figure 4B** green and blue line). A two-way ANOVA revealed a significant difference in the normalized MEP amplitude over time ($P = 0.0003$), while *post hoc* comparisons by SPSS (Cary, NC, USA) indicated that the MEP amplitudes were significantly higher than those in no-TBS controls at all time points (asterisks in **Figure 4** denote significance).

Although identical stimulus artifacts of 20 ms (50 Hz) were observed, motor responses were not evoked during TBS at any of the stimulus intensities (**Figures 2A,B**; inside dashed line boxes).

An ANOVA revealed a significant main effect of group on MEP, whereby the effects of the stimulation differed among the six groups (main effect of GROUP, $F_{(5,83)} = 127.6$, $P < 0.001$; main effect of TIME, $F_{(13,502)} = 22.273$, $P < 0.001$; interaction of GROUP × TIME, $F_{(65,502)} = 1.642$, $P < 0.001$).

A *post hoc* analysis indicated significant increases, compared to the no-TBS group, in the MEP amplitudes after the stimulation in both the 80% RMT-cTBS and RMT-iTBS for the MMB and K/X groups ($P < 0.001$).

Multiple comparisons between the 80% RMT-cTBS/MMB groups and the no-TBS group were conducted at each time point. Our results indicated the MEP amplitudes in the 80% RMT-cTBS group to be significantly increased compared with those in the no-TBS group at several time points (20, 22, and 25 min following stimulation: $P = 0.004$, 0.01, and < 0.001, respectively). Differences in the increase of MEP amplitudes were observed immediately following stimulation and persisted for more than an hour (data not shown), suggesting persistent cTBS effects on the MEP amplitudes.

The SICI at an ISI of 3 ms was significantly suppressed only after 75% RMT-cTBS under the K/X anesthesia ($P < 0.05$). In contrast, the ICF at an ISI of 11 ms was significantly suppressed only after 75% RMT-cTBS under the MMB anesthesia ($P < 0.001$), while the SICI at an ISI of 3 ms under such anesthesia tended to be suppressed, however, the result was not statistically significant (**Figure 5A**). Finally, the 75% RMT-iTBS, 80% RMT-cTBS, and 80% RMT-iTBS did not affect

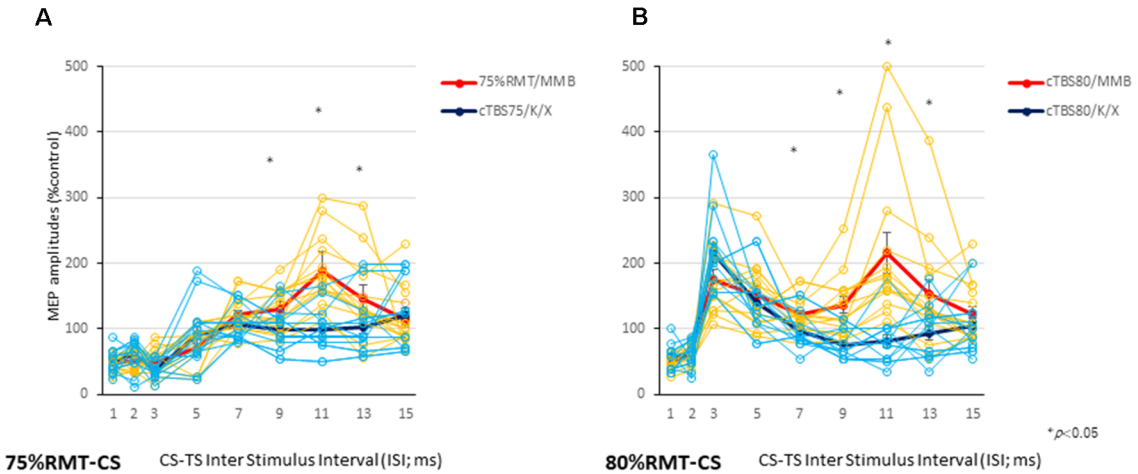

FIGURE 3 | Individual and averaged MEPs in each ISI under the MMB and K/X anesthesia conditions. Individual profiles of normalized MEPs in each ISI under the MMB and K/X anesthesia conditions **(A,B)**. Averaged normalized MEPs under the MMB (red) and K/X (blue) anesthesia conditions at a CS at 75 (left **A**) and 80 (right **B**) % of the RMT preceding test stimulus (TS)-MEPs. MMB-anesthetized rats demonstrated significant inhibition at ISIs of 3 ms and facilitation at 11 ms, whereas K/X-anesthetized rats showed significant suppression at 11 ms and facilitation at 75% of the RMT-CS. Inhibition was preserved at an ISI of 3 ms (*$P < 0.05$). MMB-anesthetized rats presented significant facilitation at ISIs of 3 and 11 ms following inhibition at 1 ms. In contrast, K/X-anesthetized rats showed significant suppression at 11 ms and facilitation at 80% RMT-CS. An analysis of variance (ANOVA) revealed that the values were significantly greater in the MMB group than in the K/X group at an ISI of 11 ms (*$P < 0.05$).

either the SICI at an ISI of 3 ms or the ICF at an ISI of 11 ms (**Figures 5B–D**).

DISCUSSION

Two main findings were reported in the present study. First, MEPs following paired electrical motor cortical stimulation showed inhibition (ISI of 3 ms) and facilitation (ISIs of 11 ms) patterns under MMB anesthesia. In contrast, the K/X anesthesia completely blocked facilitation at an ISI of 11 ms, while inhibition at an ISI of 1 ms and facilitation at an ISI of 3 ms were preserved. This phenomenon is reminiscent of the SICI and ICF in the human motor cortex observed through paired-pulse TMS. Our data indicate that ICF in the rat motor cortex is glutamate-mediated. Second, cTBS, as well as iTBS, strongly facilitated MEPs stimulus intensity for up to 25 min under both the MMB and K/X anesthesia conditions.

Differences in MEPs evoked by TMS have also been documented for different pulse shapes (monophasic vs. biphasic) and different orientations of the electric field (Nakamura et al., 2016; Shirota et al., 2017). While current density close to the electrodes is higher than that in between electrodes, it is more uniform with TMS. Stimulation focus with biphasic stimulation remains unclear (whether at the anodal or cathodal, or in between the electrodes). Preliminary direct comparison studies between epidural bipolar-biphasic-triple pulse and direct cortical monopolar stimulation resulted in similar MEPs. Advantages and limitations of the epidural cortical stimulation have been previously discussed by Kosugi et al. (2018). Given that epidural stimulation is minimally invasive and that it activates pyramidal neurons trans-synaptically *via* cortical interneuron activation, we used epidural bipolar-biphasic-triple pulse for our MEP recordings (Mishra et al., 2017).

MEP Basic Waveforms

As reported by Mishra et al. (2017), we used a train of three pulses (3-ms interval short train biphasic) to enable the selective activation and temporal summation in the motor cortex (Amassian et al., 1990). This configuration is important as a single pulse causes the activation of both the motor cortex and subcortical structures. Therefore, the MEP latencies of all our results (14.1 ± 0.88 ms in latency, not including waveforms with latencies < 5 ms) imply the activation of rat corticospinal descending motor pathways (Mishra et al., 2017). Indeed, we previously demonstrated that MEPs elicited by direct cortical stimulation (overall conduction velocity of approximately 18 m/s) disappeared after the transection of the corticospinal tract (Kamida et al., 1998). Furthermore, we confirmed that, although single-pulse stimulation also evoked MEPs, it did not activate those of interest for us, which had a higher threshold (approximately three times) and exhibited shorter (approximately 5 ms) latencies (data not shown). It should be noted that electrical stimulation of the corticospinal tract elicits excitatory post-synaptic potentials (EPSPs) in forelimb motoneurons, which are mediated by multi-synaptic excitatory corticofugal pathways and not exclusively by corticospinal axons (Alstermark et al., 2004). Indeed, a localized lesion of the rat corticospinal tract did not affect the size of the short-latency MEPs by TMS over the motor cortex, while mixed descending inputs contributed to the long latency MEPs (Nielsen et al., 2007). Also, the contribution of corticospinal axons and other descending pathways for MEPs production remains unclear (Oudega and Perez, 2012). Similarly to urethane,

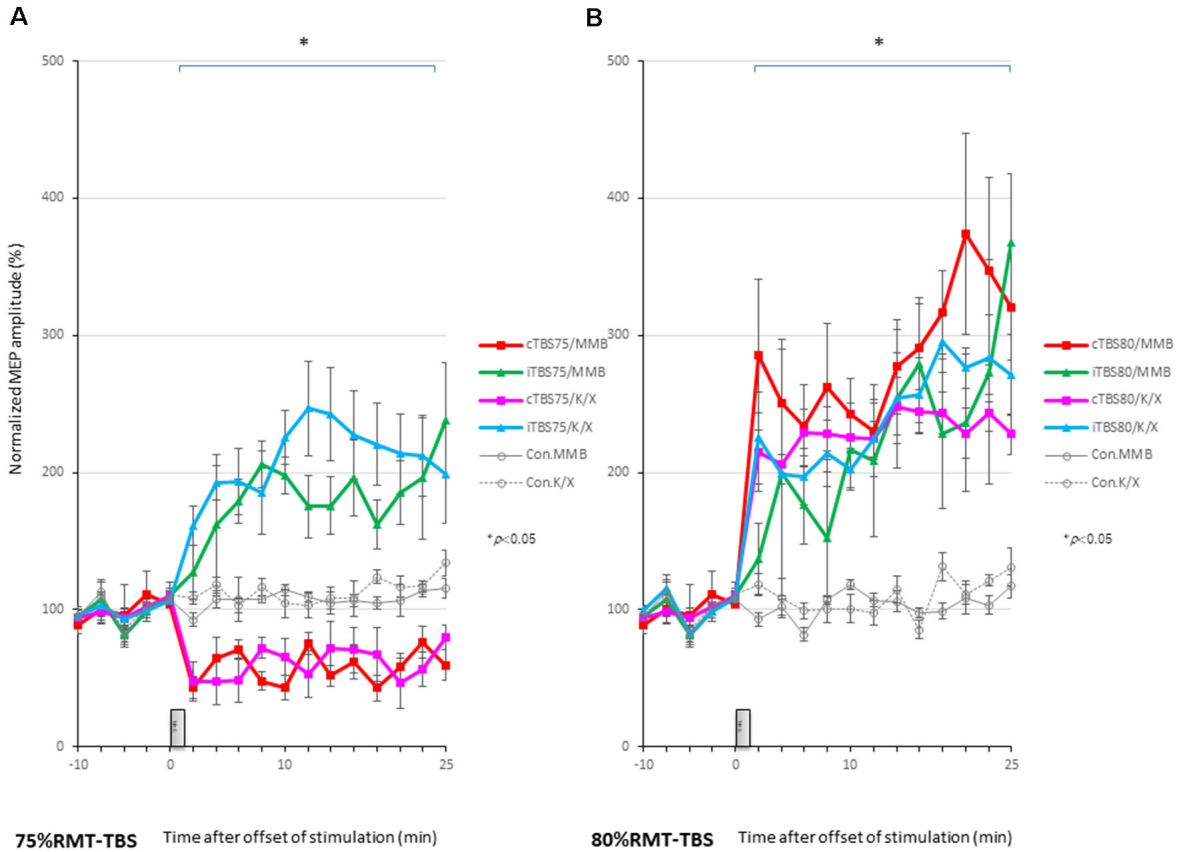

FIGURE 4 | MEP amplitudes increase in intensity in the stimulated cortex after 80% RMT-cTBS and iTBS time-series data of MEP amplitudes are expressed as the percentage change from baseline attributable to TBS. Group data are presented as the mean ± standard error of the mean. **(A)** Compared to the no-TBS group, the increase in MEP amplitudes is significantly lower in the 75% RMT-cTBS group and significantly higher in the 75%-RMT-iTBS group. **(B)** The increase in MEP amplitudes in the 80% RMT-cTBS and iTBS groups is significantly greater than that in the no-TBS group. $^*P < 0.05$.

i.e., a compound commonly used for synaptic plasticity studies (Reynolds et al., 2001; Sykes et al., 2016), we here confirmed that MMB anesthesia (applicable for survival experiments) was also favorable for multi-synaptic corticospinal MEPs and provided continuous stable conditions for MEP recordings.

SICI and ICF in the Rat Motor Cortex With an Electrical Train of Three Pulses

Contrary to reports of healthy human controls with paired-pulse TMS, a CS at 80% of the RMT preceding paired electrical motor cortical stimulation-induced inhibition (ISI of 1 ms) and facilitation (ISIs of 3 and 11 ms) patterns under the MMB anesthesia. In contrast, a CS at 75% of the RMT preceding TS-MEPs showed inhibition (ISI, 3 ms) and facilitation (ISI, 11 ms) patterns comparable with human results (Kujirai et al., 1993; Rothwell, 1997).

These results were obtained under anesthetic conditions, i.e., GABA-A agonist, midazolam-based MMB, and NMDA antagonist ketamine-based K/X. Inhibitions at an ISI of 1–2 ms were comparable between the anesthetics. Indeed, inhibitions at an ISI of 1–2 ms have been considered to include an axonal refractory period that is not mediated by GABA-A interneurons (Kujirai et al., 1993; Rothwell, 1997). Similarly, an ISI of 3 ms, which is presumed to be a GABA-A-mediated inhibitory phase in healthy humans, was facilitated and comparable between both anesthetics. Each CS-TS train consisting of three pulses (3-ms interval short train, biphasic) should be considered as both trains overlap, and each pulse may interfere at an ISI shorter than 6 ms. This differs fundamentally from the paired single pulse CS-TS TMS paradigm. Specifically, the assessment of SICI at an ISI of 3 ms with certain conditioning intensities can be contaminated by facilitatory effects, such as short ICF (Peurala et al., 2008). Given that both the CS intensities (75 and 80% of the RMT) are constantly subthreshold during TBS (see **Figure 2**; 5 μV of amplitude calibration in the fourth trace, inside dashed line-boxes), we suggest minimal intensity contamination by intracortical facilitatory influences at this level of conditioning.

Facilitation at an ISI of 11 ms, which is considered to be a glutamate-mediated facilitatory period (Ziemann et al., 2015), was completely blocked under NMDA antagonist ketamine-based K/X anesthesia. This result is consistent with a previous hypothesis proposing that ICF (facilitation at an ISI of 10–15 ms in humans) strongly correlates with excitatory glutamatergic

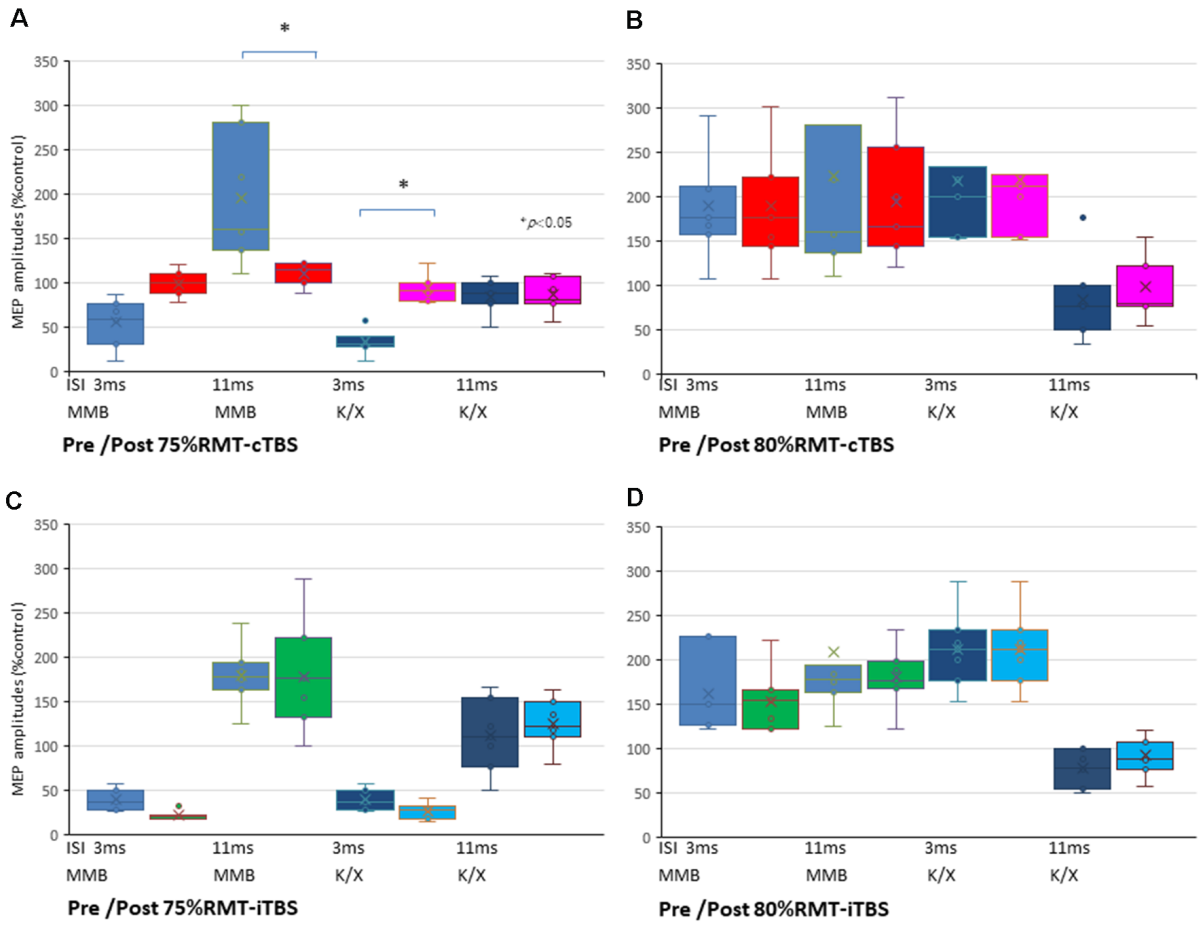

FIGURE 5 | SICI and ICF changes after cTBS and iTBS at different stimulus intensities. **(A)** A multiple comparisons test revealed that the SICI at an ISI of 3 ms was significantly suppressed only after 75% RMT-cTBS under the K/X anesthesia ($P = 0.046$, < 0.05). In contrast, the ICF at an ISI of 11 ms was significantly suppressed only after 75% RMT-cTBS under the MMB anesthesia ($P < 0.001$), while the SICI at an ISI of 3 ms under such anesthesia tended to be suppressed, however, the result was not statistically significant. **(B–D)** Finally, the 75% RMT-iTBS, 80% RMT-cTBS, and 80% RMT-iTBS did not have any effect on either the SICI at an ISI of 3 ms or the ICF at an ISI of 11 ms. Colors in the graph represent each condition pre- and post-TBS (red: cTBS/MMB, pink: cTBS/K/X; green: iTBS/MMB; light blue: iTBS/K/X at 75% and 80% of the RMT, respectively) and anesthesia (blue: MMB; dark blue: K/X, respectively). *$P < 0.05$.

interneurons within the motor cortex depending on NMDA receptor activation (Ziemann et al., 2015).

cTBS of the Rat Motor Cortex Intensity Dependently Facilitates MEP

Our results demonstrate that 75% RMT-cTBS inhibits while iTBS enhances the neuronal activity and that both 80%-cTBS and iTBS enhance neuronal activity in the cerebral cortex. There are several possible interpretations of our results, indicating that cTBS strongly facilitated MEPs in a stimulus intensity-dependent manner under both the MMB and K/X anesthetic conditions.

Our finding contrasts previous results suggesting that memantine, i.e., a non-competitive NMDA receptor antagonist, blocked both the suppressive effects of cTBS and the facilitatory effects of iTBS. Similarly, it contrasts findings showing that D-cycloserine, i.e., a partial agonist at the NMDA receptor glycine-B biding site, switched the after-effects of iTBS facilitation to inhibition in the human motor cortex (Huang et al., 2007; Teo et al., 2007). Indeed, Hsieh et al. (2015) reported iTBS-MEP facilitation and cTBS-MEP inhibition under xylazine and tiletamine-zolazepam (including tiletamine, a compound that is chemically related to ketamine and fundamentally employs the same mechanisms) anesthesia in rats. A combination of ketamine (90 mg/kg) and xylazine (10 mg/kg) is frequently used for facilitation after paired stimulation to preserve motor responses (Mishra et al., 2017). Anesthetic combinations must be carefully chosen in animal studies concerning stability, MEP preservations, "pseudo potentiation," non-survival experiments (urethane), and enhancement of GABA transmission (midazolam) or NMDA blockade (e.g., ketamine; Sykes et al., 2016). Strikingly, the present study demonstrated that MEPs were facilitated by either continuous or intermittent TBS under effective doses of anesthetics, including the GABA-A agonist, midazolam, and the NMDA antagonist, ketamine, in the rat motor cortex.

Motor cortical conditions of the subjects, including inter-individual variability (Hamada et al., 2013), and stimulus parameters, such as current direction (Shirota et al., 2017), intensity, and duration of cTBS, alter suppressive or facilitative MEP amplitudes.

An RMT stimulus intensity of 80% in the present experimental settings for anesthetized rats may exceed that of the 80% AMT in the awake human motor cortex. Indeed, cTBS increased motor cortical excitability with a relatively higher 80% AMT intensity, while it was depressed with a lower intensity. The optimal stimulus intensity was not 80% of AMT in every subject (Sasaki et al., 2018).

Similarly, low-intensity, short-interval (300 pulses) cTBS was found to depend on the intensity and to facilitate MEPs at 70% of the RMT and inhibit them at 65% of the RMT, without significant effects on the SICI (Doeltgen and Ridding, 2011). The authors speculated the 70% RMT-cTBS300 to provide sufficient stimulation to breach the activation threshold of intracortical facilitatory interneurons. In contrast, the 65% RMT-cTBS300 was suggested to both facilitate intracortical inhibitory influences and inhibit intracortical facilitatory influences on corticospinal neurons. Lower activation thresholds for intracortical inhibitory interneurons, compared to facilitatory interneurons, exist within a few percent of stimulus intensities (Kujirai et al., 1993).

In vitro, low-intensity magnetic stimulation hyperpolarizes action potential thresholds, and increases evoked spike frequency without altering the resting membrane potentials and input resistance (Tang et al., 2016a).

An epidural corticospinal MEP study revealed different intracortical facilitatory and inhibitory neuronal origins that while the 80% AMT-iTBS leads to a rapid increase in the excitability of the cortical mechanism that generates later I-waves, the cTBS preferentially affects the amplitude of the I1 wave (Di Lazzaro et al., 2008). Furthermore, TBS protocols have also been conducted for a longer time compared to reversed facilitatory and inhibitory effects (Gamboa et al., 2010).

The lack of low-intensity 75% RMT-cTBS on the SICI is consistent with previous results (Doeltgen and Ridding, 2011). Considering that the animals in the present study were under anesthetic conditions (GABA-A agonist or NMDA antagonist), the inhibitory effects on the SICI and ICF in response to cTBS may have been affected, as well as the facilitatory effects on the SICI in response to iTBS.

Ketamine, i.e., an NMDA receptor antagonist that indirectly facilitates glutamate neurotransmission through the AMPA receptor, decreased MT based on the administered dose and was shown to enhance MEP response to TMS (Di Lazzaro et al., 2003).

The effect of ketamine possibly suggests an additional contribution of fast ionotropic glutamatergic neurotransmission, most likely at the glutamatergic synapses of these axons onto corticospinal neurons (Ziemann et al., 2015).

The fact that MEPs were facilitated after cTBS or iTBS under ketamine anesthesia, while a lack of ICF was observed, may indicate that AMPA and NMDA transmission are differently involved in TBS effects and paired-pulse CS preceding TS-MEPs.

To understand the underlying mechanisms and to verify their compatibility with human results, further experiments with altered combinations of these cTBS parameters are warranted.

Limitations and Future Work

A limitation of the present study may lie in the utilization of focal short-burst triple-pulses for stable selective activation and temporal summation in the motor cortex for both CS and TS, as it represents a fundamentally different paradigm to that of the paired single pulse CS-TS TMS. Indeed, the single pulse CS-TS paradigm, even with a high threshold, should be confirmed as a strict benchmark for TMS studies. A stimulus strength of 80% of the RMT for CS and TBS, which might exceed that of 80% AMT, could be reduced in future studies.

Although an ideal-smaller-size, non-invasive animal TMS-coil design for equivalent spatial resolution has been proposed by Tang et al. (2016b), the stereotactic frame under anesthesia conditions is required. Low-intensity electrical iTBS applied to the contralesional hemisphere enhanced functional recovery even at the subacute stage after stroke (Boddington et al., 2020). Effective neuromodulation for symptomatic animal models connected to the stimulator requires repeated sessions under anesthetic drug-free, freely-moving, awake conditions. A reliable, minimally invasive, and quantitative motor mapping and MEP recording method in anesthesia-free conditions are warranted for elucidating the mechanisms underlying cortical motor reorganization. Establishing stable and reproducible conditions for RMT, AMT, and MEPs for long-term evaluations in awake, freely-moving rodents is also necessary (Kosugi et al., 2018). Furthermore, Hoogendam et al. (2010) presented—in a critical review—seven lines of evidence suggesting that neuromodulation of the rTMS is a result of the induction of synaptic changes resembling long-term potentiation and depression (LTP and LTD). Evidence includes similarities in stimulation temporal patterns required for induction, duration of changes, and sensitivity to pharmacological interventions. This is consistent with the hypothesis that motor cortex stimulation can activate MEPs, as well as cellular and molecular mechanisms underlying different forms of synaptic plasticity, such as LTP and LTD, for future neuromodulation-based therapeutic strategy (Müller-Dahlhaus and Vlachos, 2013; Rodger and Sherrard, 2015).

CONCLUSIONS

Paired-stimulation corticospinal MEPs induced inhibition and facilitation patterns that were similar, but not identical, to those of the SICI and ICF in the human motor cortex obtained when using paired-pulse TMS. Both continuous and intermittent TBS-induced MEP facilitation under two anesthetic conditions. Continuous TBS parameters in the rat motor cortex should be further explored to elucidate the underlying mechanisms.

DATA AVAILABILITY STATEMENT

The raw data supporting the conclusions of this article will be made available by the authors, without undue reservation.

ETHICS STATEMENT

The animal study was reviewed and approved by Ethical Committee of the School of Medicine, Oita University.

AUTHOR CONTRIBUTIONS

MF and YK designed the research paradigm. MF, HF, and YK performed the research investigations. MF and HF analyzed the data and wrote the article. All authors contributed to the article and approved the submitted version.

FUNDING

This work was supported by a medical research grant on traffic accidents by The General Insurance Association of Japan (MF), a grant from the Ministry of Education, Culture, Sports, Science and Technology (MF, YK, and HF), and Co-Create Knowledge for Pharma Innovation with Takeda (COCKPI-T; MF).

ACKNOWLEDGMENTS

We thank Dr. Kenji Sugita for the helpful technical advice on rat surgical procedures.

REFERENCES

Alstermark, B., Ogawa, J., and Isa, T. (2004). Lack of monosynaptic corticomotoneuronal EPSPs in rats: disynaptic EPSPs mediated *via* reticulospinal neurons and polysynaptic EPSPs *via* segmental interneurons. *J. Neurophysiol.* 91, 1832–1839. doi: 10.1152/jn.00820.2003

Amassian, V. E., Quirk, G. J., and Stewart, M. (1990). A comparison of corticospinal activation by magnetic coil and electrical stimulation of monkey motor cortex. *Electroencephalogr. Clin. Neurophysiol* 77, 390–401. doi: 10.1016/0168-5597(90)90061-h

Barry, M. D., Boddington, L. J., Igelström, K. M., Gray, J. P., Shemmell, J., Tseng, K. Y., et al. (2014). Utility of intracerebral theta burst electrical stimulation to attenuate interhemispheric inhibition and to promote motor recovery after cortical injury in an animal model. *Exp. Neurol.* 261, 258–266. doi: 10.1016/j.expneurol.2014.05.023

Boddington, L. J., Gray, J. P., Schulz, J. M., and Reynolds, J. N. J. (2020). Low-intensity contralesional electrical theta burst stimulation modulates ipsilesional excitability and enhances stroke recovery. *Exp. Neurol.* 23, 113071–113079. doi: 10.1016/j.expneurol.2019.113071

Carmel, J. B., Berrol, L. J., Brus-Ramer, M., and Martin, J. H. (2010). Chronic electrical stimulation of the intact corticospinal system after unilateral injury restores skilled locomotor control and promotes spinal axon outgrowth. *J. Neurosci.* 30, 10918–10926. doi: 10.1523/JNEUROSCI.1435-10.2010

Di Lazzaro, V., Oliviero, A., Profice, P., Pennisi, M. A., Pilato, F., Zito, G., et al. (2003). Ketamine increases human motor cortex excitability to transcranial magnetic stimulation. *J. Physiol.* 547, 485–496. doi: 10.1113/jphysiol.2002.030486

Di Lazzaro, V., Pilato, F., Dileone, M., Profice, P., Oliviero, A., Mazzone, P., et al. (2008). The physiological basis of the effects of intermittent theta burst stimulation of the human motor cortex. *J. Physiol.* 586, 3871–3879. doi: 10.1113/jphysiol.2008.152736

Doeltgen, S. H., and Ridding, M. C. (2011). Low-intensity, short-interval theta burst stimulation modulates excitatory but not inhibitory motor networks. *Clin. Neurophysiol.* 122, 1411–1416. doi: 10.1016/j.clinph.2010.12.034

Fujiki, M., Yee, K. M., and Steward, O. (2020). Non-invasive high frequency repetitive transcranial magnetic stimulation (hfrTMS) robustly activates molecular pathways implicated in neuronal growth and synaptic plasticity in select populations of neurons. *Front. Neurosci.* 14:558. doi: 10.3389/fnins.2020.00558

Gamboa, O. L., Antal, A., Moliadze, V., and Paulus, W. (2010). Simply longer is not better: reversal of theta burst after-effect with prolonged stimulation. *Exp. Brain Res.* 204, 181–187. doi: 10.1007/s00221-010-2293-4

Hamada, M., Murase, N., Hasan, A., Balaratnam, M., and Rothwell, J. C. (2013). The role of interneuron networks in driving human motor cortical plasticity. *Cereb. Cortex* 23, 1593–1605. doi: 10.1093/cercor/bhs147

Hess, G., and Donoghue, J. P. (1996). Long-term potentiation and long-term depression of horizontal connections in rat motor cortex. *Acta Neurobiol. Exp.* 56, 397–405.

Hoogendam, J. M., Ramakers, G. M., and Di Lazzaro, V. (2010). Physiology of repetitive transcranial magnetic stimulation of the human brain. *Brain Stimul.* 3, 95–118. doi: 10.1016/j.brs.2009.10.005

Hsieh, T. H., Dhamne, S. C., Chen, J. J., Pascual-Leone, A., Jensen, F. E., and Rotenberg, A. (2012). A new measure of cortical inhibition by mechanomyography and paired-pulse transcranial magnetic stimulation in unanesthetized rats. *J. Neurophysiol.* 107, 966–972. doi: 10.1152/jn.00690.2011

Hsieh, T. H., Huang, Y. Z., Rotenberg, A., Pascual-Leone, A., Chiang, Y. H., Wang, J. Y., et al. (2015). Functional dopaminergic neurons in substantia nigra are required for transcranial magnetic stimulation-induced motor plasticity. *Cereb. Cortex* 25, 1806–1814. doi: 10.1093/cercor/bht421

Huang, Y. Z., Chen, R. S., Rothwell, J. C., and Wen, H. Y. (2007). The after-effect of human theta burst stimulation is NMDA receptor dependent. *Clin. Neurophysiol.* 118, 1028–1032. doi: 10.1016/j.clinph.2007.01.021

Huang, Y. Z., Edwards, M. J., Rounis, E., Bhatia, K. P., and Rothwell, J. C. (2005). Theta burst stimulation of the human motor cortex. *Neuron* 45, 201–206. doi: 10.1016/j.neuron.2004.12.033

Kamida, T., Fujiki, M., Hori, S., and Isono, M. (1998). Conduction pathways of motor evoked potentials following transcranial magnetic stimulation: a rodent study using a "figure-8" coil. *Muscle Nerve* 21, 722–731. doi: 10.1002/(sici)1097-4598(199806)21:6<722::aid-mus3>3.0.co;2-9

Kosugi, A., Takemi, M., Tia, B., Castagnola, E., Ansaldo, A., Sato, K., et al. (2018). Accurate motor mapping in awake common marmosets using microelectro corticographical stimulation and stochastic threshold estimation. *J. Neural Eng.* 15:036019. doi: 10.1088/1741-2552/aab307

Kujirai, T., Caramia, M. D., Rothwell, J. C., Day, B. L., Thompson, P. D., Ferbert, A., et al. (1993). Corticocortical inhibition in human motor cortex. *J. Physiol.* 471, 501–519. doi: 10.1113/jphysiol.1993.sp019912

Mishra, A. M., Pal, A., Gupta, D., and Carmel, J. B. (2017). Paired motor cortex and cervical epidural electrical stimulation timed to converge in the spinal cord promotes lasting increases in motor responses. *J. Physiol.* 595, 6953–6968. doi: 10.1113/jp274663

Müller-Dahlhaus, F., and Vlachos, A. (2013). Unraveling the cellular and molecular mechanisms of repetitive magnetic stimulation. *Front. Mol. Neurosci.* 6:50. doi: 10.3389/fnmol.2013.00050

Nakamura, K., Groiss, S. J., Hamada, M., Enomoto, H., Kadowaki, S., Abe, M., et al. (2016). Variability in response to quadripulse stimulation of the motor cortex. *Brain Stimul.* 9, 859–866. doi: 10.1016/j.brs.2016.01.008

Nielsen, J. B., Perez, M. A., Oudega, M., Enriquez-Denton, M., and Aimonetti, J. M. (2007). Evaluation of transcranial magnetic stimulation for investigating transmission in descending motor tracts in the rat. *Eur. J. Neurosci.* 25, 805–814. doi: 10.1111/j.1460-9568.2007.05326.x

Oudega, M., and Perez, M. A. (2012). Corticospinal reorganization after spinal cord injury. *J. Physiol.* 590, 3647–3663. doi: 10.1113/jphysiol.2012.233189

Peurala, S. H., Müeller-Dahlhaus, F. M., Arai, N., and Ziemann, U. (2008). Interference of short-interval intracortical inhibition (SICI) and short-interval intracortical facilitation (SICF). *Clin. Neurophysiol.* 119, 2291–2297. doi: 10.1016/j.clinph.2008.05.031

Reynolds, J. N., Hyland, B. I., and Wickens, J. R. (2001). A cellular mechanism of reward-related learning. *Nature* 413, 67–70. doi: 10.1038/35092560

Rodger, J., and Sherrard, R. M. (2015). Optimising repetitive transcranial magnetic stimulation for neural circuit repair following traumatic brain injury. *Neural Regen. Res.* 10, 357–359. doi: 10.4103/1673-5374.153676

Rothwell, J. C. (1997). Techniques and mechanisms of action of transcranial stimulation of the human motor cortex. *J. Neurosci. Methods* 74, 113–122. doi: 10.1016/s0165-0270(97)02242-5

Sasaki, T., Kodama, S., Togashi, N., Shirota, Y., Sugiyama, Y., Tokushige, S. I., et al. (2018). The intensity of continuous theta burst stimulation, but not the waveform used to elicit motor evoked potentials, influences its outcome in the human motor cortex. *Brain Stimul.* 11, 400–410. doi: 10.1016/j.brs.2017.12.003

Shirota, Y., Dhaka, S., Paulus, W., and Sommer, M. (2017). Current direction-dependent modulation of human hand motor function by intermittent theta burst stimulation (iTBS). *Neurosci. Lett.* 650, 109–113. doi: 10.1016/j.neulet.2017.04.032

Sykes, M., Matheson, N. A., Brownjohn, P. W., Tang, A. D., Rodger, J., Shemmell, J. B., et al. (2016). Differences in motor evoked potentials induced in rats by transcranial magnetic stimulation under two separate anesthetics: implications for plasticity studies. *Front. Neural Circuits* 10:80. doi: 10.3389/fncir.2016.00080

Takemi, M., Castagnola, E., Ansaldo, A., Ricci, D., Fadiga, L., Taoka, M., et al. (2017). Rapid identification of cortical motor areas in rodents by high-frequency automatic cortical stimulation and novel motor threshold algorithm. *Front. Neurosci.* 11:580. doi: 10.3389/fnins.2017.00580

Tang, A. D., Hong, I., Boddington, L. J., Garrett, A. R., Etherington, S., Reynolds, J. N., et al. (2016a). Low-intensity repetitive magnetic stimulation lowers action potential threshold and increases spike firing in layer 5 pyramidal neurons *in vitro*. *Neuroscience* 335, 64–71. doi: 10.1016/j.neuroscience.2016.08.030

Tang, A. D., Lowe, A. S., Garrett, A. R., Woodward, R., Bennett, W., Canty, A. J., et al. (2016b). Construction and evaluation of rodent-specific rTMS coils. *Front. Neural Circuits* 10:47. doi: 10.3389/fncir.2016.00047

Teo, J. T., Swayne, O. B., and Rothwell, J. C. (2007). Further evidence for NMDA-dependence of the after-effects of human theta burst stimulation. *Clin. Neurophysiol.* 118, 1649–1651. doi: 10.1016/j.clinph.2007.04.010

Vahabzadeh-Hagh, A. M., Muller, P. A., Pascual-Leone, A., Jensen, F. E., and Rotenberg, A. (2011). Measures of cortical inhibition by paired-pulse transcranial magnetic stimulation in anesthetized rats. *J. Neurophysiol.* 105, 615–624. doi: 10.1152/jn.00660.2010

Yang, Q., Ramamurthy, A., Lall, S., Santos, J., Ratnadurai-Giridharan, S., Lopane, M., et al. (2019). Independent replication of motor cortex and cervical spinal cord electrical stimulation to promote forelimb motor function after spinal cord injury in rats. *Exp. Neurol.* 320:112962. doi: 10.1016/j.expneurol.2019.112962

Ziemann, U., Reis, J., Schwenkreis, P., Rosanova, M., Strafella, A., Badawy, R., et al. (2015). TMS and drugs revisited 2014. *Clin. Neurophysiol.* 126, 1847–1868. doi: 10.1016/j.clinph.2014.08.028

Conflict of Interest: The authors declare that the research was conducted in the absence of any commercial or financial relationships that could be construed as a potential conflict of interest.

frontiers in Neural Circuits

METHODS
published: 10 February 2022
doi: 10.3389/fncir.2021.789095

Using Hebbian-Type Stimulation to Rescue Arm Function After Stroke: Study Protocol for a Randomized Clinical Trial

Rong Xu[1,2†], Guang-Yue Zhu[3†], Jun Zhu[1†], Yong Wang[2], Xiang-Xin Xing[4], Lin-Yu Chen[2], Jie Li[2], Fu-Qiang Shen[2], Jian-Bing Chen[2], Xu-Yun Hua[4] and Dong-Sheng Xu[4,5*]*

[1] Shanghai Zhaxin Traditional Chinese and Western Medicine Hospital, Shanghai, China, [2] Shanghai Yangzhi Rehabilitation Hospital, Shanghai, China, [3] Tongji Hospital Affiliated to Tongji University, Shanghai, China, [4] Yueyang Hospital of Integrated Traditional Chinese and Western Medicine, Shanghai University of Traditional Chinese Medicine, Shanghai, China, [5] School of Rehabilitation Science, Shanghai University of Traditional Chinese Medicine, Shanghai, China

OPEN ACCESS

Edited by:
Nicoletta Berardi,
University of Florence, Italy

Reviewed by:
Anna Poggesi,
University of Florence, Italy
Andrea Guzzetta,
University of Pisa, Italy

***Correspondence:**
Xu-Yun Hua
swrhxy@126.com
Dong-Sheng Xu
dxu0927@shutcm.edu.cn

†These authors have contributed equally to this work

Received: 04 October 2021
Accepted: 27 December 2021
Published: 10 February 2022

Citation:
Xu R, Zhu G-Y, Zhu J, Wang Y, Xing X-X, Chen L-Y, Li J, Shen F-Q, Chen J-B, Hua X-Y and Xu D-S (2022) Using Hebbian-Type Stimulation to Rescue Arm Function After Stroke: Study Protocol for a Randomized Clinical Trial. Front. Neural Circuits 15:789095. doi: 10.3389/fncir.2021.789095

Background: Upper-extremity hemiplegia after stroke remains a significant clinical problem. The supplementary motor area (SMA) is vital to the motor recovery outcomes of chronic stroke patients. Therefore, rebuilding the descending motor tract from the SMA to the paralyzed limb is a potential approach to restoring arm motor function after stroke. Paired associative stimulation (PAS), which is based on Hebbian theory, is a potential method for reconstructing the connections in the impaired motor neural circuits. The study described in this protocol aims to assess the effects of cortico–peripheral Hebbian-type stimulation (HTS), involving PAS, for neural circuit reconstruction to rescue the paralyzed arm after stroke.

Methods: The study is a 4-month double-blind randomized sham-controlled clinical trial. We will recruit 90 post-stroke individuals with mild to moderate upper limb paralysis. Based on a 1:1 ratio, the participants will be randomly assigned to the HTS and sham groups. Each participant will undergo 5-week HTS or sham stimulation. Assessments will be conducted at baseline, immediately after the 5-week treatment, and at a 3-month follow-up. The primary outcome will be the Wolf Motor Function Test (WMFT). The secondary outcomes will be Fugl-Meyer Assessment for Upper Extremity (FMA-UE), Functional Independence Measure (FIM), and functional near-infrared spectroscopy (fNIRS) parameters. The adverse events will be recorded throughout the study.

Discussion: Upper-limb paralysis in stroke patients is due to neural circuit disruption, so the reconstruction of effective motor circuits is a promising treatment approach. Based on its anatomical structure and function, the SMA is thought to compensate for motor dysfunction after focal brain injury at the cortical level. Our well-designed randomized controlled trial will allow us to analyze the clinical efficacy of this novel

Hebbian theory-based neuromodulation strategy regarding promoting the connection between the cortex and peripheral limb. The results may have significance for the development and implementation of effective neurorehabilitation treatments.

Clinical Trial Registration: [www.ClinicalTrials.gov], identifier [ChiCTR2000039949].

Keywords: stroke, rehabilitation, plasticity, transcranial magnetic stimulation (TMS), primary motor cortex (M1), supplementary motor area (SMA)

BACKGROUND

The 2013 National Epidemiological Survey of Stroke (NESS) in China reported a large and increasing burden caused by stroke, with approximately 11 million prevalent cases of stroke, 2.4 million new-onset cases of stroke, and 1.1 million stroke-related deaths in China annually, which match the long-term trends (Wu et al., 2019). Upper-extremity hemiplegia after stroke remains a clinical challenge, with only 20% of patients currently recovering normal hand function (Kwakkel et al., 2003). Common rehabilitation options to improve arm motor function include physical fitness therapy, task-oriented practice, constraint-induced movement therapy, and robot-assisted therapy. However, the clinical outcomes tend to be modest, and several disabilities remain unresolved and need further research.

In the search for improved stroke treatments, scientists have been trying to identify the link between motor function recovery after stroke and cortical reorganization, mostly focusing on plastic changes in the sensory cortex (S1), primary motor cortex (M1), supplementary motor area (SMA), premotor cortex (PMC), and cerebellum (Qing and Li, 2015). The PMC and SMA, which contribute fibers to the corticospinal tract, are major cortical regions of voluntary action plan formation and initiation (Calautti et al., 2007). They are believed to play a role in the temporal control of movement and are critical in motor function recovery in stroke patients (Kantak et al., 2012). The SMA has been reported to be a key brain area for motor function recovery after left subcortical stroke (Wan-Wa et al., 2013). As a part of the internal capsule, about 10% of the corticospinal tract fibers arise from the SMA and terminate in the spinal cord (Baran et al., 2016). The motor neurons innervating the hand muscles are mostly located at the lower cervical segments (C7–T1). A retrograde tracer study by Dum and Strick (2002) showed that corticospinal efferents from the SMA in macaques largely project to these segments. In chronic stroke patients, the overlap index of the SMA is positively associated with the Motor Status Scale (MSS) forearm-specific score (Wan-Wa et al., 2013). Schulz et al. (2017) found that the residual motor function output of chronic stroke patients depends on the degree of disruption to the corticospinal tract and fibers connecting M1 and the ventral premotor cortex. Anne et al. (2011) reported that the positive coupling of the SMA and PMC with the ipsilesional M1 decreased during the acute phase of stroke. The coupling parameters between these regions increased with increased motor recovery, which can be used to predict improved outcomes (Anne et al., 2011). Therefore, rebuilding the descending motor tract from the SMA to the peripheral limb is a potential approach for arm motor function restoration after stroke.

Recently, it has become popular to use non-invasive neuromodulation combined with standard upper-limb rehabilitation for functional restoration in patients with post-stroke hemiplegia (Edwardson et al., 2013). Repetitive transcranial magnetic stimulation (rTMS) is a non-invasive treatment that rarely induces pain caused by skin impedance and has the advantage of non-invasively stimulating deep tissue areas. However, studies on the effects of TMS in stroke have mostly focused on the activation of single targets to promote focal neuron function recovery. In the 2014–2018 evidence-based guidelines on the therapeutic use of rTMS by International Federation of Clinical Neurophysiology (IFCN), several sham-controlled studies of ipsilesional high-frequency rTMS or intermittent theta-burst stimulation (iTBS) in post-stroke patients led to improvements (from marginal to significant) in balance or paretic hand motor function (Lefaucheur et al., 2020). Unfortunately, a key study on hand motor recovery during the chronic stroke stage found that 1-Hz rTMS over the contralesional M1 was not superior to sham rTMS (Harvey et al., 2018).

Our objective is to effectively restore neural circuits after stroke. Neural circuit reconstruction is similar to sensorimotor learning based on the Hebbian principles of neural plasticity. Donald Hebb Huibert et al. (2019) hypothesized that, if the activity in a presynaptic neuron is repeatedly temporally correlated with postsynaptic neuron activation, a long-lasting alteration in synaptic structure will ensue. It is highly likely that activation of a presynaptic neuron excites the postsynaptic neuron ("neurons that fire together wire together"). The Hebbian theory is widely utilized in artificial neural networks. We think that neural circuit reconstruction will be possible based on Hebbian synaptic plasticity.

Paired associative stimulation (PAS), based on Hebbian theory with a specific time interval, is an important means by which to reconstruct neural circuits. Traditionally, PAS

Abbreviations: SMA, Supplementary motor area; FMA-UE, Fugl-Meyer Assessment for Upper Extremity; WMFT, Wolf Motor Function Test; TMS, Transcranial magnetic stimulation; PAS, Paired associative stimulation; HTS, Hebbian-type stimulation; FIM, Functional Independence Measure; fNIRS, Functional near-infrared spectroscopy; M1, Primary motor cortex; NESS, National Epidemiological Survey of Stroke; PMC, Premotor cortex; rTMS, Repetitive transcranial magnetic stimulation; iTBS, Intermittent theta-burst stimulation; PMS, Peripheral magnetic stimulation; MMSE, Mini Mental State Examination; ICF, Classification of Functioning, Disability, and Health; SPIRIT, Standard Protocol Items: Recommendations for Interventional Trials; AEs, Adverse events; GCP, Good Clinical Practice of Pharmaceutical Products; IFCN, International Federation of Clinical Neurophysiology.

was performed by delivering a peripheral afferent volley using electronic stimulation over the radial or median nerve prior to TMS over M1. Peripheral magnetic stimulation (PMS) can also be applied, for example to the muscles, spinal nerve roots, and peripheral nerve fibers. PMS can directly recruit 1A afferent fibers or indirectly provide strong proprioceptive inflow related to muscle contraction or the change in a joint angle, while peripheral electronic stimulation generates a significant cutaneous inflow in the afferent fibers of the lemniscus and spino-thalamic tract. Unlike peripheral electronic stimulation, PMS is painless and well tolerated (Beaulieu and Schneider, 2015). A study of 16 healthy participants revealed that PMS could modulate cortical excitability (Sato et al., 2016). Krewer et al. (2014) investigated the effect of repetitive PMS on upper-limb muscular spasm caused by stroke or brain trauma. They reported short-term effects on spasticity for wrist flexors and long-term effects on spasticity for elbow extensors (Krewer et al., 2014). Another group investigated the effect of integrated PMS and TMS in healthy participants. They found that PAS can upregulate corticospinal excitability and downregulate intracortical inhibition (Sato et al., 2016).

We aim to use PAS to rebuild a neural circuit involving SMA → internal capsule → periphery in order to restore motor function. We will perform timely coupled stimulation of presynaptic and postsynaptic neurons to restore the motor circuits instead of simply upregulating excitation in the lesion area. If HTS can be induced non-invasively by magnetically stimulating the peripheral nerve after magnetically stimulating the SMA in the human brain, this method may provide a neuromodulation approach to rebuild the motor network after stroke. We hypothesize that PMS of the peripheral nerve tens of milliseconds after TMS of the SMA related to the functioning of the upper extremities will induce spike timing-dependent plasticity. This will increase targeted cortical excitability and help to reconstruct sensorimotor pathway conduction to facilitate arm motor function recovery.

OBJECTIVES

The main objectives of this clinical trial are to (1) investigate whether HTS can promote arm motor function recovery in chronic stroke and (2) explore the underlying mechanisms in the brain after HTS using functional near-infrared spectroscopy (fNIRS).

TRIAL DESIGN

This protocol has been designed according to the Standard Protocol Items: Recommendations for Interventional Trials (SPIRIT) guidelines. It is registered with the Chinese Clinical Trial Registry. Based on a 1:1 ratio, 90 participants will be randomly assigned to the HTS and sham groups. The prospective, single-center, double-blind, randomized, sham-controlled clinical trial will study the therapeutic effects of HTS vs. sham intervention. Each patient will undergo 1 session of real/sham HTS per day, always followed by general rehabilitation therapy, 5 days per week, with a total of 25 sessions. Three assessments will be performed in both groups: at baseline, immediately after the 5-week treatment, and at a 3-month follow-up. The effects will be measured using a variety of rating scales. The primary outcome will be the Wolf Motor Function Test (WMFT). The secondary outcomes will be the Fugl-Meyer Assessment for Upper Extremity (FMA-UE), Functional Independence Measure (FIM), and fNIRS parameters. To strengthen treatment compliance and minimize dropout, a doctor will contact the participants regularly.

RECRUITMENT AND SAMPLE SELECTION

Participants will be recruited from Shanghai Yangzhi Rehabilitation Hospital affiliated with Tongji University. Recruitment began on 11 Nov 2020 and will continue until the required sample size has been achieved. The volunteers will be carefully screened based on the inclusion and exclusion criteria. All participants, who will be given verbal and written details on the study purpose and process, will sign a written informed consent form.

STROKE DIAGNOSIS

Stroke will be diagnosed based on the World Health Organization definition in 1970, "stroke is rapidly developing clinical signs of focal (or global) disturbance of cerebral function, with symptoms lasting 24 h or longer, or leading to death, with no apparent cause other than of vascular origin" (Graeme, 2017).

ELIGIBILITY CRITERIA

The inclusion criteria are as follows:

(1) Having a first unilateral supratentorial, ischemic stroke, and having had a stroke in 4–12 month;

(2) Upper extremity dysfunction, with FMA-UE motor score of 30–60 out of 66 (Fugl-Meyer et al., 1975);

(3) Aged 18–80 years, regardless of sex;

(4) Mini Mental State Examination (MMSE) score > 24;

(5) Written informed consent;

(6) Right handedness.

The exclusion criteria (based on the TMS safety criteria proposed by Wassermann, 1998) are as follows:

(1) Metal implant device in the head, neck, or stimulation area;

(2) Medical implant device (cardiac pacemaker or cochlea implant);

(3) Pregnancy;

(4) Current or history of epilepsy;

(5) Current or history of medications known to affect central nervous system excitability;

(6) Intracranial hypertension;

(7) Unstable fractures or joint contracture.

(8) Taking drugs that may increase the risk of epilepsy or reduce cortical excitability.

RANDOMIZATION

The participants will be randomly assigned (using computer-generated random numbers) to one of the two groups in a 1:1 ratio after baseline assessment. A research assistant (who will not be involved in eligibility screening, the intervention, outcome assessment, or data analysis) will independently conduct the randomization process following allocation concealment. The allocation sequence will be concealed from the therapists, outcome assessors, data analysts, participants, and participants' relatives.

SAMPLE SIZE ESTIMATION

The calculation of the sample size was based on data from previous research and our per experiment (Lai et al., 2015). As the study involves two groups, the following sample size calculation for a two-sample mean comparison was used:

$$n_c = \frac{\left(Z_{1-\alpha} + Z_{1-\beta}\right)^2 \sigma^2 \left(1 + \frac{1}{K}\right)}{(\mu_T - \mu_C - \triangle)^2}$$

where, $Z_{1-\alpha}$ = 1.960, $Z_{1-\beta}$ = 0.842, μ_T =6.6 (predicted mean in HTS group); μ_C =2.3 (predicted mean in sham group), σ = 2.0 (standard deviation), K = 1 (ratio of participants in the HTS and sham groups), Δ = 3 (optimality bounds), α = 0.025 (2.5% one-tailed significance level), and β = 0.20 (80% power). The calculated required sample size was 37 participants per group. Assuming a 20% dropout rate, 45 participants per group (a total of 90 participants) need to be recruited.

INTERVENTION GROUPS

The HTS intervention group will undergo HTS with conventional rehabilitation. The control group will undergo sham HTS with conventional rehabilitation.

Blinding

The allocation sequence will be placed in sealed opaque envelopes kept in a location with restricted access. The envelopes will then be delivered to the researcher responsible for implementing the intervention the day prior to the beginning of the intervention. This process will be completed independently and the allocation sequence will be concealed from the therapists, outcome assessors, data analysts, participants, and participants' relatives. The patients and their relatives will also be blinded to group allocation. Each participant will be identified with a particular number (rather than their name), which will be used by the outcome assessor. A blinded independent data analyst (who will not be involved in recruitment, eligibility screening, intervention delivery, or outcome assessment) will conduct the data analysis.

To ensure blinding, we will follow the sham stimulation schemes used in related studies the control group. For the sham stimulation, we will use sham coils, which are similar to real coils in terms of appearance, sound, and feeling (Ruohonen et al., 2000). The sham stimulation will be performed with the same HTS procedure (without stimulation) at the same location. The parameters on the equipment display will be identical in the HTS and sham groups.

INTERVENTION

Supplementary Motor Area–Erb's Point Conduction Time

The conduction time from the SMA to Erb's point is defined as the latency between the motor evoked potential of the first dorsal interosseous muscles induced by SMA stimulation and the compound motor action potential evoked by Erb's point stimulation. The conduction time will be used as the inter-stimulus interval in PAS.

Patient Posture

The patients will be seated in a comfortable armchair, and will be asked to relax with their forearms placed on the armrest in a comfortable position. They will be awake during the whole intervention.

Transcranial Magnetic Stimulation Parameters

TMS will be applied over the ipsilesional SMA using a figure-of-eight coil with 70-mm wing diameter and a Magstim Rapid 2 stimulator (Magstim Co., Ltd., Whitland, United Kingdom) with a stimulus intensity of 120% of the resting motor threshold (RMT). The RMT is defined as the lowest stimulus intensity (with $\geq$ 50 μV peak-to-valley amplitude) that is required to induce a motor evoked potential in at least 5 out of 10 stimulations. A neuronavigation system (Brainsight TMS, Rogue Research Inc., Montréal, Canada) will be used to precisely position the coil over the SMA sites, with the anatomical references being obtained from on individual T1-weighted magnetic resonance images. The SMA is located at the posterior part of the superior frontal gyrus and is bordered inferolaterally by the superior frontal sulcus and posteriorly by the precentral sulcus (Brodmann area 6).

Peripheral Magnetic Stimulation Parameters

PMS will be applied over Erb's point on the side with hemiparesis, with the forearms placed on a stable armrest in a neutral posture. The stimulation will be delivered by a 9-cm-diameter round-shaped coil. The patient's neck will be flexed to the opposite side, about 20–30 degrees. The coil's handle will be placed parallel to the brachial plexus. The intensity will be adjusted to induce a just-visible contraction of the abductor digiti minimi muscle (Evelyne et al., 2007).

Hebbian-Type Stimulation/Paired Associative Stimulation Parameters

The PMS pulse will be delivered prior to the TMS pulse, with an inter-stimulus interval equal to the SMA–Erb's point

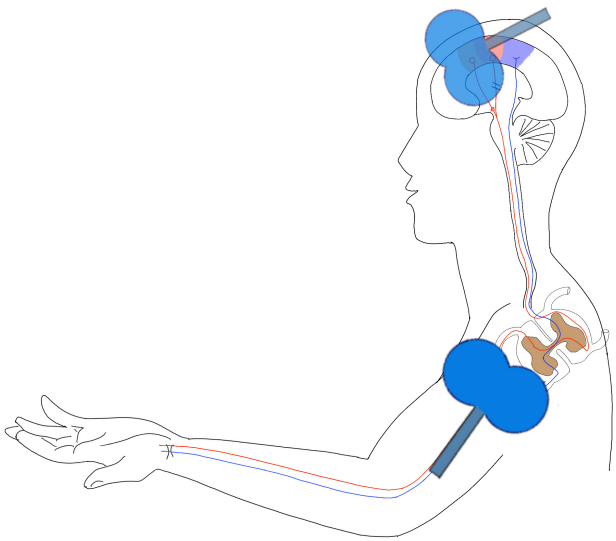

FIGURE 1 | Hebbian-type stimulation (HTS). This figure is a schema chart of the intervention model of the study. In the figure, the purple area on the head is the primary sensory area, the red area is the primary motor cortex, and the position of the coil is the SMA area. In this study, the joint stimulation of the central and peripheral was used to reconstruct the pathway from the SMA area to the peripheral nerve.

conduction time, which will be determined in advance (defined as the latency between the motor evoked potential of the first dorsal interosseous muscles induced by SMA stimulation and the compound motor action potential evoked by Erb's point stimulation). Stimuli will be delivered at 0.2 Hz, with 100 pairs, lasting for approximately 8.3 min (**Figure 1**).

Intervention Stimulation

The intervention will be conducted once a day, 5 days per week, for 25 sessions in total.

Sham Stimulation

For the sham stimulation, we will place the sham coils in the same position as in SMA TCM and PMS. The strength and frequency of the sham coil clicking noise will be similar to the real clicking noise (but with no magnetic stimulation).

Basic Stroke Management

Each participant in both groups will receive basic stroke management, including (1) assessments at the level of body function/structure, activities and participation and environmental Factors described in the International Classification of Functioning, Disability, and Health (ICF) (Svestková, 2008), (2) rehabilitation services (delivered by a multidisciplinary team of neurologists, rehabilitation physicians, rehabilitation nurses, occupational therapists, physical therapists, and speech and language therapists) based on the recommendations of clinical guidelines for patients with stroke (Winstein et al., 2016), and (3) medications(e.g., antihypertensive drugs, anti-platelet medicine, hypoglycemia agents, anti-spasm drugs etc.).

ASSESSMENTS

The clinical assessments will be performed at baseline (on the day of enrollment), immediately after the 5-week HTS/sham intervention, and at the 3-month follow-up after the intervention. After recruitment and eligibility screening, the following data will be collected: sociodemographic data (date of birth, gender, laterality, marital status, and occupational status), neuroimaging results, disease and current episode duration, blood pressure, comorbidities (psychiatric, addiction, and somatic diseases), medications, and degree of prior resistance to other treatments. These variables will be evaluated at baseline, immediately after the 5-week HTS/sham intervention, and at the 3-month follow-up (along with WMFT, FMA-UE, FIM, and fNIRS) (**Table 1**).

ADVERSE EVENTS AND SAFETY CONSIDERATIONS

Data on all potential AEs will be obtained from the participants and recorded in an observation table by the researchers (including time and date of occurrence, severity, treatment parameters, and potential causal relationship with the intervention). Monitoring of AEs will be carried out by the treating physical therapists. The principal researcher (MEAF) and data security management members will immediately be informed about severe AEs. AEs might include transient upper limb weakness, muscle soreness in the stimulation area, headache, increased muscle tone in the upper extremities, and hearing loss (caused by the coil noise during stimulation). We will give the patients earplugs to prevent hearing impairment during stimulation, and when the treatment is over, we will conduct a hearing assessment for all patients who report aural fullness, hearing loss, or tinnitus. The most serious acute AEs of TMS is epileptic seizure. Patients will be carefully asked if they have a disease that may cause epilepsy or are taking drugs that may increase the risk of epilepsy or reduce cortical excitability, and those who do will be excluded prior to randomization. If epileptic seizure occurs, the stimulation will be stopped and acute treatment will immediately be provided (Rossi et al., 2021).

MAXIMIZING TREATMENT COMPLIANCE AND MINIMIZING DROPOUT RATE

To strengthen treatment compliance and minimize dropout, a doctor will contact the participants regularly by phone to confirm the appointments, assess the effect of the treatment, and discuss the subsequent treatment and any issues that may interfere with compliance.

TABLE 1 | Study timeline.

	Enrolment	Baseline assessment	Intervention phase		Post-treatment assessment	Follow-up assessment
Time point	$-T_{1w}$	T_0	T_0	T_{5w}	T_{5w}	$T_{3months}$
Enrolment						
Eligibility screening	×					
Informed consent	×					
Allocation	×					
Interventions						
Hebbian-type stimulation (HTS)			——	——		
Sham stimulation			——	——		
Primary outcome						
Wolf Motor Function Test (WMFT)		×			×	×
Secondary outcomes						
Fugl-Meyer Assessment (FMA)		×			×	×
Functional Independence Measure (FAM)		×			×	×
Functional near-infrared spectroscopy (fNIRS) parameters		×			×	

Primary Outcomes

WMFT is highly recommended to assess the motor ability of patients with moderate to severe upper extremity motor deficits in research and clinical settings (Wolf et al., 1989). Its test-retest and inter-rater reliability and internal consistency range from 0.88 to 0.98, with most of the values being close to 0.95 (Morris et al., 2001). It will be used to assess upper limb movement ability, encompassing 17 upper-extremity motor tasks that involve starting position and verbal instructions (Wolf et al., 2001). The Functional Ability Scale score for each task ranges from 0 to 5. It is an effective and sensitive method to assess the upper extremity functional ability of patients with moderate to severe impairments after stroke (Hodics et al., 2012).

Secondary Outcomes

We will use fNIRS to assess the M1, S1, PMC, and SMA activities during six cycles of 15 s of hand grasping and 45 s of rest while sitting on a reclining chair. Each participant will be assessed at three time points (at baseline, immediately after the 5-week treatment, and at the 3-month follow-up). fNIRS parameters will be assessed and correlations with the clinical outcomes will be assessed. Other secondary outcomes will include activities of daily living, which will be determined using the FIM, and the motor section of FMA-UE will also be used to estimate upper limb movement ability (based on normal reflex activity and volitional movement of the upper extremities, along with the wrist, hand, coordination/speed, sensation, and passive joint motion domains). These stroke-associated measures will be assessed in addition to the primary outcome.

Statistical Analysis

Statistical analysis will be performed using SPSS 22.0 (SPSS Inc., Chicago, IL, United States). Database management and statistical analysis will be performed by an independent researcher, who will be blinded to group allocation. Monitoring of AEs will be carried out by the treating physical therapists. The primary analysis, which will be a per-protocol analysis, will include the patients who underwent the treatment course and completed the 3-month follow-up.

Descriptive statistics will be used to describe the baseline characteristics of the participants in both groups. The normally distributed continuous data will be presented as mean ± standard deviation, and the non-normally distributed continuous data will be presented as median (maximum and minimum). The Shapiro–Wilk test will be used to evaluate data normality. Homogeneity of variance will be assessed by Levene's test. For the normally distributed continuous data (including WMFT, UE-FMA, and FIM), paired *t*-tests will be used to compare between baseline and postintervention in each group. Additionally, unpaired *t*-tests will be used to assess the differences in the baseline characteristics and the primary and secondary outcomes between the HTS and sham groups. For the non-normally distributed continuous data, Wilcoxon tests will be used. The one-tailed significance level (α) for statistical hypothesis testing will be set at $P < 0.025$ (**Figure 2**).

DISCUSSION

Limb motor function is controlled by neural networks in several brain regions, including the default mode network and the sensory and motor networks. The motor network includes M1, pyramidal system, supplementary motor cortex (SMA)/PMC, parietal temporal cortex, basal ganglia, and cerebellum. Sensory information is integrated through the parietal temporal cortex and then connected to the brain motor neural circuits *via* a special network. Both human and animal studies have shown that the brain areas surrounding stroke lesions can promote motor function recovery (Payne and Lomber, 2001). The non-injured areas around the lateral hemisphere after stroke have a certain degree of plasticity, likely due to the reorganization of sensorimotor networks.

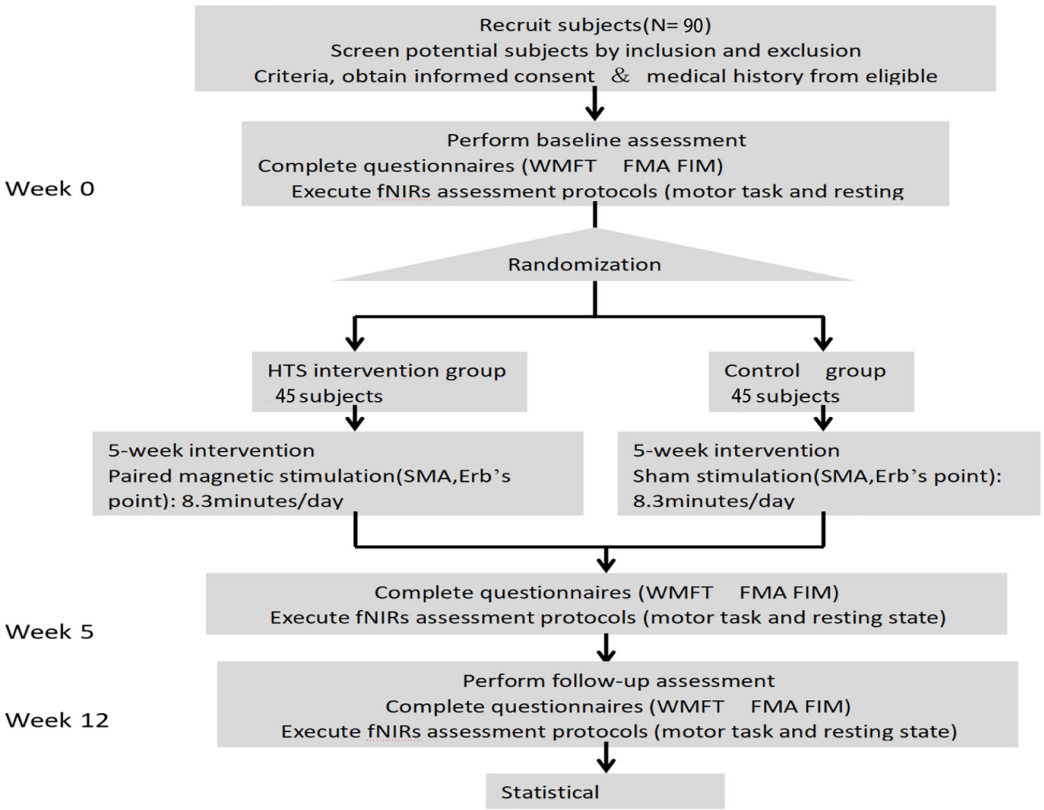

FIGURE 2 | Overview of study design.

This plasticity may depend on the functional overlapping regions in the sensorimotor network, which may compensate for the lost function after stroke. A study suggested a surrogate role for the SMA after M1 injury in monkeys. Before M1 injury, SMA neurons exhibited activity during learning (push-button task), which disappeared when performing the task after the task had been learnt. However, M1 injury led to SMA activity being restored when the task was performed again (Williams et al., 2006). This phenomenon is consistent with the ipsilesional SMA activation in stroke patients during rehabilitation (Hara, 2015). Zhang et al. (2016) found that compare to the health control functional connections between M1 and the ipsilesional parietal cortex, frontal gyrus, and SMA were increased in chronic stroke patients, while functional connections between bilateral M1 were decreased in stroke. Inman et al. (2012) found that the connections between the superior parietal cortex and M1, and the superior parietal cortex and the SMA, were significantly reduced in chronic stroke. The study of Jingchun et al. (2020) used fine map of fMRI showed that he CST originated from SMA are significantly related with motor outcomes in chronic stroke patients. The SMA/PMC is the key area for motor plan formation and movement initiation. The SMA/PMC and the prefrontal cortex form the brain's cognitive network, which predicts the movements needed for tasks to be performed and receives information from the brain's sensory integration network about the body's spatial location, generating a primary task plan. Our study aims to restore the motor circuits, based on the ideas of Donald Hebb. He hypothesized that when the axon of cell A repeatedly or continuously participates in stimulating cell B, the synaptic connection between cell A and cell B will be strengthened. On this basis, Muming Poo found that long-term potentiation or depression can be produced by exciting the postsynaptic membrane 20 ms after or before exciting the presynaptic membrane, respectively, which is known as spike timing-dependent plasticity. The difference between spike timing-dependent plasticity and Hebbian theory is that the former emphasizes the role of the sequence of presynaptic and postsynaptic membrane excitation in synaptic remodeling (Zuzanna et al., 2019).

There is a lack of guidelines on PAS HTS for stroke rehabilitation in the subacute and chronic phases. Our planned study may complement the existing stroke rehabilitation guidelines, add to the experience in this area, and provide a basis for treatment application.

CONFIDENTIALITY

The participants' personal data will be kept confidential. All human sample data (functional assessment results and functional imaging examinations) will be identified by study number rather than name. Identifiable information will not be disclosed to

members outside the study group unless permission is obtained from the subject. All study members and study sponsors were required to keep the identity of the subjects confidential. The subjects' files will be kept in a locked filing cabinet for researchers' reference only.

TRIAL STATUS

Protocol version number and date: version 1, dated February 21, 2021.
Date recruitment began: December 1, 2020.
Date when recruitment will be completed: March 3, 2022.

DATA MANAGEMENT

Two investigators will run the database which has been established in the clinical research database of Shanghai YangZhi Rehabilitation Hospital (Shanghai Sunshine Rehabilitation Center). One of them will enter data into the database, and the other researcher will be in charge of checking data accuracy. During the collection process, data will be stored in a password-protected online database accessible only to the researcher. Once the collections are completed, data will be kept in a password-protected file on the researcher's personal computer.

COORDINATING CENTER, STEERING COMMITTEE, ENDPOINT ADJUDICATION COMMITTEE

No coordinating center, steering committee, endpoint adjudication committee were constituted. The investigators will hold a monthly meeting to find out any final difficulties or mistakes. The researchers met with the intervention group every 4 months to identify and correct any final difficulties in the recruitment and follow-up process, data management, monitoring, and statistical analysis of results. They are responsible for assessing the rate of progress to ensure that the trial is carried out in accordance with the research plan. The main researchers supervised the correct development of the experiment. If any unexpected adverse reactions occur, an audit process will be conducted to identify and correct the side effects. The three therapist candidates in the study will be in charge of the evaluation. They are all experienced therapists. And all the measurements will be duplicated at least 2 times to promote data quality. The main investigators have completed the online training courses of Good Clinical Practice of Pharmaceutical Products (GCP) and got the GCP certifications.

DATA AVAILABILITY STATEMENT

The original contributions presented in the study are included in the article/**Supplementary Material**, further inquiries can be directed to the corresponding author/s.

ETHICS STATEMENT

The studies involving human participants were reviewed and approved by the Ethics Review Board of Shanghai Yangzhi Rehabilitation Hospital Affiliated to Tongji University. The patients/participants provided their written informed consent to participate in this study. Written informed consent was obtained from the individual(s) for the publication of any potentially identifiable images or data included in this article.

AUTHOR CONTRIBUTIONS

RX, JZ, J-BC, and F-QS were doctoral fellows in the project, contributed to the study design, carry out recruitment and screening of participants, set up the intervention and collect baseline data, and perform statistical analysis and interpretation of results. G-YZ and X-XX were senior researchers and carry out the intervention. YW was the occupational therapist. JL and L-YC were the physical therapists, designed the process evaluation, and performed the evaluation of cognitive and hand function. X-YH and D-SX were the chief investigators and supervisors of the project, designed the study, partake in analyzing, and interpreting the results. All authors helped draft the manuscript and consent to publication, and read and approved the final manuscript.

FUNDING

This study was supported by the research fund of Shanghai YangZhi Rehabilitation Hospital (Shanghai Sunshine Rehabilitation Center) (Project No. YZ2020-017). Additional support was provided by the National Key R&D Program of China (Grant No. 2020YFC2004202).

SUPPLEMENTARY MATERIAL

The Supplementary Material for this article can be found online at: https://www.frontiersin.org/articles/10.3389/fncir.2021.789095/full#supplementary-material

REFERENCES

Anne, K. R., Eickhoff, S. B., Wang, L. E., Fink, G. R., and Grefkes, C. (2011). Causal modeling of cortical activity from the acute to the chronic stage after stroke. *Neuroimage* 55, 1147–1158. doi: 10.1016/j.neuroimage.2011.01.014

Baran, B., Yagmurlu, K., Middlebrooks, E. H., Karadag, A., Ovalioglu, T. C., Jagadeesan, B., et al. (2016). Microsurgical and tractographic anatomy of the supplementary motor area complex in humans. *World Neurosurg.* 95, 99–107. doi: 10.1016/j.wneu.2016.07.072

Beaulieu, L.-D., and Schneider, C. (2015). Repetitive peripheral magnetic stimulation to reduce pain or improve sensorimotor impairments: a literature review on parameters of application and afferents recruitment. *Neurophysiol. Clin.* 45, 223–237. doi: 10.1016/j.neucli.2015.08.002

Calautti, C., Naccarato, M., Jones, P. S., Sharma, N., Day, D. D., Carpenter, A. T., et al. (2007). The relationship between motor deficit and hemisphere activation balance after stroke: a 3T fMRI study. *Neuroimage* 34, 322–331. doi: 10.1016/j.neuroimage.2006.08.026

Dum, R. P., and Strick, P. L. (2002). Motor areas in the frontal lobe of the primate. *Physiol. Behav.* 77, 677–682.

Edwardson, M. A., Lucas, T. H., Carey, J. R., and Fetz, E. E. (2013). New modalities of brain stimulation for stroke rehabilitation. *Exp. Brain Res.* 224, 335–358. doi: 10.1007/s00221-012-3315-1

Evelyne, C. L., Gerdelat-Mas, A., Marque, P., Loubinoux, I., and Simonetta-Moreau, M. (2007). Induction of cortical plastic changes in wrist muscles by paired associative stimulation in healthy subjects and post-stroke patients. *Exp. Brain Res.* 180, 113–122. doi: 10.1007/s00221-006-0844-5

Fugl-Meyer, A. R., Jääskö, L., Leyman, I., Olsson, S., and Steglind, S. (1975). . The post-stroke hemiplegic patient. 1. a method for evaluation of physical performance. *Scand. J. Rehabil. Med.* 7, 13–31.

Graeme, J. H. (2017). Stroke. *Lancet* 389, 641–654.

Hara, Y. (2015). Brain plasticity and rehabilitation in stroke patients. *J. Nippon Med. Sch.* 82, 4–13.

Harvey, R. L., Edwards, D., Dunning, K., Fregni, F., Stein, J., Laine, J., et al. (2018). Randomized shamcontrolled trial of navigated repetitive transcranial magnetic stimulation for motor recovery in stroke. *Stroke* 49, 2138–2146.

Hodics, T. M., Nakatsuka, K., Upreti, B., Alex, A., Smith, P. S., and Pezzullo, J. C. (2012). Wolf motor function test for characterizing moderate to severe hemiparesis in stroke patients. *Arch. Phys. Med. Rehabil.* 93, 1963–1967. doi: 10.1016/j.apmr.2012.05.002

Huibert, D. M., Verhoog, M. B., and Goriounova, N. A. (2019). Synaptic plasticity in human cortical circuits: cellular mechanisms of learning and memory in the human brain? *Curr. Opin. Neurobiol.* 54, 186–193. doi: 10.1016/j.conb.2018.06.013

Inman, C. S., James, G. A., and Hamann, S. (2012). Ahered resting-state effective connectivity of fronto-parietal motor control systems on the primary motor network following stroke[J]. *Neuroimage* 59, 227–237. doi: 10.1016/j.neuroimage.2011.07.083

Jingchun, L., Wang, C., Qin, W., Ding, H., Guo, J., Han, T., et al. (2020). Corticospinal fibers with different origins impact motor outcome and brain after subcortical stroke. *Stroke* 51, 2170–2178. doi: 10.1161/STROKEAHA.120.029508

Kantak, S. S., Stinear, J. W., Buch, E. R., and Cohen, L. G. (2012). Rewiring the brain: potential role of the premotor cortex in motor control, learning, and recovery of function following brain injury. *Neurorehabil Neural Repair* 26, 282–292. doi: 10.1177/1545968311420845

Krewer, C., Hartl, S., Müller, F., and Koenig, E. (2014). Effects of repetitive peripheral magnetic stimulation on upper-limb spasticity and impairment in patients with spastic hemiparesis: a randomized, double-blind, sham-controlled study. *Arch. Phys. Med. Rehabil.* 95, 1039–1047. doi: 10.1016/j.apmr.2014.02.003

Kwakkel, G., Kollen, B. J., van der Grond, J., and Prevo, A. J. (2003). Probability of regaining dexterity in the flaccid upper limb: impact of severity of paresis and time since onset in acute stroke. *Stroke* 34, 2181–2186. doi: 10.1161/01.STR.0000087172.16305.CD

Lai, C. J., Wang, C. P., Tsai, P. Y., Chan, R. C., Lin, S. H., Lin, F. G., et al. (2015). Corticospinal integrity and motor impairment predict outcomes after excitatory repetitive transcranial magnetic stimulation: a preliminary study. *Arch. Phys. Med. Rehabil.* 96, 69–75. doi: 10.1016/j.apmr.2014.08.014

Lefaucheur, J. P., Aleman, A., Baeken, C., and Benninger, D. H. (2020). Evidence-based guidelines on the therapeutic use of repetitive transcranial magnetic stimulation (rTMS): an update (2014-2018). *Clin. Neurophysiol.* 131, 474–528.

Morris, D. M., Uswatte, G., Crago, J. E., Cook, E. W. III, and Taub, E. (2001). The reliability of the wolf motor function test for assessing upper extremity function after stroke. *Arch. Phys. Med. Rehabil.* 82, 750–755. doi: 10.1053/apmr.2001.23183

Payne, B. R., and Lomber, S. G. (2001). Reconstructing functional systems after lesions of cerebral cortex. *Nat. Rev. Neurosci.* 2, 911–919. doi: 10.1038/35104085

Qing, T., and Li, G. (2015). Modulation of interhemispheric activation balance in motor-related areas of stroke patients with motor recovery: systematic review and meta-analysis of fMRI studies. *Neurosci. Biobehav. Rev.* 57, 392–400. doi: 10.1016/j.neubiorev.2015.09.003

Rossi, S., Antal, A., Bestmann, S., Bikson, M., and Brewer, C. (2021). Safety and recommendations for TMS use in healthy subjects and patient populations, with updates on training, ethical and regulatory issues: Expert Guidelines. *Clin. Neurophysiol.* 132, 269–306. doi: 10.1016/j.clinph.2020.10.003

Ruohonen, J., Ollikainen, M., Nikouline, V., Virtanen, J., and Ilmoniemi, R. J. (2000). Coil design for real and sham transcranial magnetic stimulation. *IEEE Trans. Biomed. Eng.* 47, 145–148. doi: 10.1109/10.821731

Sato, A., Liu, X., Iwahashi, M., and Iramina, K. (2016). Modulation of motor cortex excitability by peripheral magnetic stimulation of different stimulus sites and frequencies. *Conf. Proc. IEEE Eng. Med. Biol. Soc.* 2016, 6413–6416. doi: 10.1109/EMBC.2016.7592196

Schulz, R., Park, E., Lee, J., Chang, W. H., Lee, A., Kim, Y. H., et al. (2017). Interactions between the corticospinal tract and premotor-motor pathways for residual motor output after stroke. *Stroke* 48, 2805–2811. doi: 10.1161/STROKEAHA.117.016834

Svestková, O. (2008). International classification of functioning, disability and health of world health organization (ICF). *Prague Med. Rep.* 109, 268–274.

Wan-Wa, W., Chan, S. T., Tang, K. W., Meng, F., and Tong, K. Y. (2013). Neural correlates of motor impairment during motor imagery and motor execution in sub-cortical stroke. *Brain Inj.* 27, 651–663. doi: 10.3109/02699052.2013.771796

Wassermann, E. M. (1998). Risk and safety of repetitive transcranial magnetic stimulation: report and suggested guidelines from the international workshop on the safety of repetitivetranscranialmagnetic stimulation, june 5e7, 1996. *Electroencephalogr Clin. Neurophysiol.* 108, 1–16. doi: 10.1016/s0168-5597(97)00096-8

Williams, M., Tresilian, J. R., and Warm, J. P. (2006). *Motor Control and Learning.Encyclopedia of Cognitive Science*. Hoboken, NJ: John Wiley & Sons,Ltd, 65–88.

Winstein, C. J., Stein, J., Arena, R., and Bates, B. (2016). Guidelines for adult stroke rehabilitation and recovery: a guideline for healthcare professionals from the american heart association/american stroke association. *Stroke* 47, e98–e169.

Wolf, S. L., Catlin, P. A., Ellis, M., Archer, A. L., Morgan, B., and Piacentino, A. (2001). Assessing wolf motor function test as outcome measure for research in patients after stroke. *Stroke* 32, 1635–1639. doi: 10.1161/01.str.32.7.1635

Wolf, S. L., Lecraw, D. E., Barton, L. A., and Jann, B. B. (1989). Forced use of hemiplegic upper extremities to reverse the effect of learned nonuse among chronic stroke and head-injured patients. *Exp. Neurol.* 104, 125–132. doi: 10.1016/s0014-4886(89)80005-6

Wu, S., Wu, B., Liu, M., Chen, Z., Wang, W., Anderson, C. S., et al. (2019). Stroke in China: advances and challenges in epidemiology, prevention, and management. *Lancet Neurol.* 18, 394–405. doi: 10.1016/S1474-4422(18)30500-3

Zhang, Y., Liu, H., and Wang, L. (2016). Relationship between functional connectivity and motor function assessment in stroke patients with hemiplegia:a resting-state functional MRI study. *Neuroradiology* 58, 503–511. doi: 10.1007/s00234-016-1646-5

Zuzanna, B., Mierau, S. B., and Paulsen, O. (2019). Neuromodulation of spike-timing-dependent plasticity: past, present, and future. *Neuron* 103, 563—-581. doi: 10.1016/j.neuron.2019.05.041

Conflict of Interest: The authors declare that the research was conducted in the absence of any commercial or financial relationships that could be construed as a potential conflict of interest.

Publisher's Note: All claims expressed in this article are solely those of the authors and do not necessarily represent those of their affiliated organizations, or those of the publisher, the editors and the reviewers. Any product that may be evaluated in this article, or claim that may be made by its manufacturer, is not guaranteed or endorsed by the publisher.

frontiers | Frontiers in Human Neuroscience

TYPE Review
PUBLISHED 02 March 2023
DOI 10.3389/fnhum.2023.1125074

OPEN ACCESS

EDITED BY
Sandra Carvalho,
University of Aveiro, Portugal

REVIEWED BY
Randall Espinoza,
University of California, Los Angeles,
United States
Ki Sueng Choi,
Icahn School of Medicine at Mount Sinai,
United States

*CORRESPONDENCE
Shaquia L. Idlett-Ali
✉ shaquia.idlett-ali@cuanschutz.edu

SPECIALTY SECTION
This article was submitted to
Brain Imaging and Stimulation,
a section of the journal
Frontiers in Human Neuroscience

RECEIVED 26 December 2022
ACCEPTED 14 February 2023
PUBLISHED 02 March 2023

CITATION
Idlett-Ali SL, Salazar CA, Bell MS, Short EB and Rowland NC (2023) Neuromodulation for treatment-resistant depression: Functional network targets contributing to antidepressive outcomes.
Front. Hum. Neurosci. 17:1125074.
doi: 10.3389/fnhum.2023.1125074

Neuromodulation for treatment-resistant depression: Functional network targets contributing to antidepressive outcomes

Shaquia L. Idlett-Ali[1]*, Claudia A. Salazar[2], Marcus S. Bell[2], E. Baron Short[3] and Nathan C. Rowland[2]

[1]Department of Neurosurgery, University of Colorado Anschutz Medical Campus, Aurora, CO, United States, [2]Department of Neurosurgery, Medical University of South Carolina, Charleston, SC, United States, [3]Department of Psychiatry and Behavioral Sciences, Medical University of South Carolina, Charleston, SC, United States

Non-invasive brain stimulation is designed to target accessible brain regions that underlie many psychiatric disorders. One such method, transcranial magnetic stimulation (TMS), is commonly used in patients with treatment-resistant depression (TRD). However, for non-responders, the choice of an alternative therapy is unclear and often decided empirically without detailed knowledge of precise circuit dysfunction. This is also true of invasive therapies, such as deep brain stimulation (DBS), in which responses in TRD patients are linked to circuit activity that varies in each individual. If the functional networks affected by these approaches were better understood, a theoretical basis for selection of interventions could be developed to guide psychiatric treatment pathways. The mechanistic understanding of TMS is that it promotes long-term potentiation of cortical targets, such as dorsolateral prefrontal cortex (DLPFC), which are attenuated in depression. DLPFC is highly interconnected with other networks related to mood and cognition, thus TMS likely alters activity remote from DLPFC, such as in the central executive, salience and default mode networks. When deeper structures such as subcallosal cingulate cortex (SCC) are targeted using DBS for TRD, response efficacy has depended on proximity to white matter pathways that similarly engage emotion regulation and reward. Many have begun to question whether these networks, targeted by different modalities, overlap or are, in fact, the same. A major goal of current functional and structural imaging in patients with TRD is to elucidate neuromodulatory effects on the aforementioned networks so that treatment of intractable psychiatric conditions may become more predictable and targeted using the optimal technique with fewer iterations. Here, we describe several therapeutic approaches to TRD and review clinical studies of functional imaging and tractography that identify the diverse loci of modulation. We discuss differentiating factors associated with responders and non-responders to these stimulation modalities, with a focus on mechanisms of action for non-invasive and intracranial stimulation modalities. We advance the hypothesis that non-invasive and invasive neuromodulation approaches for TRD

are likely impacting shared networks and critical nodes important for alleviating symptoms associated with this disorder. We close by describing a therapeutic framework that leverages personalized connectome-guided target identification for a stepwise neuromodulation paradigm.

KEYWORDS

deep brain stimulation, epidural cortical stimulation, neuromodulation, transcranial magnetic stimulation (repetitive), salience network, treatment-resistant depression, electroconvulsive therapy

Introduction

Treatment-resistant depression (TRD) is defined as major depressive disorder (MDD) unresponsive to one or more conscripted treatments (Souery et al., 2006). Estimated failure rates of MDD treatment are as high as 10–30%, however, the type and number of treatments as well as the length of administration required for TRD diagnosis are inconsistently defined in the literature (Al-Harbi, 2012). Only 30% of TRD patients ever achieve remission using other means, and another 30% attempt suicide at least once in their lifetime (Bergfeld et al., 2018; Cole et al., 2022).

Measuring connectivity of brain networks for psychiatric disorders has become an increasingly used analytical technique, because it has the potential to illuminate neuromodulation targets for both non-invasive, e.g., TMS and invasive, e.g., DBS, approaches (Hollunder et al., 2022). This is especially critical since both modalities have considerable drawbacks. TMS for TRD requires up to 6 weeks of daily treatment sessions, and DBS may not show consistent efficacy in some patients until a year or more after implantation. Thus, an algorithm that helps clinicians identify and define TRD subtypes and suggests patient-specific treatments is needed.

Though many neural networks exhibit dysfunction in the setting of TRD, a close reading of the psychiatric literature consistently correlates default mode, salience, and central executive network dysfunction with TRD presentation and may suggest etiology (Hamilton et al., 2013). In contrast, a close reading of the neurosurgical literature for TRD highlights cortico-basal ganglia limbic circuits as well as cognitive control, reward and other networks that might be targeted based on specific symptom domains, including affect and attention (Williams et al., 2021). Compounding the problem of separate taxonomies in the literature is the fact that there is not enough crosstalk between the two disciplines, threatening to extend the semantic confusion surrounding these topics. Fortunately, the overall impression from examining these two bodies of literature is that the structures and networks described are very similar, if not the same, being targeted using these different approaches. As an example, functional connectivity studies show that DLPFC and subcallosal cingulate cortex (SCC), the two most common targets of TMS and DBS, respectively, are co-activated during effective treatment of TRD patients (Anderson et al., 2016). The implication is that a convergence of network anatomy and connectivity relationships among various neuromodulation treatments for TRD are needed to highlight similarities between them and advance care of TRD patients in a meaningful way.

In this review, we discuss the evidence accumulated in favor of pursuing a neuromodulatory approach for TRD. Putative mechanisms for both TMS and DBS are reviewed as well as an alternative procedure, epidural cortical stimulation, that likely engages similar circuitry. We conclude with a synthesis of network topology and argue that this may form the basis for developing a stepwise interventional approach to TRD, increasing in invasiveness only when a less invasive approach fails. In summary, much more work is needed to define clinical outcomes associated with a network-centric approach to treating TRD, however, this paper lays the important groundwork for consolidating the concepts and terminology for future *trans*-disciplinary discourse and action.

Neurobiology of transcranial magnetic stimulation

TMS is a non-invasive modality that has been FDA-approved in the United States for the management of treatment-resistant depression, smoking cessation and obsessive compulsive disorder, and is being investigated for numerous other psychiatric disorders such as addiction, chronic pain, anxiety, panic, and post-traumatic stress disorder (Cohen et al., 2022). Delivery of therapy is accomplished using a pulsatile electromagnetic field induced in a coil held at the surface of the scalp that stimulates underlying cortex (Barker et al., 1985). Electrophysiological simulations and patch-clamp studies suggest TMS-induced action potentials occur at or near somata rather than the axon hillock, the axon itself, or dendrites (Pashut et al., 2011). Computational modeling has shown that fibers running parallel to the surface of the scalp are more likely to be stimulated compared to oblique fibers, and vertical fibers are most resistant to stimulation (Tofts, 1990). Somatic

Abbreviations: TMS, transcranial magnetic stimulation; TRD, treatment-resistant depression; DBS, deep brain stimulation; DLPFC, dorsal lateral prefrontal cortex; SCC, subcallosal cingulate cortex; MDD, major depression; BDNF, brain-derived neurotrophic factor; GABA, gamma-aminobutyric acid; NMDA, N-Nitrosodimethylamine; HRSD, Hamilton Rating Scale for Depression; iTBS, intermittent theta-burst stimulation; MADRS, Montgomery-Asberg Depression Scale; RCT, randomized control trial; DWI, diffusion weighted imaging; ACC, anterior cingulate cortex; CEN, central executive network; DMN, default mode network; SN, salience network; EpCS, epidural cortical stimulation; ECT, electroconvulsive therapy; sEEG, stereotactic electroencephalogram; MRI, magnetic resonance imaging; dACC, dorsal anterior cingulate cortex; pgCC, pregenual cingulate cortex; VC/VS, ventral capsule/ventral striatum; STN, subthalamic nucleus; ATN, anterior thalamic nucleus; GPi, globus pallidus internus; VMPFC, ventromedial prefrontal cortex; PCC, posterior cingulate cortex.

depolarization drives both orthodromic and antidromic action potential propagation. Orthodromic propagation causes action potentials and activity-dependent plasticity in an anterograde manner. Antidromic propagation promotes dendritic spine growth of stimulated neurons through a local Ca^{2+} spike, leading to increased presynaptic connectivity (Pashut et al., 2011). White matter architecture changes also occur over time via synaptic strengthening and pruning (Anderson et al., 2016).

Evolution of clinical experience with TMS in treatment-resistant depression

George et al. (2000) were the first to publish results of a double-blind, sham-controlled study showing the antidepressant potential of TMS over left DLPFC in randomized subjects (George et al., 2000). TMS had been introduced years earlier by Pascual-Leone for motor cortical stimulation (Pascual-Leone et al., 1994). In the George study, 30 medication-free patients with major depressive and bipolar disorder were treated with TMS daily for 2 weeks. Twenty patients were assigned to the active TMS group, whereas 10 were assigned to the sham group. TMS sessions lasted for 20 min and occurred each weekday. All patients underwent cerebral blood flow single photon emission computed tomography (SPECT) at the start (1 day), middle (5 day), and 3 days after the end of the study. The authors concluded that daily TMS over left DLPFC produced a significant antidepressant response, defined as greater than 50% improvement in baseline Hamilton Rating Scale for Depression (HRSD) scores. In the same year, Berman et al. also assessed the efficacy of TMS in unmedicated TRD patients using a randomized, double-blind design. TRD patients enrolled in the trial were assigned to either active TMS (N = 10) or sham (N = 10) treatment. The active TMS group received 20 2 s trains of 20 Hz with 58 s intervals daily over a 2 week course (Berman et al., 2000). As in George's study, results showed statistically significant reductions in depressive symptoms compared to the sham group. These two important papers instigated a groundswell of interest in TMS for depression and many other psychiatric disorders.

Today, TMS is practiced globally, and TRD remains the primary indication. The procedure is well tolerated; individuals who receive TMS report a > 50% decrease in symptom severity (Lisanby et al., 2009; George et al., 2010; O'Reardon et al., 2010). Despite this, one obstacle that has remained in scaling its deployment even further is the burdensome requirement for multiple treatments. For example, an initial treatment regimen consists of 40–60 min sessions of active treatment, 5 days per week for 3–6 weeks (Holtzheimer et al., 2010). Because of this, innumerable attempts have been made in the two decades since George's study to modify the TMS protocol with the goal of shortening the amount of therapy needed. In 2018, the US Food and Drug Administration (FDA) approved intermittent theta-burst stimulation (iTBS) as a new variant of TMS for the treatment of TRD (Mendlowitz et al., 2019). FDA approval was contingent on several new studies of theta-burst stimulation, including a multi-center clinical trial by Blumberger et al. (2018) that compared the efficacy of iTBS to conventional TMS in patients with TRD (Blumberger et al., 2018). In their study, TRD patients were randomized to iTBS (N = 209) or 10 Hz TMS (N = 205). Patients were treated with the modality they were randomized to for 5 days a week for 4–6 weeks. The 10 Hz TMS sessions lasted 37 min and consisted of 3,000 pulses per session. The iTBS session consisted of triplet 50 Hz pulses repeated at 5 Hz for 600 pulses over only 3 min. The HRSD was administered after each of the sessions and 1-, 4-, and 12 weeks after treatment. They observed that scores significantly improved in both iTBS and TMS groups (overall reduction in HRSD-17 scores was 10.1 points in the iTBS group and 9.9 points in the 10 Hz TMS group) at baseline and 1 week after treatment. This trial became the formative study establishing iTBS as a safe, tolerable, and effective treatment for people with TRD. Furthermore, iTBS sessions last only a few min and are less costly than conventional TMS.

Cole and colleagues addressed another well-known challenge with TMS protocols: overall treatment duration. In the SAINT study, patients with TRD were enrolled (N = 22) and received 5 days of iTBS (Cole et al., 2020). Each day consisted of ten daily sessions, for a total of 18,000 pulses per day. Functional MRI identified individualized targets for iTBS in each patient - the region of left DLPFC most anticorrelated with SCC activity. Intent-to-treat analysis revealed 86.4% (N = 19) of patients met remission criteria, without negative cognitive effects. In the follow-up double-blind RCT SNT study (2022), patients with TRD were enrolled and randomly assigned to one of two groups: sham (N = 15) or iTBS stimulation (N = 14) (Cole et al., 2022). At baseline and 4 weeks following treatment, patients completed the Montgomery-Asberg Depression Scale (MADRS). Patients in the stimulation group experienced a 52% reduction in depression scores. Compared to conventional TMS, the discovery of iTBS and new accelerated protocols may result in substantial clinical responses in a shorter time frame.

Structural and functional connectivity of neural networks in depression: Salience as a key switching mechanism

Diffusion-weighted imaging (DWI) is a structural MR technique that derives several important physical tissue properties within the brain. These imaging markers can be used to extract brain network profiles and regions important for TRD pathophysiology. Fractional anisotropy and mean diffusivity, two of the most frequently reported metrics, provide information on microstructural architecture and integrity of white matter. Both metrics are obtained using diffusion tensor imaging, the analytical method forming the basis of tractography (Basser and Pierpaoli, 1996). Another variant of diffusion-weighted imaging is diffusion kurtosis imaging which quantifies the non-Gaussian quality of water diffusion (Jensen et al., 2005). Diffusion imaging has been used extensively to investigate how structural connectivity differs in TRD patients. Peng and colleagues conducted a double-blind, randomized study aimed at ascertaining whether white matter

TABLE 1 Intrinsic connectivity networks in treatment-resistant depression (TRD).

Network	Component brain regions	Function	Connectivity in TRD	References
Default mode network	VMPFC, DMPFC, PCC, inferior parietal lobe, hippocampal formation	• Decreased activity in goal-directed tasks • Increased activity during self-referential processing and resting state	• Hyperconnectivity within DMN and between DMN and thalamus • Hypoconnectivity between DMN and bilateral caudate	Greicius et al., 2007; Buckner et al., 2008; Andrews-Hanna et al., 2010; Liston et al., 2014; Kaiser et al., 2015; Anderson et al., 2016
Central executive network	DLPFC, lateral posterior parietal cortex, ventrolateral prefrontal cortex, thalamus	• Increased activity during goal-directed tasks requiring sustained attention and working memory	• Hypoconnectivity or Hyperconnectivity within the CEN	Fox et al., 2005; Seeley et al., 2007; Alexopoulos et al., 2012; Liston et al., 2014; Kaiser et al., 2015; Anderson et al., 2016
Salience network	dACC, frontoinsular cortex, amygdala, VTA	• Detection of personally salient and rewarding stimuli • Integration of external and internal emotional, homeostatic, and cognitive nature • Guiding of appropriate behavioral responses	• Hypoconnectivity within the SN relative to symptom severity • Overactivity of dACC, insula, and amygdala when presented with stimuli of negative affect	Seeley et al., 2007; Menon, 2011; Hamilton et al., 2013; Goulden et al., 2014; Manoliu et al., 2014; Uddin, 2015; Anderson et al., 2016

VMPFC, ventromedial prefrontal cortex; DMPFC, dorsomedial prefrontal cortex; PCC, posterior cingulate cortex; DLPFC, dorsolateral prefrontal cortex; dACC, dorsal anterior cingulate cortex; VTA, ventral tegmental area.

TABLE 2 Network connectivity changes in treatment-resistant depression (TRD) and resultant symptoms.

Network	Connectivity increase or decrease in TRD	Associated symptom	References
Default mode network	1. ↑ Connectivity within default mode network	1. Rumination	Sheline et al., 2010; Hamilton et al., 2015; Williams, 2016
Central executive network	1. ↓ DLPFC-parietal cortex 2. ↓ ACC-DLPFC	1. Inattention, false alarm errors 2. Cognitive dysfunction, latency	Qiu et al., 2011; Sylvester et al., 2012; Forster et al., 2015; Williams, 2016
Salience network	1. ↑ Insula-amygdala 2. ↓ Insula-ACC 3. ↓ Amygdala-subcallosal and ventral ACC 4. Striatal hypoactivation 5. ACC hyperactivation	6. Anxious avoidance 7. Negative Bias 8. Threat dysregulation 9. Anhedonia 10. Context insensitivity	Matthews et al., 2008; Stuhrmann et al., 2011; Treadway and Zald, 2011; Klumpp et al., 2013; Zhang et al., 2013; Mulders et al., 2015; Williams et al., 2016

TRD, treatment resistant depression; ACC, anterior cingulate cortex; DLPFC, dorsolateral prefrontal cortex.

abnormalities cause network dysfunction in TRD patients (Peng et al., 2012). This group enrolled 30 TRD patients and randomized subjects to sham or active TMS treatment. The investigators acquired diffusion imaging and found significant reductions in FA in the left middle frontal gyrus not observed in the sham group. Korgaonkar et al. (2014) analyzed 102 MDD patients and found that the anterior cingulate cortex (ACC) limbic white matter is a useful predictor of antidepressant treatment outcome (Korgaonkar et al., 2014). Thus, based on DWI, FA could provide a glimpse into which patients with depression might be responsive to treatment.

Measurement of gray and white matter thickness using voxel-based morphometry (VBM) as well as connectivity between brain regions, inferred as specific white matter tracts or networks, can be extracted using a combination of structural and diffusion-weighted imaging. For example, the default mode network (DMN), which is distributed over many cortical regions, and the frontoparietal central executive network (CEN), have been shown to be dysregulated in patients with depression (Liston et al., 2014). DLPFC is in fact a node within the CEN. However, tractography studies were inconclusive as to whether DLPFC modulates connectivity between the two networks. Liston et al. (2014) sought to address this knowledge gap utilizing resting-state functional MRI (Liston et al., 2014). They enrolled 17 patients with depression and 35 healthy controls. The patients received 25 sessions of TMS over a 5 week period. Clinical scales assessing depression were completed at baseline and 1–3 days after completing the treatment period. Structural and diffusion-weighted scans were acquired before and after treatment. Functional connectivity maps were generated between the CEN, and DMN, using DLPFC as a seeding region. The authors observed that TMS of the DLPFC leads to connectivity changes in the DMN. This supports the idea that structures remote from the DLPFC such as DMN are also affected by TMS, suggesting a model based on knowledge of structural connectomics. However, very few studies have combined tractography and connectivity analyses in the same cohort with DWI and fMRI to determine the correlation between the two methods, particularly with respect to DLPFC and TMS.

The salience network (SN) is also dysfunctional in TRD, though it appears to have certain predictive characteristics for TMS response not seen in DMN or CEN. Fan et al. (2019) enrolled subjects with MDD and twenty healthy controls (Fan et al., 2019). Twenty real and sham sessions of TMS were administered to the DLPFC 5 days per week. Resting state fMRI sessions were performed before and after the TMS sessions, while clinical scales measuring depression were

TABLE 3 Transcranial magnetic stimulation (TMS) studies focusing on salience network.

References	Study type	Modality	Sample	Region or network of interest	Key findings
Wada et al., 2022	N/A	TMS-EEG and MRI	60 patients with TRD and 30 healthy controls	DLPFC, SN	In patients with TRD, signal transmission from the left DLPFC to the salience network was reduced in the θ and α bands.
Iwabuchi et al., 2019	Randomized study	TMS and fMRI	27 patients with TRD	DLPFC, SN, Fronto-insular	Early response to rTMS in TRD can be predicted by fronto-insular and salience-network connections.
Hawco et al., 2018	N/A	TMS-fMRI	26 healthy young adults	DLPFC, SN	Changes induced by TMS following stimulation of the DLPFC are associated with resting state connectivity, particularly when the DLPFC target is engaged with SN.
Philip et al., 2018	Prospective trial	TMS and fMRI	33 adults receiving care at neuromodulation clinics at Brown University-affiliated hospitals.	SCC, DLPFC, SN	After TMS, symptom reduction was associated with reduced connectivity between the SCC and the default mode network, left dorsolateral prefrontal cortex, and insula, and reduced connectivity between the hippocampus and the salience network.
Schluter et al., 2018	Randomized, single-blind trial	HF-TMS	45 healthy controls	LFPN, RFPN, DMN, SN, and RN	The salience network had less functional connection when the left DLPFC was stimulated, but this network had more functional connectivity when the right DLPFC was stimulated.

MDD, major depression disorder; DMN, default mode network; SN, salience network; FPN, fronto-parietal network; CON, cingulo-opercular network; MRN, memory retrieval network; pDMN, posterior default mode network; SCC, subcallosal cingulate cortex; PCC, posterior cingulate cortex; FPN, fronto-parietal network; HF-TMS, high-frequency TMS; LFPN, left frontoparietal network; RFPN, right frontoparietal network; RN, reward network.

administered weekly. Segregation analyses were performed to index connections between and within networks. Using these analyses, the authors observed that segregation of the SN predicts symptom improvement after TMS, which adds to our understanding of the pathophysiology of depressive symptoms. Several other authors have hypothesized that SN performs a switching mechanism during effective treatment of depression, since it appears to refocus maladaptive ruminative behavior driven by DMN towards purposeful executive function and planning behavior driven by CEN (Sridharan et al., 2008; Menon, 2011; Goulden et al., 2014; Anderson et al., 2016). **Tables 1**, **2** summarize the changes in DMN, CEN, and SN associated with TRD.

Epidural cortical stimulation for treatment-resistant depression: Which is more effective – unilateral or bilateral stimulation of DLPFC?

Given the success and US FDA approval of TMS for MDD in 2008, epidural cortical stimulation (EpCS) followed as an expansion of neuromodulation tools explored for the treatment of TRD. In an open-label study of EpCS as an adjunctive therapy for TRD, 5 patients were enrolled who had previously failed electroconvulsive therapy (ECT), TMS, and vagus nerve stimulation (VNS). Each patient underwent implantation of bilateral paddle leads positioned epidurally over Brodmann's areas 10 (frontopolar prefrontal cortex) and 46 (dorsolateral prefrontal cortex) (Nahas et al., 2010). After 7 months of follow-up, patients experienced significant improvement in depressive symptoms, compared to the pre-implantation baseline—with over 50% mean improvement in metrics of depression severity and 80% of the cohort achieving remission (Nahas et al., 2010; Williams et al., 2016, 2018). Remission was sustained at the 3 and 5 year follow-up timepoints, highlighting the potential of EpCS as an adjunctive therapy for TRD, following the failure of other modalities of neuromodulation.

Similar to TMS, EpCS generates peak electric fields at the gyral crown, subjacent to the stimulation site (Wongsarnpigoon and Grill, 2008). This suggests that the antidepressive effects may depend on direct activation of gray matter, recruitment of deeper white matter and subcortical structures or both. In a meta-analysis of resting state functional imaging studies, patients with depression displayed hypoactivation of the pregenual cingulate cortex (pgCC), dorsal anterior cingulate cortex (dACC), and insula (Fitzgerald et al., 2008). Interestingly, hypoactivity was significant for bilateral dorsolateral prefrontal cortices (DLPFC) in that study (Fitzgerald et al., 2008). In addition, Salomons et al. targeted bilateral prefrontal cortices and observed changes in connectivity between SN, CEN, and DMN networks following 20 sessions of 10 Hz TMS (Salomons et al., 2014; Anderson et al., 2016). These findings support the Nahas and Williams trials which resulted in up to 80% sustained remission (Nahas et al., 2010; Williams et al., 2016, 2018) while, in a separate study, unilateral (left-sided) conventional DLPFC stimulation produced an average of 30% remission (Kopell et al., 2011). This also highlights the potential to utilize EpCS as an alternative approach in TRD patients non-responsive to TMS, perhaps drawing on similar key mechanisms (Fitzgerald et al., 2008; Grimm et al., 2008).

In addition to direct modulation of hypoactivated DLPFC, EpCS of DLPFC could improve symptoms of TRD by altering connectivity with the subcallosal cingulate cortex (SCC), similar to TMS (Fox et al., 2012) or by indirectly modulating SN. As mentioned, the SN is hypothesized to act as a "switch" that serves to transition between other core

TABLE 4 Deep brain stimulation (DBS) for treatment-resistant depression (TRD) focusing on salience network.

References	Study type	Modality	Sample	Region or network of interest	Key findings
Yan et al., 2021	Systematic review	DBS	4 cases of self-injurious behavior	SN, NAcc, ALIC	Abnormal pain processing is related to alterations of salience network connectivity which in turn may influence SIB.
Riva-Posse et al., 2019	Randomized trial	DBS	9 patients with TRD	SN, SCC	Salience of behavioral responses are associated with SCC DBS-induced autonomic changes.
Ellard et al., 2018	N/A	DBS	35 unipolar depressed patients, 24 bipolar depressed patients, and 39 healthy controls	SN, DMN, ECN	Patients with bipolar disease displayed weaker functional connectivity between right dorsal AI and right VLPFC (SN). Greater impairment in perceived control in unipolar depression correlated with stronger right dorsal AI – right VLPFC (SN) functional connectivity.
Downar et al., 2016	Review	DBS	N/A	SN, dACC, anterior insula	Behavioral self-control, emotion regulation, and social cognition show functional correlations with SN activity. aCIN, part of the SN, may be a potential neuropsychiatric DBS target.
Choi et al., 2015	Case series	DBS	9 TRD patients undergoing DBS	SN, SCC	Proximity to bilateral VMFC (via forceps minor and left uncinate fasciculus) and CC (via left cingulum bundle) correlate with higher structural connectivity and clinical response

Acin, anterior cingulo-insular; NAcc, nucleus accumbens; ALIC, anterior limb of the internal capsule; SIB, self-injurious behavior; SCC, subcallosal cingulate cortex; VMFC, ventromedial frontal cortex; CC, cingulate cortex; ECN, fronto-parietal executive control; AI, anterior insula; SCC, subcallosal cingulate.

functional networks (including CEN and DMN) recruited during emotion regulation and social cognition. Nodes in the SN include dACC and bilateral insular cortices. These regions have been designated "common core" regions with aberrant activation in many psychiatric disorders, including obsessive-compulsive and post-traumatic stress disorders (Downar et al., 2016). These relationships suggest a functional interaction between DLPFC and the SN that is possibly exploited via TMS (**Table 3**) and EpCS for the modulation of TRD. DLPFC may act as a superficial access point to drive modulation of the deeper salience network, functioning to improve mood regulation by normalizing the activation balance and promoting transitions between intrinsic and task-evoked circuits.

Deep brain stimulation for treatment-resistant depression: Novel ideas emerge from clinical trials

Deep brain stimulation (DBS) is an invasive modality applied via stereotactic insertion of one or more intracranial leads. Its initial utility was investigated in the context of movement disorders, inspired by evidence that high frequency stimulation (100–200 Hz) of the ventral intermediate thalamic nucleus could alleviate tremor (Albe Fessard et al., 1963). In 1996, thalamic DBS received FDA approval in the US for essential and Parkinsonian tremors. Approvals for subthalamic nucleus (STN) and globus pallidus internus (GPi) DBS followed in 2003 for Parkinson's Disease (Miocinovic et al., 2013) and anterior thalamic nucleus (ATN) DBS for epilepsy in 2018 (Salanova et al., 2015; Kim et al., 2017). Evidence-based application of DBS for TRD has proven complex given the promising outcomes in open-label investigations that have not been reproduced in randomized clinical trials (RCT) (Morishita et al., 2014). In cohort studies of nucleus accumbens DBS, 40–45% of the TRD cohort responded with > 50% reduction in depressive symptoms. For ventral capsule/ventral striatum (VC/VS) DBS cohort studies, response rates were 53% at 12 months, and 71% by the long-term endpoint (mean of 37 months) (Malone et al., 2009; Malone, 2010). Despite these positive results, the multicenter RCT of VC/VS DBS failed to meet its primary endpoint (Dougherty et al., 2015). Similarly, positive effects of subcallosal cingulate cortex (SCC) DBS were reported in multiple case reports (Neimat et al., 2008; Guinjoan et al., 2010; Holtzheimer and Mayberg, 2010; Hamani et al., 2012) and cohort studies demonstrating > 60% responder rate (Mayberg et al., 2005; Kennedy et al., 2011). A subsequent multicenter trial showed a 29% responder rate at 12 months (Lozano et al., 2012), while a single-blinded study by Holtzheimer et al. reported 91% response rate and 58% remission rate (Holtzheimer et al., 2012). Of note the later study utilized higher intensity stimulation (6–10 mA) than the former (5.2 mA). These led to the BROADEN trial, which was conducted as a multicenter, randomized controlled trial for SCC DBS. Subjects underwent bilateral SCC implantation and were randomized to active or sham DBS for 6 months. Following the first endpoint of 6 months, no group differences were found, and the study was discontinued following a futility analysis. Nevertheless, two novel findings emerged from this study. First, a retrospective tractography study observed that SCC DBS responders were more likely to have the active contacts located at the convergence of four white matter pathways: forceps minor, uncinate fasciculus, cingulum bundle, and fronto-striatal fibers (Riva-Posse et al., 2014). Second, when subjects were followed longitudinally (2–8 years), the response and remission rates rose to 81 and

54%, respectively (Crowell et al., 2019). These follow-up studies provide encouragement for the therapeutic potential of DBS for TRD, as increasing evidence suggests that heterogeneity of psychiatric disorders may warrant an individualized approach, including connectomics and tractography, for patient-specific target identification (Riva-Posse et al., 2018; Allawala et al., 2021; Hollunder et al., 2022).

DBS antidepressive mechanisms

An advantage of SCC DBS is that it directly targets the white matter tracts underlying the subgenual cingulate cortex and thus gains access to functional networks involving the cingulum bundle. In contrast, the stimulus area accessed by ECT, TMS and EpCS is less focused. Notwithstanding, Tsolaki and colleagues demonstrated differences in responsivity to ECT based on SCC connectivity, again supporting the idea that non-invasive and invasive modalities share network coupling dynamics (Tsolaki et al., 2021). DBS contacts apply a three-dimensional electric field to surrounding tissue, resulting in depolarization or hyperpolarization of neighboring dendrites and axons (McIntyre and Foutz, 2013). The therapeutic effects are generated via high frequency stimulation (~100–130 Hz) of a target selected for its ability to modulate an aspect of neurologic dysfunction such as ATN for epilepsy and STN for Parkinson's disease. Initial functional studies in patients with depression demonstrated increased glucose metabolism in the SCC and pregenual cingulate cortex (pgCC) (Sacher et al., 2012). Mayberg and colleagues observed that hypermetabolism in SCC was attenuated with pharmacologic antidepressants (Mayberg et al., 1997, 2000), identifying SCC as a potential target for modulation of TRD with DBS. As suggested by tractography studies (Riva-Posse et al., 2014; Tsolaki et al., 2017), SCC DBS likely activates white matter tracts in close proximity to the electrode contacts, such as the cingulum bundle and uncinate fasciculus. The cingulum is a large white matter tract superficial to the corpus callosum and involved in executive control, emotion, pain, and memory (Bubb et al., 2018). Axons from the subgenual and anterior cingulate subsections have terminations in the anterior cingulate cortex (ACC), prefrontal cortex (dorsolateral, medial and orbital), amygdala, insula and superior temporal cortex (Bubb et al., 2018). Each of these structures have been strongly implicated in the SN and serve as potential sites of modulation for emotion dysregulation. Moreover, in a study of error rate in an emotional empathy task after ischemic stroke, Oishi et al. showed that right uncinate fasciculus lesions were associated with greater error rate. This demonstrated the role of the uncinate fasciculus, a tract with connections to orbitofrontal cortex, anterior insula, temporal pole, and amygdala, in emotional empathy (Oishi et al., 2015). SCC DBS at the intersection of these and other tracts may provide a locus for modulation of the SN given apparent overlap with key nodes: dorsal anterior cingulate cortex, anterior insula, temporal pole, and the amygdala (Friston, 2017). Direct access to the SN may provide a useful clue as to the potential mechanism for DMN and CEN activation via SCC DBS. **Table 4** summarizes key clinical evidence of SN modulation with DBS.

Multi-modality neuromodulation for TRD: A network-centric clinical algorithm

Given the complexity and heterogeneity associated with TRD, it would be advantageous to create a systematic therapeutic approach. We propose an heuristic clinical pathway that utilizes available neuromodulation technologies, tiered by invasiveness, to find the optimal, personalized treatment plan for individuals with TRD. This stepwise neuromodulation clinical pathway, paired with individualized target identification via tractography and functional connectomics, could result in more consistent patient outcomes.

In this pathway, patients that have failed three or more antidepressants and ECT will be treated with *Level 1A* neuromodulation—conventional DLPFC TMS protocol (6 weeks). If symptoms persist (<50% improvement in symptoms), patients may undergo additional testing including functional connectivity imaging, tractography, behavioral and cognitive testing for characterization of patient-specific TRD neurobiology contributing to depressive symptoms. Unique TRD profiles in certain patients have been suggested by several authors proposing that specific depressive symptoms map onto distinct functional networks (Williams, 2016; Hollunder et al., 2022). Imaging data would be used to identify personalized targets for subsequent neuromodulation. *The next step, Level 1B* neuromodulation, consists of accelerated TMS such as the 5 day SAINT protocol, using iTBS. If this fails, evidence of abnormal activation in DMN (hyperactivation) or CEN (hypoactivation) would be an indicator for *Level 2* neuromodulation—bilateral DLPFC and frontopolar PFC EpCS for 6 months. If imaging identifies hypoactivation of SN, *Level 3* neuromodulation—SCC DBS, would be recommended. VNS, which has been implicated in DLPFC activation via connections to the locus coeruleus, is an alternative if intracranial surgery is contraindicated (Conway et al., 2006, 2018; Dorr and Debonnel, 2006; Roosevelt et al., 2006; Kamel et al., 2022). Broader network dysfunction in DMN, CEN, and SN or severe, refractory cases would be an indication for *Level 4* neuromodulation—stereotactic electroencephalography (sEEG)-informed adaptive DBS. For this level, sEEG would assist with identifying symptom-specific biomarkers and targets for personalized closed-loop DBS. Scangos and colleagues used this approach and reported favorable outcomes with VC/VS stimulation for modulation of symptom-associated gamma power in the amygdala of one patient with TRD (Scangos et al., 2021). In that study, machine learning (ML) algorithms were used to analyze biomarkers in one structure while stimulating in a remote site. While specific white matter pathways were not considered in that study, it is interesting that the ML algorithms modeling the data identified a target other than SCC as most effective in ameliorating the patient's symptoms. The findings support the idea that not only may TRD manifest differently in each individual, structures outside the traditional DMN, SN or CEN networks, such as the amygdala, may provide useful biomarker correlations. A schematic of the proposed clinical pathway is depicted in **Figure 1**.

As previously described, depression is associated with hyperactivation of the DMN which may contribute to symptoms of rumination and pessimism (Anderson et al., 2016). This

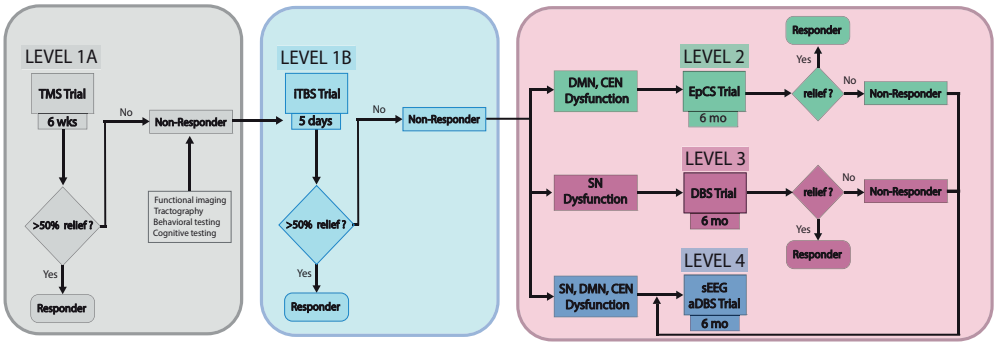

FIGURE 1
TRD neuromodulation clinical pathway. This schematic depicts the proposed stepwise pathway for optimizing individualized management of treatment-resistant depression sEEG, stereotactic electroencephalography; aDBS, adaptive deep brain stimulation.

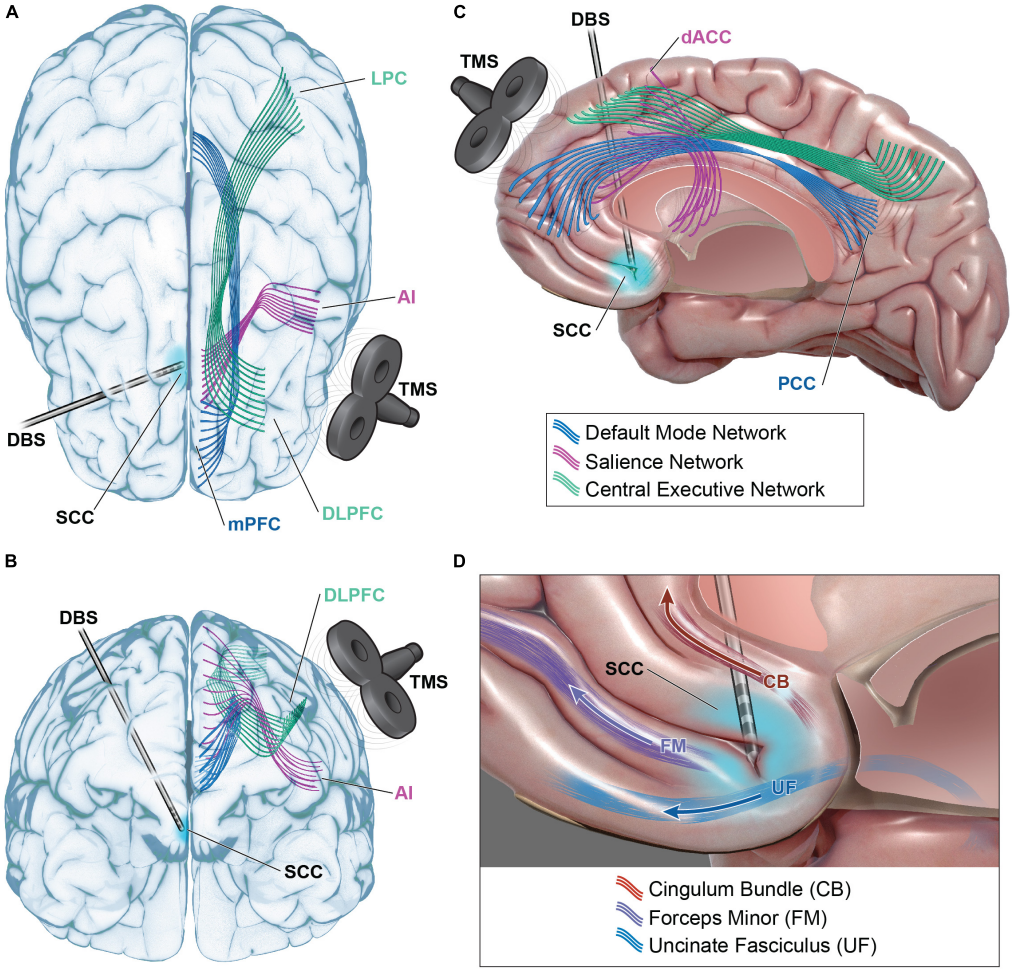

FIGURE 2
Functional network modulation in TRD. Default mode network (DMN – blue), salience network (SN – purple), and central executive network (CEN – green) are accessible for modulation with transcranial magnetic stimulation (TMS) and deep brain stimulation (DBS). Dorsal lateral prefrontal cortex (DLPFC) TMS may modulate CEN via direct modulation of DLPFC and its projections to lateral parietal cortex (LPC) **(A–C)**. DLPFC TMS could indirectly modulate SN via functional connections with anterior cingulate cortex (ACC), anterior insula (AI), or DMN via functional connections with medial prefrontal cortex (mPFC) and posterior cingulate cortex (PCC). DBS at the intersection of subcallosal cingulate cortex (SCC), the cingulum bundle (CB), uncinate fasciculus (UF), and forceps minor (FM) may modulate SN via projections to dorsal anterior cingulate cortex (dACC) and AI **(C,D)**. Functional connections to DLPFC, mPFC, and PCC also present avenues for modulation of CEN and DMN. Please see **Table 1** for full listing of network structures.

may or may not be cosynchronous with SN and CEN hypoactivation, resulting in aberrant responses to salient stimuli, memory deficits, and attentional dysfunction (Anderson et al., 2016). The neuromodulation clinical pathway we have proposed enables a multifaceted approach for treating depression by targeting nodes within each of these networks. This provides a systematic approach for implementing neuromodulation to find the target and therapy that works optimally for each patient.

In summary, the imbalance between network activity may prime individuals to preferentially respond to a particular stimulation locus and modality. TMS at the DLPFC directly modulates the node of the central executive network. But this region also has functional connections with nodes of the SN (ACC and anterior insula) and the DMN (ventromedial prefrontal cortex (VMPFC), posterior cingulate cortex (PCC) and lateral parietal cortex) (**Figures 2A–C**). Patients with pathologic hypoactivation of DLPFC as the primary insult may be responders to TMS. Bilateral DLPFC and frontopolar stimulation with EpCS likely alters activity of the CEN and DMN but also has downstream effects on the salience network. DBS at the intersection of the SCC, cingulum, and uncinate fasciculus likely modulates the SN via dACC and anterior insula (**Figures 2C, D**). This is probably paired with effects on the CEN and DMN through functional connections with DLPFC and VMPFC to PCC, respectively. Patients with hypoactivation of the salience network may preferentially respond to SCC DBS. A network-centric clinical pathway brings together multiple disciplines and proposes a new common language with the aim of enhancing care for treatment-resistant depression.

Author contributions

NR and ES helped to frame to scope of the manuscript and provided the editorial support. SI-A, CS, MB, and NR composed the manuscript, figures, and tables. All authors contributed to the article and approved the submitted version.

Conflict of interest

The authors declare that the research was conducted in the absence of any commercial or financial relationships that could be construed as a potential conflict of interest.

Publisher's note

References

Albe Fessard, D., Arfel, G., Guiot, G., Derome, P., Dela, H., Korn, H., et al. (1963). Characteristic electric activities of some cerebral structures in man. *Ann. Chir.* 17, 1185–1214.

Alexopoulos, G., Hoptman, M., Kanellopoulos, D., Murphy, C., Lim, K., and Gunning, F. (2012). Functional connectivity in the cognitive control network and the default mode network in late-life depression. *J. Affect. Disord.* 139, 56–65. doi: 10.1016/j.jad.2011.12.002

Al-Harbi, K. (2012). Treatment-resistant depression: therapeutic trends, challenges, and future directions. *Patient Prefer Adher.* 6, 369–388. doi: 10.2147/PPA.S29716

Allawala, A., Bijanki, K., Goodman, W., Cohn, J., Viswanathan, A., Yoshor, D., et al. (2021). A novel framework for network-targeted neuropsychiatric deep brain stimulation. *Neurosurgery* 89, E116–E121. doi: 10.1093/neuros/nyab112

Anderson, R., Hoy, K., Daskalakis, Z., and Fitzgerald, P. (2016). Repetitive transcranial magnetic stimulation for treatment resistant depression: Re-establishing connections. *Clin. Neurophysiol.* 127, 3394–3405. doi: 10.1016/j.clinph.2016.08.015

Andrews-Hanna, J., Reidler, J., Sepulcre, J., Poulin, R., and Buckner, R. (2010). Functional-anatomic fractionation of the brain's default network. *Neuron* 65, 550–562. doi: 10.1016/j.neuron.2010.02.005

Barker, A., Jalinous, R., and Freeston, I. (1985). Non-invasive magnetic stimulation of human motor cortex. *Lancet* 1, 1106–1107. doi: 10.1016/s0140-6736(85)92413-4

Basser, P., and Pierpaoli, C. (1996). Microstructural and physiological features of tissues elucidated by quantitative-diffusion-tensor MRI. *J. Magn. Reson. B.* 111, 209–219. doi: 10.1006/jmrb.1996.0086

Bergfeld, I., Mantione, M., Figee, M., Schuurman, P., Lok, A., and Denys, D. (2018). Treatment-resistant depression and suicidality. *J. Affect. Disord.* 235, 362–367. doi: 10.1016/j.jad.2018.04.016

Berman, R., Narasimhan, M., Sanacora, G., Miano, A., Hoffman, R., Hu, X., et al. (2000). A randomized clinical trial of repetitive transcranial magnetic stimulation in the treatment of major depression. *Biol. Psychiatry* 47, 332–337. doi: 10.1016/s0006-3223(99)00243-7

Blumberger, D., Vila-Rodriguez, F., Thorpe, K., Feffer, K., Noda, Y., Giacobbe, P., et al. (2018). Effectiveness of theta burst versus high-frequency repetitive transcranial magnetic stimulation in patients with depression (THREE-D): A randomised non-inferiority trial. *Lancet* 391, 1683–1692. doi: 10.1016/S0140-6736(18)30295-2

Bubb, E., Metzler-Baddeley, C., and Aggleton, J. (2018). The cingulum bundle: Anatomy, function, and dysfunction. *Neurosci. Biobehav. Rev.* 92, 104–127. doi: 10.1016/j.neubiorev.2018.05.008

Buckner, R., Andrews-Hanna, J., and Schacter, D. (2008). The brain's default network: Anatomy, function, and relevance to disease. *Ann. N. Y. Acad. Sci.* 1124, 1–38. doi: 10.1196/annals.1440.011

Choi, K., Riva-Posse, P., Gross, R., and Mayberg, H. (2015). Mapping the "Depression Switch" During Intraoperative Testing of Subcallosal Cingulate Deep Brain Stimulation. *JAMA Neurol.* 72, 1252–1260. doi: 10.1001/jamaneurol.2015.2564

Cohen, S., Bikson, M., Badran, B., and George, M. S. (2022). A visual and narrative timeline of US FDA milestones for Transcranial Magnetic Stimulation (TMS) devices. *Brain Stimul.* 15, 73–75. doi: 10.1016/j.brs.2021.11.010

Cole, E., Phillips, A., Bentzley, B., Stimpson, K., Nejad, R., Barmak, F., et al. (2022). Stanford Neuromodulation Therapy (SNT): A double-blind randomized controlled trial. *Am. J. Psychiatry* 179, 132–141. doi: 10.1176/appi.ajp.2021.20101429

Cole, E., Stimpson, K., Bentzley, B., Gulser, M., Cherian, K., Tischler, C., et al. (2020). Stanford accelerated intelligent neuromodulation therapy for treatment-resistant depression. *Am. J. Psychiatry* 177, 716–726. doi: 10.1176/appi.ajp.2019.19070720

Conway, C., Kumar, A., Xiong, W., Bunker, M., Aaronson, S., and Rush, A. (2018). Chronic vagus nerve stimulation significantly improves quality of life in treatment-resistant major depression. *J. Clin. Psychiatry* 79:18m12178. doi: 10.4088/JCP.18m12178

Conway, C., Sheline, Y., Chibnall, J., George, M., Fletcher, J., and Mintun, M. (2006). Cerebral blood flow changes during vagus nerve stimulation for depression. *Psychiatry Res.* 146, 179–184. doi: 10.1016/j.pscychresns.2005.12.007

Crowell, A., Riva-Posse, P., Holtzheimer, P., Garlow, S., Kelley, M., Gross, R., et al. (2019). Long-Term outcomes of subcallosal cingulate deep brain stimulation for treatment-resistant depression. *Am. J. Psychiatry* 176, 949–956. doi: 10.1176/appi.ajp.2019.18121427

Dorr, A., and Debonnel, G. (2006). Effect of vagus nerve stimulation on serotonergic and noradrenergic transmission. *J. Pharmacol. Exp. Ther.* 318, 890–898. doi: 10.1124/jpet.106.104166

Dougherty, D., Rezai, A., Carpenter, L., Howland, R., Bhati, M., O'Reardon, J., et al. (2015). A Randomized Sham-Controlled Trial of Deep Brain Stimulation of the Ventral Capsule/Ventral Striatum for Chronic Treatment-Resistant Depression. *Biol. Psychiatry* 78, 240–248. doi: 10.1016/j.biopsych.2014.11.023

Downar, J., Blumberger, D., and Daskalakis, Z. (2016). The neural crossroads of psychiatric illness: An emerging target for brain stimulation. *Trends Cogn. Sci.* 20, 107–120. doi: 10.1016/j.tics.2015.10.007

Ellard, K., Zimmerman, J., Kaur, N., Van Dijk, K., Roffman, J., Nierenberg, A., et al. (2018). Functional connectivity between anterior insula and key nodes of frontoparietal executive control and salience networks distinguish bipolar depression from unipolar depression and healthy control subjects. *Biol. Psychiatry Cogn. Neurosci. Neuroimaging* 3, 473–484. doi: 10.1016/j.bpsc.2018.01.013

Fan, J., Tso, I., Maixner, D., Abagis, T., Hernandez-Garcia, L., and Taylor, S. (2019). Segregation of salience network predicts treatment response of depression to repetitive transcranial magnetic stimulation. *Neuroimage Clin.* 22:101719. doi: 10.1016/j.nicl.2019.101719

Fitzgerald, P., Laird, A., Maller, J., and Daskalakis, Z. J. (2008). A meta-analytic study of changes in brain activation in depression. *Hum. Brain Mapp.* 29, 683–695. doi: 10.1002/hbm.20426

Forster, S., Nunez Elizalde, A., Castle, E., and Bishop, S. (2015). Unraveling the anxious mind: Anxiety, worry, and frontal engagement in sustained attention versus off-task processing. *Cereb. Cortex* 25, 609–618. doi: 10.1093/cercor/bht248

Fox, M., Buckner, R., White, M., Greicius, M., and Pascual-Leone, A. (2012). Efficacy of transcranial magnetic stimulation targets for depression is related to intrinsic functional connectivity with the subgenual cingulate. *Biol. Psychiatry* 72, 595–603. doi: 10.1016/j.biopsych.2012.04.028

Fox, M., Snyder, A., Vincent, J., Corbetta, M., Van Essen, D., and Raichle, M. (2005). The human brain is intrinsically organized into dynamic, anticorrelated functional networks. *Proc. Natl. Acad. Sci. U.S.A.* 102, 9673–9678. doi: 10.1073/pnas.0504136102

Friston, K. (2017). Precision Psychiatry. *Biol. Psychiatry Cogn. Neurosci. Neuroimaging* 2, 640–643. doi: 10.1016/j.bpsc.2017.08.007

George, M., Lisanby, S., Avery, D., McDonald, W., Durkalski, V., Pavlicova, M., et al. (2010). Daily left prefrontal transcranial magnetic stimulation therapy for major depressive disorder: A sham-controlled randomized trial. *Arch. Gen. Psychiatry* 67, 507–516. doi: 10.1001/archgenpsychiatry.2010.46

George, M., Nahas, Z., Molloy, M., Speer, A., Oliver, N., Li, X., et al. (2000). A controlled trial of daily left prefrontal cortex TMS for treating depression. *Biol. Psychiatry* 48, 962–970. doi: 10.1016/s0006-3223(00)01048-9

Goulden, N., Khusnulina, A., Davis, N., Bracewell, R., Bokde, A., McNulty, J., et al. (2014). The salience network is responsible for switching between the default mode network and the central executive network: Replication from DCM. *Neuroimage* 99, 180–190. doi: 10.1016/j.neuroimage.2014.05.052

Greicius, M., Flores, B., Menon, V., Glover, G., Solvason, H., Kenna, H., et al. (2007). Resting-state functional connectivity in major depression: Abnormally increased contributions from subgenual cingulate cortex and thalamus. *Biol. Psychiatry* 62, 429–437. doi: 10.1016/j.biopsych.2006.09.020

Grimm, S., Beck, J., Schuepbach, D., Hell, D., Boesiger, P., Bermpohl, F., et al. (2008). Imbalance between left and right dorsolateral prefrontal cortex in major depression is linked to negative emotional judgment: An fMRI study in severe major depressive disorder. *Biol. Psychiatry* 63, 369–376. doi: 10.1016/j.biopsych.2007.05.033

Guinjoan, S., Mayberg, H., Costanzo, E., Fahrer, R., Tenca, E., Antico, J., et al. (2010). Asymmetrical contribution of brain structures to treatment-resistant depression as illustrated by effects of right subgenual cingulum stimulation. *J. Neuropsychiatry Clin. Neurosci.* 22, 265–277. doi: 10.1176/jnp.2010.22.3.265

Hamani, C., Giacobbe, P., Diwan, M., Balbino, E., Tong, J., Bridgman, A., et al. (2012). Monoamine oxidase inhibitors potentiate the effects of deep brain stimulation. *Am. J. Psychiatry* 169, 1320–1321. doi: 10.1176/appi.ajp.2012.12060754

Hamilton, J., Chen, M., and Gotlib, I. (2013). Neural systems approaches to understanding major depressive disorder: An intrinsic functional organization perspective. *Neurobiol. Dis.* 52, 4–11. doi: 10.1016/j.nbd.2012.01.015

Hamilton, J., Farmer, M., Fogelman, P., and Gotlib, I. (2015). Depressive rumination, the default-mode network, and the dark matter of clinical neuroscience. *Biol. Psychiatry* 78, 224–230. doi: 10.1016/j.biopsych.2015.02.020

Hawco, C., Voineskos, A., Steeves, J., Dickie, E., Viviano, J., Downar, J., et al. (2018). Spread of activity following TMS is related to intrinsic resting connectivity to the salience network: A concurrent TMS-fMRI study. *Cortex* 108, 160–172. doi: 10.1016/j.cortex.2018.07.010

Hollunder, B., Rajamani, N., Siddiqi, S., Finke, C., Kühn, A., Mayberg, H., et al. (2022). Toward personalized medicine in connectomic deep brain stimulation. *Prog. Neurobiol.* 210:102211. doi: 10.1016/j.pneurobio.2021.102211

Holtzheimer, P., Kelley, M., Gross, R., Filkowski, M., Garlow, S., Barrocas, A., et al. (2012). Subcallosal cingulate deep brain stimulation for treatment-resistant unipolar and bipolar depression. *Arch. Gen. Psychiatry* 69, 150–158. doi: 10.1001/archgenpsychiatry.2011.1456

Holtzheimer, P., and Mayberg, H. (2010). Deep brain stimulation for treatment-resistant depression. *Am. J. Psychiatry* 167, 1437–1444. doi: 10.1176/appi.ajp.2010.10010141

Holtzheimer, P., McDonald, W., Mufti, M., Kelley, M., Quinn, S., Corso, G., et al. (2010). Accelerated repetitive transcranial magnetic stimulation for treatment-resistant depression. *Depress Anxiety* 27, 960–963. doi: 10.1002/da.20731

Iwabuchi, S., Auer, D., Lankappa, S., and Palaniyappan, L. (2019). Baseline effective connectivity predicts response to repetitive transcranial magnetic stimulation in patients with treatment-resistant depression. *Eur. Neuropsychopharmacol.* 29, 681–690. doi: 10.1016/j.euroneuro.2019.02.012

Jensen, J., Helpern, J., Ramani, A., Lu, H., and Kaczynski, K. (2005). Diffusional kurtosis imaging: The quantification of non-gaussian water diffusion by means of magnetic resonance imaging. *Magn. Reson. Med.* 53, 1432–1440. doi: 10.1002/mrm.20508

Kaiser, R., Andrews-Hanna, J., Wager, T., and Pizzagalli, D. (2015). Large-scale network dysfunction in major depressive disorder: A meta-analysis of resting-state functional connectivity. *JAMA Psychiatry* 72, 603–611. doi: 10.1001/jamapsychiatry.2015.0071

Kamel, L., Xiong, W., Gott, B., Kumar, A., and Conway, C. (2022). Vagus nerve stimulation: An update on a novel treatment for treatment-resistant depression. *J. Neurol. Sci.* 434:120171. doi: 10.1016/j.jns.2022.120171

Kennedy, S., Giacobbe, P., Rizvi, S., Placenza, F., Nishikawa, Y., Mayberg, H., et al. (2011). Deep brain stimulation for treatment-resistant depression: Follow-up after 3 to 6 years. *Am. J. Psychiatry* 168, 502–510. doi: 10.1176/appi.ajp.2010.10081187

Kim, S., Lim, S., Kim, J., Son, B., Lee, K., and Shon, Y. (2017). Long-term follow-up of anterior thalamic deep brain stimulation in epilepsy: A 11-year, single center experience. *Seizure* 52, 154–161. doi: 10.1016/j.seizure.2017.10.009

Klumpp, H., Post, D., Angstadt, M., Fitzgerald, D., and Phan, K. (2013). Anterior cingulate cortex and insula response during indirect and direct processing of emotional faces in generalized social anxiety disorder. *Biol. Mood Anxiety Disord.* 3:7. doi: 10.1186/2045-5380-3-7

Kopell, B., Halverson, J., Butson, C., Dickinson, M., Bobholz, J., Harsch, H., et al. (2011). Epidural cortical stimulation of the left dorsolateral prefrontal cortex for refractory major depressive disorder. *Neurosurgery* 69, 1015–1029. doi: 10.1227/NEU.0b013e318229cfcd

Korgaonkar, M., Williams, L., Song, Y., Usherwood, T., and Grieve, S. (2014). Diffusion tensor imaging predictors of treatment outcomes in major depressive disorder. *Br. J Psychiatry* 205, 321–328. doi: 10.1192/bjp.bp.113.140376

Lisanby, S., Husain, M., Rosenquist, P., Maixner, D., Gutierrez, R., Krystal, A., et al. (2009). Daily left prefrontal repetitive transcranial magnetic stimulation in the acute treatment of major depression: Clinical predictors of outcome in a multisite, randomized controlled clinical trial. *Neuropsychopharmacology* 34, 522–534. doi: 10.1038/npp.2008.118

Liston, C., Chen, A., Zebley, B., Drysdale, A., Gordon, R., Leuchter, B., et al. (2014). Default mode network mechanisms of transcranial magnetic stimulation in depression. *Biol. Psychiatry* 76, 517–526. doi: 10.1016/j.biopsych.2014.01.023

Lozano, A., Giacobbe, P., Hamani, C., Rizvi, S., Kennedy, S., Kolivakis, T., et al. (2012). A multicenter pilot study of subcallosal cingulate area deep brain stimulation for treatment-resistant depression. *J. Neurosurg.* 116, 315–322. doi: 10.3171/2011.10.JNS102122

Malone, D. (2010). Use of deep brain stimulation in treatment-resistant depression. *Cleve. Clin J. Med.* 77(Suppl. 3), S77–S80. doi: 10.3949/ccjm.77.s3.14

Malone, D., Dougherty, D., Rezai, A., Carpenter, L., Friehs, G., Eskandar, E., et al. (2009). Deep brain stimulation of the ventral capsule/ventral striatum for treatment-resistant depression. *Biol. Psychiatry* 65, 267–275. doi: 10.1016/j.biopsych.2008.08.029

Manoliu, A., Riedl, V., Zherdin, A., Mühlau, M., Schwerthöffer, D., Scherr, M., et al. (2014). Aberrant dependence of default mode/central executive network interactions on anterior insular salience network activity in schizophrenia. *Schizophr. Bull.* 40, 428–437. doi: 10.1093/schbul/sbt037

Matthews, S., Strigo, I., Simmons, A., Yang, T., and Paulus, M. (2008). Decreased functional coupling of the amygdala and supragenual cingulate is related to increased depression in unmedicated individuals with current major depressive disorder. *J. Affect. Disord.* 111, 13–20. doi: 10.1016/j.jad.2008.05.022

Mayberg, H., Brannan, S., Mahurin, R., Jerabek, P., Brickman, J., Tekell, J., et al. (1997). Cingulate function in depression: A potential predictor of treatment response. *Neuroreport* 8, 1057–1061. doi: 10.1097/00001756-199703030-00048

Mayberg, H., Brannan, S., Tekell, J., Silva, J., Mahurin, R., McGinnis, S., et al. (2000). Regional metabolic effects of fluoxetine in major depression: Serial changes and relationship to clinical response. *Biol. Psychiatry* 48, 830–843. doi: 10.1016/s0006-3223(00)01036-2

Mayberg, H., Lozano, A., Voon, V., McNeely, H., Seminowicz, D., Hamani, C., et al. (2005). Deep brain stimulation for treatment-resistant depression. *Neuron* 45, 651–660. doi: 10.1016/j.neuron.2005.02.014

McIntyre, C., and Foutz, T. (2013). Computational modeling of deep brain stimulation. *Handb. Clin. Neurol.* 116, 55–61. doi: 10.1016/B978-0-444-53497-2.00005-X

Mendlowitz, A., Shanbour, A., Downar, J., Vila-Rodriguez, F., Daskalakis, Z., Isaranuwatchai, W., et al. (2019). Implementation of intermittent theta burst stimulation compared to conventional repetitive transcranial magnetic stimulation in patients with treatment resistant depression: A cost analysis. *PLoS One* 14:e0222546. doi: 10.1371/journal.pone.0222546

Menon, V. (2011). Large-scale brain networks and psychopathology: A unifying triple network model. *Trends Cogn. Sci.* 15, 483–506. doi: 10.1016/j.tics.2011.08.003

Miocinovic, S., Somayajula, S., Chitnis, S., and Vitek, J. (2013). History, applications, and mechanisms of deep brain stimulation. *JAMA Neurol.* 70, 163–171. doi: 10.1001/2013.jamaneurol.45

Morishita, T., Fayad, S., Higuchi, M., Nestor, K., and Foote, K. (2014). Deep brain stimulation for treatment-resistant depression: Systematic review of clinical outcomes. *Neurotherapeutics* 11, 475–484. doi: 10.1007/s13311-014-0282-1

Mulders, P., van Eijndhoven, P., Schene, A., Beckmann, C., and Tendolkar, I. (2015). Resting-state functional connectivity in major depressive disorder: A review. *Neurosci. Biobehav. Rev.* 56, 330–344. doi: 10.1016/j.neubiorev.2015.07.014

Nahas, Z., Anderson, B., Borckardt, J., Arana, A., George, M., Reeves, S., et al. (2010). Bilateral epidural prefrontal cortical stimulation for treatment-resistant depression. *Biol. Psychiatry* 67, 101–109. doi: 10.1016/j.biopsych.2009.08.021

Neimat, J., Hamani, C., Giacobbe, P., Merskey, H., Kennedy, S., Mayberg, H., et al. (2008). Neural stimulation successfully treats depression in patients with prior ablative cingulotomy. *Am. J. Psychiatry* 165, 687–693. doi: 10.1176/appi.ajp.2008.07081298

Oishi, K., Faria, A., Hsu, J., Tippett, D., Mori, S., and Hillis, A. (2015). Critical role of the right uncinate fasciculus in emotional empathy. *Ann. Neurol.* 77, 68–74. doi: 10.1002/ana.24300

O'Reardon, J., Solvason, H., Janicak, P., Sampson, S., Isenberg, K., Nahas, Z., et al. (2010). Reply regarding "efficacy and safety of transcranial magnetic stimulation in the acute treatment of major depression: A multisite randomized controlled trial". *Biol. Psychiatry* 67, e15–e17. doi: 10.1016/j.biopsych.2009.06.027

Pascual-Leone, A., Valls-Solé, J., Wassermann, E., and Hallett, M. (1994). Responses to rapid-rate transcranial magnetic stimulation of the human motor cortex. *Brain* 117, 847–858. doi: 10.1093/brain/117.4.847

Pashut, T., Wolfus, S., Friedman, A., Lavidor, M., Bar-Gad, I., Yeshurun, Y., et al. (2011). Mechanisms of magnetic stimulation of central nervous system neurons. *PLoS Comput. Biol.* 7:e1002022. doi: 10.1371/journal.pcbi.1002022

Peng, H., Zheng, H., Li, L., Liu, J., Zhang, Y., Shan, B., et al. (2012). High-frequency rTMS treatment increases white matter FA in the left middle frontal gyrus in young patients with treatment-resistant depression. *J. Affect. Disord.* 136, 249–257. doi: 10.1016/j.jad.2011.12.006

Philip, N., Barredo, J., van 't Wout-Frank, M., Tyrka, A., Price, L., and Carpenter, L. (2018). Network Mechanisms of Clinical Response to Transcranial Magnetic Stimulation in Posttraumatic Stress Disorder and Major Depressive Disorder. *Biol. Psychiatry* 83, 263–272. doi: 10.1016/j.biopsych.2017.07.021

Qiu, C., Liao, W., Ding, J., Feng, Y., Zhu, C., Nie, X., et al. (2011). Regional homogeneity changes in social anxiety disorder: A resting-state fMRI study. *Psychiatry Res.* 194, 47–53. doi: 10.1016/j.pscychresns.2011.01.010

Riva-Posse, P., Choi, K., Holtzheimer, P., Crowell, A., Garlow, S., Rajendra, J., et al. (2018). A connectomic approach for subcallosal cingulate deep brain stimulation surgery: Prospective targeting in treatment-resistant depression. *Mol. Psychiatry* 23, 843–849. doi: 10.1038/mp.2017.59

Riva-Posse, P., Choi, K., Holtzheimer, P., McIntyre, C., Gross, R., Chaturvedi, A., et al. (2014). Defining critical white matter pathways mediating successful subcallosal cingulate deep brain stimulation for treatment-resistant depression. *Biol. Psychiatry* 76, 963–969. doi: 10.1016/j.biopsych.2014.03.029

Riva-Posse, P., Inman, C., Choi, K., Crowell, A., Gross, R., Hamann, S., et al. (2019). Autonomic arousal elicited by subcallosal cingulate stimulation is explained by white matter connectivity. *Brain Stimul.* 12, 743–751. doi: 10.1016/j.brs.2019.01.015

Roosevelt, R., Smith, D., Clough, R., Jensen, R., and Browning, R. (2006). Increased extracellular concentrations of norepinephrine in cortex and hippocampus following vagus nerve stimulation in the rat. *Brain Res.* 1119, 124–132. doi: 10.1016/j.brainres.2006.08.048

Sacher, J., Neumann, J., Fünfstück, T., Soliman, A., Villringer, A., and Schroeter, M. (2012). Mapping the depressed brain: A meta-analysis of structural and functional alterations in major depressive disorder. *J. Affect. Disord.* 140, 142–148. doi: 10.1016/j.jad.2011.08.001

Salanova, V., Witt, T., Worth, R., Henry, T., Gross, R., Nazzaro, J., et al. (2015). Long-term efficacy and safety of thalamic stimulation for drug-resistant partial epilepsy. *Neurology* 84, 1017–1025. doi: 10.1212/WNL.0000000000001334

Salomons, T., Dunlop, K., Kennedy, S., Flint, A., Geraci, J., Giacobbe, P., et al. (2014). Resting-state cortico-thalamic-striatal connectivity predicts response to dorsomedial prefrontal rTMS in major depressive disorder. *Neuropsychopharmacology* 39, 488–498. doi: 10.1038/npp.2013.222

Scangos, K., Khambhati, A., Daly, P., Makhoul, G., Sugrue, L., Zamanian, H., et al. (2021). Closed-loop neuromodulation in an individual with treatment-resistant depression. *Nat. Med.* 27, 1696–1700. doi: 10.1038/s41591-021-01480-w

Schluter, R., Jansen, J., van Holst, R., van den Brink, W., and Goudriaan, A. (2018). Differential Effects of Left and Right Prefrontal High-Frequency Repetitive Transcranial Magnetic Stimulation on Resting-State Functional Magnetic Resonance Imaging in Healthy Individuals. *Brain Connect.* 8, 60–67. doi: 10.1089/brain.2017.0542

Seeley, W., Menon, V., Schatzberg, A., Keller, J., Glover, G., Kenna, H., et al. (2007). Dissociable intrinsic connectivity networks for salience processing and executive control. *J. Neurosci.* 27, 2349–2356. doi: 10.1523/JNEUROSCI.5587-06.2007

Sheline, Y., Price, J., Yan, Z., and Mintun, M. (2010). Resting-state functional MRI in depression unmasks increased connectivity between networks via the dorsal nexus. *Proc. Natl. Acad. Sci. U.S.A.* 107, 11020–11025. doi: 10.1073/pnas.1000446107

Souery, D., Papakostas, G. I., and Trivedi, M. H. (2006). Treatment-Resistant Depression. *J. Clin. Psychiatry* 67(Suppl. 6), 16–22.

Sridharan, D., Levitin, D., and Menon, V. (2008). A critical role for the right fronto-insular cortex in switching between central-executive and default-mode networks. *Proc. Natl. Acad. Sci. U.S.A.* 105, 12569–12574. doi: 10.1073/pnas.0800005105

Stuhrmann, A., Suslow, T., and Dannlowski, U. (2011). Facial emotion processing in major depression: A systematic review of neuroimaging findings. *Biol. Mood Anxiety Disord.* 1:10. doi: 10.1186/2045-5380-1-10

Sylvester, C., Corbetta, M., Raichle, M., Rodebaugh, T., Schlaggar, B., Sheline, Y., et al. (2012). Functional network dysfunction in anxiety and anxiety disorders. *Trends Neurosci.* 35, 527–535. doi: 10.1016/j.tins.2012.04.012

Tofts, P. (1990). The distribution of induced currents in magnetic stimulation of the nervous system. *Phys. Med Biol.* 35, 1119–1128. doi: 10.1088/0031-9155/35/8/008

Treadway, M., and Zald, D. (2011). Reconsidering anhedonia in depression: Lessons from translational neuroscience. *Neurosci. Biobehav. Rev.* 35, 537–555. doi: 10.1016/j.neubiorev.2010.06.006

Tsolaki, E., Espinoza, R., and Pouratian, N. (2017). Using probabilistic tractography to target the subcallosal cingulate cortex in patients with treatment resistant depression. *Psychiatry Res. Neuroimaging* 261, 72–74. doi: 10.1016/j.pscychresns.2017.01.006

Tsolaki, E., Narr, K., Espinoza, R., Wade, B., Hellemann, G., Kubicki, A., et al. (2021). Subcallosal Cingulate Structural Connectivity Differs in Responders and Nonresponders to Electroconvulsive Therapy. *Biol. Psychiatry Cogn. Neurosci. Neuroimaging* 6, 10–19. doi: 10.1016/j.bpsc.2020.05.010

Uddin, L. (2015). Salience processing and insular cortical function and dysfunction. *Nat. Rev. Neurosci.* 16, 55–61. doi: 10.1038/nrn3857

Wada, M., Nakajima, S., Honda, S., Takano, M., Taniguchi, K., Tsugawa, S., et al. (2022). Reduced signal propagation elicited by frontal transcranial magnetic stimulation is associated with oligodendrocyte abnormalities in treatment-resistant depression. *J. Psychiatry Neurosci.* 47, E325–E335. doi: 10.1503/jpn.220102

Williams, L. M. (2016). Precision psychiatry: A neural circuit taxonomy for depression and anxiety. *Lancet Psychiatry* 3, 472–480. doi: 10.1016/S2215-0366(15)00579-9

Williams, N., Bentzley, B., Hopkins, T., Pannu, J., Sahlem, G., Takacs, I., et al. (2018). Optimization of epidural cortical stimulation for treatment-resistant depression. *Brain Stimul.* 11, 239–240. doi: 10.1016/j.brs.2017.09.001

Williams, N., Short, E., Hopkins, T., Bentzley, B., Sahlem, G., Pannu, J., et al. (2016). Five-Year Follow-Up of Bilateral Epidural Prefrontal Cortical Stimulation for Treatment-Resistant Depression. *Brain Stimul.* 9, 897–904. doi: 10.1016/j.brs.2016.06.054

Williams, N., Sudheimer, K., Cole, E., Varias, A., Goldstein-Piekarski, A., Stetz, P., et al. (2021). Accelerated neuromodulation therapy for Obsessive-Compulsive Disorder. *Brain Stimul.* 14, 435–437. doi: 10.1016/j.brs.2021.02.013

Wongsarnpigoon, A., and Grill, W. (2008). Computational modeling of epidural cortical stimulation. *J. Neural Eng.* 5, 443–454. doi: 10.1088/1741-2560/5/4/009

Yan, H., Elkaim, L., Loh, A., Boutet, A., Germann, J., Elias, G., et al. (2021). Lesions causing self-injurious behavior engage putative networks modulated by deep brain stimulation. *Brain Stimul.* 14, 273–276. doi: 10.1016/j.brs.2021.01.009

Zhang, W., Chang, S., Guo, L., Zhang, K., and Wang, J. (2013). The neural correlates of reward-related processing in major depressive disorder: A meta-analysis of functional magnetic resonance imaging studies. *J. Affect. Disord.* 151, 531–539. doi: 10.1016/j.jad.2013.06.039

frontiers | Frontiers in Neural Circuits

TYPE Brief Research Report
PUBLISHED 21 March 2023
DOI 10.3389/fncir.2023.1124221

OPEN ACCESS

EDITED BY
Raffaella Ricci,
University of Turin, Italy

REVIEWED BY
Ying-hui Chou,
University of Arizona, United States
Mariagiovanna Cantone,
Gaspare Rodolico Hospital, Italy

*CORRESPONDENCE
Joshua C. Brown
jbrown@mclean.harvard.edu

RECEIVED 14 December 2022
ACCEPTED 24 February 2023
PUBLISHED 21 March 2023

CITATION
Kweon J, Vigne MM, Jones RN, Carpenter LL and Brown JC (2023) Practice makes plasticity: 10-Hz rTMS enhances LTP-like plasticity in musicians and athletes.
Front. Neural Circuits 17:1124221.
doi: 10.3389/fncir.2023.1124221

Practice makes plasticity: 10-Hz rTMS enhances LTP-like plasticity in musicians and athletes

Jamie Kweon[1], Megan M. Vigne[1], Richard N. Jones[2,3], Linda L. Carpenter[1,2] and Joshua C. Brown[1,2,3]*

[1]Neuromodulation Research Facility, TMS Clinic, Butler Hospital, Providence, RI, United States, [2]Department of Psychiatry and Human Behavior, Warren Alpert Medical School of Brown University, Providence, RI, United States, [3]Department of Neurology, Warren Alpert Medical School of Brown University, Providence, RI, United States

Motor skill learning has been linked to functional and structural changes in the brain. Musicians and athletes undergo intensive motor training through the practice of an instrument or sport and have demonstrated use-dependent plasticity that may be subserved by long-term potentiation (LTP) processes. We know less, however, about whether the brains of musicians and athletes respond to plasticity-inducing interventions, such as repetitive transcranial magnetic stimulation (rTMS), differently than those without extensive motor training. In a pharmaco-rTMS study, we evaluated motor cortex excitability before and after an rTMS protocol in combination with oral administration of D-cycloserine (DCS) or placebo. In a secondary covariate analysis, we compared results between self-identified musicians and athletes (M&As) and non-musicians and athletes (non-M&As). Three TMS measures of cortical physiology were used to evaluate plasticity. We found that M&As did not have higher baseline corticomotor excitability. However, a plasticity-inducing protocol (10-Hz rTMS in combination with DCS) strongly facilitated motor-evoked potentials (MEPs) in M&As, but only weakly in non-M&As. Placebo and rTMS produced modest facilitation in both groups. Our findings suggest that motor practice and learning create a neuronal environment more responsive to plasticity-inducing events, including rTMS. These findings may explain one factor contributing to the high inter-individual variability found with MEP data. Greater capacity for plasticity holds implications for learning paradigms, such as psychotherapy and rehabilitation, by facilitating LTP-like activation of key networks, including recovery from neurological/mental disorders.

KEYWORDS

repetitive transcranial magnetic simulation, plasticity, LTP, motor-evoked potential (MEP), D-cycloserine (D-CYC: partial NMDA receptor agonist), NMDA-receptor

1. Introduction

Motor skill training, defined as the acquisition and subsequent refinement of novel movement sequences in a progressive manner, has the ability to change the structure and function of the motor cortex (Adkins et al., 2006). Animal studies have found that training in a specific motor task produces an expansion of cortical representation of the exercised body part which parallels improved performance (reviewed in Adkins et al., 2006). In humans,

6 weeks of practice in a visuomotor task increased corticospinal excitability as measured by motor-evoked potentials (MEPs), with learning-dependent greater increases in those who engaged in increasingly difficult training (Christiansen et al., 2020). It is hypothesized that motor skill development on a short- and long-term scale can induce changes in synaptic strength between corticospinal neurons and engage synaptic plasticity to reorganize cortical maps (Monfils et al., 2005). Increased dendritic branching and synapse numbers have been found within the motor cortex of rats after motor skill training, suggesting learning-related synaptogenesis (Greenough et al., 1985; Kleim et al., 1996). Blocking receptors critical to synaptic plasticity abolishes practice-dependent effects at both cellular (animal) and behavioral (human) levels (see Monfils et al., 2005 for a comprehensive review).

Musicians and athletes (M&As) are two groups who engage in consistent, deliberate, motor skill acquisition through the practice of an instrument or sport. Studies have identified structural and functional differences in the brains of experienced M&As compared to non-M&As, specifically in regions engaged in consistent skill training (Herholz and Zatorre, 2012; Duru and Balcioglu, 2018). Pantev et al. (1998) showed brain responses to piano tones were 25% larger in musicians than in non-musicians, with larger effects for tones from each musician's specific instrument. Another study found that skilled pianists demonstrated a rapid increase in motor cortex activation relative to non-musicians when performing a novel tapping task during a single fMRI scan (Hund-Georgiadis and von Cramon, 1999). Athletes also demonstrate this use-dependent plasticity phenomenon. One study using MRI found that golf experts engage less brain area than novices during a motor planning task, suggesting less recruitment necessary due to greater synaptic efficiency in skilled golfers (Milton et al., 2007). These changes in function are associated with changes in structure as evidenced by increased gray matter volume in hand areas of the motor cortex for handball players and increased gray matter volume in foot areas for ballet dancers (Meier et al., 2016). These results appear to suggest that motor learning maps onto generally associated regions of the motor cortex.

Transcranial magnetic stimulation (TMS) has been widely used to study motor cortex plasticity. 10-Hz repetitive TMS (rTMS) stimulation may induce long-term potentiation (LTP; Vlachos et al., 2012; Lenz et al., 2015; Brown et al., 2022), a form of synaptic plasticity which is critically dependent upon n-methyl-d-aspartate (NMDA) receptors (Huang et al., 2007). In humans, LTP-like processes can be assessed indirectly with quantitative neurophysiology and pharmacology capable of enhancing or diminishing key receptor activity while delivering rTMS. More specifically, 10-Hz rTMS to the motor cortex can increase MEP amplitudes (Maeda et al., 2000; Jung et al., 2008; Hoogendam et al., 2010) by enhancing LTP-like plasticity (Brown et al., 2020, 2021; Kweon et al., 2022). Plasticity induction is not unique to concurrent NMDA activation and 10-Hz rTMS, but has also been demonstrated with transcranial direct current stimulation (tDCS), transcranial alternating current stimulation (tACS), quadripulse stimulation (QPS), and continuous and intermittent theta burst stimulation (c/iTBS) including modified protocols [cTBS(mod)], to name a few, as reviewed in Brown et al. (2022) and Suppa et al. (2022). Importantly, MEPs utilize a corticomotor pathway to hand muscles that have been strengthened in M&As through motor skill training. M&As have demonstrated greater plasticity induction as measured by MEPs and recruitment (input-output) curves after paired-associative stimulation (PAS; Rosenkranz et al., 2007; Kumpulainen et al., 2015). We, therefore, hypothesized that subjects who routinely engaged in extensive motor learning and practice would have greater plasticity than those who did not. We present a secondary covariate analysis examining M&A status from a replication study (Kweon et al., 2022) designed to determine whether 10-Hz rTMS increases MEP amplitude through LTP-like mechanisms by assessing whether NMDA receptor agonism with d-cycloserine was sufficient to further enhance MEPs, as shown previously (Brown et al., 2020).

2. Materials and methods

We analyzed results from 10 healthy adults (six women, 21–39 years old) from a randomized, double-blind, crossover study, as described previously (Kweon et al., 2022). In that study, subjects received a single dose of either 100 mg dose of D-cycloserine (DCS, an NMDA receptor partial agonist) or placebo, then the other capsule, in random order, at least 1 week apart. We collected baseline MEP (bins of 20 single- or paired-pulse jittered 4–7 s apart) measures ∼1 h after dosing, followed by the rTMS plasticity protocol ∼2 h after dosing, and finally, post-rTMS MEP measures, as shown in **Figure 1A**. All subjects were right-handed.

All TMS single-pulses and rTMS pulse trains were delivered with the PowerMag stimulator system (Mag and More, Germany). Briefly, 10-Hz rTMS was delivered at 80% of the resting motor threshold in 1.5 s trains with 58.5 s rest for 20 min (300 pulses). All pulses were neuronavigated within 0.5 mm of the left motor cortex (M1) (Brainsight, Rogue Research, Quebec, Canada). Procedures for obtaining resting motor threshold (rMT) were described in the original study (Kweon et al., 2022). We collected one bin of 40 single-pulses (SP) at 120% rMT, and one SP at every percent intensity from 20% to 100% of maximum machine stimulator output in randomized order fit to a Boltzmann sigmoidal recruitment curve (RC). Pulses were jittered at 4–7 s intervals. Paired pulses were separated by inter-stimulus interval of 3 ms for SICI and 15 ms for ICF conditioning stimulus (CS), with a subthreshold intensity (80% rMT) and the testing stimulus (TS) of 120% rMT. LICI consisted of two pulses at 120% rMT spaced 100 ms apart.

As a part of our demographic questionnaire, we asked participants if they were an "experienced musician or athlete" who currently practiced said skill. Those who selected "yes" were asked to record the number of years and hours per week they spent practicing. Four of the 10 participants identified as a musician or athlete, with an average length of practice of 14.5 years, and a range of 4–6 h per week (**Table 1**).

As before, we analyzed SP data over a 1-h time course, normalized to baseline, using a mixed repeated measure analysis of variance (ANOVA). We examined the effects of drug, time, and drug-time interaction, controlling for order in the crossover design. Given the small sample size, we could not assume normality; therefore, a Kruskal-Wallis test was used to compare differences at baseline and each post-rTMS time point between the four drug (DCS, placebo) × group (M&A, non-M&A) conditions. The

10.3389/fncir.2023.1124221

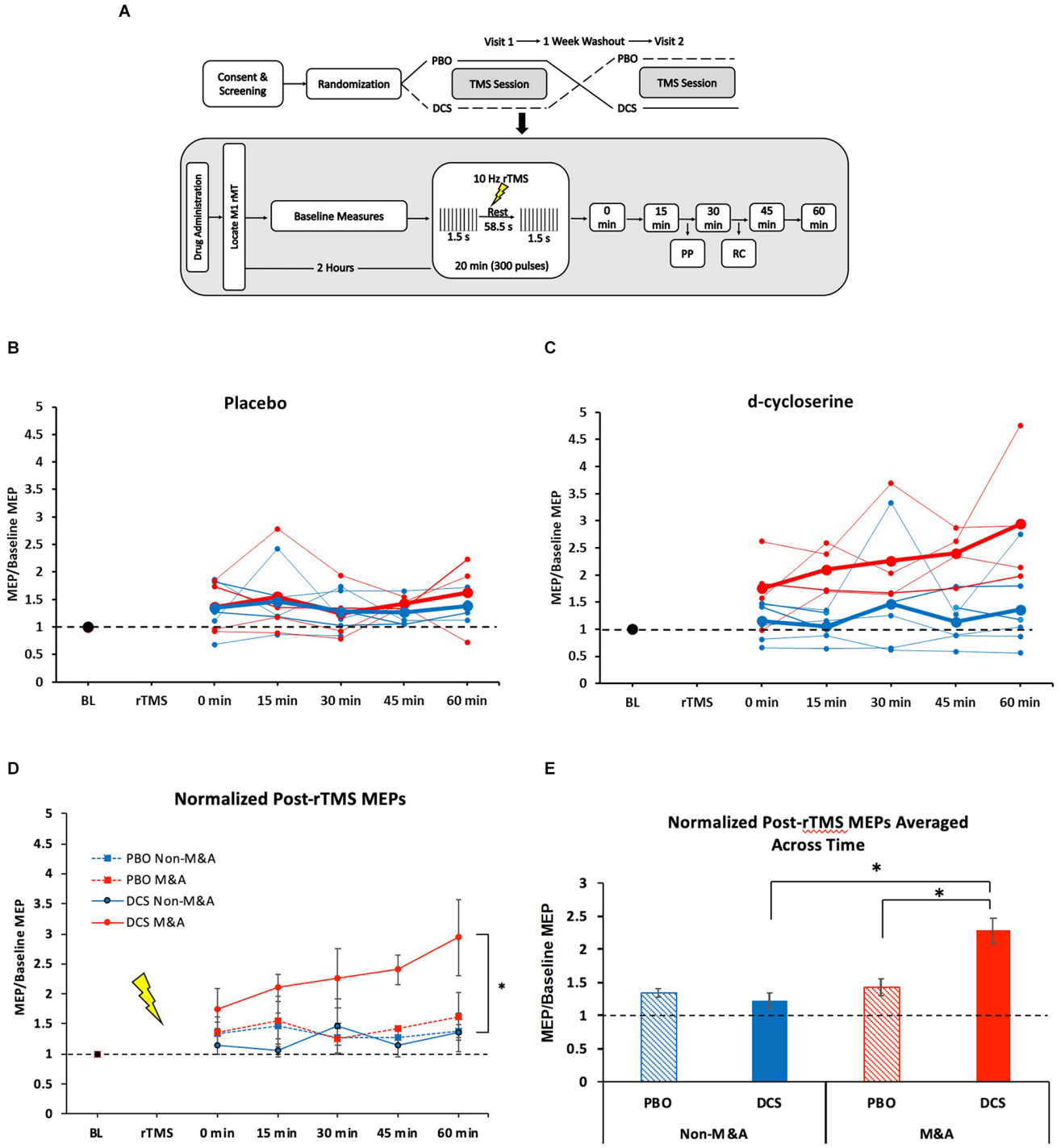

FIGURE 1
NMDA receptor partial agonist D-cycloserine (DCS) enhances 10-Hz rTMS-induced motor-evoked potentials (MEPs) exclusively for Musicians and Athletes. **(A)** Study design. Top: Overview of full experiment. Below: TMS session protocol. Baseline measures include SP, PP, and RC. MT and SP bins were recorded at every 15-min post-rTMS time points. **(B)** Individual subject MEP values for each time point after 10-Hz rTMS for placebo condition. Blue = Non-M&As, Red = M&As. Group averages are in bold. **(C)** Individual subject MEP values for each time point after 10-Hz rTMS for d-cycloserine condition. Blue = Non-M&As, Red = M&As. Group averages are in bold. **(D)** Averaged (normalized to baseline) MEP values with standard error of the mean (error bars) for each time point after 10-Hz rTMS for all conditions: 0 min: Non-M&As (1.15 ± 0.14), M&As (1.75 ± 0.34), $H_{(3)} = 3.06$, $p = 0.383$; 15 min: Non-M&As (1.06 ± 0.11), M&As (2.1 ± 0.23), $H_{(3)} = 7.69$, $p = 0.053$; 30 min: Non-M&As (1.47 ± 0.45), M&As (2.26 ± 0.49), $H_{(3)} = 4.93$, $p = 0.024$; 45 min: Non-M&As (1.14 ± 0.18), M&As (2.4 ± 0.24), $H_{(3)} = 9.48$, $p = 0.024$; 60 min: Non-M&As (1.37 ± 0.32), M&As (2.94 ± 0.64), $H_{(3)} = 6.70$, $p = 0.082$. **(E)** Normalized MEP values averaged across time with standard error of the mean (error bars) for all conditions: PBO Non-M&As (1.35 ± 0.07), DCS Non-M&As (1.23 ± 0.12), PBO M&As (1.43 ± 0.12), DCS M&As (2.29 ± 0.019). *$p < 0.05$. PBO, Placebo; DCS, D-cycloserine; SP, single-pulse; PP, paired-pulse; RC, recruitment curve; rMT, resting motor threshold; rTMS, repetitive Transcranial Magnetic Stimulation; MEPs, motor-evoked potentials; M&As, Musicians and Athletes; ICF, intracortical facilitation.

TABLE 1 Characteristics of musicians/athletes.

Musician/Athlete	Male (M)/Female (F)	Age (years)	Instrument/Sport	Number of Years	Practice intensity (hours/week)
1	F	39	Piano	33	4
2	F	35	Piano	8	4.5
3	F	28	Guitar	4	4.5
4	F	22	Volleyball	14	6

overall effect was also analyzed with a Kruskal-Wallis test of the grand average of all post-rTMS MEP amplitudes (across time) between the four conditions. Paired-pulse (PP) measures were derived from a ratio of PP/SP, and these ratios were compared before and after rTMS to generate a percent change, as described previously (Brown et al., 2021). The Kruskal-Wallis test was used to compare averages across the four conditions. Mann-Whitney U test was used to analyze characteristics between groups and visits (i.e., age, motor threshold). Recruitment curves were fitted with the Levenberg-Marquard nonlinear least-mean squares algorithm to fit raw data to a Boltzmann sigmoidal function using Signal software (Cambridge Electronic Devices, UK) as before (Kweon et al., 2022). Wilcoxon signed-rank test compared the change in recruitment curve intercept, slope, and height before and after rTMS and between drug conditions. Analyses were performed with R software (R core team, Vienna, Austria). We set *a priori* level of significance at $p < 0.05$.

3. Results

We found no differences between Non-M&As and M&As regarding age [U ($N_{Non\text{-}M\&As}$ = 6, $N_{M\&As}$ = 4) = 7.5, p = 0.39] or resting motor threshold (rMT) averaged across the two visits [U ($N_{Non\text{-}M\&As}$ = 6, $N_{M\&As}$ = 4) = 32, p = 0.23]. We also found no difference in baseline MEPs between Non-M&As and M&As in either drug condition (Kruskal-Wallis, $H_{(3)}$ = 7.02, p = 0.07; **Supplementary Figure 1A**).

3.1. Single pulse time course

Figures 1B,C displays individual subject MEP values for each time point after 10-Hz rTMS by drug condition. In the placebo condition, M&As did not differ from non-M&As by group ($F_{(1,4)}$ = 0.87, p = 0.404), time ($F_{(4,16)}$ = 0.53, p = 0.713), or interaction ($F_{(4,16)}$ = 1.93, p = 0.155), as shown in **Figure 1D**. There was a group effect when taking DCS, however, with M&As having greater normalized MEP amplitudes repeated across time compared with Non-M&As ($F_{(1,4)}$ = 7.8, p = 0.027, η^2 = 0.40; **Figure 1D**), without a definitive effect of time ($F_{(4,16)}$ = 2.5, p = 0.06) or group-by-time interaction ($F_{(4,16)}$ = 0.97, p = 0.44).

Grand averages of all normalized time points across the four conditions yielded a marked increase for M&A with DCS ($H_{(3)}$ = 29.23, $p < 0.001$; **Figure 1E**), including direct comparisons between drug conditions for M&As [U (N_{PBO} = 19, N_{DCS} = 20) = 63, $z = -3.57$, $p < 0.001$], and between M&As and non-M&As within the DCS condition [U ($N_{Non\text{-}M\&As}$ = 29, $N_{M\&As}$ = 20) = 62, $Z = -4.64$, $p < 0.001$].

3.2. Paired pulse

We did not detect a difference with our small sample size in the degree of ICF change before and after rTMS between the four combinations of drug × group ($H_{(2)}$ = 1.079, p = 0.583, **Supplementary Figures 2A,D**). We also detected no differences in SICI measures ($H_{(3)}$ = 1.541, p = 0.673, **Supplementary Figures 2B,E**), or LICI measures ($H_{(3)}$ = 1.512, p = 0.680, **Supplementary Figures 2C,F**).

3.3. Recruitment curve

We did not detect any differences in recruitment curve intercepts, slopes, or heights either between conditions or before and after rTMS. We did find a trend-level decrease in intercept after rTMS for M&As in the DCS condition ($z = -1.826$, p = 0.068, **Supplementary Figure 3**).

4. Discussion

These data appear to be consistent with our hypothesis that motor learning can enhance the capacity to respond to plasticity-inducing events. Specifically, we observed that 10-Hz rTMS + d-cycloserine robustly increased MEPs over 1-h for M&As. We also observed that trend level increases in intracortical facilitation and excitatory shifts in recruitment curves. However, it is important to note that these results are from a post-hoc covariate analysis from a small sample size of 10 subjects (20 visits), and therefore we cannot reach conclusions, but we present these data to assist in future study design. This limitation acknowledged, we speculate on what these results, if true, might mean with implications for repetitious practice and plasticity (i.e., rTMS, psychotherapy, rehabilitation, etc.).

DCS has previously been shown to enhance the excitatory effects of 10-Hz rTMS on MEPs in healthy participants (Brown et al., 2020; Kweon et al., 2022), purportedly through NMDA receptor agonism. LTP requires NMDA receptor activity (Brown et al., 2022), as do the LTP-like changes found in animal hippocampal slices after 10-Hz repetitive magnetic stimulation (Vlachos et al., 2012). More specifically, LTP (and learning) can be enhanced by increasing NMDA activity, as demonstrated in transgenic mice overexpressing an NMDA receptor subunit (Tang et al., 1999, 2001). Thus, the enhancement of 10-Hz rTMS-induced MEPs through d-cycloserine augmentation may reasonably be thought to enact LTP-like mechanisms by associating NMDA receptor activation with neuronal stimulation. Extensive motor practice in M&As incorporates the long-term effects of increased

learning, which is known to be subserved by NMDA-receptor dependent LTP (Whitlock et al., 2006; Brown et al., 2021). The applicability of these results outside of the motor cortex and healthy subjects has been supported by Cole and colleagues who found that DCS was sufficient to enhance both motor physiology (Cole et al., 2021), and clinical outcomes in depressed patients (Cole et al., 2022).

Interestingly, baseline MEPs for M&As showed a trend-level decrease (see **Supplementary Figure 1A**). If true, this would suggest that M&As do not have higher baseline corticomotor excitability, but rather with *a greater capacity to undergo change*, the definition of plasticity (Brown et al., 2022). To speculate further on the molecular mechanism of these changes, we can consider what is known from animal studies. Baseline excitability (synaptic transmission) is mediated primarily by α-amino-3-hydroxy-5-methyl-4-isoxazolepropionic acid (AMPA) receptors (Muller et al., 1988). Increased excitability is mediated by an acute increase in the GluA1 subtype of AMPA receptors (Brown et al., 2022) which has already been demonstrated to occur with 10-Hz magnetic stimulation (Vlachos et al., 2012) and learning (Whitlock et al., 2006). NMDA receptors, on the other hand, are not important for baseline transmission but are critical for governing AMPA receptor trafficking into the synapse, that is, LTP (Brown et al., 2021). If we extrapolate these animal-level findings to M&As, it may be that M&As have less M1 AMPA receptors at baseline, but can quickly upregulate AMPA receptors possibly as a result of increased NMDA receptors. This appears plausible given that LTP upregulates NMDA receptor expression, and that this is necessary for subsequent learning (Yang et al., 2022). Increased NMDA receptors in M&As would indicate a greater capacity to induce LTP with appropriate synaptic activation.

In promoting plasticity induction, it is often tempting to apply the expression "more is better". However, with non-invasive brain stimulation, we often see this is not the case. Rather, an inverted U-shape curve indicates a "sweet spot" for much of plasticity induction (Caulfield and Brown, 2022). In fact, in many cases, more stimulation may reverse results, such as by doubling iTBS pulse numbers (Gamboa et al., 2010). It is not yet known whether protocols involving DCS could be further enhanced. We administered a single session of 300 pulses. It remains to be seen whether plasticity induction could be further increased with clinical protocols involving 3,000 pulses for 36 sessions, or if mechanisms would be invoked and effects reversed (Thomson and Sack, 2020). This may explain the long-term depression (LTD)-like effects seen with 600 pulses of iTBS with DCS (Teo et al., 2007). While this would seem counterintuitive in the acute sense, chronic learning or repeated LTP would engage homeostatic plasticity mechanisms which effectively serve to prevent ceiling effects (saturation) and enable continuous learning through whole-neuron AMPA receptor expression reduction while still retaining relative synaptic strength (Turrigiano, 2012). Homeostatic metaplasticity may also explain our observation that M&As trended towards lower baseline MEPs, theoretically reflecting a decrease in AMPA receptors, but an increase in NMDA receptors (Yang et al., 2022), which do not mediate most of baseline synaptic transmission (Muller et al., 1988). Whether homeostatic AMPA receptor removal and LTP-induced NMDA receptor upregulation is independent of one another, or possibly connected in the same manner that GluA2 receptors replace GluA1 receptors (Shi et al., 2001) is an intriguing question. Regardless, if MEP excitability is mediated by AMPA receptors, these results appear consistent with M&As having decreased AMPA receptors at baseline, while the marked increase as a result of a plasticity protocol may be orchestrated by increased NMDA receptors from mature synapses.

These data provide preliminary support that repeated learning (as experienced by M&As) may enhance synaptic plasticity (Rosenkranz et al., 2007; Kumpulainen et al., 2015) induced by 10-Hz rTMS and NMDA receptor activation. However, a larger sample size is necessary to reach conclusions, and a prospective study design (examining before and after musical/athletic training) would be needed to determine causality (i.e., whether increased plasticity is produced by learning or whether people with innately enhanced plasticity are more likely to become M&As). Furthermore, our sample included three types of instruments and sports, which likely activate plasticity in various brain regions to different extents. This is both a limitation of our *post-hoc* naturalistic study design as well as valuable information regarding the generalizability of motor practices on specific muscle groups. Future studies may determine how generalizable these changes are by comparing, for example, pianists and violinists. We have speculated about underlying mechanisms which can only be guessed at without parallel human and animal experimental designs. M&As may have driven previously reported differences following 10-Hz rTMS (Brown et al., 2020), and may contribute to the high inter-individual variability frequently found in MEP studies (Corp et al., 2020, 2021). Of broader interest is whether motor network learning translates to other networks, such as those theoretically targeted with dorsolateral prefrontal cortex rTMS for depression. It is tempting to consider whether prior extensive application of psychotherapeutic techniques (enhancing plasticity capacity of relevant circuits) promotes responsiveness to clinical rTMS, or whether rTMS alone accomplishes this in responders. These preliminary results suggest that learning may facilitate LTP-like activity in relevant neural circuits with implications for therapeutic contexts like stroke rehabilitation, cognitive-behavioral therapy, or clinical rTMS.

Data availability statement

The raw data supporting the conclusions of this article will be made available by the authors, without undue reservation.

Ethics statement

The studies involving human participants were reviewed and approved by Care New England-Butler Hospital Institutional Review Board. The patients/participants provided their written informed consent to participate in this study.

Author contributions

JK collected data and wrote the manuscript. MV collected data and significantly contributed to the manuscript. RJ provided

statistics support and manuscript edits. JB as principal investigator and head of lab, significantly contributed to manuscript. LC as head of the transcranial magnetic stimulation clinic provided equipment and resources as well as manuscript edits. All authors contributed to the article and approved the submitted version.

Funding

Research reported in this publication was supported by the National Institute of General Medical Sciences of the National Institutes of Health under award number P20GM130452 and Center for Biomedical Research Excellence, Center for Neuromodulation.

Acknowledgments

We would like to thank Frances Kronenberg and Luke Acuff for their editorial support.

Conflict of interest

The authors declare that the research was conducted in the absence of any commercial or financial relationships that could be construed as a potential conflict of interest.

Publisher's note

All claims expressed in this article are solely those of the authors and do not necessarily represent those of their affiliated organizations, or those of the publisher, the editors and the reviewers. Any product that may be evaluated in this article, or claim that may be made by its manufacturer, is not guaranteed or endorsed by the publisher.

Supplementary material

The Supplementary Material for this article can be found online at: https://www.frontiersin.org/articles/fncir.2023.1124221/full#supplementary-material.

References

Adkins, D. L., Boychuk, J., Remple, M. S., and Kleim, J. A. (2006). Motor training induces experience-specific patterns of plasticity across motor cortex and spinal cord. *J. Appl. Physiol. (1985)* 101, 1776–1782. doi: 10.1152/japplphysiol.00515.2006

Brown, J. C., DeVries, W. H., Korte, J. E., Sahlem, G. L., Bonilha, L., Short, E. B., et al. (2020). NMDA receptor partial agonist, d-cycloserine, enhances 10 Hz rTMS-induced motor plasticity, suggesting long-term potentiation (LTP) as underlying mechanism. *Brain Stimul.* 13, 530–532. doi: 10.1016/j.brs.2020.01.005

Brown, J. C., Higgins, E. S., and George, M. S. (2022). Synaptic plasticity 101: the story of the AMPA receptor for the brain stimulation practitioner. *Neuromodulation* 25, 1289–1298. doi: 10.1016/j.neurom.2021.09.003

Brown, J. C., Yuan, S., DeVries, W. H., Armstrong, N. M., Korte, J. E., Sahlem, G. L., et al. (2021). NMDA-receptor agonist reveals LTP-like properties of 10-Hz rTMS in the human motor cortex. *Brain Stimul.* 14, 619–621. doi: 10.1016/j.brs.2021.03.016

Caulfield, K. A., and Brown, J. C. (2022). The problem and potential of TMS' infinite parameter space: a targeted review and road map forward. *Front. Psychiatry* 13:867091. doi: 10.3389/fpsyt.2022.867091

Christiansen, L., Larsen, M. N., Madsen, M. J., Grey, M. J., Nielsen, J. B., and Lundbye-Jensen, J. (2020). Long-term motor skill training with individually adjusted progressive difficulty enhances learning and promotes corticospinal plasticity. *Sci. Rep.* 10:15588. doi: 10.1038/s41598-020-72139-8

Cole, J., Selby, B., Ismail, Z., and McGirr, A. (2021). D-cycloserine normalizes long-term motor plasticity after transcranial magnetic intermittent theta-burst stimulation in major depressive disorder. *Clin. Neurophysiol.* 132, 1770–1776. doi: 10.1016/j.clinph.2021.04.002

Cole, J., Sohn, M. N., Harris, A. D., Bray, S. L., Patten, S. B., and McGirr, A. (2022). Efficacy of adjunctive D-Cycloserine to intermittent theta-burst stimulation for major depressive disorder: a randomized clinical trial. *JAMA Psychiatry* 79, 1153–1161. doi: 10.1001/jamapsychiatry.2022.3255

Corp, D. T., Bereznicki, H. G. K., Clark, G. M., Youssef, G. J., Fried, P. J., Jannati, A., et al. (2021). Large-scale analysis of interindividual variability in single and paired-pulse TMS data. *Clin. Neurophysiol.* 132, 2639–2653. doi: 10.1016/j.clinph.2021.06.014

Corp, D. T., Bereznicki, H. G. K., Clark, G. M., Youssef, G. J., Fried, P. J., Jannati, A., et al. (2020). Large-scale analysis of interindividual variability in theta-burst stimulation data: results from the "big TMS data collaboration". *Brain Stimul.* 13, 1476–1488. doi: 10.1016/j.brs.2020.07.018

Duru, A. D., and Balcioglu, T. H. (2018). Functional and structural plasticity of brain in elite karate athletes. *J. Healthc. Eng.* 2018:8310975. doi: 10.1155/2018/8310975

Gamboa, O. L., Antal, A., Moliadze, V., and Paulus, W. (2010). Simply longer is not better: reversal of theta burst after-effect with prolonged stimulation. *Exp. Brain Res.* 204, 181–187. doi: 10.1007/s00221-010-2293-4

Greenough, W. T., Larson, J. R., and Withers, G. S. (1985). Effects of unilateral and bilateral training in a reaching task on dendritic branching of neurons in the rat motor-sensory forelimb cortex. *Behav. Neural Biol.* 44, 301–314. doi: 10.1016/s0163-1047(85)90310-3

Herholz, S. C., and Zatorre, R. J. (2012). Musical training as a framework for brain plasticity: behavior, function and structure. *Neuron* 76, 486–502. doi: 10.1016/j.neuron.2012.10.011

Hoogendam, J. M., Ramakers, G. M. J., and Di Lazzaro, V. (2010). Physiology of repetitive transcranial magnetic stimulation of the human brain. *Brain Stimul.* 3, 95–118. doi: 10.1016/j.brs.2009.10.005

Huang, Y.-Z., Chen, R.-S., Rothwell, J. C., and Wen, H.-Y. (2007). The after-effect of human theta burst stimulation is NMDA receptor dependent. *Clin. Neurophysiol.* 118, 1028–1032. doi: 10.1016/j.clinph.2007.01.021

Hund-Georgiadis, M., and von Cramon, D. Y. (1999). Motor-learning-related changes in piano players and non-musicians revealed by functional magnetic-resonance signals. *Exp. Brain Res.* 125, 417–425. doi: 10.1007/s002210050698

Jung, S. H., Shin, J. E., Jeong, Y.-S., and Shin, H.-I. (2008). Changes in motor cortical excitability induced by high-frequency repetitive transcranial magnetic stimulation of different stimulation durations. *Clin. Neurophysiol.* 119, 71–79. doi: 10.1016/j.clinph.2007.09.124

Kleim, J. A., Lussnig, E., Schwarz, E. R., Comery, T. A., and Greenough, W. T. (1996). Synaptogenesis and Fos expression in the motor cortex of the adult rat after motor skill learning. *J. Neurosci.* 16, 4529–4535. doi: 10.1523/JNEUROSCI.16-14-04529.1996

Kumpulainen, S., Avela, J., Gruber, M., Bergmann, J., Voigt, M., Linnamo, V., et al. (2015). Differential modulation of motor cortex plasticity in skill- and endurance-trained athletes. *Eur. J. Appl. Physiol.* 115, 1107–1115. doi: 10.1007/s00421-014-3092-6

Kweon, J., Vigne, M., Jones, R., George, M. S., Carpenter, L. L., and Brown, J. C. (2022). A replication study of NMDA receptor agonism sufficiency to enhance 10-Hz rTMS-induced motor cortex plasticity. *Brain Stimul.* 15, 1372–1374. doi: 10.1016/j.brs.2022.09.014

Lenz, M., Platschek, S., Priesemann, V., Becker, D., Willems, L. M., Ziemann, U., et al. (2015). Repetitive magnetic stimulation induces plasticity of excitatory postsynapses on proximal dendrites of cultured mouse CA1 pyramidal neurons. *Brain Struct. Funct.* 220, 3323–3337. doi: 10.1007/s00429-014-0859-9

Maeda, F., Keenan, J. P., Tormos, J. M., Topka, H., and Pascual-Leone, A. (2000). Modulation of corticospinal excitability by repetitive transcranial magnetic stimulation. *Clin. Neurophysiol.* 111, 800–805. doi: 10.1016/s1388-2457(99)00323-5

Meier, J., Topka, M. S., and Hanggi, J. (2016). Differences in cortical representation and structural connectivity of hands and feet between professional handball players and ballet dancers. *Neural Plast.* 2016:6817397. doi: 10.1155/2016/6817397

Milton, J., Solodkin, A., Hlustik, P., and Small, S. L. (2007). The mind of expert motor performance is cool and focused. *Neuroimage* 35, 804–813. doi: 10.1016/j.neuroimage.2007.01.003

Monfils, M.-H., Plautz, E. J., and Kleim, J. A. (2005). In search of the motor engram: motor map plasticity as a mechanism for encoding motor experience. *Neuroscientist* 11, 471–483. doi: 10.1177/1073858405278015

Muller, D., Joly, M., and Lynch, G. (1988). Contributions of quisqualate and NMDA receptors to the induction and expression of LTP. *Science* 242, 1694–1697. doi: 10.1126/science.2904701

Pantev, C., Oostenveld, R., Engelien, A., Ross, B., Roberts, L. E., and Hoke, M. (1998). Increased auditory cortical representation in musicians. *Nature* 392, 811–814. doi: 10.1038/33918

Rosenkranz, K., Williamon, A., and Rothwell, J. C. (2007). Motorcortical excitability and synaptic plasticity is enhanced in professional musicians. *J. Neurosci.* 27, 5200–5206. doi: 10.1523/JNEUROSCI.0836-07.2007

Shi, S., Hayashi, Y., Esteban, J. A., and Malinow, R. (2001). Subunit-specific rules governing AMPA receptor trafficking to synapses in hippocampal pyramidal neurons. *Cell* 105, 331–343. doi: 10.1016/s0092-8674(01)00321-x

Suppa, A., Asci, F., and Guerra, A. (2022). Transcranial magnetic stimulation as a tool to induce and explore plasticity in humans. *Handb. Clin. Neurol.* 184, 73–89. doi: 10.1016/B978-0-12-819410-2.00005-9

Tang, Y. P., Shimizu, E., Dube, G. R., Rampon, C., Kerchner, G. A., Zhuo, M., et al. (1999). Genetic enhancement of learning and memory in mice. *Nature* 401, 63–69. doi: 10.1038/43432

Tang, Y. P., Wang, H., Feng, R., Kyin, M., and Tsien, J. Z. (2001). Differential effects of enrichment on learning and memory function in NR2B transgenic mice. *Neuropharmacology* 41, 779–790. doi: 10.1016/s0028-3908(01)00122-8

Teo, J. T. H., Swayne, O. B., and Rothwell, J. C. (2007). Further evidence for NMDA-dependence of the after-effects of human theta burst stimulation. *Clin. Neurophysiol.* 118, 1649–1651. doi: 10.1016/j.clinph.2007.04.010

Thomson, A. C., and Sack, A. T. (2020). How to design optimal accelerated rTMS protocols capable of promoting therapeutically beneficial metaplasticity. *Front. Neurol.* 11:599918. doi: 10.3389/fneur.2020.599918

Turrigiano, G. (2012). Homeostatic synaptic plasticity: local and global mechanisms for stabilizing neuronal function. *Cold Spring Harb. Perspect. Biol.* 4:a005736. doi: 10.1101/cshperspect.a005736

Vlachos, A., Muller-Dahlhaus, F., Rosskopp, J., Lenz, M., Ziemann, U., and Deller, T. (2012). Repetitive magnetic stimulation induces functional and structural plasticity of excitatory postsynapses in mouse organotypic hippocampal slice cultures. *J. Neurosci.* 32, 17514–17523. doi: 10.1523/JNEUROSCI.0409-12.2012

Whitlock, J. R., Heynen, A. J., Shuler, M. G., and Bear, M. F. (2006). Learning induces long-term potentiation in the hippocampus. *Science* 313, 1093–1097. doi: 10.1126/science.1128134

Yang, X., Gong, R., Qin, L., Bao, Y., Fu, Y., Gao, S., et al. (2022). Trafficking of NMDA receptors is essential for hippocampal synaptic plasticity and memory consolidation. *Cell Rep.* 40:111217. doi: 10.1016/j.celrep.2022.111217

frontiers | Frontiers in Neural Circuits

TYPE Original Research
PUBLISHED 05 April 2023
DOI 10.3389/fncir.2023.1120410

OPEN ACCESS

EDITED BY
Kevin Caulfield,
Medical University of South Carolina, United States

REVIEWED BY
Luis Hernandez-Garcia,
University of Michigan, United States
Daniel McCalley,
Stanford University, United States

*CORRESPONDENCE
Taylor Kuhn
✉ tkuhn@mednet.ucla.edu

†These authors have contributed equally to this work

RECEIVED 09 December 2022
ACCEPTED 14 March 2023
PUBLISHED 05 April 2023

CITATION
Kuhn T, Spivak NM, Dang BH, Becerra S, Halavi SE, Rotstein N, Rosenberg BM, Hiller S, Swenson A, Cvijanovic L, Dang N, Sun M, Kronemyer D, Berlow R, Revett MR, Suthana N, Monti MM and Bookheimer S (2023) Transcranial focused ultrasound selectively increases perfusion and modulates functional connectivity of deep brain regions in humans. *Front. Neural Circuits* 17:1120410. doi: 10.3389/fncir.2023.1120410

Transcranial focused ultrasound selectively increases perfusion and modulates functional connectivity of deep brain regions in humans

Taylor Kuhn[1]*, Norman M. Spivak[1,2,3†], Bianca H. Dang[1†], Sergio Becerra[1], Sabrina E. Halavi[1], Natalie Rotstein[1], Benjamin M. Rosenberg[4], Sonja Hiller[1], Andrew Swenson[5], Luka Cvijanovic[5], Nolan Dang[1], Michael Sun[6], David Kronemyer[1], Rustin Berlow[7], Malina R. Revett[1], Nanthia Suthana[1,2,4,8], Martin M. Monti[1,2,4] and Susan Bookheimer[1]

[1]Department of Psychiatry and Biobehavioral Sciences, University of California, Los Angeles, Los Angeles, CA, United States, [2]Department of Neurosurgery, University of California, Los Angeles, Los Angeles, CA, United States, [3]UCLA-Caltech Medical Scientist Training Program, Los Angeles, CA, United States, [4]Department of Psychology, University of California, Los Angeles, Los Angeles, CA, United States, [5]Neuroscience Interdepartmental Program, University of California, Los Angeles, Los Angeles, CA, United States, [6]Department of Psychological and Brain Sciences, Dartmouth College, Hanover, NH, United States, [7]American Brain Stimulation Clinic, Del Mar, CA, United States, [8]Department of Bioengineering, University of California, Los Angeles, Los Angeles, CA, United States

Background: Low intensity, transcranial focused ultrasound (tFUS) is a re-emerging brain stimulation technique with the unique capability of reaching deep brain structures non-invasively.

Objective/Hypothesis: We sought to demonstrate that tFUS can selectively and accurately target and modulate deep brain structures in humans important for emotional functioning as well as learning and memory. We hypothesized that tFUS would result in significant longitudinal changes in perfusion in the targeted brain region as well as selective modulation of BOLD activity and BOLD-based functional connectivity of the target region.

Methods: In this study, we collected MRI before, simultaneously during, and after tFUS of two deep brain structures on different days in sixteen healthy adults each serving as their own control. Using longitudinal arterial spin labeling (ASL) MRI and simultaneous blood oxygen level dependent (BOLD) functional MRI, we found changes in cerebral perfusion, regional brain activity and functional connectivity specific to the targeted regions of the amygdala and entorhinal cortex (ErC).

Results: tFUS selectively increased perfusion in the targeted brain region and not in the contralateral homolog or either bilateral control region. Additionally, tFUS directly affected BOLD activity in a target specific fashion without engaging auditory cortex in any analysis. Finally, tFUS resulted in selective modulation of the targeted functional network connectivity.

Conclusion: We demonstrate that tFUS can selectively modulate perfusion, neural activity and connectivity in deep brain structures and connected networks. Lack

of auditory cortex findings suggests that the mechanism of tFUS action is not due to auditory or acoustic startle response but rather a direct neuromodulatory process. Our findings suggest that tFUS has the potential for future application as a novel therapy in a wide range of neurological and psychiatric disorders associated with subcortical pathology.

KEYWORDS

transcranial focused ultrasound, functional connectivity, brain perfusion, amygdala, entorhina cortex

Introduction

Non-invasive methods for treating psychiatric and neurological disorders by modulating neural activity in humans include techniques such as transcranial magnetic stimulation (TMS) (Barker et al., 1985) and transcranial direct current stimulation (tDCS) (Perlson, 1945). However, these techniques are limited by their inability to target deep brain regions (e.g., amygdala or hippocampus (HC)), which are currently only effectively modulated by invasive, higher-risk deep brain stimulation (DBS) (Obeso et al., 2001). Here, we provide initial evidence that low intensity transcranial focused ultrasound (tFUS) can non-invasively modulate neural activity in the human amygdala and hippocampus by measuring changes in cerebral blood perfusion using arterial spin labeling (ASL) magnetic resonance imaging (MRI) and functional connectivity (FC) during simultaneous tFUS and blood oxygenation level dependent (BOLD) functional MRI (fMRI).

Focused ultrasound has recently been explored as a novel neuromodulation technology (Pasquinelli et al., 2019; Toccaceli et al., 2019; Stern et al., 2021). At high intensities, ultrasound can be used to cause ablations (e.g., for neurosurgical pallidotomy) (Moosa et al., 2019). Low intensity tFUS can penetrate the skull and dura (Hynynen and Jolesz, 1998), thereby affecting neuron populations in the brain, likely through cellular modulation (Tufail et al., 2011). By changing the parameters of the ultrasound such as pulse repetition frequency and duty cycle, it is possible to create potentiating or disruptive effects at the network level (Spivak et al., 2022), without also causing tissue damage via the heating effects seen at higher intensities (Schafer et al., 2021). Consequently, tFUS can circumvent the limitations of current neuromodulation techniques while maintaining high safety levels (Pasquinelli et al., 2019).

tFUS is thought to modulate neural activity either via mechanical stretching or neuronal intramembrane cavitation excitation (NICE). The mechanical stretching model suggests that tFUS physically stretches the cell soma resulting in membrane depolarization by way of voltage gated ion channel influx (Morris and Juranka, 2007; Tyler et al., 2008; Kubanek et al., 2016). Many ion channels have been shown to be influenced by ultrasonic stimulation, including mechanosensitive two-pore-domain potassium channels (Kubanek et al., 2016), and channels not typically classified as mechanosensitive (i.e., sodium and calcium voltage-gated channels) (Morris and Juranka, 2007). Alternatively, the NICE model proposes that tFUS causes spaces to form and disappear between the hydrophobic tails of the phospholipids comprising the cell bilayer (Plaksin et al., 2016). The law of conservation of charge establishes that greater distance between the charges (inside and outside the cell) results in greater electric potential, thereby changing the membrane potential. Whether this change is potentiating (akin to tDCS) or directly modulating (akin to TMS) is as of yet unclear.

Regardless of its precise mechanism, early histology and animal studies of tFUS demonstrate reversible physiologic effects on neuron clusters such as dentate gyrus and CA1 subregions (Tyler et al., 2008). Such effects include increased neuronal and astrocytic ionic conductance resulting in amplified cellular and synaptic activity, as measured by whole-cell patch clamps and confocal imaging of *ex vivo* neural cell cultures subjected to low intensity ultrasound (Tyler et al., 2008). Using real-time fMRI of macaque monkeys, tFUS produced transient disruption FC between the amygdala and its functional network (Folloni et al., 2019). In humans, tFUS has been shown to modulate BOLD signal in sensorimotor cortex (Ai et al., 2016), primary motor cortex (Ai et al., 2016, 2018), primary visual cortex (Lee et al., 2016) as well as the right inferior frontal gyrus and its functional network (Sanguinetti et al., 2020). Recently, tFUS in humans has been shown to modulate BOLD signal in basal ganglia regions including the globus pallidus (Cain et al., 2021b) and caudate (Ai et al., 2016), as well as the thalamus (Li et al., 2021) with associated changes in subjective reporting of pain and level of consciousness. When targeting a different thalamic nucleus, tFUS also appears to affect levels of consciousness in coma patients (Monti et al., 2016; Cain et al., 2021a). Importantly, nearly all of these studies compared BOLD signal before and after tFUS rather than reporting real-time changes in network connectivity during tFUS sonication. Neuroimaging data acquired simultaneously with tFUS administration is critical to maximize the likelihood of precise targeting of brain regions and engagement of their functional networks (Spivak and Kuhn, 2019). To our knowledge, no other studies report effects of tFUS on perfusion, BOLD or FC of the amygdala or entorhinal cortex (ErC) in humans. The capacity to successfully and non-invasively target and modulate these deep brain regions has wide-ranging implications for clinical neuromodulation

of disorders involving anxiety, emotion regulation, learning and memory.

Non-invasive TMS has a large clinical effect size for Major Depressive Disorder (MDD), Posttraumatic Stress Disorder (PTSD), Obsessive-Compulsive Disorder (OCD) and Generalized Anxiety Disorder (GAD) (Cirillo et al., 2019). TMS, however, is unable to directly target deep brain structures such as the amygdala, which prior studies suggest is a meaningful target for treating anxiety disorders. Rather, TMS and tDCS indirectly engage deep brain regions via downstream modulation achieved by targeting dorsal cortical regions that are functionally connected to those deep targets. DBS of the amygdala has been shown to reduce hypervigilance in rodent models of PTSD (Langevin et al., 2010; Stidd et al., 2013). Additionally, in a single human patient with PTSD, DBS of the amygdala resulted in increased pleasant memories and regulated sleep (Langevin et al., 2016). The demonstrated potential of DBS to modulate amygdalar activity and associated behavior provides promise for similar findings in non-invasive tFUS.

Similarly, DBS of the ErC improved memory in a small sample of patients with Alzheimer's disease (AD) (Suthana et al., 2012; Suthana and Fried, 2014). In rodent models, direct stimulation of the perforant pathway—the afferent connections arising from the ErC projecting to the dentate gyrus and CA1 region of the HC—enhanced memory and HC neurogenesis (Toda et al., 2008). Similar findings have been reported using theta burst electrical stimulation in the ErC and perforant pathway area prior to learning, which improved subsequent memory (Titiz et al., 2017). Replicating these ErC DBS findings using tFUS would be a major advancement in non-invasive brain stimulation therapies for amnestic syndromes such as amnestic mild cognitive impairment (aMCI) and AD.

In the present study, we administered tFUS simultaneously with BOLD fMRI to examine brain circuit modulation in two key deep brain structures: the amygdala, implicated in many anxiety and mood disorders (Fox and Shackman, 2019), and the ErC, implicated in memory formation (Montchal et al., 2019) and impaired episodic memory in AD (Gómez-Isla et al., 1996; Olajide et al., 2021). Similar to the macaque study (Folloni et al., 2019) and directly related to our goal of disrupting amygdala connectivity, we used a sonication paradigm intended to inhibit/disrupt (Spivak et al., 2022) amygdala activity. Conversely, we also used a sonication paradigm hypothesized to excite/stimulate (Spivak et al., 2022) the ErC with the goal of increasing ErC connectivity. In order to ensure accurate targeting and engagement of the target brain region, we used longitudinal arterial spin labeling (ASL) MRI to quantify tFUS-related perfusion changes in the targeted brain regions.

Hypotheses

This study sought to demonstrate proof-of-principle evidence that tFUS can evidence target-specific brain perfusion and functional connectivity changes indicative of neuromodulation. We were able to perform perfusion MRI before and after tFUS. Because tFUS is MRI compatible, we were also able to collect resting state FC MRI simultaneously during tFUS administration. We performed tFUS on a group of sixteen healthy aging adults targeting both regions (amygdala and ErC) two weeks apart, order counterbalanced and data collected and examined blindly, to determine the effect on perfusion, regional brain activity and associated FC (**Figure 1**). We expected that we would see tFUS-induced 1) increased perfusion only in the targeted brain region and not the control region 2) changes in brain function measured using BOLD associated with tFUS and 3) modulation of FC of the targeted region and its functionally connected regions.

Results

tFUS-related increased regional perfusion

Within-subject, partial volume corrected ASL MRI demonstrated increased perfusion in the region of the brain targeted by tFUS as compared to the control region. When sonicating the right amygdala, increased perfusion was found in the sonicated amygdala (Cohen's d: 0.97, mean ASL signal change = 19.52%; $SD_{ROI} = 0.93$, $SD_{sample} = 0.38$, $p < 0.001$; **Figure 2**) and not in the left ErC (Cohen's d: 0.2; mean ASL signal change = 6.72%; $SD_{ROI} = 0.34$, $SD_{sample} = 0.29$, $p > 0.1$) or right ErC (Cohen's d: 0.11; mean ASL signal change = 1.13%; $SD_{ROI} = 0.33$, $SD_{sample} = 0.26$, $p > 0.1$). Similarly, when sonicating the left ErC, increased left ErC perfusion (Cohen's d: 0.8; mean ASL signal change = 15.75%; $SD_{ROI} = 1.02$, $SD_{sample} = 0.23$, $p < 0.001$; **Figure 2**) without increased right amygdala (Cohen's d: 0.08; mean ASL signal change = 7.07%; $SD_{ROI} = 0.35$, $SD_{sample} = 0.25$, $p > 0.1$) or left amygdala perfusion (Cohen's d: 0.05; mean ASL signal change = 3.35%; $SD_{ROI} = 0.35$, $SD_{sample} = 0.17$, $p > 0.1$) was found. Additionally, significantly increased perfusion was found only in the targeted brain structure ipsilateral to the tFUS transducer and not in the contralateral homologue region. Specifically, the sonicated right amygdala evidenced increased perfusion following sonication (as described above) while the left amygdala, which was not targeted, did not display a significant change in perfusion (Cohen's d: 0.31; mean ASL signal change = 10.48%; $SD_{ROI} = 0.72$, $SD_{sample} = 0.23$, $p > 0.1$). Similarly, only the targeted left ErC, and not the right ErC, evidenced statistically significant tFUS-related increased perfusion (Cohen's d: 0.1; mean ASL signal change = 8.24%; $SD_{ROI} = 0.77$, $SD_{sample} = 0.36$, $p > 0.1$). Further, statistically significantly increased (all p's < 0.001) perfusion was observed in regions known to be functionally connected to the targeted areas. Amygdala-focused tFUS increased amygdala and medial prefrontal cortex (PFC) perfusion (Cohen's d: 0.32); mean ASL signal change = 11.63%). ErC-focused tFUS increased ErC perfusion as well as perfusion in the HC (Cohen's d: 0.17; mean ASL signal change = 6.20%), anterior cingulate (Cohen's d: 0.26; mean ASL signal change = 14.42%), and bilateral basal ganglia regions including the thalamus (Cohen's d: 0.26; mean ASL signal change = 14.38%).

FIGURE 1
Study design. A visual representation of the randomized, double-blind, within-subject crossover study design. Participants completed two study visits, separated by a 14-day between-session window. During each session, participants underwent a baseline MRI assessment of regional blood flow using Arterial Spin Labeling (ASL) MRI. Thereafter, participants received tFUS in the MRI with simultaneously collected blood oxygenation level-dependent (BOLD) MRI. After tFUS was administered, ASL was collected again to compare to baseline. The brain region targeted during each study session was randomized and counterbalanced across participants such that 47% received amygdala tFUS during the first study session and 53% received ErC tFUS during their first session. Examples of amygdala and ErC tFUS targeting are provided, as well as a chart detailing sample demographics.

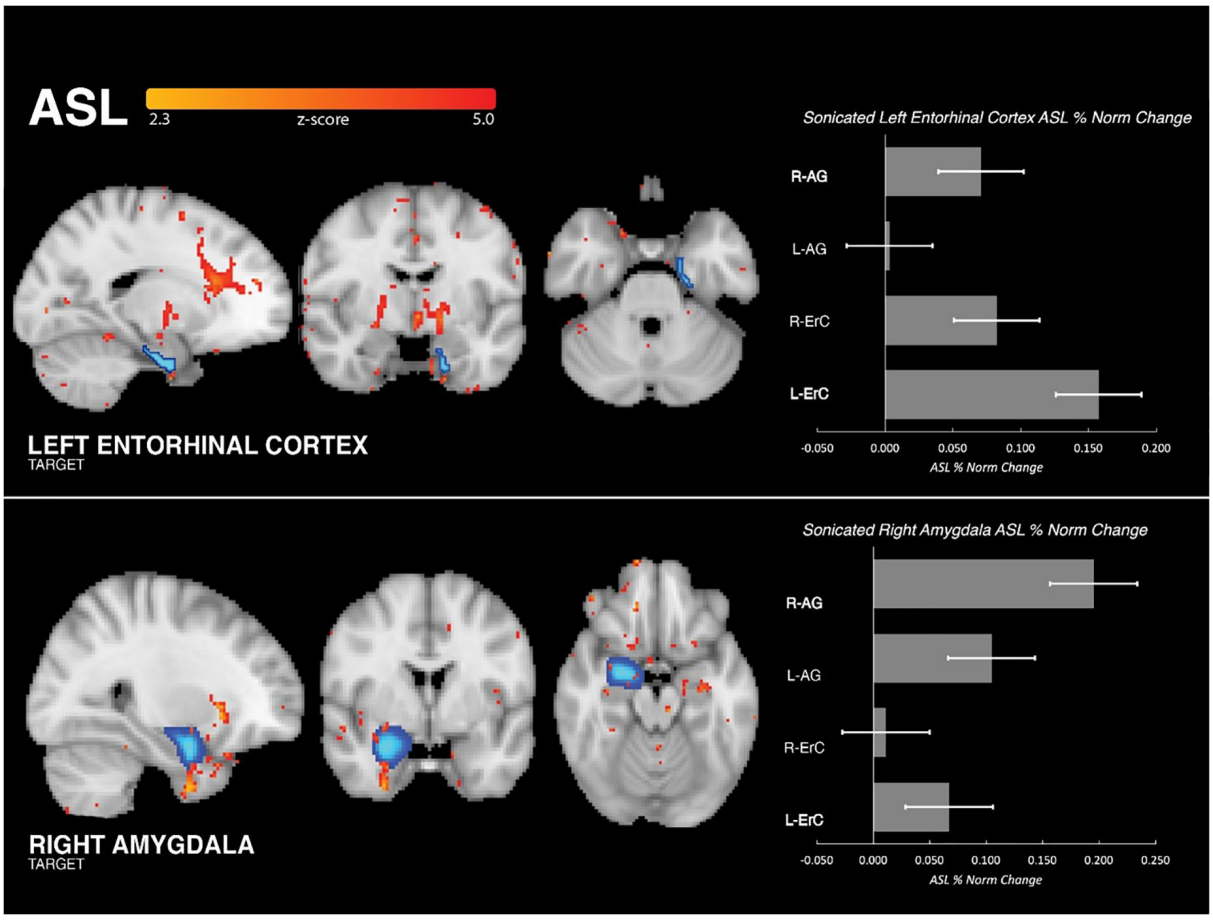

FIGURE 2
Group perfusion findings. **(Left Column)** Analysis of ASL MRI demonstrated that tFUS was associated with significant increase in perfusion to the targeted region and not the control region (i.e., when targeting ErC, increased perfusion to ErC and not amygdala, and vice versa). Increased perfusion was also seen in functionally connected regions. For ErC: anterior cingulate cortex, medial prefrontal cortex and basal ganglia regions including anterior thalamus. For amygdala: medial prefrontal cortex and ventral forebrain. **(Right Column)** Bar graph illustrating the mean, normalized percent perfusion change associated with tFUS in the four regions of interest: right amygdala, left amygdala, right entorhinal cortex, left entorhinal cortex. When sonicating the left ErC, increased perfusion was found in the sonicated left ErC and not the right ErC or bilateral amygdala. Similarly, when sonicating the right amygdala increased perfusion was found in the sonicated right amygdala and not the left amygdala or bilateral ErC.

tFUS-related brain activation

Functional BOLD MRI data was collected at the same time as tFUS sonication. The main effect of tFUS on brain activity was modeled using a traditional block-design paradigm matching the alternating 30s blocks during which the transducer was on and off. The results of this analysis (**Figure 3**) revealed that tFUS targeting the right amygdala resulted in significantly decreased BOLD activity in the amygdala, posterior cingulate, supplemental motor area cortex, dorsolateral prefrontal cortex and pons. There were no areas of significantly increased BOLD when targeting the right amygdala (all FDR-corrected p-values > 0.05).

When targeting the left ErC, tFUS was associated with significantly increased BOLD in small areas of the ErC, temporo-occipito-parietal junction, occipital cortex and right cerebellum. Additionally, left ErC tFUS was associated with significantly reduced BOLD in anterior frontal, anterior temporal including entorhinal/parahippocampal areas, and posterior parietal cortices. Importantly, neither amygdala or ErC analysis revealed significant or trending towards significant changes in BOLD in either auditory cortex (all FDR-corrected p values > 0.05), suggesting that these effects were indeed due to a neuromodulatory effect of tFUS and not due to an auditory startle response (as shown by Guo et al. (2018) and Sato et al. (2018)) or an acoustic reaction to bone conduction from the vibration of the transducer (Dobrev et al., 2017). For both targets, all participants demonstrated positive correlations between their unique individual BOLD changes and the group changes, which is to say that all participants demonstrated BOLD changes in the expected direction consistently with the group findings.

tFUS-related network connectivity changes

For each participant, a standard MNI152 atlas mask of the targeted brain region was used as the seed region for a psychophysiological interaction analysis (PPI), which shows regions of modulated connectivity between brain areas during sonication but not during rest. PPI analyses were conducted for each perfusion seed (amygdala and ErC) on the BOLD data collected simultaneously with the tFUS sonication experiment. By analyzing the PPI of both sonication target seeds, regional specificity of FC changes was assessed. As such, one seed corresponded to the brain region targeted by tFUS during the BOLD acquisition, and the other seed corresponded to the brain region targeted during the other tFUS session (control region). As a second control analysis, we also ran PPI analyses using the target seed on the BOLD data collected when targeting the control region.

Sonicating the right amygdala, group PPI analysis (**Figure 3**) revealed tFUS-related decreased FC between the right amygdala and posterior cingulate, anterior cingulate, medial prefrontal and posterior parietal regions. Using the ErC as a control region, we confirmed that these tFUS-evoked FC changes were specific to the right amygdala. Importantly, PPI analysis of the BOLD data collected when targeting the amygdala using an ErC seed did not yield any significant FC changes associated with the ErC (all p's > 0.05 FDR corrected). Similarly, PPI analyses conducted using the BOLD acquired during ErC tFUS with the amygdala seed did not yield any amygdala-related FC changes (all FDR-corrected p-values > 0.05).

Group PPI analysis of data collected when sonicating the left ErC revealed tFUS-related increased connectivity between the left ErC and left dorsolateral prefrontal cortex (**Figure 3**). Again importantly, PPI analyses using the above amygdala seed applied to the BOLD data collected while the ErC was sonicated did not yield any amygdala-related FC changes (all p's > 0.05 FDR corrected). Finally, PPI analyses conducted using the BOLD acquired during amygdala tFUS with the ErC seed did not yield any ErC-related FC changes (all FDR-corrected p-values > 0.05).

Across all PPI analyses, there was no significant effect found in the auditory cortex (all FDR-corrected p-values > 0.05). For both targets, all participants demonstrated positive correlations between their unique individual PPI-based functional connectivity changes and the group changes, which is to say that all participants demonstrated connectivity changes in the expected direction consistently with the group findings.

Discussion

In these investigations we combined tFUS with ASL MRI and simultaneous BOLD fMRI to examine the impact of focused ultrasound on deep brain areas of the human brain. The results indicate differential impacts of tFUS on amygdala and ErC perfusion, BOLD activity and FC. The findings suggest that tFUS can preferentially increase regional blood flow and modulate network connectivity of subcortical regions, potentially in a desired direction. tFUS sonication parameters hypothesized to disrupt activity yielded decreased FC in the amygdala network including prefrontal cortex, cingulate and brainstem. Conversely, tFUS sonication parameters hypothesized to increase functional activity resulted in generally, though not exclusively, increased BOLD activity and FC in the targeted ErC and its network (e.g. HC). tFUS of the ErC also activated visual regions, likely through the integration of visual input through the ErC via efferent downstream projections (Schultz et al., 2015). Interestingly, both tFUS protocols resulted in increased perfusion in the targeted brain region - not the control region nor the contralateral homolog of the targeted region. This double dissociation in perfusion and FC supports our hypothesis that the modulatory effects of tFUS are focal and directly related to the targeted region. Supporting the conclusion that these findings were due to neuromodulatory effects of tFUS, none of our analyses found engagement of the auditory cortex. Indeed, no participant reported any auditory or visual effects during sonication. Without evidence of auditory cortex activation associated with tFUS, it is unlikely that our findings are related to auditory startle response (38) or acoustic reactions to bone conduction (39). Effective targeting of tFUS is critical for successful modulation of the desired brain region(s) and associated cognitive and/or affective functions and ASL. fMRI appears to be an effective way to measure target engagement in the brain. The present findings suggest that ASL is an effective method of confirming engagement of tFUS-targeted brain regions.

This study also supports prior ones which found that tFUS can be used to modulate BOLD activity in cortical and subcortical regions (Ai et al., 2016, 2018; Lee et al., 2016; Monti et al., 2016;

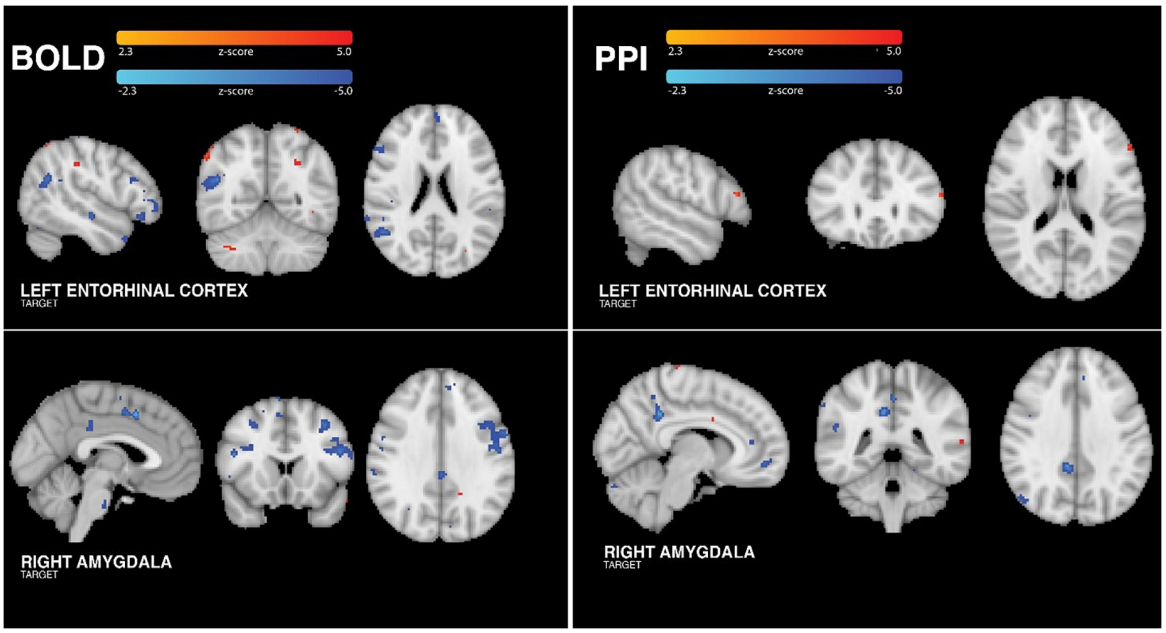

FIGURE 3
Group BOLD findings. **(Left Column)** Analysis of tFUS on BOLD showed significantly increased activity in small areas of the temporo-occipito-parietal junction, occipital cortex and right cerebellum. Additionally, left ErC tFUS was associated with significantly reduced BOLD in anterior frontal, anterior temporal, and posterior parietal cortices. tFUS targeting the right amygdala resulted in significantly decreased BOLD activity in the posterior cingulate, pre-sensorimotor cortex, dorsolateral prefrontal cortex and pons. **(Right Column)** When sonicating the ErC, group PPI analysis revealed tFUS-related increased connectivity between the left ErC and left dorsolateral prefrontal cortex. Group PPI analysis of data collected when sonicating the amygdala revealed tFUS-related decreased FC between the right amygdala and posterior cingulate, anterior cingulate, medial prefrontal and posterior parietal regions. PPI control analyses confirmed that these findings were specific to the target region.

Sanguinetti et al., 2020; Cain et al., 2021a,b; Li et al., 2021), adding the amygdala and entorhinal cortex to the list of deep brain regions that can be modulated with tFUS. However, our findings were not directionally consistent with those of Cain et al., who sonicated the thalamus using the 100Hz paradigm (ErC) and the 10 Hz paradigm (amygdala). Cain et al. found reduced perfusion and FC using the same sonication parameters as we used when targeting the ErC (100Hz) and no FC changes using the parameters we used when targeting the amygdala (10Hz). These different findings are possibly due to the differences in vasculature (e.g., thalamostriate vs. major/middle cerebral arteries) and connectivity of the thalamus compared to the medial temporal lobe structures in the present study. Further, our findings contribute to this literature by providing additional evidence that tFUS selectively increases regional perfusion while modulating both regional activity and functional connectivity. These results extend the possible clinical applications of tFUS by confirming the ability of tFUS to engage deep brain regions in humans important for emotion regulation as well as memory formation and retrieval. Our amygdala sonication results closely align with those of the amygdala tFUS study conducted in macaques (Folloni et al., 2019), which was influential to the design of this project. Interestingly, those investigators found that the tFUS-related FC changes persisted for the 80-minute duration of their resting state fMRI (rs-fMRI) assessment. It will be important to determine the duration of tFUS effects in humans for the design of clinical trials and eventual clinical implementation of tFUS. Additional work in a larger sample with varying time windows between tFUS application and post-tFUS evaluation also is required.

The differential effects of amygdala tFUS present an opportunity for further investigation of non-invasive techniques for the treatment of anxiety disorders and other psychiatric pathologies. For example, it seems likely that the timing of amygdala tFUS will be relative to the acquisition, generalization and extinction of fear and anxiety. If tFUS can disrupt the new learning of fear, then it may be useful in emergency departments to help lessen the severity of or prevent the development of PTSD. Alternatively, if tFUS is able to accelerate the extinction of previously learned fear, then it could be an adjunctive treatment for patients with already established anxiety-related syndromes such as GAD, PTSD, Social Anxiety Disorder (SAD), panic disorder, or OCD. tFUS may offer a treatment for "treatment-resistant" anxiety and mood disorders. Further work in this area will be important to determine the extent to which tFUS is a viable "affective neural prosthetic" for interventional use in psychiatric disorders.

Similarly, tFUS of the ErC could be a meaningful non-invasive intervention for diseases affecting learning and memory, such as MCI and AD. As with the amygdala, further research is needed to determine the optimal timing for ErC sonication. One study in humans found improvement in spatial memory performance when DBS to the entorhinal cortex was administered during learning trials (Suthana et al., 2012). It's possible that tFUS may have an enhanced effect on learning and subsequent memory when sonication is applied concurrently during the initial learning and/or retrieval of memory events. The sonication parameters used in this study hypothesized to excite/engage the ErC network resulted in both increased and decreased BOLD and functional connectivity. Further exploration of ErC tFUS

sonication parameters and sonication-to-stimuli timing protocol, as well as ErC tFUS effects in participants with learning and memory disorders, is needed to validate and optimize tFUS as a non-invasive cognitive prosthetic tool.

No adverse events occurred during this study. Participants were followed every day for three days following each tFUS session and exhibited no negative reactions, including physical discomfort or heightened anxiety. Given its nascency in humans, it will be important to monitor these and other pertinent safety variables. A recently published review of the current findings on tFUS safety in humans and animals reported that adverse events following tFUS are rare, occurring only in studies that administered tFUS at intensities above the currently approved limit for use in humans (Pasquinelli et al., 2019). With FDA approval and oversight, one group recently administered tFUS to temporal lobe in patients with intractable temporal lobe epilepsy scheduled for surgical resection of the epileptogenic tissue of the temporal lobe (Stern et al., 2021). Histological examination following excision of the previously sonicated tissue did not indicate any tissue damage, including thermal or cavitation effects, following tFUS intensities up to eight times higher than that used in this study. Another study sonicating prepared slices of brain tissue saw no damage until intensities nearly 20x the intensities used in present study (Spivak et al., 2021). These outcomes support a conclusion that low intensity tFUS does not work via a thermal or tissue damaging cavitation mechanism, and is safe for use in humans. Additional safety work is needed to further establish safety guidelines for clinical use across a variety of patient populations, brain targets and clinical use cases.

The preliminary nature of this study entails limitations shared by all early-stage studies of novel technology. One limitation is that the somewhat small sample size leads to decreased statistical power. However, the moderate to large effect sizes of the tFUS-related brain changes indicate that the study was sufficiently powered to detect changes in perfusion, BOLD activity and functional connectivity, at both the group and single-participant level. Further, the sample comprised only individuals undergoing healthy aging. It did not compare tFUS effects between healthy individuals and those with neurologic and psychiatric disorders associated with the targeted brain regions (e.g., GAD, PTSD, and AD). Additionally, during the simultaneous tFUS-BOLD analysis, an assumption underlying the statistical PPI model was that tFUS resulted in instantaneous effects on the BOLD signal which were appropriately modeled using a block design which followed the on-off blocks of the sonication administration. It is possible that effect of tFUS builds up over time and therefore an evolving matrix, rather than an on-off block, model would be more appropriate. However, to our knowledge, this is not yet known in the field and our attempts generate, using our data, an empirical model of tFUS effects other than this block design were unsuccessful. Therefore, currently, the block design appeared to be the best model. However, larger-scale future analyses should further investigate this possibility. Similarly, longitudinal BOLD analyses are warranted to help determine the time scale of the tFUS effects on functional connectivity. The macaque study that informed the amygdala portion of the present study demonstrated ongoing FC effects of tFUS throughout the 2 hour duration of the BOLD study.

The purposes of this study were to demonstrate the feasibility of an alternative to other more invasive and less effective treatments for neurologic and psychiatric disorders affecting learning, memory, anxiety and emotion regulation, and to suggest directions for further research. Other research has shown that tFUS can reliably target desired areas of the deep brain without engaging nearby structures. For example, the ErC and amygdala lie within 1cm of one another in the brain, yet neither was affected by targeting the other. That being so, it is unclear whether all participants were stimulated in the exact same sub-region within the amygdala and ErC. Even though perfusion data suggested that the majority of the targeted brain region was sonicated, given that sub-regional activation may vary subject-to-subject, further work is necessary to enhance targeting precision and more fully understand the impact of tFUS on regional subnuclei. In this vein, the amygdala is a larger target region than the ErC and therefore the sonication likely effected a different proportion of target tissue. Advances in focal beam technology and the impact of varying sonication shapes and sizes will likely assist in the effective clinical implementation of tFUS technology.

Materials and methods

Study design

Participants completed two experimental sessions conducted exactly two weeks apart. Pre-tFUS, simultaneous-tFUS, and post-tFUS MRI data were collected during each experimental session. tFUS was performed in the MRI scanner and targeted one brain region per experimental session: one session targeting the right amygdala and one targeting the left ErC (**Figure 1**). The order of the brain regions targeted by tFUS was randomized and counterbalanced across participants. Participants were blinded to which brain region was sonicated during each session; they were only aware that the tFUS transducer was placed on the left side of their head during one session (ErC) and the right side of their head during the other session (amygdala). Study staff performing statistical analyses were blinded to the tFUS target associated with the data. For MRI data, this involved masking the data so that the tFUS transducer could not be seen on the images prior to beginning the processing pipeline. As such, the design was a double-blind randomized, within-subjects crossover clinical trial. Prior to participant enrollment and data collection, both studies were registered in the National Clinical Trials archive (ClinicalTrials.gov, 2018a,b).

Demographics

From twenty-one screened adults, eighteen healthy adults were recruited for this study. Due to motion artifacts rendering some MRI data unusable, two participants were removed from analyses, yielding a final sample size of sixteen healthy aging adults. These participants were, on average, 61.38 (7.75) years old, 56% female, and were 37% Caucasian American, 31% Latinx American, 19% African American and 13% Asian American. Given our group's plan to expand the ErC tFUS protocol into studies involving participant populations with neurodegenerative diseases, healthy aging adults were specifically recruited for this project.

Screening procedures

All procedures were in accordance with the Declaration of Helsinki and approved by the University of California, Los Angeles (UCLA) Institutional Review Board prior to enrollment. All participants provided written informed consent. Screening protocols were adapted from the study Mapping the Human Connectome During Typical Aging (Bookheimer et al., 2019) to obtain a sample representative of healthy adult aging. Included in this screening was a set of questions ensuring safety to undergo MRI examination. Potential participants were excluded for prior diagnosis and/or treatment of major psychiatric disorders (e.g., schizophrenia, bipolar disorder), neurological disorders (e.g., stroke, brain tumors, Parkinson's Disease), or severe depression that required treatment for 12 months or longer in the past five years. In individuals 60 years and older, potential participants were excluded based on impaired cognitive abilities as assessed by a cognitive screener: the Telephone Interview for Cognitive Status modified (TICS-M) (Knopman et al., 2010). To be eligible for the study, potential participants were required to score 30 or greater on the TICS-M, after adjusting for educational background. After obtaining written informed consent, the Montreal Cognitive Assessment (Nasreddine et al., 2005) was administered to ensure that participants who did not earn the minimum score for their age bracket were excluded from the study.

MRI-guided tFUS targeting

The tFUS sonications were delivered using a single-element transducer placed above the ear at the temporal window, one of the thinnest parts of the skull bone, and targeted using real-time structural MRI navigation inside the MRI. tFUS of the amygdala used sonication parameters hypothesized to decrease or disrupt activity in the sonicated emotion region. This was modeled in part off of the Foloni study in Macaques (Folloni et al., 2019) and was done based on the hypothesis that disruption of amygdala and its functional network may serve as the foundation for investigating tFUS clinical applications in anxiety disorders. tFUS of the ErC used sonication parameters hypothesized to increase activity in the targeted memory region. This was based on the hypothesis, based in part on our collaborators work in ErC DBS (Suthana et al., 2012; Suthana and Fried, 2014), that stimulation of the ErC may lead to improved learning and memory. Both paradigms used a 5% duty cycle, in 10 cycles of 30 s on, 30 s off, for a total of 5 min of non-consecutive tFUS (**Figure 4**). The paradigm targeting the amygdala used a 5 ms pulse width repeated at a 10 Hz pulse repetition frequency (PRF), while the paradigm targeting the ErC used a 0.5 ms pulse width repeated at a 100 Hz PRF. In both instances, the fundamental frequency was 0.65 MHz and the $I_{spta.3}$ was 720 mW/cm^2, which was determined by applying the derating equation with a derating factor of 0.3 dB/cm-MHz. Prior testing using cadaveric skulls in degassed water has shown that the skull acts to broaden the −6dB focal width by 1.5 mm and lengthen the −6dB axial focal length by 1.4 mm with a minimal lateral shift of less than 1mm (Schafer et al., 2021).

tFUS was performed inside the MRI scanner using typical targeting approaches for low intensity tFUS (Spivak and Kuhn, 2019). This involved a 30-s SCOUT imaging sequence to visualize the tFUS transducer and its orthogonal line of targeting into the brain. The tFUS transducer had a focal sonication depth of 65 mm (BrainSonix Corp., Sherman Oaks, CA, USA (Schafer et al., 2021)). The MRI scanning console computer was used to visualize the transducer and, using fiducial markers built into the transducer, a line orthogonal to the center of the transducer was drawn on screen into the brain at 65 mm depth from the interface of the transducer

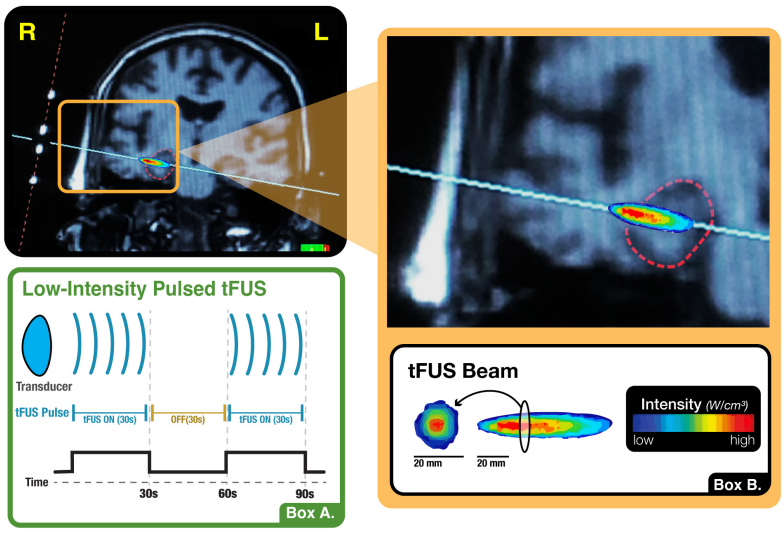

FIGURE 4
tFUS paradigm. **(A)** Illustration of the present study's sonication block design, wherein the transducer alternated between 30-s blocks of active stimulation and no stimulation. This cycle occurred ten times, totaling five minutes of non-consecutive tFUS. **(B)** Visualization of the shape, orientation and intensity distribution of the tFUS beam. When measured in a water tank using a hydrophone, the tFUS beam appears ellipsoid in shape with a central focus of higher intensity and a surround of lower intensity. The longitudinal dimension is approximately 2 cm in length while the cross section, which also evidences a higher intensity centroid, is approximately 0.5 cm in diameter.

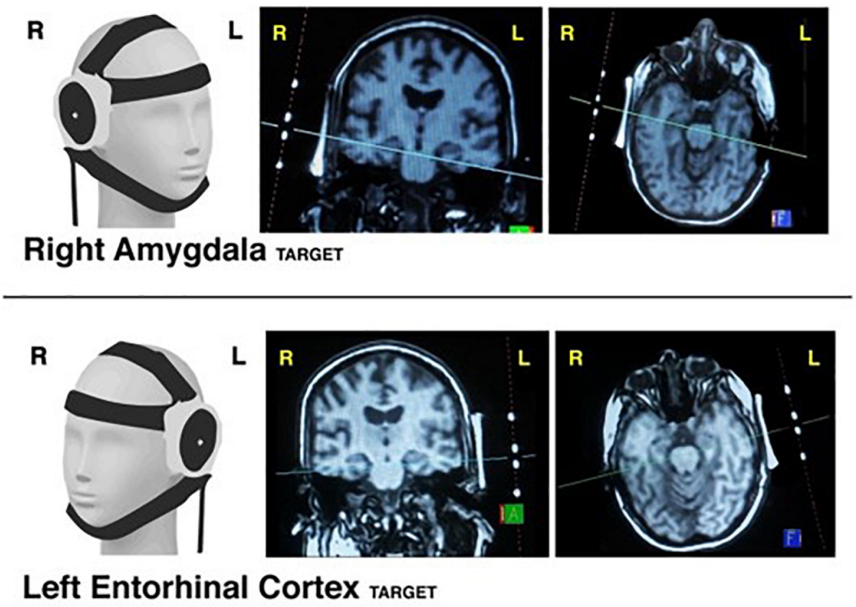

FIGURE 5
tFUS targeting. Visualization of transducer placement on 3D model (1st column) when targeting the right amygdala **(Top Row)** and left entorhinal cortex **(Bottom Row)**. Examples of MRI-console guided targeting using transducer fiducial markers are provided in coronal view (2nd column) and axial view (3rd column).

and gel pad (Figure 5). The transducer was then manually moved as necessary to correct its position such that the targeted brain region was ultimately confirmed via SCOUT MRI as either the right amygdala or left ErC. Specifically, we attempted to target the centromedian aspect of the amygdala by aiming the targeting line through the middle of the body of the amygdala. We attempted to target the interface of the ErC and the perforant pathway by aiming the orthogonal line through the central axis of the angular bundle, which carries the perforant pathway, and subsequently the central region of the ErC.

Neuroimaging acquisition

All MRI data were collected using a 3T Siemens MAGNETOM Prisma fit scanner (Siemens Medical Solution, Erlangen, Germany) located at the UCLA Center for Cognitive Neuroscience. ASL, multi-slice BOLD and T1 anatomical scans were collected from sixteen healthy aging adults. In order to accommodate the tFUS transducer into the MRI head coil, the 20-channel head coil was used for all acquisition sequences. This required minor modification to MP-RAGE scan borrowed from the Lifespan Human Connectome Project (Bookheimer et al., 2019) to ensure compatibility with the 20-channel coil (rather than 32-channel used in the HCP). ASL scans were collected before and after tFUS with a pulsed ASL sequence using 3.0 mm slices, FOV = 192 mm (AP) x 120 mm (FH), TR = 4,600 ms, TE = 16.18 ms, flip angle = 180°, bolus duration = 700 ms, inversion time = 1,990 ms, FAIR-QII Perfusion, 1 average, pre-scan normalization filter, gray, white and fat suppression filters and 1.5 mm x 1.5 mm x 3 mm voxels and total scan time of 4 min 59 s for each ASL sequence. Simultaneous tFUS BOLD data were collected using an optimized SMS GRE EPI sequence involving TR = 700 ms, TE = 33 ms, flip angle = 70°, FOV = 192 mm (AP) x 135 mm (FH) and 2.5 mm isotropic voxels with total scan time of 11 min 49 s. Framewise Integrated Real-time MRI Monitoring (FIRMM) (Dosenbach et al., 2017) was used during the collection of all BOLD data to monitor for participant motion. Prior to tFUS administration, structural MP-RAGE T1-weighted scans were acquired with 120 1.0-mm sagittal slices, FOV = 256 mm (AP) x 192 mm (FH), matrix = 256 × 192, TR = 450 ms, TE = 10 ms, flip angle = 8°, and voxel size = 1.0 mm x 0.94 mm x 0.94 mm. All images were quality controlled and visually inspected prior to being preprocessed and analyzed. The tFUS transducer was placed inside the MRI head coil for the resting state fMRI scan during which the tFUS was administered. For all other MRI sequences, the tFUS transducer was removed from the head coil and the scanner. It took approximately five minutes to extract the participant from the scanner, either place or remove the transducer, and replace the participant in the scanner.

Perfusion analysis

Pulsed Arterial Spin Labeling (PASL) scans produce a perfusion image with voxel values representing local perfusion rates. For each subject, pre-stimulation PASL images were linearly registered to each subject's T1. Perfusion images were processed by using the BASIL (Chappell et al., 2008) toolbox, includimmg partial volume correction, then transferred to MNI space using non-linear registration in FSL. Using FSL Version 6.0,[1] a voxel-wise comparison of pre-vs-post tFUS sonication was conducted individually for each subject by subtracting the registered pre-sonication perfusion map from the post-sonication perfusion map. A 2 × 2 repeated measures analysis of variance (ANOVA),

1 www.fmrib.ox.ac.uk/fsl

corrected for multiple comparisons using False Discovery Rate (FDR), compared the longitudinal perfusion changes between amygdala sonication and ErC sonication at the voxel-wise level. Results of this ANOVA are reported along with the mean and standard deviation perfusion change within each region of interest as well as across the study sample.

Simultaneous tFUS-BOLD analysis

10-minute tFUS experiments were administered as BOLD data was collected inside the MRI scanner. Sonication-synced BOLD functional data processing included motion correction to the mean image, spatial smoothing (Gaussian Kernel FWHM = 5 mm), high-pass temporal filtering ($t > 0.01$ Hz) and regression-based removal of outliers (ICA-Aroma (Pruim et al., 2015)). To examine the main effect of tFUS on BOLD, a whole brain general linear model was set up specifying the onset and duration (30s) of the tFUS sonication blocks. Resulting statistical maps estimating the voxel-wise magnitude of neural activation associated with tFUS were corrected for multiple comparisons using FDR and thresholded at $z = 2.3$ and FDR-correct $p < 0.001$.

Further, to examine tFUS-related network connectivity, a seed-based approach was used to examine whole brain connectivity with the tFUS target of interest and compare between stimulation (on-off) conditions using PPI modeling. FSL FEAT module was used to conduct these analyses. The seed regions used for this PPI analysis were right amygdala, automatically segmented from each participant's structural MRI using FSL First (Patenaude et al., 2011), and left ErC, adopted from a standard, functionally-derived atlas (Maass et al., 2015). Both ROIs were registered initially to each participant's fMRI. Group analyses were then conducted following registration of the functional data to standard MNI space. The mean time series from this seed region in the preprocessed BOLD image was extracted using fslmaths and entered as the first explanatory variable. The block-design entered as the second explanatory variable was computed from the timed on-off tFUS sonication blocks (main effect of tFUS described above). The third explanatory variable was the interaction of the tFUS-target-seed mean time series and the sonication on-off blocks. The time series variable was centered at zero and the block design was centered at the mean. The resulting statistical maps were corrected for multiple comparisons using FDR and thresholded at $z = 2.3$ and FDR-corrected $p < 0.001$. We also ran correlation analyses to determine the number of participants whose individual tFUS-related changes were associated with the group findings.

Data availability statement

The raw data supporting the conclusions of this article will be made available by the authors, without undue reservation.

Ethics statement

The studies involving human participants were reviewed and approved by UCLA IRB. The patients/participants provided their written informed consent to participate in this study.

Author contributions

TK, SBo, MM, NSu, NSp, and RB: conceptualization. TK, SBe, SBo, MM, NSu, RB, NSp, BD, and SHi: methodology. TK, SBe, NSp, BD, SHi, SBo, BR, AS, LC, MS, DK, and MR: investigation. TK, BD, SBe, SHa, and NR: visualization. TK, SBo, and MR: funding acquisition. TK, SBo, BD, and NSp: project administration. TK, SBo, NSp, BD, and MR: supervision. TK, SBe, NSp, BD, SBo, SHa, and NR: writing – original draft. All authors: writing – review and editing.

Funding

UCLA Staglin IMHRO Center for Cognitive Neuroscience Pilot Funding (TK). UCLA Semel Institute for Neuroscience and Behavior (TK). Alzheimer's Association Zenith Award ZEN-20-643042: Modulation of Hippocampal Circuitry with Focused Ultrasound in MCI (SBo and TK).

Acknowledgments

The authors would like to acknowledge the following groups and individuals for their assistance and collaboration with this project: Jared Gilbert (UCLA), Andrew W. Bismark (UCSD), Tyler Wishard (UCLA), Cory Inman (UCLA), the *BrainSonix* Corporation: (Alexander Bystritsky, MD, Ph.D.; Alexander Korb, Ph.D.; Mark E. Schafer, Ph.D.) and the *transcranial Focused Ultrasound (tFUS) Consortium* (Mark George, MD (Medical University of South Carolina); Greg Fonzo, Ph.D. (Dell Medical School); Darin Dougherty, MD (Harvard-MGH); Benjamin Greenberg, MD, Ph.D. (Brown University); Noah Philip, MD (Brown University); Wayne Goodman, MD (Baylor College of Medicine).

Conflict of interest

NSu was a consultant for BrainSonix Corporation.

The remaining authors declare that the research was conducted in the absence of any commercial or financial relationships that could be construed as a potential conflict of interest.

Publisher's note

References

Ai, L., Bansal, P., Mueller, J. K., and Legon, W. (2018). Effects of transcranial focused ultrasound on human primary motor cortex using 7T fMRI: A pilot study. *BMC Neurosci.* 19:56. doi: 10.1186/s12868-018-0456-6

Ai, L., Mueller, J. K., Grant, A., Eryaman, Y., and Legon, W. (2016). Transcranial focused ultrasound for BOLD fMRI signal modulation in humans. *Annu. Int. Conf. IEEE Eng. Med. Biol. Proc.* 38, 1758–1761. doi: 10.1109/EMBC.2016.7591057

Barker, A. T., Jalinous, R., and Freeston, I. L. (1985). Non-invasive magnetic stimulation of human motor cortex. *Lancet* 1, 1106–1107. doi: 10.1016/S0140-6736(85)92413-4

Bookheimer, S. Y., Salat, D. H., Terpstra, M., Ances, B. M., Barch, D. M., Buckner, R. L., et al. (2019). The lifespan human connectome project in aging: An overview. *Neuroimage* 185, 335–348. doi: 10.1016/j.neuroimage.2018.10.009

Cain, J. A., Visagan, S., Johnson, M. A., Crone, J., Blades, R., Spivak, N. M., et al. (2021b). Real time and delayed effects of subcortical low intensity focused ultrasound. *Sci. Rep.* 11:6100. doi: 10.1038/s41598-021-85504-y

Cain, J. A., Spivak, N. M., Coetzee, J. P., Crone, J. S., Johnson, M. A., Lutkenhoff, E. S., et al. (2021a). Ultrasonic thalamic stimulation in chronic disorders of consciousness. *Brain Stimul.* 14, 301–303. doi: 10.1016/j.brs.2021.01.008

Chappell, M. A., Groves, A. R., Whitcher, B., and Woolrich, M. W. (2008). Variational Bayesian inference for a nonlinear forward model. *IEEE Trans. Signal Process.* 57, 223–236. doi: 10.1109/TSP.2008.2005752

Cirillo, P., Gold, A. K., Nardi, A. E., and Ornelas, A. C. (2019). Transcranial magnetic stimulation in anxiety and trauma-related disorders: A systematic review and meta-analysis. *Brain Behav.* 9:e01284. doi: 10.1002/brb3.1284

ClinicalTrials.gov (2018a). *Low intensity focused ultrasound for emotion regulation (LIFUPEMOT)*. Available online at: https://clinicaltrials.gov/ct2/show/results/NCT03782194 (accessed December 17, 2018).

ClinicalTrials.gov (2018b). *Low intensity focused ultrasound for learning and memory (LIFUPMEM)*. Available online at: https://clinicaltrials.gov/ct2/show/NCT03717922 (accessed October 22, 2018).

Dobrev, I., Sim, J. H., Stenfelt, S., Ihrle, S., Gerig, R., Pfiffner, F., et al. (2017). Sound wave propagation on the human skull surface with bone conduction stimulation. *Hear. Res.* 355, 1–13. doi: 10.1016/j.heares.2017.07.005

Dosenbach, N. U. F., Koller, J. M., Earl, E. A., Miranda-Dominguez, O., Klein, R. L., Van, A. N., et al. (2017). Real-time motion analytics during brain MRI improve data quality and reduce costs. *Neuroimage* 161, 80–93. doi: 10.1016/j.neuroimage.2017.08.025

Folloni, D., Verhagen, L., Mars, R. B., Fouragnan, E., Constans, C., Aubry, J.-F., et al. (2019). Manipulation of subcortical and deep cortical activity in the primate brain using transcranial focused ultrasound stimulation. *Neuron* 101, 1109–1116. doi: 10.1016/j.neuron.2019.01.019

Fox, A. S., and Shackman, A. J. (2019). The central extended amygdala in fear and anxiety: Closing the gap between mechanistic and neuroimaging research. *Neurosci. Lett.* 693, 58–67. doi: 10.1016/j.neulet.2017.11.056

Gómez-Isla, T., Price, J. L., McKeel, D. W. Jr., Morris, J. C., Growdon, J. H., and Hyman, B. T. (1996). Profound loss of layer II entorhinal cortex neurons occurs in very mild Alzheimer's disease. *J. Neurosci.* 16, 4491–4500. doi: 10.1523/JNEUROSCI.16-14-04491.1996

Guo, H., Hamilton, M. II., Offutt, S. J., Gloeckner, C. D., Li, T., Kim, Y., et al. (2018). Ultrasound produces extensive brain activation via a cochlear pathway. *Neuron* 98, 1020–1030.e4.

Hynynen, K., and Jolesz, F. A. (1998). Demonstration of potential noninvasive ultrasound brain therapy through an intact skull. *Ultrasound Med. Biol.* 24, 275–283. doi: 10.1016/S0301-5629(97)00269-X

Knopman, D. S., Roberts, R. O., Geda, Y. E., Pankratz, V. S., Christianson, T. J. H., Petersen, R. C., et al. (2010). Validation of the telephone interview for cognitive status-modified in subjects with normal cognition, mild cognitive impairment, or dementia. *Neuroepidemiology* 34, 34–42. doi: 10.1159/000255464

Kubanek, J., Shi, J., Marsh, J., Chen, D., Deng, C., and Cui, J. (2016). Ultrasound modulates ion channel currents. *Sci. Rep.* 6:24170. doi: 10.1038/srep24170

Langevin, J. P., Chen, J. W. Y., Koek, R. J., Sultzer, D. L., Mandelkern, M. A., Schwartz, H. N., et al. (2016). Deep brain stimulation of the basolateral amygdala: Targeting technique and electrodiagnostic findings. *Brain Sci.* 6:28. doi: 10.3390/brainsci6030028

Langevin, J. P., De Salles, A. A. F., Kosoyan, H. P., and Krahl, S. E. (2010). Deep brain stimulation of the amygdala alleviates post-traumatic stress disorder symptoms in a rat model. *J. Psychiatr. Res.* 44, 1241–1245. doi: 10.1016/j.jpsychires.2010.04.022

Lee, W., Kim, H. C., Jung, Y., Chung, Y. A., Song, I.-U., Lee, J. H., et al. (2016). Transcranial focused ultrasound stimulation of human primary visual cortex. *Sci. Rep.* 6:34026. doi: 10.1038/srep34026

Li, X., Badran, B., Dowdle, L., Caulfield, K., Summers, P., Short, B., et al. (2021). Imaged-guided Transcranial focused ultrasound on the right thalamus modulates ascending pain pathway to somatosensory cortex in healthy participants. *Brain Stimul.* 14:1638. doi: 10.1016/j.brs.2021.10.160

Maass, A., Berron, D., Libby, L. A., Ranganath, C., and Düzel, E. (2015). Functional subregions of the human entorhinal cortex. *eLife* 4:e06426. doi: 10.7554/eLife.06426

Montchal, M. E., Reagh, Z. M., and Yassa, M. A. (2019). Precise temporal memories are supported by the lateral entorhinal cortex in humans. *Nat. Neurosci.* 22, 284–288. doi: 10.1038/s41593-018-0303-1

Monti, M. M., Schnakers, C., Korb, A. S., Bystritsky, A., and Vespa, P. M. (2016). Non-invasive ultrasonic thalamic stimulation in disorders of consciousness after severe brain injury: A first-in-man report. *Brain Stimul.* 9, 940–941. doi: 10.1016/j.brs.2016.07.008

Moosa, S., Martínez-Fernández, R., Elias, W. J., Del Alamo, M., Eisenberg, H. M., and Fishman, P. S. (2019). The role of high-intensity focused ultrasound as a symptomatic treatment for Parkinson's disease. *Mov. Disord.* 34, 1243–1251. doi: 10.1002/mds.27779

Morris, C. E., and Juranka, P. F. (2007). Nav channel mechanosensitivity: Activation and inactivation accelerate reversibly with stretch. *Biophys. J.* 93, 822–833. doi: 10.1529/biophysj.106.101246

Nasreddine, Z. S., Phillips, N. A., Bédirian, V., Charbonneau, S., Whitehead, V., Collin, I., et al. (2005). The Montreal cognitive assessment, MoCA: A brief screening tool for mild cognitive impairment. *J. Am. Geriatr. Soc.* 53, 695–699. doi: 10.1111/j.1532-5415.2005.53221.x

Obeso, J. A., Olanow, C. W., Rodriguez-Oroz, M. C., Krack, P., Kumar, R., and Lang, A. E. (2001). Deep-brain stimulation of the subthalamic nucleus or the pars interna of the globus pallidus in Parkinson's disease. *N. Engl. J. Med.* 345, 956–963. doi: 10.1056/NEJMoa000827

Olajide, O. J., Suvanto, M. E., and Chapman, C. A. (2021). Molecular mechanisms of neurodegeneration in the entorhinal cortex that underlie its selective vulnerability during the pathogenesis of Alzheimer's disease. *Biol. Open* 10:bio056796. doi: 10.1242/bio.056796

Pasquinelli, C., Hanson, L. G., Siebner, H. R., Lee, H. J., and Thielscher, A. (2019). Safety of transcranial focused ultrasound stimulation: A systematic review of the state of knowledge from both human and animal studies. *Brain Stimul.* 12, 1367–1380. doi: 10.1016/j.brs.2019.07.024

Patenaude, B., Smith, S. M., Kennedy, D. N., and Jenkinson, M. (2011). A Bayesian model of shape and appearance for subcortical brain segmentation. *Neuroimage* 56, 907–922. doi: 10.1016/j.neuroimage.2011.02.046

Perlson, J. (1945). Psychologic studies on a patient who received two hundred and forty-eight shock treatments. *Arch. Neurol. Psychiatry* 54, 409–411. doi: 10.1001/archneurpsyc.1945.02300110093015

Plaksin, M., Kimmel, E., and Shoham, S. (2016). Cell-type-selective effects of intramembrane cavitation as a unifying theoretical framework for ultrasonic neuromodulation. *eNeuro* 3:ENEURO.0136-15.2016. doi: 10.1523/ENEURO.0136-15.2016

Pruim, R. H. R., Mennes, M., van Rooij, D., Llera, A., Buitelaar, J. K., and Beckmann, C. F. (2015). ICA-AROMA: A robust ICA-based strategy for removing motion artifacts from fMRI data. *Neuroimage* 112, 267–277. doi: 10.1016/j.neuroimage.2015.02.064

Sanguinetti, J. L., Hameroff, S., Smith, E. E., Sato, T., Daft, C. M., Tyler, W. J., et al. (2020). Transcranial focused ultrasound to the right prefrontal cortex improves mood and alters functional connectivity in humans. *Front. Hum. Neurosci.* 14:52. doi: 10.3389/fnhum.2020.00052

Sato, T., Shapiro, M. G., and Tsao, D. Y. (2018). Ultrasonic neuromodulation causes widespread cortical activation via an indirect auditory mechanism. *Neuron* 98, 1031–1041.e5. doi: 10.1016/j.neuron.2018.05.009

Schafer, M. E., Spivak, N. M., Korb, A. S., and Bystritsky, A. (2021). Design, development, and operation of a low-intensity focused ultrasound pulsation (LIFUP) system for clinical use. *IEEE Trans. Ultrason. Ferroelectr. Freq. Control* 68, 54–64. doi: 10.1109/TUFFC.2020.3006781

Schultz, H., Sommer, T., and Peters, J. (2015). The role of the human entorhinal cortex in a representational account of memory. *Front. Hum. Neurosci.* 9:628. doi: 10.3389/fnhum.2015.00628

Spivak, N. M., and Kuhn, T. P. (2019). Variations in targeting techniques of focused ultrasound for use in neuromodulation. *Brain Stimul.* 12, 1595–1596. doi: 10.1016/j.brs.2019.07.021

Spivak, N. M., Korb, A. S., Reyes, S. D., Bych, B. P., Schafer, S. F., Khanlou, N., et al. (2021). Histological examination of focused ultrasound effects on human brain tissue. *Brain Stimul.* 14, 1486–1488. doi: 10.1016/j.brs.2021.09.015

Spivak, N. M., Sanguinetti, J. L., and Monti, M. M. (2022). Focusing in on the future of focused ultrasound as a translational tool. *Brain Sci.* 12:158. doi: 10.3390/brainsci12020158

Stern, J. M., Spivak, N. M., Becerra, S. A., Kuhn, T. P., Korb, A. S., Kronemyer, D., et al. (2021). Safety of focused ultrasound neuromodulation in humans with temporal lobe epilepsy. *Brain Stimul.* 14, 1022–1031. doi: 10.1016/j.brs.2021.06.003

Stidd, D. A., Vogelsang, K., Krahl, S. E., Langevin, J.-P., and Fellous, J.-M. (2013). Amygdala deep brain stimulation is superior to paroxetine treatment in a rat model of posttraumatic stress disorder. *Brain Stimul.* 6, 837–844. doi: 10.1016/j.brs.2013.05.008

Suthana, N., and Fried, I. (2014). Deep brain stimulation for enhancement of learning and memory. *Neuroimage* 85, 996–1002. doi: 10.1016/j.neuroimage.2013.07.066

Suthana, N., Haneef, Z., Stern, J., Mukamel, R., Behnke, E., Knowlton, B., et al. (2012). Memory enhancement and deep-brain stimulation of the entorhinal area. *N. Engl. J. Med.* 366, 502–510. doi: 10.1056/NEJMoa1107212

Titiz, A. S., Hill, M. R. H., Mankin, E. A., Aghajan, Z. M., Eliashiv, D., Tchemodanov, N., et al. (2017). Theta-burst microstimulation in the human entorhinal area improves memory specificity. *eLife* 6:e29515. doi: 10.7554/eLife.29515

Toccaceli, G., Barbagallo, G., and Peschillo, S. (2019). Low-intensity focused ultrasound for the treatment of brain diseases: Safety and feasibility. *Theranostics* 9, 537–539. doi: 10.7150/thno.31765

Toda, H., Hamani, C., Fawcett, A. P., Hutchison, W. D., and Lozano, A. M. (2008). The regulation of adult rodent hippocampal neurogenesis by deep brain stimulation. *J. Neurosurg.* 108, 132–138. doi: 10.3171/JNS/2008/108/01/0132

Tufail, Y., Yoshihiro, A., Pati, S., Li, M. M., and Tyler, W. J. (2011). Ultrasonic neuromodulation by brain stimulation with transcranial ultrasound. *Nat. Protoc.* 6, 1453–1470. doi: 10.1038/nprot.2011.371

Tyler, W. J., Tufail, Y., Finsterwald, M., Tauchmann, M. L., Olson, E. J., and Majestic, C. (2008). Remote excitation of neuronal circuits using low-intensity, low-frequency ultrasound. *PLoS One* 3:e3511. doi: 10.1371/journal.pone.0003511

frontiers | Frontiers in Neural Circuits

TYPE Original Research
PUBLISHED 03 May 2023
DOI 10.3389/fncir.2023.1161826

OPEN ACCESS

EDITED BY
Kevin Caulfield,
Medical University of South Carolina,
United States

REVIEWED BY
Sybren Van Hoornweder,
University of Hasselt, Belgium
Adam Stern,
Beth Israel Deaconess Medical Center and
Harvard Medical School, United States

*CORRESPONDENCE
Noah S. Philip
✉ noah_philip@brown.edu

RECEIVED 08 February 2023
ACCEPTED 10 April 2023
PUBLISHED 03 May 2023

CITATION
Cosmo C, Zandvakili A, Petrosino NJ, Toutain TGLdO, Miranda JGV and Philip NS (2023) Examining the neural mechanisms of rTMS: a naturalistic pilot study of acute and serial effects in pharmacoresistant depression. *Front. Neural Circuits* 17:1161826. doi: 10.3389/fncir.2023.1161826

Examining the neural mechanisms of rTMS: a naturalistic pilot study of acute and serial effects in pharmacoresistant depression

Camila Cosmo[1,2], Amin Zandvakili[1,2], Nicholas J. Petrosino[1,2], Thaise Graziele L. de O. Toutain[3], José Garcia Vivas Miranda[4] and Noah S. Philip[1,2]*

[1]Department of Psychiatry and Human Behavior, The Warren Alpert Medical School, Brown University, Providence, RI, United States, [2]VA RR&D Center for Neurorestoration and Neurotechnology, VA Providence Healthcare System, Providence, RI, United States, [3]Institute of Health Sciences, Federal University of Bahia, Salvador, Brazil, [4]Institute of Physics, Federal University of Bahia, Salvador, Brazil

Introduction: Previous studies have demonstrated the effectiveness of therapeutic repetitive transcranial magnetic stimulation (rTMS) to treat pharmacoresistant depression. Nevertheless, these trials have primarily focused on the therapeutic and neurophysiological effects of rTMS following a long-term treatment course. Identifying brain-based biomarkers of early rTMS therapeutic response remains an important unanswered question. In this pilot study, we examined the effects of rTMS on individuals with pharmacoresistant depression using a graph-based method, called Functional Cortical Networks (FCN), and serial electroencephalography (EEG). We hypothesized that changes in brain activity would occur early in treatment course.

Methods: A total of 15 patients with pharmacoresistant depression underwent five rTMS sessions (5Hz over the left dorsolateral prefrontal cortex, 120%MT, up to 4,000 pulses/session). Five participants received additional rTMS treatment, up to 40 sessions. Resting EEG activity was measured at baseline and following every five sessions, using 64-channel EEG, for 10 minutes with eyes closed. An FCN model was constructed using time-varying graphs and motif synchronization. The primary outcome was acute changes in weighted-node degree. Secondary outcomes included serial FFT-based power spectral analysis and changes in depressive symptoms measured by the 9-Item Patient Health Questionnaire (PHQ-9) and the 30-item Inventory of Depressive Symptoms-Self Report (IDS-SR).

Results: We found a significant acute effect over the left posterior area after five sessions, as evidenced by an increase in weighted-node degree of 37,824.59 (95% CI, 468.20 to 75,180.98) and a marginal enhancement in the left frontal region ($t(14) = 2.0820$, $p = 0.056$). One-way repeated measures ANOVA indicated a significant decrease in absolute beta power over the left prefrontal cortex ($F(7, 28) = 2.37$, $p = 0.048$) following ten rTMS sessions. Furthermore, a significant clinical improvement was observed following five rTMS sessions on both PHQ-9 ($t(14) = 2.7093$, $p = 0.017$) and IDS-SR ($t(14) = 2.5278$, $p = 0.024$) and progressed along the treatment course.

Discussion: Our findings suggest that FCN models and serial EEG may contribute to a deeper understanding of mechanisms underlying rTMS treatment. Additional research is required to investigate the acute and serial effects of rTMS in pharmacoresistant depression and assess whether early EEG changes could serve as predictors of therapeutic rTMS response.

KEYWORDS

functional cortical networks, repetitive transcranial magnetic stimulation (rTMS), non-invasive brain stimulation (NIBS), pharmacoresistant depression, treatment-resistant depression (TRD), qEEG, power spectral analysis (FFT), naturalistic study

Introduction

Recent data from the World Health Organization's Global Health Estimate report indicate that depressive disorders are a significant public health concern that affects a substantial proportion of the American population, with a prevalence of 5.9% (World Health Organization, 2017). Specifically, these data suggested that 8.4% of Years Lived with Disability and Disability-Adjusted Life Years could be attributed to the impact of depression, indicating a significant burden on the population (World Health Organization, 2017). Furthermore, the Centers for Disease Control and Prevention's 2019 National Health Interview Survey reported that 4.7% of adults aged 18 or older exhibited regular symptoms of depression, and 18.5% experienced some degree of depressive symptoms (Clarke et al., 2019). The 2020 National Survey on Drug Use and Health also found a high prevalence of Major Depressive Disorder (MDD), with an estimated 8.4% of the adult population affected (Center for Behavioral Health Statistics and RTI International, 2021). In addition, the survey revealed that 6% of U.S. adults experienced at least one episode of depression with severe impairment (Center for Behavioral Health Statistics and RTI International, 2021). Notably, among individuals with a severe presentation, 71% underwent treatment (Center for Behavioral Health Statistics and RTI International, 2021). The absence of a standardized definition for pharmacoresistant depression, also referred to as treatment-resistant depression (TRD), has led to considerable variation in its reported prevalence across the literature (Zhdanava et al., 2021). In a recent study, Zhdanava et al. found that the estimated annual prevalence of American adults undergoing pharmacotherapy for MDD was 8.9 million, with 30.9% of these individuals presenting TRD (Zhdanava et al., 2021). Although there is no consensus regarding the concept of pharmacoresistant depression, it is generally defined as the lack of remission of depressive symptoms following a minimum of two optimal trials of evidence-based pharmacological treatment (McIntyre et al., 2014; Cosmo et al., 2021; Zhdanava et al., 2021; Denee et al., 2022).

Repetitive transcranial magnetic stimulation (rTMS) is a non-invasive technique that induces an electrical current in the cortex through magnetic pulses, modifying brain networks (Carpenter et al., 2012; Gaynes et al., 2014; Cosmo et al., 2021). In 2008, the US Food and Drug Administration cleared rTMS for the treatment of pharmacoresistant depression. A pivotal study, a large multisite trial comprising 307 participants, assessed the effectiveness of therapeutic rTMS in treatment-resistant depression utilizing a naturalistic approach (Carpenter et al., 2012). It consisted of an acute phase treatment with an average of 28.3 rTMS sessions [with a standard deviation (SD) of 10.1]. The primary outcome measure was the Clinical Global Impressions-Severity of Illness scale. A significant improvement in depression symptoms and severity was observed from baseline to endpoint. The findings of this study are consistent with subsequent controlled trials and support the use of rTMS as an effective, safe, and well-tolerated treatment for TRD (Avery and Holtzheimer, 2006; Demitrack and Thase, 2009; Carpenter et al., 2012; Connolly et al., 2012; Benadhira et al., 2017; Cosmo et al., 2021).

Since its initial clearance, rTMS has been increasingly utilized in TRD (Carpenter et al., 2012; Gaynes et al., 2014; Anderson et al., 2016; Cosmo et al., 2021), with emerging data supporting its use in a broad range of neuropsychiatric disorders (Carpenter et al., 2012; Anderson et al., 2016; Zandvakili et al., 2019; Alyagon et al., 2020; Cosmo et al., 2021; McIntyre et al., 2021; Khedr et al., 2022). Despite its clinical successes, the mechanism of action of rTMS and its effects during treatment have yet to be fully elucidated. Prior studies utilizing quantitative electroencephalography (qEEG) yielded promising findings of underlying mechanisms of rTMS (Spronk et al., 2008; Valiulis et al., 2012; Noda et al., 2013; Wozniak-Kwasniewska et al., 2015; Kallioniemi and Daskalakis, 2022; Morris et al., 2023). The effects of high-frequency and low-frequency rTMS protocols on EEG power spectral analysis were assessed in a sample of 45 patients with TRD. While clinical efficacy was similar for both frequencies, distinct electrophysiological measures were observed. The low-frequency group showed increased frontal alpha power asymmetry toward the right hemisphere and higher beta power in frontal, central, parietal, and left temporal areas. In contrast, the high-frequency group demonstrated more widespread changes, including increased delta power in the left hemisphere, and increased alpha power in the right (Valiulis et al., 2012). Similar to other rTMS studies, this trial has primarily applied a pre- vs. post-treatment comparison (Spronk et al., 2008; Valiulis et al., 2012; Noda et al., 2013; Morris et al., 2023). Since clinical improvement does not always progress linearly over time, multiple EEG acquisitions over the course of rTMS may yield novel observations that may enhance our understanding of mechanisms underlying TMS and inform the development of novel treatment protocols. Furthermore, the identification of brain-based biomarkers of early therapeutic response remains an important and unanswered question in the field.

Graph theory provides a robust framework for analyzing brain networks (Sporns, 2018). Using graph-based analytical methods, such as functional cortical network (FCN), it is possible to investigate the connectivity patterns among distinct brain regions, and how these patterns evolve over time in response to interventions or stimuli (Sporns, 2018). Graph-based models have demonstrated promising results as an approach to characterizing brain connectivity patterns in neuropsychiatric disorders (Toutain et al., 2022, 2023), and evaluating acute neurophysiological effects following brain stimulation (Polania et al., 2011; Cosmo et al., 2015).

To this end, we utilized Functional Cortical Networks and EEG power spectral analysis, to examine the acute and serial effects of rTMS on patients diagnosed with treatment-resistant depression. qEEG and FCN are two distinct but complementary approaches for investigating brain dynamics. Combining these methods may lead to a comprehensive understanding of the neural mechanisms underlying rTMS effects. We hypothesized that the therapeutic effects of repetitive transcranial magnetic stimulation on treatment-resistant depression would be observable early in the treatment course, as assessed by FCN, qEEG, and standardized clinical assessment scales.

Materials and methods

This naturalistic pilot study was conducted at the VA Providence Medical Center upon chart review of patients with pharmacoresistant depression that underwent rTMS treatment from October 2018 to December 2020. Methods were approved by VA Providence Institutional Review Board.

Participants

Fifteen veterans (12 males and 3 females) with pharmacoresistant depression (mean age ± SD: 52 ± 10.5 years) were enrolled in this study. Inclusion criteria were (1) a primary diagnosis of MDD consistent with the Diagnostic and Statistical Manual of Mental Disorders, fifth edition (DSM-V), and confirmed by an experienced psychiatrist; (2) had failed at least two antidepressant trials; and (3) were recommended by their primary providers to undergo rTMS as a therapeutic strategy. The exclusion criteria were (1) former or current presence of psychotic features or diagnosis of primary psychotic disorder; (2) cognitive impairment; (3) having any contraindication for iTBS (e.g., implanted devices/metal, pregnancy, unstable medical conditions, history of seizure, etc.); or (4) active suicidality. Given the naturalistic nature of this study, participants continued in any ongoing treatment (i.e., medications, therapy, etc.) while having adjunctive rTMS sessions. Consistent with clinical practice, other treatments were largely held stable during rTMS unless clinically indicated.

Procedures and TMS parameters

In the acute effects group, participants underwent five sessions of rTMS at 5 Hz, 120% of motor threshold (MT), and up to 4,000 pulses per session. The number of pulses varied from 3,000 to 4,000 according to psychiatrist-advised protocol and patients' tolerability. Due to the time required for serial EEG recording, five male participants (mean age ± SD: 59 ± 6.93 years) agreed to receive additional rTMS treatment, with the same parameters, in a five consecutive sessions-block (up to 40 sessions), forming the serial effects subgroup. The remaining ten patients continued the rTMS treatment course without EEG recording.

After MT determination, the coil was placed over the left dorsolateral prefrontal cortex (DLPFC), approximately between F3 and F5 electrode locations (using the international 10/20 EEG system). rTMS was delivered by applying the Magstim® Rapid^2 Plus^1 system (Magstim, UK).

The left dorsolateral prefrontal cortex, a known pathophysiological target of depression, has been shown to be deeply connected with limbic structures responsible for regulating mood (Pandya et al., 2012; Zhang et al., 2018). High-frequency TMS delivered at this region has been associated with polysynaptic effects and, consequently, effective reduction of depressive symptoms (Philip et al., 2015; Cosmo et al., 2021).

Outcome measures

EEG acquisition and analysis

Ten minutes eyes closed, resting-state EEG was recorded at baseline, and at the end of each block of five rTMS sessions. The brain electrical activity was recorded by a 64-channel EEG cap, placed in accordance with the 10-10 system, an extension of the international 10–20 system, with CPz as reference, and using an EEG gel system (eego, ANT, Enschede, the Netherlands) with Ag/AgCl electrodes. Electrode-skin impedance was set below 20 kΩ, and data were sampled at 600 Hz.

EEG preprocessing and analysis were performed using EEGLAB, running on MATLAB [R2021b (9.11), The Mathworks, Inc.]. EEG signals were filtered with a band-pass filter ranging from 0.5 to 50 Hz and segmented into 1s epochs. Independent Component Analysis (ICA) was automatically performed to remove ocular, electrocardiographic, and electromyographic artifacts. In addition, an automatic procedure was employed to reject epochs containing signal amplitudes >100 μV or <-100 μV. Subsequently, a manual visual inspection was carried out to eliminate any remaining artifacts. Then, power spectral density (PSD) analyses of artifact-free 1s epochs (without overlap) were carried out by applying customed MATLAB scripts. We applied Welch's power spectral density to estimate the mean PSD for all epochs of the signal. The average PSD values for each frequency band were estimated. Power was calculated for the following four frequency bands: delta (1–4 Hz), theta (4–8 Hz), alpha (8–13 Hz), and beta (13–30 Hz). For Fast Fourier Transform (FFT) analyses, the Bonferroni procedure was applied to correct for multiple comparisons across the four frequency bands.

In summary, EEG data were used to (1) build functional cortical networks to assess the acute effects of rTMS on the connectivity between the brain regions, and (2) compute power spectral changes in a series analysis of rTMS effects at the end of every 5-session block (up to 8 blocks).

Functional cortical network model

An FCN model was developed by using time-varying graphs (TVG) and motif synchronization methods (Rosário et al., 2015). It consists of applying local oscillation patterns (motifs) to synchronize traces of pairs of EEG channels over time, creating a TVG. This graph includes a set of nodes and edges—the first corresponding to the electrodes, and the second representing the synchronization between these electrode regions. Each pair of electrodes are compared in a defined time window (1,000 ms), and for every window, a network (i.e., graph) is constructed, and connectivity is estimated for each electrode. Based on a sliding time window along the EEG recording, 72,000 graphs were generated and overlapped, creating a weighted static aggregate network. On this weighted network, weights indicate the number of connections over time; namely, the number of times synchronization between pairs of electrodes occurred. For this study, functional cortical networks were developed based on the following parameters: threshold (0.80), window length (60 points); lag window (1), τ minimum (3), τ maximum (15), TVG step (1), motif lag (1), sample rate (600 Hz), resulting in 72,000 points for a total period

of 120,000 ms. These parameters were applied to ensure that the resulting synchronization had only a 1% chance of being due to chance. Two resting state networks, pre- and post- 5 rTMS sessions block, were created for each patient.

FCN analyses were conducted by grouping electrodes into clusters based on corresponding brain regions as follows: left frontal: AF7, AF3, F7, F5, F3, F1, FC5, FC3, FC1 electrodes; right frontal: AF8, AF4, F8, F6, F4, F2, FC6, FC4, FC2; left centrotemporal: T7, C5, C3, C1, TP7, CP5, CP3, CP1; right centrotemporal: T8, C6, C4, C2, TP8, CP6, CP4, CP2; left posterior: P7, P5, P3, P1, PO7, PO5, PO3, O1; and right posterior: P8, P6, P4, P2, PO8, PO6, PO4, O2. Electrode grouping was performed for the computation of topological indices of the functional cortical networks. Specifically, the indices were estimated for each electrode separately and subsequently averaged across electrodes within each region. Therefore, regional connectivity represents the average connectivity of the corresponding electrodes.

Our primary outcome was acute changes in weighted-node degree. This metric reflects how many times and how long the nodes (i.e., EEG electrodes) were synchronized over time, displaying the network evolution after five rTMS sessions, which we refer to as acute changes. For further information on the FCN methods, please refer to (Cosmo et al., 2015; Rosário et al., 2015). Secondary outcomes included serial FFT-based power spectral analysis and changes in depressive symptoms severity as measured by the 9-Item Patient Health Questionnaire (PHQ-9) and the 30-item Inventory of Depressive Symptoms-Self Report (IDS-SR), as further explained below.

Self-reported clinical rating scales

Depressive symptom severity was measured by applying the PHQ-9 and IDS-SR (Gili et al., 2011). These clinical scales are sensitive instruments and can be applied in a one-week window to assess changes in symptom severity. They were designed to grade the nine main depressive symptomatology domains in accordance with the Diagnostic and Statistical Manual of Mental Disorders, fourth edition (DSM-IV), with the IDS-SR having additional items to rate melancholic and atypical features. The IDS-SR total score ranges from 0 to 84, with a rating of 18 or more implying clinically significant depression, 39–48 indicating severe presentation, and above 49, very severe symptomatology (Gili et al., 2011). As far as PHQ-9, its total score varies from 0 to 27, with a result between 10 and 14 indicating moderate depression, 15 and 19 implying moderately severe depression, and a score of 20 or more suggesting severe depression.

Statistical analysis

Clinical and demographic features were assessed using descriptive statistical procedures such as central tendency and dispersion measures. The Shapiro–Wilk test was used to assess the data normality, and Mauchly's sphericity test was applied, determining that the assumption of sphericity was met as required for the repeated-measures ANOVA. Parameters of all the electrodes were analyzed for each individual, and a weighted-node degree was generated for each electrode, with p-values corrected using the Bonferroni technique. The primary outcome measure, weighted-node degree, was analyzed by applying paired t-test to compare within-group changes (i.e., baseline vs. the fifth rTMS session). One-way repeated measures ANOVA was performed to assess serial clinical and absolute/relative power data. Power was calculated based on FFT analysis, with absolute and relative power estimated for each frequency band. For the FFT analyses, the Bonferroni procedure was applied to correct for multiple comparisons across the four frequency bands. Additional paired t-tests were carried out to compare baseline (T0) and post (T1, end of 5 rTMS sessions; T2, after 10 sessions; T3, 15 sessions; T4, 20 sessions;

TABLE 1 Demographic features at baseline.

	Acute effects ($n = 15$)	Serial effects ($n = 5$)
Age (years)[a]	52 (10.53)	59 (6.93)
Female sex (%)	20	0
Race (%)		
African American	0	0
American Indian/Alaska native	0	0
Multiracial	7.69	0
White	92.31	100
Ethnicity		
Not of Hispanic origin	93.33	100
Hispanic origin	6.67	0
Marital status[b]		
Single	20	0
Married	33.33	60
Separated	6.67	0
Divorced	33.33	40
Employment status[b]		
Full time	33.33	40
Part time	6.67	0
Unemployed	13.33	0
Multiple status	20	0
Service-connected disability (mental health)	78.57	80

[a]Age presented as mean ± standard deviation (SD).
[b]Totals do not sum up to 100% due to participants non-response.

TABLE 2 Acute effects of rTMS on clinical features.

	T0	T1	Within-groups (p)[‡]
PHQ-9[a]	15.4 (6.71)	13.5 (6.16)	0.017
IDS-SR[a]	41 (13.54)	34.4 (12.76)	0.024

[a]Clinical variables of 15 participants described as mean ± SD; PHQ-9, 9-Item Patient Health Questionnaire; IDS-SR, 30-item Inventory of Depressive Symptoms-Self Report; rTMS, repetitive Transcranial Magnetic Stimulation; SD, Standard deviation.
[‡]p-values correspond to paired t-test.

T5, 25 sessions; T6, after last rTMS session; and T7, 1 week after the end of treatment) data of each secondary outcome within-group. Statistical analyses were performed using the Stata software program, version 16.1 (StataCorp LP, College Station, TX, USA). Statistical significance was determined at alpha = 5%, and all p-values were two-tailed.

Results

Demographic and clinical characteristics

Baseline demographic features for both groups—(a) rTMS acute effects ($n = 15$); and (b) rTMS serial effects (SE; $n = 5$) are shown in Table 1. The severity of depressive symptoms was similar for both groups at baseline, indicating moderately severe depression, based on PHQ-9 measures (acute effects: 15.4 ± 6.71; serial effects: 16.4 ± 4.83) and severe presentation according to IDS-SR scores (acute effects: 41 ± 13.54; serial effects: 39.2 ± 7.08) (Tables 2, 3).

Acute effects—FCN

After five rTMS sessions, an acute effect was observed over the left posterior area, evidenced by a statistically significant increase of 37,824.59 in the weighted-node degree mean of the electrodes located in this region [95% CI, 468.20 to 75,180.98, t (14) = 2.172, $p = 0.047$, with a medium effect size ($d = 0.561$)]. Increased synchronization was also noted in the left frontal electrodes [t (14) = 2.082, $p = 0.056$; medium effect size ($d = 0.537$)], although with nominal statistical significance (Figure 1).

Serial effects—Power spectral analysis

One-way repeated measures ANOVA showed a statistically significant decrease in the absolute power in the beta band over the left prefrontal cortex [F (7, 28) = 2.37, $p = 0.048$], with notable effects observed as early as after 10 rTMS sessions [t (4) = 3.225, $p = 0.032$; with a large effect size ($d = -1.442$)]. Upon analysis of each prefrontal EEG channel, an absolute beta power decrease was mainly observed in F5 [F (7, 28) = 2.85, $p = 0.022$], with a significant reduction at T2 [t (4) = 2.922, $p = 0.043$; with a large effect size ($d = -1.307$)], compared to baseline (T0); and there was no significant difference in the beta power at other brain regions ($p \geq 0.05$) (Figure 2). In addition, no significant changes were observed in the absolute or relative power in the delta, theta, or alpha bands following the stimulation sessions ($p \geq 0.05$).

Clinical effects—PHQ-9 and IDS-SR

To assess whether the acute and serial neurophysiological effects of rTMS treatment reflected changes in depressive symptoms, clinical outcomes (PHQ-9 and IDS-SR) were analyzed in both groups [acute effects ($n = 15$) and serial effects ($n = 5$)].

Consistent with the FCN findings, a statistically significant clinical improvement was observed following five rTMS sessions. The acute effects were observed on both the PHQ-9 [t (14) = 2.709, $p = 0.017$; $d = 0.699$] and IDS-SR [t (14) = 2.528, $p = 0.024$; d = 0.653] (Table 2).

Concerning rTMS serial effects on clinical outcomes, a significant improvement was noted over time on both the PHQ-9 [F (7, 28) = 4.93, $p = 0.001$] and IDS-SR scales [F (7, 28) = 5.82, $p < 0.001$] (Table 3). Interestingly, PHQ-9 was more sensitive in detecting early clinical response, as improvement was observed following 10 sessions, corresponding to the observed absolute beta power reduction at the same timepoint (T2). In contrast, clinical improvement as measured by the IDS-SR was not noted until after 15 sessions. Despite this finding, PHQ-9 only detected statistically significant clinical improvement at specific time points (T2, T6, and T7). IDS-SR demonstrated a greater consistency in detecting the longitudinal effects, with a sustained significant response observed over treatment.

Discussion

This study indicates that FCN models may provide a sensitive measure of acute changes in neural mechanisms underlying therapeutic rTMS. Five rTMS sessions were sufficient to evoke higher synchronization between electrodes in the left posterior and prefrontal areas, with a statistically significant increase observed in the first. Additionally, this pilot data indicates the potential of serial EEG to monitor rTMS-induced changes in cortical networks during the treatment course. Our results demonstrate that rTMS elicited a reduction in beta power over time in the left prefrontal area, starting as early as after the first ten sessions. In line with the FCN and qEEG findings, statistically significant clinical improvement was observed following five and ten rTMS sessions, respectively. Clinical naturalistic therapeutic response was observed over time on both—the PHQ-9 and IDS-SR, with the latter being more consistent in detecting longitudinal improvement

TABLE 3 Serial effects of rTMS on clinical features.

	T0	T1	T2	T3	T4	T5	T6	T7[#]	Within-groups (p)[‡]
PHQ-9[a]	16.4 (4.83)	14.8 (5.40)	10.6 (7.44)	12 (7.31)	10 (9.25)	9.4 (9.50)	9 (8.69)	8.2 (9.18)	0.001
IDS-SR[a]	39.2 (7.08)	35 (16.11)	31.2 (14.10)	30 (13.91)	28.6 (15.34)	26 (16.14)	24.8 (16.81)	20.8 (16.75)	<0.001

[a]Clinical variables of 5 participants described as mean ± SD; PHQ-9, 9-Item Patient Health Questionnaire (); IDS-SR, 30-item Inventory of Depressive Symptoms-Self Report; rTMS, repetitive Transcranial Magnetic Stimulation; SD, Standard deviation.
[#]One week after the last rTMS session.
[‡]p-values correspond to repeated measures ANOVA.

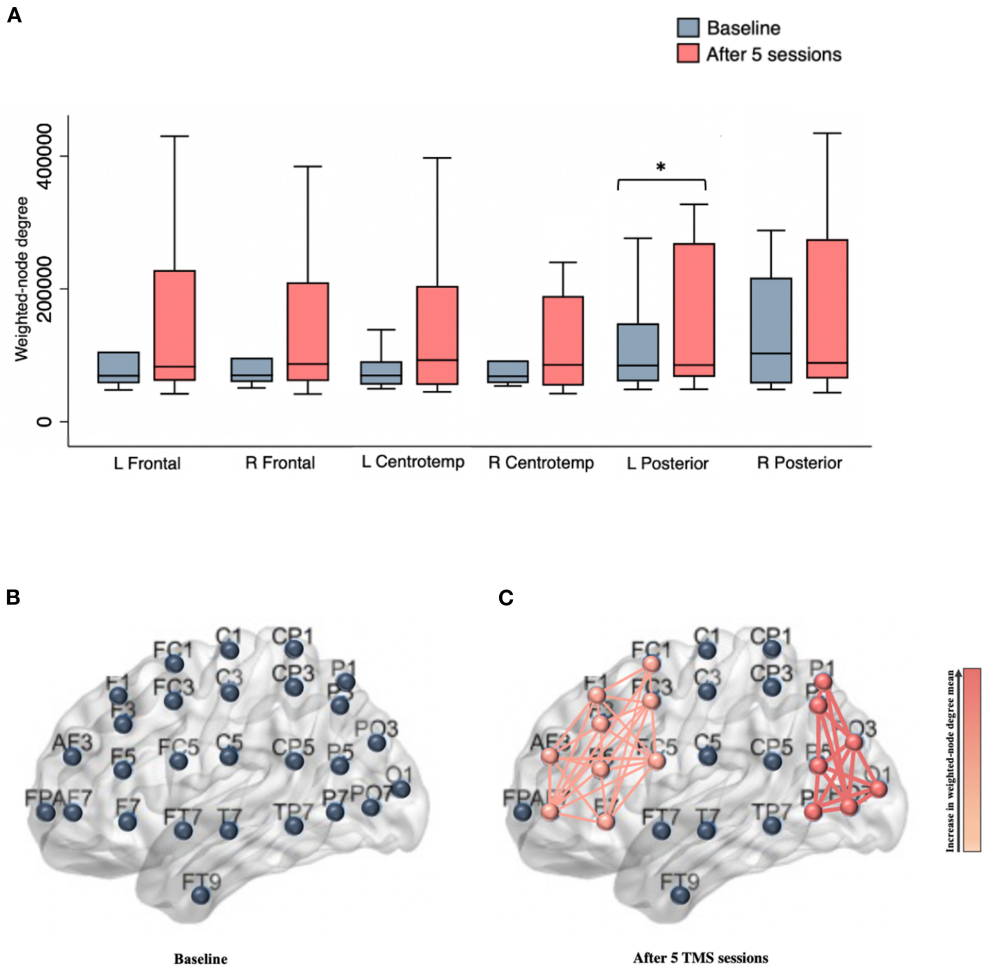

FIGURE 1
(A) Box plots show the weighted-node degree mean for brain regions at baseline and after five rTMS sessions. An acute effect was observed over the left posterior area, evidenced by a statistically significant increase in the weighted-node degree mean ($p = 0.047$); **(B)** Illustration showing left electrodes (e.g., nodes) distribution; **(C)** Schematic representation of left frontal and posterior clusters following five rTMS sessions. The thickness of the edges and the gradient color represents the strength of association between the network nodes. L, left; R, Right; Centrotemp, centrotemporal. *Indicates statistical significance.

over the course of rTMS treatment. The hypotheses generated by this naturalistic study require further investigation through a more rigorous research design, such as randomized clinical trials, to examine the clinical efficacy of rTMS in individuals with treatment-resistant depression, as well as the corresponding acute and serial neurophysiological changes induced by this neuromodulation technique.

Although rTMS has been widely investigated as a neuromodulatory tool for numerous neuropsychiatric disorders, its neurophysiological mechanisms remain unclear (Carpenter et al., 2012; Anderson et al., 2016; Zandvakili et al., 2019; Alyagon et al., 2020; Cosmo et al., 2021; McIntyre et al., 2021; Khedr et al., 2022). The use of the FCN model in this study is innovative as it offers a novel approach to understanding the acute effects of rTMS on dynamic patterns of brain connectivity over time. This EEG-based model is able to describe brain connectivity by analyzing the temporal synchronization between electrodes (i.e., nodes), providing insight into the evolution of the networks (Cosmo et al., 2015; Rosário et al., 2015). Furthermore, this technique is feasible and cost-effective compared to neuroimaging methods and allows the identification of changes in the cortical connectivity induced by rTMS early on in the course of treatment.

Based on the FCN model, an enhancement in the degree of synchronization in electrodes located in the left posterior and frontal regions was observed, as a result of the administration of five rTMS sessions. Previous studies have demonstrated that rTMS delivered over the left DLPFC led to modulation of brain regions extending beyond the target area, including posterior networks (Liston et al., 2014; Lan et al., 2016; Cardenas et al., 2022), which could be a result of the activation of the central executive network—a frontoparietal system. In our study, a statistically significant increase was noted only in the left posterior area. It is important to note that a statistically significant improvement in clinical outcomes, as quantified by both the PHQ-9 and IDS-SR, was also observed as an acute effect of stimulation. Nevertheless, the potential association between FCN and clinical findings remains uncertain as no correlation analysis was performed given the absence of a linear relationship. Prior trials that have shown

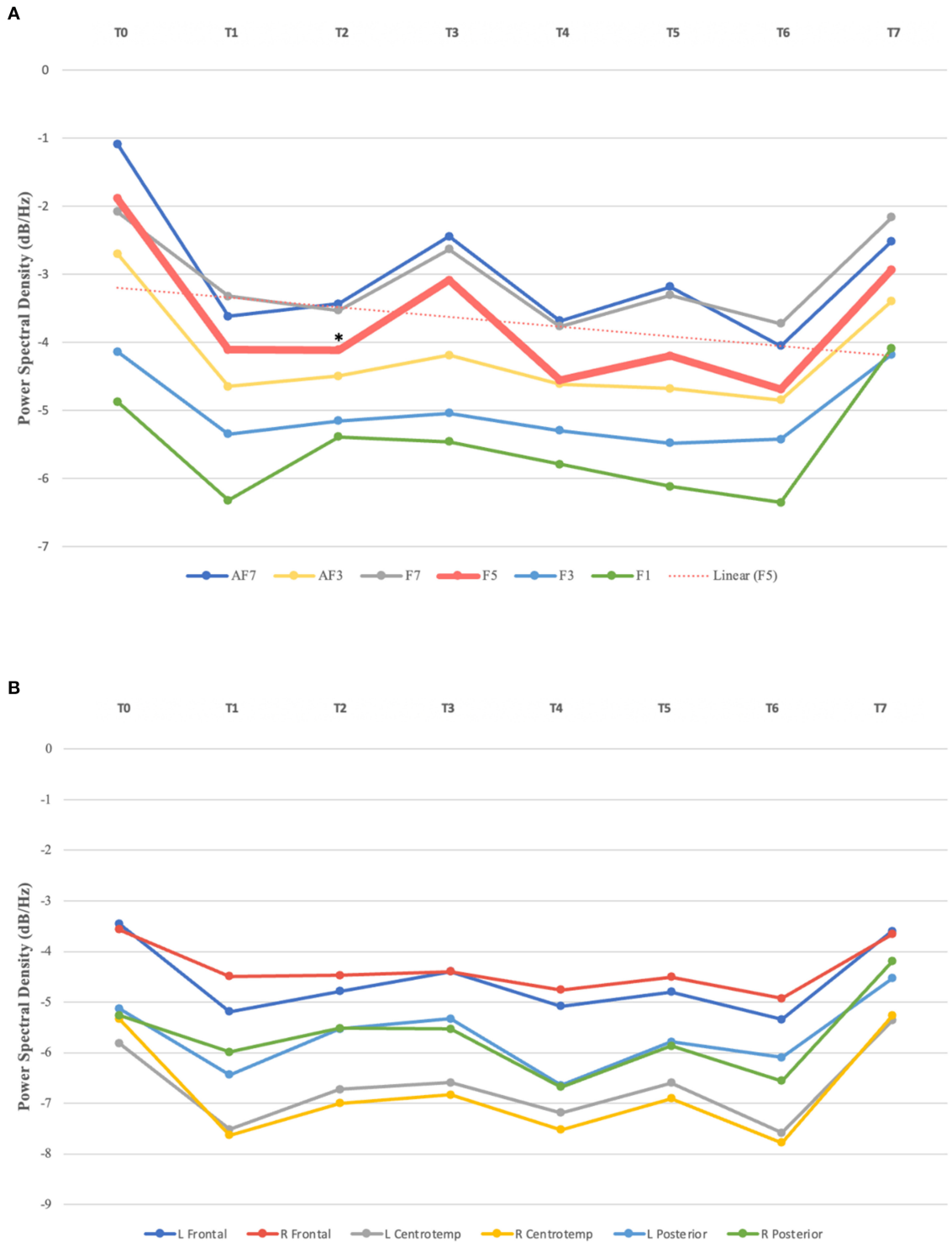

FIGURE 2
(A) Absolute beta power in left prefrontal channels over time. Statistically significant absolute power decrease observed in F5 after 10 sessions (T2), compared to baseline (T0); linear trendline for F5. **(B)** Absolute beta power in brain regions from T0–T7. L, left; R, Right; Centrotemp, centrotemporal. *Indicates statistical significance.

that increased left frontal activity might be linked to decreased negative and increased positive affect, while increased left posterior activity is thought to reflect improved emotional processing. Research assessing the relationship between emotional processing and neural networks has established a correlation between the left hemisphere and the experience of positive affect (Spielberg et al., 2008). Previous studies investigating the neural basis of depression have shown a link between depressive symptoms

and frontal brain asymmetry, with a reduction in left frontal activity (Henriques and Davidson, 1990, 1991; Eric and Hall, 1999; Palmiero and Piccardi, 2017). It has been suggested that an increase in left frontal activity might be linked to less negative and more positive affect. Hypoactivation of this area has been associated with increased responsivity to negative stimuli, which in turn enhances the likelihood of developing mood disorders, particularly depression (Henriques and Davidson, 1991; Eric and Hall, 1999; Palmiero and Piccardi, 2017). Studies utilizing both EEG and functional magnetic resonance imaging (fMRI) have demonstrated a correlation between left frontal activation and a reduction in negative affect, and an increase in positive affect (Eric and Hall, 1999; Davidson, 2004a,b; Cerqueira et al., 2008; Machado and Cantilino, 2017; Palmiero and Piccardi, 2017). Specifically, fMRI trials have suggested that this link may be mediated by top-down regulation via an inhibitory input to the amygdala (Ochsner et al., 2002; Roalf et al., 2011). Concerning the left posterior brain region, previous research has demonstrated functional impairment in this area in individuals with depression, particularly in the inferior parietal cortex (IPC) (Muller et al., 2013; Mel'nikov et al., 2018). This region plays a crucial role in emotional processing, as well as social cognition, specifically in the affective component of social cognition (Muller et al., 2013; Bzdok et al., 2016; Numssen et al., 2021). It is thought that the dysregulation of the IPC and its resulting impairments in emotional processing and social cognition may be caused by a dysfunction in the connections between the inferior parietal cortex and correlated cortical and subcortical areas (Muller et al., 2013; Numssen et al., 2021).

Although the available data support our findings, it is essential to further investigate the acute effects of rTMS over the left DLPFC and the potential correlation between clinical improvement and the neurophysiological findings observed in our study. The enhancement of synchronization in the left DLPFC, in conjunction with a significant increase in connectivity in the left posterior region, may have led to clinical improvement through different mechanisms. These mechanisms may include an enhancement of positive affect, an improvement in emotional processing and social cognition, or a combination of both. Additional studies are required to determine the existence of a potential clinical-neurophysiological correlation and the precise nature of this relationship.

Furthermore, our results provide evidence for the potential use of serial EEG in monitoring rTMS-induced neurophysiological changes along the treatment course. A reduction in absolute beta power over the left prefrontal cortex was observed as early as after ten sessions, which was consistent with the clinical response as measured by PHQ-9. These findings align with previous research linking beta power to therapeutic response evidenced by reduced depressive symptoms (Paquette et al., 2009). In addition, as suggested by Wyczesany et al., beta frequency band has been associated with negative emotions and increased psychological distress, potentially reflecting automatic responses to negative stimuli (Wyczesany et al., 2018). A recent review of EEG frequency bands in mental health disorders, which analyzed data from 18 studies on depression, concluded that increased absolute beta and theta power, for both eyes-open and eyes-closed conditions, were the main findings in this population (Newson et al., 2018). Taken together, these data support our findings suggesting that the reduction of absolute beta power over the left prefrontal cortex may be associated with improved clinical outcomes in individuals with depression undergoing rTMS treatment.

The current study had several limitations, most prominently (1) the naturalistic design that may have introduced potential sources of observer bias and prevented the use of standardized procedures. Nevertheless, it is noteworthy that the naturalistic data has the advantage of emulating real-life circumstances, providing a high ecological validity, and yielding data that are more generalizable, increasing external validity. By using a naturalistic approach, we aimed to enhance our understanding of how rTMS works in real-world settings, with study participants more accurately representing our clinical population; (2) the small sample size that might have resulted in type II error due to its limited power, also precluding hypothesis testing and more complex analyses; (3) the convenience sample that made the study more prone to sampling bias, and might have introduced confounding factors related to comorbidities and ongoing treatment; (4) population primarily composed of male veterans, possibly affecting the external validity; (5) challenges related to power spectral analysis, particularly its modest spatial resolution and the overlap of spectral properties across some psychiatric disorders; and (6) lack of correction for multiple comparisons across time points and for clinical outcomes, requiring careful interpretation of our findings. As indicated above, veterans received rTMS as an adjunct treatment to ongoing pharmacotherapy, although other treatments remained stable. Furthermore, another important limitation of our study is the lack of a sham control group, which is particularly relevant given the use of self-reported clinical instruments. The potential influence of a placebo effect on these clinical scales needs to be taken into consideration when interpreting our results. Despite these limitations, our pilot study provides an exploratory examination of the effects of rTMS in individuals with pharmacoresistant depression under real-life clinical conditions, along the treatment course.

In summary, this naturalistic pilot study assessed the acute and serial effects of rTMS on brain activity utilizing a Functional Cortical Network model and EEG power spectral analysis, respectively. Our results indicate that FCN models might work as a sensitive measure of acute changes in neural mechanisms underlying therapeutic rTMS. Five rTMS sessions were sufficient to evoke higher synchronization between electrodes in the left posterior and frontal regions, with statistically significant findings observed in the first area. These findings are consistent with previous studies that have demonstrated that increased left posterior activity may reflect improved emotional processing, while enhanced activity in the left frontal region may be associated with improved affect. Furthermore, our results suggest the potential of serial EEG in monitoring rTMS-induced cortical changes throughout the treatment course. Specifically, we observed a reduction in beta power over the left prefrontal cortex as early as after ten sessions, which was consistent with the observed clinical response. This is in line with prior research associating beta power with therapeutic response and support the development of serial EEG as a biomarker of rTMS response, which may aid in tracking and potentially predicting stimulation effects over the course of treatment. These findings may serve as a foundation for future, more rigorous studies utilizing a randomized, double-blind,

sham-controlled design to further investigate the acute and serial effects of rTMS in individuals with pharmacoresistant depression and inform the optimization of therapeutic stimulation protocols.

Data availability statement

Data is available upon request, following to US Department of Veterans Affairs regulations.

Ethics statement

The studies involving human participants were reviewed and approved by VA Providence Institutional Review Board. The patients/participants provided their written informed consent to participate in this study.

Author contributions

AZ and NSP designed and conducted the study. CC performed the data analysis and prepared the manuscript draft with intellectual input from AZ, NJP, TT, JM, and NSP. CC, AZ, TT, JM, NJP, and NSP performed a critical review of the manuscript. All authors approved the final manuscript.

Funding

Effort on this manuscript was supported by R25 MH101076 and the VA Office of Research Rehabilitation and Development (RR&D) Center for Neurorestoration and Neurotechnology at VA Providence and the Department of Veterans Affairs grant IK2CX002115. The funders had no role in the design of the study, data analysis, or decision to publish.

Conflict of interest

NJP received clinical trial support (through US Department of Veteran Affairs) from Wave Neuro and Neurolief. NSP serves on the scientific advisory board for Pulvinar Neuro.

The remaining authors declare that the research was conducted in the absence of any commercial or financial relationships that could be construed as a potential conflict of interest.

Publisher's note

All claims expressed in this article are solely those of the authors and do not necessarily represent those of their affiliated organizations, or those of the publisher, the editors and the reviewers. Any product that may be evaluated in this article, or claim that may be made by its manufacturer, is not guaranteed or endorsed by the publisher.

Author disclaimer

The views expressed in this article are those of the authors and do not necessarily reflect the position or policy of the VA or NIH.

References

Alyagon, U., Shahar, H., Hadar, A., Barnea-Ygael, N., Lazarovits, A., Shalev, H., et al. (2020). Alleviation of ADHD symptoms by non-invasive right prefrontal stimulation is correlated with EEG activity. *Neuroimage Clin.* 26, 102206. doi: 10.1016/j.nicl.2020.102206

Anderson, R. J., Hoy, K. E., Daskalakis, Z. J., and Fitzgerald, P. B. (2016). Repetitive transcranial magnetic stimulation for treatment resistant depression: Re-establishing connections. *Clin. Neurophysiol.* 127, 3394–3405. doi: 10.1016/j.clinph.2016.08.015

Avery, D. H., and Holtzheimer, P. E. (2006). 3rd, Fawaz W, Russo J, Neumaier J, Dunner DL, et al. A controlled study of repetitive transcranial magnetic stimulation in medication-resistant major depression. *Biol. Psychiatry.* 59, 187–194. doi: 10.1016/j.biopsych.2005.07.003

Benadhira, R., Thomas, F., Bouaziz, N., Braha, S., Andrianisaina, P. S., Isaac, C., et al. (2017). A randomized, sham-controlled study of maintenance rTMS for treatment-resistant depression (TRD). *Psychiatry Res.* 258, 226–233. doi: 10.1016/j.psychres.2017.08.029

Bzdok, D., Hartwigsen, G., Reid, A., Laird, A. R., Fox, P. T., Eickhoff, S. B., et al. (2016). Left inferior parietal lobe engagement in social cognition and language. *Neurosci. Biobehav. Rev.* 68, 319–334. doi: 10.1016/j.neubiorev.2016.02.024

Cardenas, V. A., Bhat, J. V., Horwege, A. M., Ehrlich, T. J., Lavacot, J., Mathalon, D. H., et al. (2022). Anatomical and fMRI-network comparison of multiple DLPFC targeting strategies for repetitive transcranial magnetic stimulation treatment of depression. *Brain Stimul.* 15, 63–72. doi: 10.1016/j.brs.2021.11.008

Carpenter, L. L., Janicak, P. G., Aaronson, S. T., Boyadjis, T., Brock, D. G., Cook, I. A., et al. (2012). Transcranial magnetic stimulation (TMS) for major depression: a multisite, naturalistic, observational study of acute treatment outcomes in clinical practice. *Depress. Anxiety.* 29, 587–596. doi: 10.1002/da.21969

Center for Behavioral Health Statistics and RTI International (2021). In: Services USDoHaH, editor. *Key Substance Use and Mental Health Indicators in the United States: Results From the 2020 National Survey on Drug Use and Health.* Rockville, MD: Center for Behavioral Health Statistics and Quality, Substance Abuse and Mental Health Services Administration.

Cerqueira, C. T., Almeida, J. R., Gorenstein, C., Gentil, V., Leite, C. C., Sato, J. R., et al. (2008). Engagement of multifocal neural circuits during recall of autobiographical happy events. *Braz. J. Med. Biol. Res.* 41, 1076–1085. doi: 10.1590/S0100-879X2008001200006

Clarke, T. C., Schiller, J. S., and Boersma, P. (2019). *Early Release of Selected Estimates Based on Data From the 2019 National Health Interview Survey*. Atlanta, GA: Centers for Disease Control and Prevention, National Center for Health Statistics: U.S. Department of Health and Human Services. p. 2.

Connolly, K. R., Helmer, A., Cristancho, M. A., Cristancho, P., and O'Reardon, J. P. (2012). Effectiveness of transcranial magnetic stimulation in clinical practice post-FDA approval in the United States: results observed with the first 100 consecutive cases of depression at an academic medical center. *J. Clin. Psychiatry.* 73, e567–e573. doi: 10.4088/JCP.11m07413

Cosmo, C., Ferreira, C., and Miranda, J. G., do Rosario, R. S., Baptista, A. F., Montoya, P., et al. (2015). Spreading effect of tDCS in individuals with attention-deficit/hyperactivity disorder as shown by functional cortical networks: a randomized, double-blind, sham-controlled trial. *Front. Psychiatry.* 6, 111. doi: 10.3389/fpsyt.2015.00111

Cosmo, C., Zandvakili, A., Petrosino, N. J., Berlow, Y. A., and Philip, N. S. (2021). Repetitive transcranial magnetic stimulation for treatment-resistant depression: recent critical advances in patient care. *Curr. Treat Options Psychiatry* 8, 47–63. doi: 10.1007/s40501-021-00238-y

Davidson, R. J. (2004a). Well-beingand affective style: neural substrates and biobehavioural correlates. *Philos. Trans. R. Soc. Lond. B. Biol. Sci.* 359, 1395–1411. doi: 10.1098/rstb.2004.1510

Davidson, R. J. (2004b). What does the prefrontal cortex "do" in affect: perspectives on frontal EEG asymmetry research. *Biol. Psychol.* 67, 219–233. doi: 10.1016/j.biopsycho.2004.03.008

Demitrack, M. A., and Thase, M. E. (2009). Clinical significance of transcranial magnetic stimulation (TMS) in the treatment of pharmacoresistant depression: synthesis of recent data. *Psychopharmacol. Bull.* 42, 5–38.

Denee, T., Kerr, C., Eva, J., Vincent, S. A., Young, A. H., Jacobsen, N., et al. (2022). The impact of treatment-resistant depression on the lives of carers: a mixed-methods study. *J. Affect. Disord.* 325, 194–205. doi: 10.1016/j.jad.2022.12.135

Eric, E., and Hall, S. J. P. (1999). Frontal asymmetry, dispositional affect, and physical activity in older adults. *J Aging Phys Activity.* 7, 76–90. doi: 10.1123/japa.7.1.76

Gaynes, B. N., Lloyd, S. W., Lux, L., Gartlehner, G., Hansen, R. A., Brode, S., et al. (2014). Repetitive transcranial magnetic stimulation for treatment-resistant depression: a systematic review and meta-analysis. *J. Clin. Psychiatry.* 75, 477–489. doi: 10.4088/JCP.13r08815

Gili, M., Luciano, J. V., Bauza, N., Aguado, J., Serrano, M. J., Armengol, S., et al. (2011). Psychometric properties of the IDS-SR30 for the assessment of depressive symptoms in Spanish population. *BMC Med. Res. Methodol.* 11, 131. doi: 10.1186/1471-2288-11-131

Henriques, J. B., and Davidson, R. J. (1990). Regional brain electrical asymmetries discriminate between previously depressed and healthy control subjects. *J. Abnorm. Psychol.* 99, 22–31. doi: 10.1037/0021-843X.99.1.22

Henriques, J. B., and Davidson, R. J. (1991). Left frontal hypoactivation in depression. *J. Abnorm. Psychol.* 100, 535–545. doi: 10.1037/0021-843X.100.4.535

Kallioniemi, E., and Daskalakis, Z. J. (2022). Identifying novel biomarkers with TMS-EEG - Methodological possibilities and challenges. *J. Neurosci. Methods.* 377, 109631. doi: 10.1016/j.jneumeth.2022.109631

Khedr, E. M., Elbeh, K., Saber, M., Abdelrady, Z., and Abdelwarith, A. (2022). A. double blind randomized clinical trial of the effectiveness of low frequency rTMS over right DLPFC or OFC for treatment of obsessive-compulsive disorder. *J. Psychiatr. Res.* 156, 122–131. doi: 10.1016/j.jpsychires.2022.10.025

Lan, M. J., Chhetry, B. T., Liston, C., Mann, J. J., and Dubin, M. (2016). Transcranial magnetic stimulation of left dorsolateral prefrontal cortex induces brain morphological changes in regions associated with a treatment resistant major depressive episode: an exploratory analysis. *Brain Stimul.* 9, 577–583. doi: 10.1016/j.brs.2016.02.011

Liston, C., Chen, A. C., Zebley, B. D., Drysdale, A. T., Gordon, R., Leuchter, B., et al. (2014). Default mode network mechanisms of transcranial magnetic stimulation in depression. *Biol. Psychiatry.* 76, 517–526. doi: 10.1016/j.biopsych.2014.01.023

Machado, L., and Cantilino, A. (2017). A systematic review of the neural correlates of positive emotions. *Braz J Psychiatry.* 39, 172–179. doi: 10.1590/1516-4446-2016-1988

McIntyre, R. S., Filteau, M. J., Martin, L., Patry, S., Carvalho, A., Cha, D. S., et al. (2014). Treatment-resistant depression: definitions, review of the evidence, and algorithmic approach. *J. Affect. Disord.* 156, 1–7. doi: 10.1016/j.jad.2013.10.043

McIntyre, R. S., Lee, Y., Rodrigues, N. B., Nasri, F., Lao, G., Zeng, W., et al. (2021). Repetitive transcranial magnetic stimulation for cognitive function in adults with bipolar disorder: A pilot study. *J. Affect. Disord.* 293, 73–77. doi: 10.1016/j.jad.2021.05.075

Mel'nikov, M. E., Petrovskii, E. D., Bezmaternykh, D. D., Kozlova, L. I., Shtark, M. B., Savelov, A. A., et al. (2018). fMRI response of parietal brain areas to sad facial stimuli in mild depression. *Bull. Exp. Biol. Med.* 165, 741–745. doi: 10.1007/s10517-018-4255-y

Morris, A. T., Temereanca, S., Zandvakili, A., Thorpe, R., Sliva, D. D., Greenberg, B. D., et al. (2023). Fronto-central resting-state 15-29Hz transient beta events change with therapeutic transcranial magnetic stimulation for posttraumatic stress disorder and major depressive disorder. *medRxiv [Preprint].* doi: 10.1101/2023.03.11.23286902

Muller, V. I., Cieslik, E. C., Laird, A. R., Fox, P. T., and Eickhoff, S. B. (2013). Dysregulated left inferior parietal activity in schizophrenia and depression: functional connectivity and characterization. *Front. Hum. Neurosci.* 7, 268. doi: 10.3389/fnhum.2013.00268

Newson, J. J., Thiagarajan, T. C., and Frequency Bands in, E. E. G. (2018). Psychiatric disorders: a review of resting state studies. *Front. Hum. Neurosci.* 12, 521. doi: 10.3389/fnhum.2018.00521

Noda, Y., Nakamura, M., Saeki, T., Inoue, M., Iwanari, H., Kasai, K., et al. (2013). Potentiation of quantitative electroencephalograms following prefrontal repetitive transcranial magnetic stimulation in patients with major depression. *Neurosci. Res.* 77, 70–77. doi: 10.1016/j.neures.2013.06.002

Numssen, O., Bzdok, D., and Hartwigsen, G. (2021). Functional specialization within the inferior parietal lobes across cognitive domains. *Elife.* 10, e63591. doi: 10.7554/eLife.63591

Ochsner, K. N., Bunge, S. A., Gross, J. J., and Gabrieli, J. D. (2002). Rethinking feelings: an FMRI study of the cognitive regulation of emotion. *J. Cogn. Neurosci.* 14, 1215–1229. doi: 10.1162/089892902760807212

Palmiero, M., and Piccardi, L. (2017). Frontal EEG asymmetry of mood: a mini-review. *Front. Behav. Neurosci.* 11, 224. doi: 10.3389/fnbeh.2017.00224

Pandya, M., Altinay, M., and Malone, D. A., Anand, A. (2012). Where in the brain is depression? *Curr. Psychiatry Rep.* 14, 634–642. doi: 10.1007/s11920-012-0322-7

Paquette, V., Beauregard, M., and Beaulieu-Prevost, D. (2009). Effect of a psychoneurotherapy on brain electromagnetic tomography in individuals with major depressive disorder. *Psychiatry Res.* 174, 231–239. doi: 10.1016/j.pscychresns.2009.06.002

Philip, N. S., Carpenter, S. L., Ridout, S. J., Sanchez, G., Albright, S. E., Tyrka, A. R., et al. (2015). 5Hz Repetitive transcranial magnetic stimulation to left prefrontal cortex for major depression. *J. Affect. Disord.* 186, 13–17. doi: 10.1016/j.jad.2014.12.024

Polania, R., Nitsche, M. A., and Paulus, W. (2011). Modulating functional connectivity patterns and topological functional organization of the human brain with transcranial direct current stimulation. *Hum. Brain Mapp.* 32, 1236–1249. doi: 10.1002/hbm.21104

Roalf, D. R., Pruis, T. A., Stevens, A. A., and Janowsky, J. S. (2011). More is less: emotion induced prefrontal cortex activity habituates in aging. *Neurobiol. Aging.* 32, 1634–1650. doi: 10.1016/j.neurobiolaging.2009.10.007

Rosário, R. S., Cardosco, P. T., Muñoz, M. A., Montoya, P., and Miranda, J. G. V. (2015). Motif-synchronization: a new method for analysis of dynamic brain networks with EEG. *Physica A.* 439, 7–19. doi: 10.1016/j.physa.2015.07.018

Spielberg, J. M., Stewart, J. L., Levin, R. L., Miller, G. A., and Heller, W. (2008). Prefrontal cortex, emotion, and approach/withdrawal motivation. *Soc. Personal. Psychol. Compass.* 2, 135–153. doi: 10.1111/j.1751-9004.2007.00064.x

Sporns, O. (2018). Graph theory methods: applications in brain networks. *Dialogues Clin. Neurosci.* 20, 111–121. doi: 10.31887/DCNS.2018.20.2/osporns

Spronk, D., Arns, M., Bootsma, A., van Ruth, R., and Fitzgerald, P. B. (2008). Long-term effects of left frontal rTMS on EEG and ERPs in patients with depression. *Clin. EEG Neurosci.* 39, 118–124. doi: 10.1177/155005940803900305

Toutain, T., Alba, G., and Miranda, J. G. V., Silva do Rosario, R., Munoz, M., de Sena, E. P. (2022). Brain asymmetry in pain affective modulation. *Pain Med.* 23, 686–696. doi: 10.1093/pm/pnab232

Toutain, T. G. L. d. O., Miranda, J. G. V., do Rosário, R. S., and de Sena, E. P. (2023). Brain instability in dynamic functional connectivity in schizophrenia. *J. Neural Transm.* 130, 171–180. doi: 10.1007/s00702-022-02579-1

Valiulis, V., Gerulskis, G., Dapsys, K., Vistartaite, G., Siurkute, A., Maciulis, V., et al. (2012). Electrophysiological differences between high and low frequency rTMS protocols in depression treatment. *Acta Neurobiol. Exp.* 72, 283–295.

World Health Organization (2017). *Depression and Other Common Mental Disorders: Global Health Estimates.* Geneva: World Health Organization.

Wozniak-Kwasniewska, A., Szekely, D., Harquel, S., Bougerol, T., and David, O. (2015). Resting electroencephalographic correlates of the clinical response to repetitive transcranial magnetic stimulation: A preliminary comparison between unipolar and bipolar depression. *J. Affect. Disord.* 183, 15–21. doi: 10.1016/j.jad.2015.04.029

Wyczesany, M., Capotosto, P., Zappasodi, F., and Prete, G. (2018). Hemispheric asymmetries and emotions: evidence from effective connectivity. *Neuropsychologia.* 121, 98–105. doi: 10.1016/j.neuropsychologia.2018.10.007

Zandvakili, A., Philip, N. S., Jones, S. R., Tyrka, A. R., Greenberg, B. D., Carpenter, L. L., et al. (2019). Use of machine learning in predicting clinical response to transcranial magnetic stimulation in comorbid posttraumatic stress disorder and major depression: A resting state electroencephalography study. *J. Affect. Disord.* 252, 47–54. doi: 10.1016/j.jad.2019.03.077

Zhang, F. F., Peng, W., Sweeney, J. A., Jia, Z. Y., and Gong, Q. Y. (2018). Brain structure alterations in depression: psychoradiological evidence. *CNS Neurosci. Ther.* 24, 994–1003. doi: 10.1111/cns.12835

Zhdanava, M., Pilon, D., Ghelerter, I., Chow, W., Joshi, K., Lefebvre, P., et al. (2021). The prevalence and national burden of treatment-resistant depression and major depressive disorder in the United States. *J. Clin. Psychiatry.*82, 20m13699. doi: 10.4088/JCP.20m13699

frontiers | Frontiers in Neural Circuits

TYPE Brief Research Report
PUBLISHED 15 June 2023
DOI 10.3389/fncir.2023.1179096

OPEN ACCESS

EDITED BY
Joshua C. Brown,
Harvard Medical School, United States

REVIEWED BY
Brian Theyel,
Brown University, United States
Roger Cachope,
CHDI Foundation, United States

*CORRESPONDENCE
Jennifer Rodger
✉ jennifer.rodger@uwa.edu.au

RECEIVED 03 March 2023
ACCEPTED 16 May 2023
PUBLISHED 15 June 2023

CITATION
Tomar M, Rodger J and Moretti J (2023) Dorsal striatum c-Fos activity in perseverative ephrin-A2A5$^{-/-}$ mice and the cellular effect of low-intensity rTMS.
Front. Neural Circuits 17:1179096.
doi: 10.3389/fncir.2023.1179096

Dorsal striatum c-Fos activity in perseverative ephrin-A2A5$^{-/-}$ mice and the cellular effect of low-intensity rTMS

Maitri Tomar[1,2], Jennifer Rodger[1,2]* and Jessica Moretti[1,2]

[1]School of Biological Sciences, University of Western Australia, Crawley, WA, Australia, [2]Brain Plasticity Lab, Perron Institute for Neurological and Translational Science, Nedlands, WA, Australia

Introduction: Overreliance on habit is linked with disorders, such as drug addiction and obsessive-compulsive disorder, and there is increasing interest in the use of repetitive transcranial magnetic stimulation (rTMS) to alter neuronal activity in the relevant pathways and for therapeutic outcomes. In this study, we researched the brains of ephrin-A2A5$^{-/-}$ mice, which previously showed perseverative behavior in progressive-ratio tasks, associated with low cellular activity in the nucleus accumbens. We investigated whether rTMS treatment had altered the activity of the dorsal striatum in a way that suggested altered hierarchical recruitment of brain regions from the ventral striatum to the dorsal striatum, which is linked to abnormal habit formation.

Methods: Brain sections from a limited number of mice that underwent training and performance on a progressive ratio task with and without low-intensity rTMS (LI-rTMS) were taken from a previous study. We took advantage of the previous characterization of perseverative behavior to investigate the contribution of different neuronal subtypes and striatal regions within this limited sample. Striatal regions were stained for c-Fos as a correlate of neuronal activation for DARPP32 to identify medium spiny neurons (MSNs) and for GAD67 to identify GABA-ergic interneurons.

Results and discussion: Contrary to our hypothesis, we found that neuronal activity in ephrin-A2A5$^{-/-}$ mice still reflected the typical organization of goal-directed behavior. There was a significant difference in the proportion of neuronal activity across the striatum between experimental groups and control but no significant effects identifying a specific regional change. However, there was a significant group by treatment interaction which suggests that MSN activity is altered in the dorsomedial striatum and a trend suggesting that rTMS increases ephrin-A2A5$^{-/-}$ MSN activity in the DMS. Although preliminary and inconclusive, the analysis of this archival data suggests that investigating circuit-based changes in striatal regions may provide insight into chronic rTMS mechanisms that could be relevant to treating disorders associated with perseverative behavior.

KEYWORDS

habit formation, dorsal striatum, nucleus accumbens, rTMS, ephrin, c-Fos

1. Introduction

Repetitive transcranial magnetic stimulation (rTMS) is a non-invasive brain stimulation technique that is currently approved for the treatment of depression (O'Reardon et al., 2007) and obsessive compulsive disorder (OCD) (Carmi et al., 2018). However, the mechanisms of how rTMS achieve therapeutic outcomes are not well understood, and increased understanding can be useful in refining its use.

Currently, we know that rTMS can modulate neuronal activity (Aydin-Abidin et al., 2008; Moretti et al., 2022) and the activity of various neurotransmitters, including dopamine (Keck et al., 2002; Moretti et al., 2020), which is thought to contribute to rTMS-induced changes.

Previously, a transgenic ephrin-A2A5$^{-/-}$ mouse strain has been used in conjunction with rTMS to measure structural and functional plasticity induced within abnormal neural pathways. Ephrins are membrane-bound ligands of Eph tyrosine kinase receptors and are important in cell migration and axon guidance during development (Wilkinson, 2001). As a result, ephrin-A2A5$^{-/-}$ mice, which lack the ephrin-A2 and ephrin-A5 ligands, show disorganized axonal projections in neuronal circuits throughout the brain due to disrupted Eph/ephrin signaling. These mice display abnormal visual topography and visuomotor behavior which are both partially rescued by low-intensity rTMS (LI-rTMS) (Rodger et al., 2012; Makowiecki et al., 2014; Poh et al., 2018). In addition, the mice show reduced dopaminergic innervation of the striatum (Sieber et al., 2004; Cooper et al., 2009) associated with abnormal behavioral patterns in goal-directed behavior (Poh et al., 2018), but the effects of LI-rTMS on this phenotype are less well understood.

A previous study (Moretti et al., 2021) explored whether the different goal-directed behaviors of ephrin-A2A5$^{-/-}$ mice, compared to wildtype mice, were due to abnormal motivation processing, by comparing the performance of both strains in progressive ratio (PR) tasks. PR tasks are a good measure of motivation as they involve an increasing instrumental response requirement for a reward. Highly motivated animals will continue to respond consistently, while animals with low motivation stop or slow their response (Hodos, 1961; Aberman et al., 1998). The potential ameliorating effect of chronic excitatory LI-rTMS delivered during the PR task was also examined. Unexpectedly, the results did not support a motivation phenotype: ephrin-A2A5$^{-/-}$ mice showed perseverative behavior in the PR task, with a greater number of responses compared to wildtype mice despite increasing task difficulty (Moretti et al., 2021). Compared to wildtype mice, ephrin-A2A5$^{-/-}$ mice also showed reduced c-Fos expression in the nucleus accumbens (NAc) after 2 weeks' performance on the PR task (Moretti et al., 2021).

It had been suggested that the behavioral phenotype of perseverative responding and reduced accumbal activity in ephrin-A2A5$^{-/-}$ mice may reflect an accelerated dorsal shift in neuronal activity characteristic of habitual behavior (Segovia et al., 2012). The behavioral shift from goal-directed to habitual behavior involves dopaminergic pathways and hierarchical recruitment of brain regions from the ventral striatum to the dorsal striatum, which would correspond to the reduced activity in the nucleus accumbens (ventral striatum) in ephrin-A2A5$^{-/-}$ mice (Segovia et al., 2012; Liu et al., 2013).

Interestingly, chronic excitatory LI-rTMS delivered to ephrin-A2A5$^{-/-}$ mice during the PR task did not significantly alter behavior but did ameliorate the reduced c-Fos expression in the ventral striatum of ephrin-A2A5$^{-/-}$ mice, resulting in expression that was similar to wildtype levels (Moretti et al., 2021). Therefore, in ephrin-A2A5$^{-/-}$ mice, LI-rTMS may mitigate abnormal activity along the mesolimbic pathway associated with behavioral inflexibility and habit. One possibility is that it delays or interferes with an accelerated shift in neuronal activity toward the dorsal striatum.

However, Moretti et al. (2021) did not include the analysis of the c-Fos activity in the dorsal striatum. Therefore, in this study, we aim to understand whether (1) the altered dorsal striatum activity occurred in ephrin-A2A5$^{-/-}$ mice, which could partially explain the perseverative behavior in these mice and (2) whether LI-rTMS treatment altered the dorsal striatal activity in ephrin-A2A5$^{-/-}$ mice. In this study, we used the archival tissue from the study by Moretti et al. (2021) to identify and compare the activation of neuronal populations across the entire striatum, investigating the dorsomedial striatum (DMS), dorsolateral striatum (DLS), and nucleus acccumbens (NAc) in wildtype and ephrin-A2A5$^{-/-}$ mice that either received active rTMS or sham stimulation, using c-Fos immunohistochemistry. Due to the archival nature of this tissue, our sample size is not sufficient to warrant firm conclusions, and without multiple timepoints, we cannot definitively demonstrate a change in the progression of hierarchical recruitment. However, we present these data as supporting evidence to Moretti et al. (2021) to determine, at least at this single timepoint, whether activity in the striatum reflects a relative difference in striatal activity contribution. This brief report acts as preliminary data to support whether the hypothesis that rTMS alters circuit function and/or hierarchical recruitment of activity has any potential for future research, especially research interested in the transition from goal-directed to habitual behavior, such as drug addiction (Everitt and Robbins, 2005) and OCD (Gillan et al., 2011). However, future research requires greater sample sizes and multiple time points to fully characterize such changes.

2. Materials and methods

2.1. Animal tissue

All experiments were approved by the University of Western Australia Animal Ethics Committee (AEC 100/1639). Sagittal mouse brain sections (40 μm) from 11 adult (8–24-week-old) wildtype C57BL6/J mice (sham: 6 mice (2 male and 4 female mice); rTMS: 5 mice (2 male and 3 female mice) and 10 ephrin-A2A5$^{-/-}$ mice [sham: 6 (4 male and 2 female mice); rTMS: 4 mice (1 male and 3 female mice)] (Moretti et al., 2021) were used. The ephrin-A2A5$^{-/-}$ mice were backcrossed onto C57BL6/J mice for >20 generations, bred from heterozygous ephrin-A2$^{-/-}$A5$^{+/-}$ parents and genotyped at weaning (Feldheim et al., 2000). In the previous study, following habituation to the LI-rTMS coil and training in the operant box, mice performed 1 week of an exponential PR task (required responses increase under an exponential equation) followed by 1 week of PR7 (requirement started at 7 responses and increased by 7 with each reinforcement) (Moretti et al., 2021). Mice received 14 days of biomimetic high-frequency stimulation (BHFS) LI-rTMS or sham during the first 10 min of the daily PR task and were euthanized 90 min after the beginning of the final PR task to correspond with the peak of c-Fos expression (Moretti et al., 2021). A summary of the experimental design from Moretti et al. (2021) is reproduced in Figure 1. The previous study showed perseverative behavior in both treated and untreated ephrin-A2A5-/- mice, as well as low c-Fos expression in the NAc of untreated mice, which

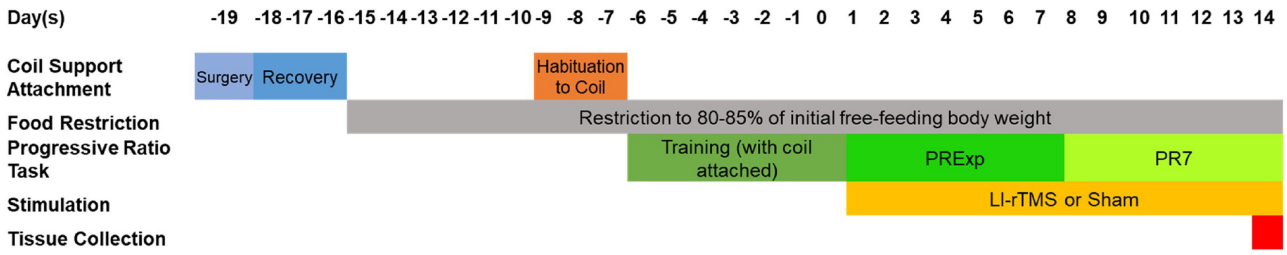

FIGURE 1
Outline of the experimental paradigm performed by Moretti et al. (2021). Reproduced from Moretti et al. (2021) Copyright 2021, with permission from Elsevier. http://www.sciencedirect.com/journal/behavioural-brain-research.

showed improvement following LI-rTMS (Moretti et al., 2021). It was speculated that the low c-Fos expression in the NAc may reflect an accelerated shift from goal-directed to habit in untreated ephrin-A2A5$^{-/-}$ mice, which could have been delayed at a cellular level by LI-rTMS (Moretti et al., 2021). However, in the previous study, neuronal activation in the dorsal striatum was not investigated. In the current study, we used additional tissues from the same animals as Moretti et al. (2021) to confirm the shift in neuronal activity from regions involved in goal-directed behavior to form a habit and whether LI-rTMS delayed it at a cellular level.

2.2. Immunofluorescence

Every fifth sagittal brain section which contained the dorsal striatum was identified using the mouse brain atlas (Paxinos and Franklin, 2012). These sections were stained for three different antibodies: c-Fos (rabbit polyclonal c-Fos antibody, 1:5000, Abcam, ab190289), a marker for neuronal activity (Bullitt, 1990); cAMP-regulated phosphoprotein-32 kD (DARPP32) (purified mouse anti-DARPP32, 1:2000, BD Transduction Laboratories, 611520), a marker for MSNs (Anderson and Reiner, 1991); and glutamate decarboxylase 67 (GAD67) (anti-Goat, 1:750, R&D systems, AF2086-SP), a marker for GABAergic neurons (Lazarus et al., 2015).

Free-floating sections were washed 3× in PBS (5 min each), permeabilized by washing in 0.1% Triton-X in PBS (PBS-T) for 15 min, and incubated for 2 h in a blocking buffer of 2% bovine serum albumin (Sigma) and 3% normal donkey serum (Sigma) diluted in 0.1% PBS-T. Then, sections were incubated with primary antibodies in a blocking buffer overnight at 4°C. Sections were washed in PBS-T 3× (10 min each) and incubated for 2 h with secondary antibodies diluted in blocking buffer to 1:600 (donkey anti-rabbit IgG Alexa Fluor 488, Invitrogen, Thermo Fisher, A21206; donkey anti-mouse IgG Alexa Fluor 555, Invitrogen, Thermo Fisher, A21202; and donkey anti-goat IgG H&L Alexa Fluor 647, ab150131). Sections were then washed in PBS-T 3× (10 min each) and incubated for 10 min in Hoescht in PBS (1:1000, Invitrogen). Finally, the sections were washed in PBS 3× (10 min each) and mounted on gelatin-subbed slides, coverslipped with a mounting medium (Dako, Glostrup, Denmark), and sealed with nail polish. Slides were stored at 4°C in a light-controlled environment until imaging.

2.3. Imaging and quantification

For accurate locations of DMS and DLS in sagittal sections, we used the Chon et al. (2019) atlas annotated onto a 3D magnetic resonance imaging (MRI) data of the P56 mouse brain atlas using the software ITK-SNAP (Yushkevich et al., 2006). Sections were imaged through z-stacks (2 µm apart) on a Nikon C2 confocal microscope (Nikon, Tokyo, Japan) at 40× magnification. During imaging, sections from one ephrin-A2A5$^{-/-}$-rTMS animal were excluded due to poor staining (ephrin-A2A5$^{-/-}$-rTMS $n = 3$). Cell counts were performed using stereological principles using ImageJ software and were carried out blinded to the experimental group after all images were captured.

The total number of c-Fos single-labeled cells, c-Fos^{+}/DARPP32^{+} double-labeled cells, and c-Fos^{+}/GAD67^{+}/DARPP32^{-} double-labeled cells were identified and counted for each image (Figure 2). The combination of DARPP32^{+} and GAD67^{+} double labeling was not assessed since DARPP32^{+} cells are also GAD67^{+} because they are GABAergic in nature. c-Fos^{+} cells not colocalized with DARPP32 were classified as unspecified c-Fos.

2.4. Statistical analysis

For analysis, the total c-Fos cells/mm^3, the percentage of c-Fos cells colocalized with DARPP32, and GAD67 were calculated for each animal.

Assumptions of normality and homogeneity were checked. For DLS counts, the assumptions of normality were not met for percentage c-Fos-GAD67 and total c-Fos cells/mm^3 counts ($p < 0.05$). The homogeneity of variance was checked, and it was met for all datasets (Levene's test, $p > 0.05$). For DMS counts, the assumptions of normality were not met for percentage c-Fos-DARPP32, percentage c-Fos-GAD67, and total c-Fos cells/mm^3 ($p < 0.05$). The assumption of homogeneity of variance was not met for percentage c-Fos-DARPP32 data (Levene's test, $p < 0.05$) but was corrected with logarithmic transformation.

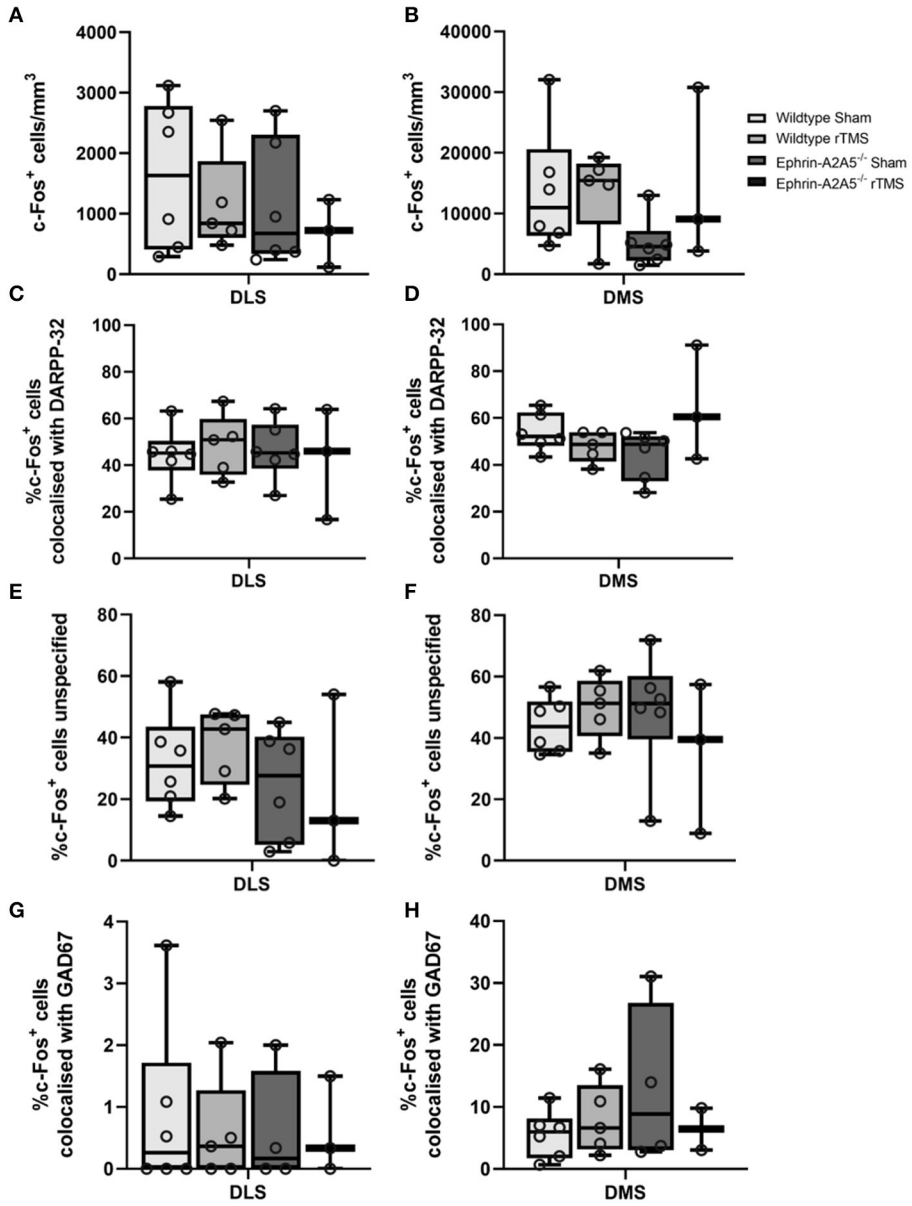

FIGURE 2
c-Fos activation in DMS and DLS across rTMS treated and untreated wildtype and ephrin-A2A5$^{-/-}$mice. Total c-Fos density (cells/mm^3) **(A, B)**; % of c-Fos$^+$ cells colocalized with DARPP32$^+$ cells **(C, D)**; unspecified c-Fos$^+$ cells **(E, F)**; and c-Fos$^+$ cells colocalized with GAD67$^+$-DARPP32$^-$ **(G, H)**. Points represent individual animal counts. Overall, c-Fos activation did not differ between strains or treatment groups. However, the significant omnibus test indicated a difference in DMS c-Fos-DARPP32 colocalization. Results suggested that in ephrin-A2A5$^{-/-}$, rTMS increased the percentage of c-Fos-DARPP32 colocalization but pairwise *post hoc* comparisons did not survive multiple corrections.

To compare whether cell counts changed across groups, multiple two-way analyses of variance (ANOVAs) were used with the independent variables of strain and treatment. Each ANOVA had the dependent variable of either total c-Fos cells/mm^3, percentage c-Fos-DARPP32, or percentage unspecified c-Fos cell count data and was run separately for both DLS and DMS. ANOVA was also performed for c-Fos$^+$/GAD67$^+$/DARPP32$^-$ cell counts for the DLS region. For the DMS regions, due to a small sample size, the ephrin-rTMS group was excluded from statistical analysis for c-Fos$^+$/GAD67$^+$/DARPP32$^-$ dataset, and Student *t*-tests were performed to compare the remaining experimental groups.

Additional data for the percentage of c-Fos$^+$/GAD67$^+$/DARPP32$^-$ cell counts were also obtained for the NAc core and shell when the regions were present in the stained tissue (NAc core, Group: wildtype-sham $n = 5$, wildtype-rTMS $n = 4$, ephrin-A2A5$^{-/-}$-sham $n = 4$, and ephrin-A2A5$^{-/-}$-rTMS $n = 2$; NAc shell, Group: wildtype-sham $n = 6$, wildtype-rTMS $n = 5$, ephrin-A2A5$^{-/-}$-sham $n = 4$, and ephrin-A2A5$^{-/-}$-rTMS $n = 3$). This was combined with total c-Fos cells/mm^3 and percentage c-Fos-DARPP32 cell counts for NAc core and shell from the previous study (Moretti et al., 2021). The percentage of the c-Fos-GAD67 dataset in the NAc core and shell did not meet the assumptions of normality and heterogeneity. Therefore,

non-parametric Mann–Whitney *U*-tests were performed to compare the percentage of c-Fos$^+$/GAD67$^+$/DARPP32$^-$ cell counts between sham and treatment for both wildtype and ephrin-A2A5$^{-/-}$ groups.

3. Results

3.1. Total c-Fos cells/mm^3

In DLS and DMS, there was no significant strain, treatment, or interaction effects [DLS: $F_{(1,16)} < 1.04$, $p > 0.323$; DMS: $F_{(1,16)} < 1.378$, $p > 0.258$].

3.2. c-Fos colocalization in MSNs

In DLS, there was no overall effect of the strain, treatment, or interaction [$F_{(1,16)} < 0.376$, $p > 0.548$] (Figure 2). Similarly, in DMS, there was no significant difference in the percentage of colocalization between strains or treatment [$F_{(1,16)} < 1.26$, $p > 0.279$]. However, there was a significant strain*treatment interaction [$F_{(1,16)} = 5.1062$, $p = 0.038$, $\eta^2 = 0.228$]. To understand the interaction, we followed up with pairwise *post hoc* comparisons using Tukey's test. There was an increase in the percentage of c-Fos-DARPP32 colocalization after treatment in ephrin-A2A5$^{-/-}$ mice compared to the ephrin-sham group (Figure 2); however, the effect did not survive multiple comparison correction [uncorrected $p = 0.041$, $t_{(16)} = -2.225$, corrected $p = 0.159$] despite the significant omnibus interaction. All other groups were non-significantly different from each other.

3.3. Percentage of unspecified c-Fos cells

In DLS and DMS, there was a significant effect of strain, treatment, or interaction [DLS: $F_{(1,16)} < 1.9052$, $p > 0.186$; DMS: $F_{(1,16)} < 1.738$, $p > 0.206$] (Figure 2).

3.3.1. Confirmatory analysis for unspecified c-Fos-labeled cells

Across all experimental groups, approximately 60 and 40% of c-Fos labeled cells in the ventral and dorsal striatum, respectively, were unidentified (i.e., not MSNs). Therefore, the sections included staining for GABAergic interneurons to identify unspecified c-Fos labeled cells.

For the percentage of c-Fos$^+$/GAD67$^+$/DARPP32$^-$ colocalization, there were no effects of strain, treatment, or interaction for the DLS [$F_{(1,14)} < 0.088$, $p > 0.771$], and in the DMS, there was no significant change in c-Fos$^+$/GAD67$^+$/DARPP32$^-$ colocalization between wildtype-sham and wildtype-rTMS mice [$t_{(9)} = -0.864$, $p = 0.410$], and there was no significant difference between strains, wildtype-sham and ephrin-sham [$t_{(8)} = -1.32$, $p = 0.222$].

In the NAc core, there was no significant difference in the percentage of c-Fos$^+$/GAD67$^+$/DARPP32$^-$ colocalization following treatment in both wildtype (U = 8.5, $p = 0.771$) and ephrin-A2A5$^{-/-}$ mice (U = 2, $p = 0.289$) and no significant difference between strains, wildtype-sham and ephrin-sham (U = 6, $P = 0.240$). Similarly, in the NAc shell, there was no significant difference in the percentage of c-Fos$^+$/GAD67$^+$/DARPP32$^-$ colocalization following treatment in both wildtype (U = 12, $p = 0.597$) and ephrin-A2A5$^{-/-}$ mice (U = 5, $p = 0.825$). There was also no significant strain difference between wildtype-sham and ephrin-sham (U = 11, $p = 0.896$).

3.4. Comparison of c-Fos activity across regions and groups

The initial 4*4 contingency χ^2 test was significant [$\chi^2(9, N = 666{,}524) = 8{,}030$, $p < 0.001$, V = 0.0634]. The follow-up 2*4 contingency χ^2 test was performed to understand where the difference was and showed that proportions of the striatal c-Fos activity per region (Figure 3) differed in comparison with wildtype-sham for all groups although the test may be overly sensitive due to the large sample size [wildtype-rTMS: $\chi^2(3, N = 436{,}329) = 642$, $p < 0.001$, V = 0.0384; ephrin-sham: $\chi^2(3, N = 335{,}837) = 2156$, $p < 0.001$, V = 0.0801; and ephrin-rTMS: $\chi^2(3, N = 384{,}288) = 2446$, $p < 0.001$, V = 0.0798]. Although there are significant differences, the effect sizes for each comparison are small.

Finally, a region-by-region comparison of experimental groups against wildtype-sham is presented in Table 1. Despite significant comparisons on the group level, no regions appeared to be statistically different. Therefore, no single regional difference drove the difference between wildtype sham and the other experimental groups. However, numerically, it does appear that the proportion of DLS activation increases in the ephrin-sham group and decreases in the ephrin-rTMS group relative to wildtype mice.

4. Discussion

Prior evidence of a habitual behavioral responding pattern in ephrin-A2A5$^{-/-}$ mice led to the hypothesis that these mice would display greater neuronal activity in striatal regions involved in habit formation (Moretti et al., 2021). The majority of the neuronal activity in the striatum of these mice remained localized in regions responsible for goal-directed behavior. However, the proportion of c-Fos labeling across the striatum was significantly different in all experimental groups compared to control animals although no specific region was identified as driving this difference.

We also hypothesized that the LI-rTMS change in c-Fos densities seen previously in ephrin-A2A5$^{-/-}$ mice NAc would extend to the dorsal striatum. In partial support, we did not observe a change in average c-Fos density after LI-rTMS in ephrin-A2A5$^{-/-}$ mice for the dorsostriatal regions, but in the DMS, there was a trend that suggested increased MSN activation in ephrin-A2A5$^{-/-}$ mice following stimulation.

The proportional activity across the striatum showed significant differences between wildtype-sham and the other experimental groups when considering the distribution of activity across all regions (i.e., wildtype-sham overall proportion distribution vs. wildtype rTMS overall proportion distribution), but when comparing group differences within specific regions (i.e., the

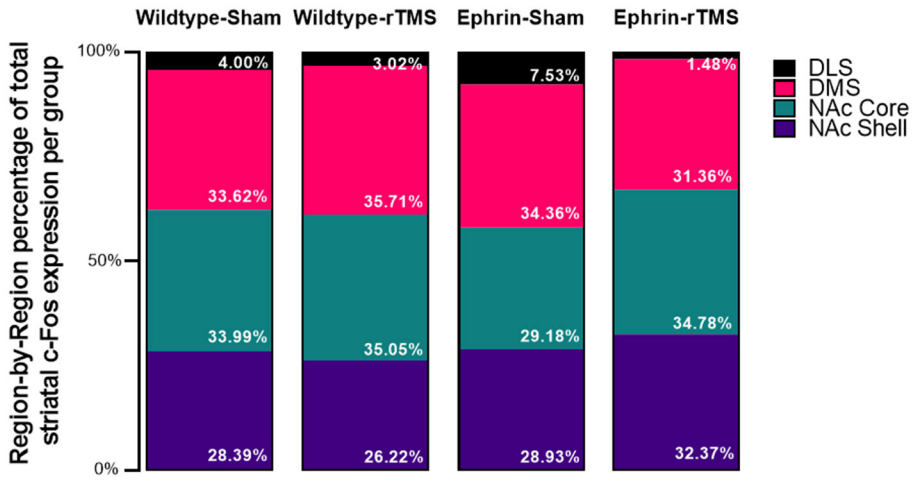

FIGURE 3
Average region-by-region proportion of the total striatal activity in the experimental groups. An initial 4*4 (group*region) contingency χ^2 test inclusive of all groups was significant, as were follow-up 2*4 (group*region) contingency χ^2 tests comparing each experimental group with wildtype-sham. However, Mann–Whitney U comparisons did not identify significant differences at the region level (e.g., wildtype-sham DLS vs. ephrin-sham DLS).

TABLE 1 Region-by-region comparison for the proportion of c-Fos in the striatum.

Group comparison (wildtype-sham vs. experimental groups)	Mann-Whitney U	*p*	Effect size (rank biserial correlation)	Mean difference	95% confidence interval	
					Lower	Upper
Wildtype-rTMS						
Region comparison						
DLS	14	0.926	0.0667	0.271	−2	4
DMS	11	0.537	0.267	−5.5	−22	21
NAc core	14.5	1	0.0333	0.00368	−18	14
NAc shell	12	0.662	0.200	5.5	−11	17
Ephrin-sham						
Region comparison						
DLS	11.5	0.333	0.361	−3.88	−21	3
DMS	15	0.699	0.167	−5	−24	20
NAc core	11	0.31	0.389	9.5	−9	27
NAc shell	17	0.936	0.056	3	−13	13
Ephrin-rTMS						
Region comparison						
DLS	4.5	0.276	0.500	2	−2	6
DMS	7	0.714	0.222	4.5	−20	42
NAc core	9	1	0	−0.0727	−23	17
NAc shell	6	0.548	0.333	−4.5	−21	8

Mann–Whitney U comparisons, following significant 2*4 contingency χ^2 tests, assessed region-specific changes in the proportion of striatal c-Fos (wildtype-sham vs. experimental groups).

difference in NAc proportion between two groups), there were no significant differences. We found absolute differences between the means for the DLS of ephrin-A2A5$^{-/-}$ mice and the wildtype-sham group where proportional DLS activity was greater in ephrin-A2A5$^{-/-}$ sham mice than wildtype mice and lower in ephrin-A2A5$^{-/-}$ mice than LI-rTMS. This is in line with the hypotheses, but the differences did not reach statistical significance. Greater sample size and specific experimental design are required

to appropriately understand whether the progression of activity within the striatum is altered with LI-rTMS.

Additionally, we assessed the GABA-ergic interneuron activity throughout the striatum but saw no significant changes in GAD67 activity between groups. Apart from the DMS, which had approximately 5–10% GABA-ergic interneuron activity, low GABA-ergic interneuron activity was observed in the NAc core, shell (<2%), and DLS (<4%).

4.1. Caveats

The hierarchical recruitment of striatal regions from goal-directed to habitual behavior was partly characterized by the progression of c-Fos expression during training in a fixed-ratio (FR) task, from higher c-Fos activity in the NAc shell on the first day of the task, toward the NAc core, DMS, and finally to DLS as training progresses (Segovia et al., 2012). In our study, a caveat is that, unlike previous studies (Segovia et al., 2012), our c-Fos data indirectly reflect the neuronal activity only at the final timepoint, after the completion of the PR task. In a PR task, unlike in an FR schedule, the response requirement changes over time, so mice cannot generally predict how much work is required to obtain a reward based on previous trials. Although we can assume a similar hierarchical progression of activity within the striatum, the variable nature of the PR task could impact the behavioral and cellular response differently than suggested for the FR framework (Segovia et al., 2012).

5. Conclusion

The present study did not fully support the assumptions made by our previous study (Moretti et al., 2021) in which it was hypothesized that the neuronal activity in ephrin-A2A5$^{-/-}$ mice with repetitive and perseverative responding behavior would have shifted to the striatal region involved in habit formation. Rather, in this study, we found that activity remained dominant in regions involved in goal-directed behaviors. However, there was a trend that suggested increased MSN activation in the DMS for ephrin-A2A5$^{-/-}$ following stimulation. The relative proportion of c-Fos activity in the striatum was significantly different in experimental groups compared to the control. However, it is unclear, using the current sample sizes, whether the difference could be statistically attributed to altered dorsal striatum activity.

Although the possibility that rTMS interferes with habit formation is exciting, the current findings remain limited and preliminary. Some of this initial evidence, in addition to recent evidence, for LI-rTMS-induced changes to the striatal activity and network connectivity (Moretti et al., 2022) does provide some direction for potential mechanisms of rTMS involving the modulation of subcortical circuits. This could have implications for the mechanism by which rTMS plays a role in the treatment of conditions such as drug addiction and OCD. Future studies should look at experiments that specifically investigate circuit function and changes over time. Combination with electrophysiological recordings from the striatum could also help map any causal relationship. Overall, LI-rTMS shows some promise for altered hierarchical recruitment of specific striatal regions on a cellular level; however, the current experimental design and sample size limit conclusions. Nonetheless, this evidence supports further circuit-based investigations in larger studies, potentially with more clinically relevant animal models to probe rTMS mechanisms.

Data availability statement

The raw data supporting the conclusions of this article will be made available by the authors, without undue reservation.

Ethics statement

The animal study was reviewed and approved by the University of Western Australia Animal Ethics Committee.

Author contributions

MT: methodology, writing—original draft, writing—review and editing, formal analysis, investigation, and visualization. JR: writing—review and editing and supervision. JM: conceptualization, writing—review and editing, methodology, formal analysis, visualization, and supervision. All authors contributed to the article and approved the submitted version.

Funding

JR was supported by a fellowship from Multiple Sclerosis Western Australia (MSWA) and the Perron Institute for Neurological and Translational Science. JM was supported by an Australian Government Research Training Program (RTP) scholarship and Byron Kakulas Prestige scholarship.

Acknowledgments

We thank Dr. Bhedita Seewoo and Mr. Samuel J. Bolland for their guidance in creating the mouse brain atlas for this study.

Conflict of interest

The authors declare that the research was conducted in the absence of any commercial or financial relationships that could be construed as a potential conflict of interest.

Publisher's note

References

Aberman, J. E., Ward, S. J., and Salamone, J. D. (1998). Effects of dopamine antagonists and accumbens dopamine depletions on time-constrained progressive-ratio performance. *Pharmacol. Biochem. Behav.* 61, 341–348. doi: 10.1016/S0091-3057(98)00112-9

Anderson, K. D., and Reiner, A. (1991). Immunohistochemical localization of DARPP-32 in striatal projection neurons and striatal interneurons: implications for the localization of D1-like dopamine receptors on different types of striatal neurons. *Brain Res.* 568, 235–243. doi: 10.1016/0006-8993(91)91403-N

Aydin-Abidin, S., Trippe, J., Funke, K., Eysel, U. T., and Benali, A. (2008). High- and low-frequency repetitive transcranial magnetic stimulation differentially activates c-Fos and zif268 protein expression in the rat brain. *Exp. Brain Res.* 188, 249–261. doi: 10.1007/s00221-008-1356-2

Bullitt, E. (1990). Expression ofC-fos-like protein as a marker for neuronal activity following noxious stimulation in the rat. *J. Comp. Neurol.* 296, 517–530. doi: 10.1002/cne.902960402

Carmi, L., Alyagon, U., Barnea-Ygael, N., Zohar, J., Dar, R., and Zangen, A. (2018). Clinical and electrophysiological outcomes of deep TMS over the medial prefrontal and anterior cingulate cortices in OCD patients. *Brain Stimul.* 11, 158–165. doi: 10.1016/j.brs.2017.09.004

Chon, U., Vanselow, D. J., Cheng, K. C., and Kim, Y. (2019). Enhanced and unified anatomical labeling for a common mouse brain atlas. *Nat. Commun.* 10, 5067. doi: 10.1038/s41467-019-13057-w

Cooper, M. A., Kobayashi, K., and Zhou, R. (2009). Ephrin-A5 regulates the formation of the ascending midbrain dopaminergic pathways. *Dev. Neurobiol.* 69, 36–46. doi: 10.1002/dneu.20685

Everitt, B. J., and Robbins, T. W. (2005). Neural systems of reinforcement for drug addiction: From actions to habits to compulsion. *Nat. Neurosci.* 8, 1481–1489. doi: 10.1038/nn1579

Feldheim, D. A., Kim, Y.-I. I., Bergemann, A. D., Frisén, J., Barbacid, M., and Flanagan, J. G. (2000). Genetic analysis of ephrin-A2 and ephrin-A5 shows their requirement in multiple aspects of retinocollicular mapping. *Neuron* 25, 563–574. doi: 10.1016/S0896-6273(00)81060-0

Gillan, C. M., Papmeyer, M., Morein-Zamir, S., Sahakian, B. J., Fineberg, N. A., Robbins, T. W., et al. (2011). Disruption in the balance between goal-directed behavior and habit learning in obsessive-compulsive disorder. *Am. J. Psychiat.* 168, 718–726. doi: 10.1176/appi.ajp.2011.10071062

Hodos, W. (1961). Progressive Ratio as a Measure of Reward Strength. *Science.* 134, 943–944. doi: 10.1126/science.134.3483.943

Keck, M. E., Welt, T., Muller, M. B., Erhardt, A., Ohl, F., Toschi, N., et al. (2002). Repetitive transcranial magnetic stimulation increases the release of dopamine in the mesolimbic and mesostriatal system. *Neuropharmacology* 43, 101–109. doi: 10.1016/S0028-3908(02)00069-2

Lazarus, M. S., Krishnan, K., and Huang, Z. J. (2015). GAD67 deficiency in parvalbumin interneurons produces deficits in inhibitory transmission and network disinhibition in mouse prefrontal cortex. *Cereb. Cortex* 25, 1290–1296. doi: 10.1093/cercor/bht322

Liu, H.-S., Chefer, S., Lu, H., Guillem, K., Rea, W., Kurup, P., et al. (2013). Dorsolateral caudate nucleus differentiates cocaine from natural reward-associated contextual cues. *Proc. Natl. Acad. Sci.* 110, 4093–4098. doi: 10.1073/pnas.1207531110

Makowiecki, K., Harvey, A. R., Sherrard, R. M., and Rodger, J. (2014). Low-intensity repetitive transcranial magnetic stimulation improves abnormal visual cortical circuit topography and upregulates BDNF in Mice. *J. Neurosci.* 34, 10780–10792. doi: 10.1523/JNEUROSCI.0723-14.2014

Moretti, J., Poh, E. Z., Bolland, S. J., Harvey, A. R., Albrecht, M. A., and Rodger, J. (2021). Concurrent LI-rTMS induces changes in c-Fos expression but not behavior during a progressive ratio task with adult ephrin-A2A5-/- mice. *Behav. Brain Res.* 400, 113011. doi: 10.1016/j.bbr.2020.113011

Moretti, J., Poh, E. Z., and Rodger, J. (2020). rTMS-Induced Changes in Glutamatergic and Dopaminergic Systems: Relevance to Cocaine and Methamphetamine Use Disorders. *Front. Neurosci.* 14, 137. doi: 10.3389/fnins.2020.00137

Moretti, J., Terstege, D. J., Poh, E. Z., Epp, J. R., and Rodger, J. (2022). Low intensity repetitive transcranial magnetic stimulation modulates brain - wide functional connectivity to promote anti - correlated c - Fos expression. *Sci. Rep.* 12, 20571. doi: 10.1038/s41598-022-24934-8

O'Reardon, J. P., Solvason, H. B., Janicak, P. G., Sampson, S., Isenberg, K. E., Nahas, Z., et al. (2007). Efficacy and safety of transcranial magnetic stimulation in the acute treatment of major depression: a multisite randomized controlled trial. *Biol. Psychiatry* 62, 1208–1216. doi: 10.1016/j.biopsych.2007.01.018

Paxinos, G., and Franklin, K. (2012). *Paxinos and Franklin's the Mouse Brain in Stereotaxic Coordinates.* 4th ed. Cambridge, MAq: Academic Press.

Poh, E. Z., Harvey, A. R., Makowiecki, K., and Rodger, J. (2018). Online LI-rTMS during a Visual Learning Task : differential Impacts on Visual Circuit and Behavioural Plasticity in Adult Ephrin-A2A5 Mice. *eNeuro* 5, 17. doi: 10.1523/ENEURO.0163-17.2018

Rodger, J., Mo, C., Wilks, T., Dunlop, S. A., and Sherrard, R. M. (2012). Transcranial pulsed magnetic field stimulation facilitates reorganization of abnormal neural circuits and corrects behavioral deficits without disrupting normal connectivity. *FASEB J.* 26, 1593–1606. doi: 10.1096/fj.11-194878

Segovia, K. N., Correa, M., Lennington, J. B., Conover, J. C., and Salamone, J. D. (2012). Changes in nucleus accumbens and neostriatal c-Fos and DARPP-32 immunoreactivity during different stages of food-reinforced instrumental training. *Eur. J. Neurosci.* 35, 1354–1367. doi: 10.1111/j.1460-9568.2012.08036.x

Sieber, B. A., Kuzmin, A., Canals, J. M., Danielsson, A., Paratcha, G., Arenas, E., et al. (2004). Disruption of EphA/ephrin-A signaling in the nigrostriatal system reduces dopaminergic innervation and dissociates behavioral responses to amphetamine and cocaine. *Mol. Cell. Neurosci.* 26, 418–428. doi: 10.1016/j.mcn.2004.03.009

Wilkinson, D. G. (2001). Multiple roles of eph receptors and ephrins in neural development. *Nat. Rev. Neurosci.* 2, 155–164. doi: 10.1038/35058515

Yushkevich, P. A., Piven, J., Hazlett, H. C., Smith, R. G., Ho, S., Gee, J. C., et al. (2006). User-guided 3D active contour segmentation of anatomical structures: Significantly improved efficiency and reliability. *Neuroimage* 31, 1116–1128. doi: 10.1016/j.neuroimage.2006.01.015

frontiers | Frontiers in Human Neuroscience

TYPE Original Research
PUBLISHED 20 July 2023
DOI 10.3389/fnhum.2023.1229618

OPEN ACCESS

EDITED BY
Kevin A. Caulfield,
Medical University of South Carolina, United States

REVIEWED BY
Nicole R. Nissim,
Mayo Clinic Florida, United States
Aprinda Indahlastari,
University of Florida, United States

*CORRESPONDENCE
Shirley Fecteau
✉ shirley.fecteau@fmed.ulaval.ca

RECEIVED 30 May 2023
ACCEPTED 06 July 2023
PUBLISHED 20 July 2023

CITATION
Bouchard AE, Renauld E and Fecteau S (2023) Changes in resting-state functional MRI connectivity during and after transcranial direct current stimulation in healthy adults. *Front. Hum. Neurosci.* 17:1229618. doi: 10.3389/fnhum.2023.1229618

Changes in resting-state functional MRI connectivity during and after transcranial direct current stimulation in healthy adults

Amy E. Bouchard, Emmanuelle Renauld and Shirley Fecteau*

Department of Psychiatry and Neurosciences, Faculty of Medicine, CERVO Brain Research Centre, Centre intégré universitaire en santé et services sociaux de la Capitale-Nationale, Université Laval, Québec City, QC, Canada

Introduction: Transcranial direct current stimulation (tDCS) applied over the dorsolateral prefrontal cortex (DLPFC) at rest can influence behaviors. However, its mechanisms remain poorly understood. This study examined the effect of a single session of tDCS over the bilateral DLPFC on resting-state functional connectivity using fMRI (rs-fcMRI) during and after stimulation in healthy adults. We also investigated whether baseline rs-fcMRI predicted tDCS-induced changes in rs-fcMRI.

Methods: This was a randomized, sham-controlled, double-blind, crossover study. We delivered tDCS for 30 min at 1 mA with the anode and cathode over the left and right DLPFC, respectively. We used seed-based analyses to measure tDCS-induced effects on whole-brain rs-fcMRI using a 3 (before, during, after stimulation) × 2 (active, sham stimulation) ANOVA.

Results: There were four significant Time × Stimulation interactions on the connectivity scores with the left DLPFC seed (under the anode electrode) and no interactions for the right DLPFC seed (under the cathode electrode). tDCS changed rs-fcMRI between the left DLPFC seed and parieto-occipital, parietal, parieto-occipitotemporal, and frontal clusters during and after stimulation, as compared to sham. Furthermore, rs-fcMRI prior to stimulation predicted some of these tDCS-induced changes in rs-fcMRI during and after stimulation. For instance, rs-fcMRI of the fronto-parietooccipital network predicted changes observed after active stimulation, rs-fcMRI of the fronto-parietal network predicted changes during active stimulation, whereas rs-fcMRI of the fronto-parieto-occipitotemporal and the frontal networks predicted changes both during and after active stimulation.

Discussion: Our findings reveal that tDCS modulated rs-fcMRI both during and after stimulation mainly in regions distal, but also in those proximal to the area under the anode electrode, which were predicted by rs-fcMRI prior to tDCS. It might be worth considering rs-fcMRI to optimize response to tDCS.

KEYWORDS

concurrent tDCS-fMRI, functional connectivity, DLPFC, healthy adults, parietal cortex

1. Introduction

In recent years, we have seen an exponential use of transcranial direct current stimulation (tDCS) in humans. This popularity mainly comes from the fact that tDCS is an easy, inexpensive, and non-invasive neuromodulatory technique with the potential to modulate brain activity that will, consequently, improve cognition, behaviors or alleviate symptoms. Unfortunately, the hasty use of tDCS has led to conflicting reports on the neural effects of tDCS in humans. True, the availability of tDCS devices that can be concurrently combined with neuroimaging is relatively recent and such investigations are not trivial to conduct. However, one remaining pitfall in the field is to take for granted the premises that anodal and cathodal tDCS, respectively, facilitates and inhibits cortical excitability, which is mainly based on the direct current stimulation literature, and that such local effects are causally related to the observed behavioral effects. Such premises derived from direct current stimulation to postulate mechanisms of tDCS are oversimplified and have created misleading data interpretations in the field of tDCS in humans (Jackson et al., 2016; Fecteau, 2022). Precise mechanisms of tDCS remain largely unknown (Bestmann and Walsh, 2017). This is unfortunate since a non-invasive approach that could reliably modify human brain activity would be impactful.

One fundamental need in the field of tDCS is to characterize and understand its effects on resting state brain activity. Indeed, little is still known on how tDCS influences brain activity, even when participants are simply at rest, without behavioral or cognitive confounding factors, such as performing cognitive tasks before, during or after stimulation. It seems important to investigate if tDCS alone reaches the cortex and sufficiently modulates brain activity. Characterization of the tDCS effects on resting state brain activity will contribute to developing hypotheses on how tDCS, by strengthening or weakening activity in brain regions and networks, may consequently improve cognitive performance. It will also contribute to identifying when it is relevant to deliver tDCS at rest, rather than combining it with a specific cognitive task. Further, characterization of tDCS effects during and after stimulation will contribute to identifying when it is best to combine it with cognitive tasks, whether they should be combined concurrently or subsequently.

Although tDCS delivered over the dorsolateral prefrontal cortex (DLPFC) is among the most used tDCS protocols in healthy individuals and patients with psychiatric conditions, there is still a paucity of studies on the effects of tDCS while delivered at rest on resting state functional connectivity (rs-fcMRI) using functional magnetic resonance imaging (fMRI), during and after stimulation. There seem to be only three studies that investigated the effects of tDCS at rest on rs-fcMRI after stimulation as compared to before stimulation. Keeser et al. (2011) conducted a double-blind, crossover tDCS study in 13 men who received tDCS with the anode and cathode over the left DLPFC and the right supraorbital area at 2 mA for 20 min. Rs-fcMRI was collected for 5 min while subjects had their eyes closed before and no later than 5 min after tDCS. Coactivation was increased in frontal regions, parts of the left frontal-parietal network and the right posterior cingulate cortex, as well as parts of the right frontal-parietal network after active than sham tDCS. Peña-Gómez et al. (2012) conducted a crossover, partially randomized (sham was always before active tDCS) study in 10 adults who received stimulation with the anode and cathode over the left DLPFC and right supraorbital area, respectively, and the opposite montage, at 2 mA for 20 min. Rs-fcMRI was collected for 10 min before and after tDCS. Temporal functional connectivity between prefrontal and parietal regions was stronger and spatial robustness of the default mode network was more reduced after active than after sham. Park et al. (2013) conducted a single-blind, parallel tDCS study, applying the anode over the left DLPFC and the cathode over the right supraorbital area at 1 mA for 20 min in healthy adults (25 in the active and 14 in the sham group). Rs-fcMRI was collected while subjects had their eyes closed immediately before and after tDCS. tDCS increased rs-fcMRI between the left DLPFC and frontal, temporal and subcortical regions in the right hemisphere and decreased it between the left DLPFC and frontal regions around the stimulation site in the left hemisphere.

There seem to be only two concurrent tDCS-fMRI studies reporting changes in rs-fcMRI in healthy humans while receiving tDCS over the DLPFC at rest. We previously conducted a sham-controlled, double-blind, crossover tDCS-fMRI study in 13 adults who received the anode and cathode electrodes over the left and right DLPFC, respectively, at 1 mA for 30 min (Mondino et al., 2020). Rs-fcMRI was collected for 5 min before tDCS, 30 min during tDCS and 10 min after tDCS while subjects had their eyes closed. Rs-fcMRI was increased between the left DLPFC seed under the anode electrode and bilateral parietal regions during stimulation, which long lasted for at least 10 min after stimulation. Leaver et al. (2022) conducted a single-blind, crossover tDCS-fMRI study in 37 adults who received 2 mA active and sham tDCS for 5 min, within the same session separated by 10–15 min. The anode and cathode were over the left DLPFC and right ventrolateral PFC, respectively. During active as compared to sham stimulation, rs-fcMRI increased within the orbitofrontal network, whereas it decreased between a frontoparietal network and a node near the subgenual anterior cingulate cortex, as well as a node near the right superior parietal lobule.

In sum, the number of studies that delivered tDCS over the DLPFC at rest and measured rs-fcMRI, without any confounding factors such as administering a task before, during and or after stimulation, remains limited. Although results between studies still show some variability, the main effects indicate modulation of large-scale circuits involving proximal and distal regions to the DLPFC (especially frontal and parietal areas).

The main goal of this work was to examine the tDCS effects on rs-fcMRI delivered over the DLPFC while healthy adults were at rest, and if so, whether baseline rs-fcMRI predicts such effects. Specifically, we investigated (1) the type of changes induced by tDCS (i.e., increases rs-fcMRI, further positively correlates brain regions, decreases rs-fcMRI, further anticorrelates brain regions); (2) the location of these changes (i.e., between the whole brain and each region under the anode and cathode electrodes, the left and right DLPFC); (3) the time course of these changes (during and/or after stimulation); and (4) if baseline rs-fcMRI predicts these changes, if any. We based our hypotheses on the study by Mondino et al. (2020) since it seems to be the only study that investigated tDCS effects on rs-fcMRI while targeting the bilateral DLPFC in healthy adults at rest both during and after stimulation. We expected that tDCS will increase fronto-parietal rs-fcMRI, both during and after stimulation.

2. Materials and methods

2.1. Design

This was a randomized, crossover, sham-controlled, double-blind study. Participants underwent two concurrent tDCS-fMRI sessions, one with active and one with sham tDCS, separated by 7 days (on the same weekday and time of day to minimize variability). They were randomized using a Latin square, counterbalancing the order of active and sham tDCS. Blinding integrity was assessed in participants and the outcome assessor using a standardized form to determine whether they believed the session was active or sham tDCS. Participants were also assessed on potential tDCS-related side effects at each tDCS session using a standardized questionnaire.

2.2. Participants

Sixteen healthy participants enrolled in this project. They were free of general medical, neurological, and psychiatric conditions and eligible for tDCS (Keel et al., 2001) and MRI. They provided their written informed consent prior to their participation in this study. The institutional review board of the local institute approved this project. Fourteen participants completed the study (two participants withdrew). We excluded one participant due to MRI artifacts. Thus, 13 participants (nine women; mean age = 26.1, standard deviation = 4.6 years; one left-handed, one ambidextrous, eleven right-handed evaluated using the Edinburgh Handedness Inventory, Oldfield, 1971) were entered into the analyses. A sample of 13 participants was needed to detect a large effect size (dz = 0.85) with 80% power and α of 0.05, for a two-tailed paired samples *t*-test (Faul et al., 2007, 2009).

2.3. tDCS

We administered tDCS using an MR-compatible battery-driven stimulator (neuroConn GmbH, Ilmenau, Germany) with two 7 × 5 cm^2 rubber electrodes. We used an electrode paste (≈3 mm layer) to offer stability (e.g., less chance to drip and bridge between the electrodes than saline water) and prevent drying out over the scanning session. Active tDCS was delivered at a current intensity of 1 mA (maximum current intensity applicable for the stimulator used in this study) for 30 min. Sham stimulation was delivered for 30 min with ramp up and ramp down periods of 30 s, the remaining time with no active current (Gandiga et al., 2006). The anode and cathode electrodes were placed over the left (F3) and right (F4) DLPFC, respectively, using the international electroencephalography 10–20 system. We chose to apply the anode and cathode electrodes over the left and right DLPFC, respectively, since this montage previously led to results of interest in our research program on substance use disorders. We observed that this montage modulated decision-making behaviors relevant for substance use disorders (Fecteau et al., 2010), such as reducing risk taking behaviors (Fecteau et al., 2007) and elevation of salivary cortisol during decision making under stress condition (Brunelin and Fecteau, 2021). This montage also reduced cue-provoked craving for alcohol (Boggio et al., 2008), smoking (Boggio et al., 2009), and food (Fregni et al., 2008; see Bouchard et al., 2021 for a review). We now pursue investigation of this montage by combining it concurrently with neuroimaging. So far, we found that this montage elevated prefrontal N-acetylaspartate and striatal glutamate + glutamine (Hone-Blanchet et al., 2016) and rs-fcMRI between the left DLPFC and bilateral parietal regions (Mondino et al., 2020). Our ultimate goal is to identify the mechanisms of this montage to eventually offer a neuromodulatory method that will reliably engage specific brain targets.

2.4. MRI

2.4.1. Data acquisition

We acquired data as follows: 5 min of fMRI before tDCS, 25 min of fMRI during tDCS (onset of fMRI acquisition was 5 min after the start of stimulation), 5 min of fMRI after tDCS, and the anatomical scan. For the fMRI scans, we instructed participants to rest and keep their eyes open. Whole-brain MR scans were acquired with a Philips 3T Achieva scanner and a standard 8-channel head coil (Philips Healthcare, Best, Netherlands). T1-weighted structural magnetic images were obtained with a magnetization prepared rapid acquisition gradient-echo sequence with the following parameters: TR = 8.2 ms, TE = 3.7 ms, FoV = 250 mm, flip angle = 8°, 256 × 256 matrix, 180 slices/volume, slice thickness = 1 mm, no gap. For the rs-fcMRI scans, EPI BOLD images were acquired as follows: TR = 3,000 ms, TE = 30 ms, FoV = 224 mm × 224 mm × 140 mm, flip angle = 70°, 64 × 64 matrix, dynamic scans 100, voxel size = 3.5 mm × 3.5 mm × 3.5 mm, slice thickness = 3.5 mm, no gap.

2.4.2. fMRI preprocessing

We preprocessed structural and functional volumes with CONN (Whitfield-Gabrieli and Nieto-Castanon, 2012) (version 19.c) and SPM 12 on MATLAB R2019a (Mathworks, Inc., USA). We used CONN's default preprocessing pipeline (Nieto-Castanon, 2020). We smoothed volumes with 7 mm full width at half Gaussian kernel. We used ART[1] to identify outlier scans with intermediate settings (97th percentile in normative sample). We defined outliers using a global signal z-value threshold of 5 and a subject-motion mm threshold of 0.9 mm. We excluded one participant because he had more than 20% outlier scans. We denoised data using Compcor (Behzadi et al., 2007) to regress out physiological noise sources (white matter and cerebrospinal fluid signals with 10 confound dimensions in addition to their first-order derivatives). Moreover, we regressed out movement-related covariates (scrubbing and realignment, with its first-order derivatives). We also regressed out the effect of each session (before, during and after tDCS), with their first-order derivatives. We performed band pass filtering of 0.008–0.09 Hz (Hallquist et al., 2013) and linear detrending. Lastly, we verified preprocessing and denoising procedures with CONN's quality analysis reports. We labeled cortical and subcortical regions using the Harvard-Oxford Atlas (Desikan et al., 2006) and cerebellar areas with the

1 https://www.nitrc.org/projects/artifact_detect

automated anatomical labeling atlas (Tzourio-Mazoyer et al., 2002), as implemented in CONN.

2.4.3. Seed-based rs-fcMRI analyses

We conducted seed-based rs-fcMRI analyses with the left and right DLPFC as seeds ($x = \pm 36$, $y = 29$, $z = 38$; with 5 mm radii) using CONN. These analyses measure the level of rs-fcMRI between the seed and each voxel in the brain (Nieto-Castanon, 2020). We performed a 3 × 2 (Time × Stimulation) repeated-measures ANOVA to investigate potential tDCS-induced changes on rs-fcMRI. We used a voxel threshold of p-uncorrected < 0.001 and cluster threshold cluster size of p-FDR-corrected < 0.05 (Friston et al., 1994). We calculated average connectivity values within the cluster(s) with REX,[2] as implemented in CONN. We used SPSS 29 (IBM Corp., USA) to conduct *post hoc* analyses. We performed linear regression analyses to investigate whether baseline rs-fcMRI predicted tDCS-induced changes in rs-fcMRI of the significant clusters. *Post hoc* and linear regression analyses were bootstrapped with 1,000 bootstrap samples and 95% confidence intervals to confirm robustness.

3. Results

3.1. Effects of tDCS on rs-fcMRI during and after stimulation

We first compared baseline rs-fcMRI between active and sham conditions and found no differences for both seeds (left DLPFC: p-FDR = 0.540; right DLPFC: p-FDR ≥ 0.282). We then assessed the effects of tDCS on rs-fcMRI. Seed-based analyses for the left DLPFC seed (under the anode electrode) revealed four significant Time × Stimulation interactions (**Table 1** and **Figure 1**). First, rs-fcMRI changed between the left DLPFC seed and a cluster mainly containing the bilateral cuneus (**Figure 1A**). Rs-fcMRI was greater (positively correlated) post-tDCS as compared to during tDCS and post-sham. Also, rs-fcMRI increased (changed from an anticorrelation to a positive correlation) from pre-sham to during sham, and then decreased (anticorrelated) from during sham to post-sham. Second, rs-fcMRI changed between the left DLPFC seed and a cluster in the right precuneus (**Figure 1B**). Rs-fcMRI was weaker during active than during sham, but greater post-tDCS as compared to pre-tDCS, during tDCS and post-sham (changed from an anticorrelation to a positive correlation). Also, rs-fcMRI was weaker post-sham as compared to during sham. Third, rs-fcMRI changed between the left DLPFC seed and a cluster mainly encompassing the bilateral precuneus, extending to the right lingual gyrus (**Figure 1C**). Rs-fcMRI was weaker during active than sham, and greater (changed from an anticorrelation to a positive correlation) post-tDCS as compared to pre-tDCS, during tDCS and post-sham. Fourth, rs-fcMRI changed between the left DLPFC seed and a cluster in the left orbitofrontal cortex (OFC) (**Figure 1D**). Rs-fcMRI was greater during active than sham, and weaker post-tDCS as compared to pre-tDCS, during tDCS and post-sham. There were no significant Time × Stimulation interactions on rs-fcMRI for the right DLPFC seed (under the cathode electrode; p-FDR = 0.584).

4. Impact of baseline rs-fcMRI on tDCS effects during and after stimulation

We then examined if rs-fcMRI prior to tDCS predicted rs-fcMRI changes in the four significant Time × Stimulation interactions involving the left DLPFC seed, under the anode electrode. We conducted regression analyses with baseline rs-fcMRI as the predictor and tDCS-induced changes in rs-fcMRI as the criterion variable [Bonferroni threshold $p \leq 0.05/15 = 0.00333$: 3 comparisons for the first interaction (after active, during sham, after sham), 4 comparisons for each of the three other interactions (during and after active, during and after sham), totaling 15, **Table 2** and **Figure 2**]. For the first interaction, baseline rs-fcMRI between the left DLPFC seed and the cluster mainly containing the bilateral cuneus predicted changes after tDCS ($p = 0.001$), accounting for 67.4% ($R^2 = 0.674$) of the variance, but did not significantly predict changes during or after sham (during: $p = 0.016$; after: $p = 0.051$). For the second interaction, baseline rs-fcMRI between the left DLPFC seed and the right precuneus predicted changes during active stimulation ($p < 0.001$), which accounted for 70.0% ($R^2 = 0.700$) of the variance. Baseline rs-fcMRI did not predict changes after active ($p = 0.073$) or sham stimulation ($p = 0.068$). For the third interaction, baseline rs-fcMRI between the left DLPFC seed and the cluster mainly containing the bilateral precuneus, extending to the right lingual gyrus, predicted changes during ($p < 0.001$) and after ($p < 0.001$) tDCS, accounting for 85.0% ($R^2 = 0.850$) and 75.8% ($R^2 = 0.758$) of the variance, respectively. Finally, for the fourth interaction, baseline rs-fcMRI between the left DLPFC seed and the cluster in the left OFC predicted changes during ($p = 0.002$) and after ($p < 0.001$) tDCS, accounting for 59.9% ($R^2 = 0.599$) and 71.2% ($R^2 = 0.712$) of the variance, respectively.

4.1. Side effects and integrity of blinding

There were no differences between active and sham tDCS for the number and intensity level of reported side effects ($p > 0.1$), nor mood ($p > 0.4$). There was no significant difference in blinding ratings between active and sham conditions ($p > 0.7$). The majority of participants were blind to the stimulation conditions they received (4 participants correctly guessed their stimulation condition with a confidence level higher than 90%). The rs-fcMRI assessor had minimal interaction with the participants and stayed blinded to the stimulation conditions with a 100% confidence level.

5. Discussion

In this sham-controlled, double-blind, crossover study, 30 min of tDCS delivered while healthy adults were at rest, with the anode and cathode electrode over the left and right DLPFC, respectively,

2 https://www.nitrc.org/projects/rex/

TABLE 1 tDCS-induced rs-fcMRI changes in healthy individuals revealed by time (before, during, after tDCS) × tDCS (active, sham) repeated measures ANOVA (significant *post hoc* results are bolded).

Left dorsolateral prefrontal cortex seed [$x = -36$, $y = 29$, $z = 38$]			
Right/Left cuneus, right precuneus			
Cluster size: 99 voxels	Peak MNI coordinates: [$x = 0$, $y = -84$, $z = 36$]		Size p-FDR = 0.0009
Post hoc comparison *t*-tests	*t*	*p*	Glass' Δ
Before active vs. sham	−1.647	0.132	
During active vs. sham	2.071	0.071	
After active vs. sham	−5.968	**0.001**	
Before vs. during sham	−2.644	**0.033**	0.701
Before vs. during active	0.624	0.527	−0.182
Before vs. after sham	1.736	0.126	−0.520
Before vs. after active	−2.183	0.065	0.793
During vs. after sham	4.382	**0.004**	−1.497
During vs. after active	−4.156	**0.008**	3.003
Right precuneus			
Cluster size: 55 voxels	Peak MNI coordinates: [$x = 18$, $y = -56$, $z = 26$]		Size p-FDR = 0.0186
Before active vs. sham	−0.166	0.859	
During active vs. sham	3.163	**0.013**	
After active vs. sham	−5.563	**0.003**	
Before vs. during sham	−1.737	0.109	0.473
Before vs. during active	0.364	0.738	−0.107
Before vs. after sham	1.612	0.122	−0.492
Before vs. after active	−3.443	**0.021**	1.016
During vs. after sham	5.066	**0.002**	−1.751
During vs. after active	−4.434	**0.006**	1.899
Right/Left precuneus, right lingual gyrus			
Cluster size: 42 voxels	Peak MNI coordinates: [$x = 6$, $y = -58$, $z = 10$]		Size p-FDR = 0.0438
Before active vs. sham	1.576	0.137	
During active vs. sham	3.704	**0.004**	
After active vs. sham	−3.880	**0.005**	
Before vs. during sham	−1.426	0.185	0.365
Before vs. during active	−0.621	0.552	0.201
Before vs. after sham	0.864	0.387	−0.363
Before vs. after active	−4.137	**0.008**	1.229
During vs. after sham	1.805	0.110	−1.065
During vs. after active	−5.544	**0.001**	2.236
Left orbitofrontal cortex			
Cluster size: 38 voxels	Peak MNI coordinates: [$x = -38$, $y = 30$, $z = -4$]		Size p-FDR = 0.0496
Before active vs. sham	0.784	0.448	
During active vs. sham	−2.243	**0.048**	
After active vs. sham	5.792	**0.002**	
Before vs. during sham	0.795	0.418	−0.241
Before vs. during active	−1.708	0.097	0.360

(Continued)

TABLE 1 (Continued)

Left dorsolateral prefrontal cortex seed [$x = -36$, $y = 29$, $z = 38$]			
Right/Left cuneus, right precuneus			
Cluster size: 99 voxels	Peak MNI coordinates: [$x = 0$, $y = -84$, $z = 36$]		Size p-FDR = 0.0009
Post hoc comparison t-tests	t	p	Glass' Δ
Before vs. after sham	−1.029	0.337	0.477
Before vs. after active	2.855	**0.020**	−1.346
During vs. after sham	−1.813	0.097	1.072
During vs. after active	4.681	**0.001**	−2.692
Right dorsolateral prefrontal cortex seed [$x = 36$, $y = 29$, $z = 38$]			Size p-FDR = 0.5844

FDR, false discovery rate; MNI, Montreal Neurological Institute. *P*-values for *post hoc* comparison *t*-tests are bootstrapped.

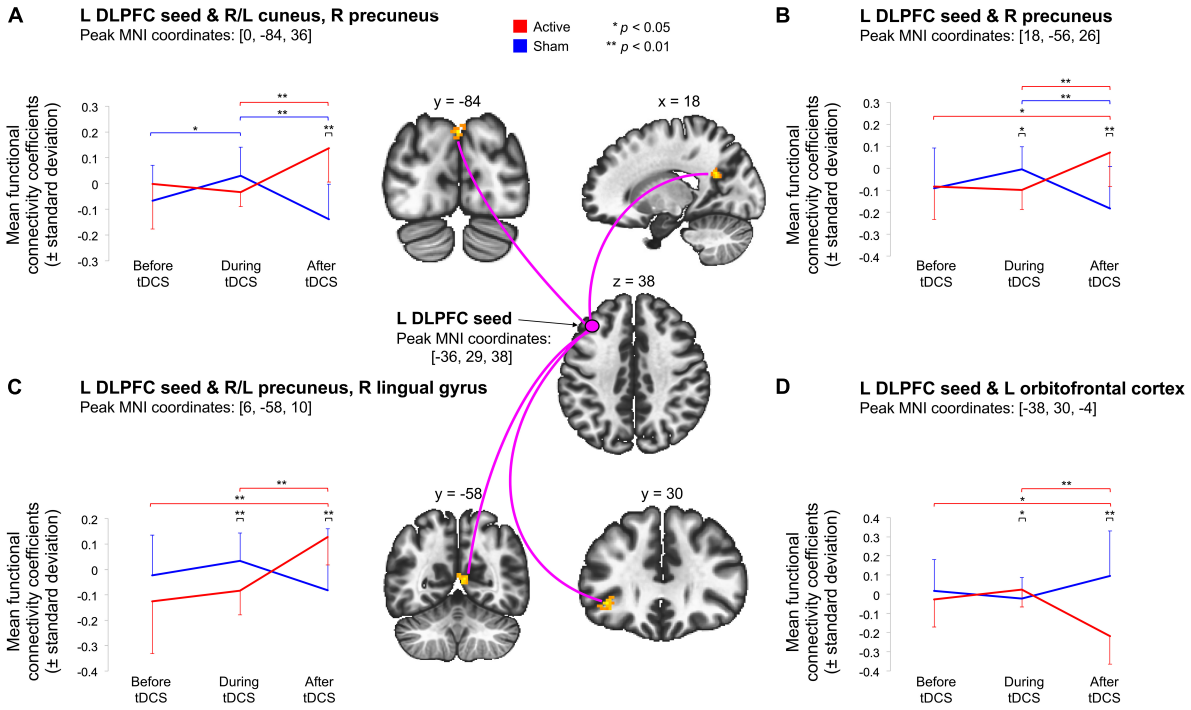

FIGURE 1
Illustration of the significant Time (pre-tDCS, during tDCS-post-tDCS) × Stimulation (active, sham) interactions indicate that active tDCS modulated rs-fcMRI between the left DLPFC seed (under the anodal electrode) and four clusters, during or after stimulation. First, **(A)** shows that active tDCS modulated rs-fcMRI between the left DLPFC seed and a parieto-occipital cluster. Second, **(B)** demonstrates that active tDCS modulated rs-fcMRI between the left DLPFC seed and a parietal cluster. Third, **(C)** indicates that active tDCS modulated rs-fcMRI between the left DLPFC seed and a parieto-occipitotemporal cluster. Last, **(D)** shows that active tDCS modulated rs-fcMRI between the left DLPFC seed and a frontal cluster. Voxel-threshold of $p < 0.001$ (p-uncorrected); cluster threshold of $p < 0.05$ (p-FDR-corrected). The red and blue error bars represent within-group differences for the active and sham condition, respectively. Asterisks denote significant *post hoc* comparisons (*$p < 0.05$; **$p < 0.01$).

modulated rs-fcMRI. Briefly, regarding our four specific aims, tDCS induced rs-fcMRI changes: (1) leading to increased (further positively correlated) and decreased (further negatively correlated or anticorrelated) rs-fcMRI, (2) in regions proximal and distal to the anode electrode, (3) in the same direction during and after stimulation (i.e., a change observed during stimulation was further increased after stimulation rather than reverted), with stronger changes after than during stimulation, and (4) some changes were predicted by baseline rs-fcMRI.

There were four significant stimulation (active, sham) by time (before, during, after tDCS) interactions. Interestingly, all rs-fcMRI changes were found with the left DLPFC seed, under the anode electrode, and none were found with the right DLPFC seed, under the cathode electrode.

Three out of the four stimulation by time interactions involved clusters contralateral and distal to the anode electrode. These interactions indicated rs-fcMRI changes between the left DLPFC seed and parietal, occipitoparietal and parieto-occipitotemporal networks. Further, baseline rs-fcMRI predicted some of these changes either during or after stimulation. These predictions indicate that it may be worth selecting participants based on their rs-fcMRI to optimize tDCS response. For instance, participants

TABLE 2 Predictions from baseline rs-fcMRI (immediately before tDCS) on subsequent tDCS-induced rs-fcMRI changes in healthy individuals during and after stimulation between the left DLPFC seed and the fronto-parieto-occipital, fronto-parietal, fronto-parieto-occipitotemporal, and frontal circuits (significant *post hoc* results are bolded).

					Bootstrap	
	β	R^2	*t*	*p*	Bca 95% CI	*p*
Right/Left cuneus, right precuneus						
After active	−0.821	0.674	−4.767	**0.001**	[−1.442, −0.531]	**0.020**
During sham	−0.653	0.426	−2.860	**0.016**	[−0.959, −0.0506]	**0.019**
After sham	−0.551	0.303	−2.187	0.051	[−0.990, −0.272]	**0.013**
Right precuneus						
During active	−0.837	0.700	−5.070	< **0.001**	[−1.217, −0.515]	**0.002**
After active	−0.512	0.262	−1.978	0.073	[−1.539, 0.244]	0.306
During sham	−0.846	0.715	−5.253	< **0.001**	[−1.104, −0.565]	**0.001**
After sham	−0.520	0.271	−2.020	0.068	[−0.860, −0.208]	**0.008**
Right/Left precuneus, right lingual gyrus						
During active	−0.922	0.850	−7.888	< **0.001**	[−1.381, −0.827]	**0.001**
After active	−0.871	0.758	−5.878	< **0.001**	[−1.270, −0.559]	**0.002**
During sham	−0.750	0.563	−3.765	**0.003**	[−1.282, −0.293]	**0.001**
After sham	−0.332	0.110	−1.166	0.268	[−1.193, 0.670]	0.132
Left orbitofrontal cortex						
During active	−0.774	0.599	−4.050	**0.002**	[−1.085, −0.427]	**0.006**
After active	−0.844	0.712	−5.217	< **0.001**	[−1.725, −0.851]	**0.001**
During sham	−0.799	0.638	−4.401	**0.001**	[−1.385, −0.248]	**0.002**
After sham	−0.526	0.276	−2.050	0.065	[−1.789, 0.789]	0.256

Bca 95% CI, bias corrected accelerated 95% confidence interval.

with stronger rs-fcMRI of the fronto-parietal network would respond better to tDCS during stimulation, whereas those with stronger rs-fcMRI in the fronto-parietooccipital network would respond better to tDCS after stimulation. This also might help improve study designs, such as identifying the best time point to test outcomes, whether during or after stimulation.

Most previous studies also reported that tDCS over the DLPFC increases rs-fcMRI in fronto-parietal networks, involving various parietal nodes (Keeser et al., 2011; Peña-Gómez et al., 2012; Mondino et al., 2020; Leaver et al., 2022). One also found strengthened rs-fcMRI in fronto-temporal networks (Park et al., 2013). In regard to modulating rs-fcMRI between frontal and parietooccipital nodes, it seems that this study might be the first one to report such a result. Generally, the prefrontal cortex in these large resting state networks presumably exerts top-down control of these parietal, temporal, and occipital nodes. It is still unclear in the rs-fcMRI literature how to interpret such tDCS-induced modulation leading these large networks to decorrelate. Intrinsic anticorrelations are observed between regions involved in externally oriented (e.g., attention) and internally oriented (e.g., self-referential processing) functions, possibly reflecting the separation of regions/networks with opposing or competing roles (Fox et al., 2005; Fox and Raichle, 2007; Buckner et al., 2008; Buckner and DiNicola, 2019), and possibly the capacity to switch between them (Whitfield-Gabrieli and Ford, 2012).

Interestingly, the fourth stimulation by time interaction differed from the three other interactions, that is rs-fcMRI change involved a cluster proximal and ipsilateral to the anode electrode. This change was observed between the left DLPFC and OFC. It indicated that active tDCS further anticorrelated rs-fcMRI of these regions after stimulation, as compared to before and during stimulation. Also, rs-fcMRI was greater during active than sham stimulation. Further, these changes during and after active stimulation were predicted by baseline rs-fcMRI of this frontal network. Park et al. (2013) found decreased rs-fcMRI in the left middle and inferior frontal gyri, ipsilateral to the anode electrode (with the cathode over the right supraorbital area), similar to our results, but increased in regions contralateral to the anode electrode (or ipsilateral to the cathode electrode). Others reported increased rs-fcMRI in bilateral OFC (Leaver et al., 2022) and in frontal regions ipsilateral to the anode electrode (Keeser et al., 2011). Little is known regarding frontal networks containing strictly the DLPFC and OFC in rs-fcMRI in healthy populations. However, their interactions via separate networks are associated with cognitive control. The frontoparietal (central executive) network is anchored in the DLPFC, supports executive functions, and integrates information from other networks such as the default mode network (Vincent et al., 2008; Uddin et al., 2019). Anticorrelated rs-fcMRI between these two networks is associated with better cognitive functioning in healthy individuals (e.g., Hampson et al., 2010; Keller et al., 2015; Ng et al., 2016). Regions within the default mode network might also be worth targeting with tDCS such as the precuneus which may modulate rs-fcMRI of key executive control regions (e.g., DLPFC). It will also be of interest to

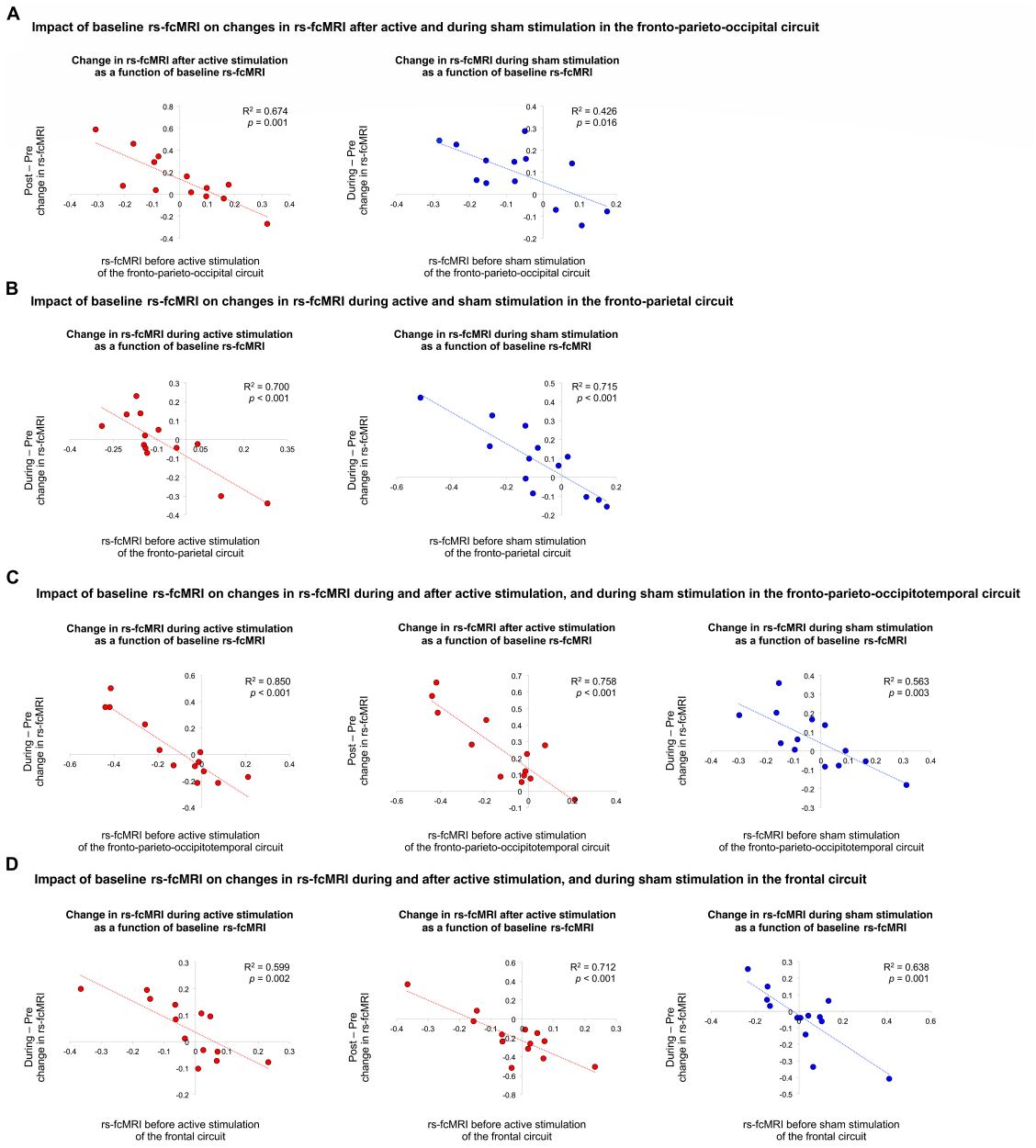

FIGURE 2
Impact of baseline rs-fcMRI on changes in rs-fcMRI during and after active and sham stimulation. First, **(A)** illustrates the impact of baseline rs-fcMRI on changes in rs-fcMRI after active and during sham stimulation in the fronto-parieto-occipital circuit. Second, **(B)** demonstrates the impact of baseline rs-fcMRI on changes in rs-fcMRI during active and sham stimulation in the fronto-parietal circuit. Third, **(C)** shows the impact of baseline rs-fcMRI on changes in rs-fcMRI during and after active stimulation, as well as during sham stimulation, in the fronto-parieto-occipitotemporal circuit. Last, **(D)** illustrates the impact of baseline rs-fcMRI on changes in rs-fcMRI during and after active stimulation, as well as during sham stimulation, in the frontal circuit. The red and blue trendlines and data points represent the active and sham conditions, respectively.

investigate whether repeated tDCS sessions engage these networks and enhance cognitive functions associated with these networks, such as rs-fcMRI of the fronto-parietal network known to be related with attentional processes (Seeley et al., 2007).

There were also changes with sham stimulation involving two of these networks, the fronto-parietal and the fronto-parietooccipital networks. Specifically, rs-fcMRI between the frontal and parietal network decreased after sham stimulation, which was not predicted by baseline rs-fcMRI. Also, rs-fcMRI between the frontal and parietooccipital network increased during sham, but decreased after sham stimulation. Several studies also reported changes in rs-fcMRI involving the DLPFC with sham tDCS, especially implicating the parietal cortex (Peña-Gómez et al., 2012; Mondino et al., 2020; Leaver et al., 2022), the primary auditory association cortex (Peña-Gómez et al., 2012), and the cerebellum (Park et al., 2013). Interestingly, Leaver et al. (2022) compared sham tDCS with a no-tDCS condition. They observed significant decreased rs-fcMRI for the no-tDCS condition as compared to sham tDCS in several networks with the DLPFC, including the superior parietal lobule, the posterior cingulate

cortex, the dorsal anterior cingulate, the primary visual cortex, the primary auditory cortex, and the primary somatosensory cortex. We previously discussed that such decrease as we observed in fronto-parietal networks may be linked to a time effect considering that participants stayed at a resting state for more than half an hour, in which DLPFC activity may weaken and decorrelate from the other nodes of resting state networks (as observed in healthy individuals, Mondino et al., 2020). Although rs-fcMRI research has rapidly grown over the last two decades, several questions remain to be addressed. Resting-state networks are generally stable, however, some studies reported that rs-fcMRI does not remain static and fluctuates with time during scanning sessions (Hutchison et al., 2013; Preti et al., 2017; Lurie et al., 2020). This becomes even more pertinent for repeated rs-fcMRI scans within the same scanning period as in our work, such as collecting rs-fcMRI for 5–10 min before tDCS, for 25–30 min during tDCS, and for 5–10 min after tDCS (typically limiting the entire MRI session to 1 h). Hence, this highlights the importance of including no-tDCS conditions, as well as further characterizing rs-fcMRI during repeated acquisitions.

The electrical current travels from the anode to the cathode electrode. However, it is important to highlight here that tDCS did not modulate rs-fcMRI between the regions under the anode and cathode electrodes, here the left and right DLPFC, during or after stimulation. This lack of rs-fcMRI changes was also observed in previous studies applying the tDCS electrodes over both DLPFCs (Mondino et al., 2020), over the left DLPFC and contralateral supraorbital area (Keeser et al., 2011; Peña-Gómez et al., 2012; Park et al., 2013), and over the left DLPFC and contralateral ventrolateral PFC (Leaver et al., 2022). These findings compel us to be cautious when interpreting the impact of tDCS on cognition or behaviors as solely due to brain activity changes in regions under the electrodes, at least when applied over the DLPFC. Likewise, it is tempting to speculate how findings from this work are relevant for clinical populations since the DLPFC is among, if not, the most targeted region with tDCS, especially psychiatric disorders (Fregni et al., 2021). However, it is often expected that patients display different rs-fcMRI as compared to healthy controls (Kaiser et al., 2015; Taebi et al., 2022), thus the tDCS effects on rs-fcMRI might be different in patients from those in healthy individuals.

This study has limitations that should be addressed, such as the small sample size, which limits generalizability. Despite this, we strictly controlled for type 1 error, which should help power analyses for future studies. Also, potential sex-related differences were not studied, which could be examined with an appropriate power analysis in future work. Additionally, the scan time during stimulation was longer than the scanning durations before and after stimulation, which may reduce reliability (Birn et al., 2013). It may be interesting to compare different rs-fcMRI times (e.g., 5-min increments) in future work. To note, in our previous concurrent tDCS-rs-fcMRI study, there were no significant differences in tDCS-induced effects on rs-fcMRI changes in fronto-parietal circuitry when comparing two 15-min time bins during 30 min of tDCS in healthy individuals (Mondino et al., 2020).

In sum, tDCS delivered over the bilateral DLPFC modulates rs-fcMRI of several circuits comprising regions distal (parietal, occipital, temporal) and proximal (frontal) to the anodal electrode, both during and after stimulation. Further, rs-fcMRI prior to tDCS predicted tDCS effects during and after stimulation, which may be useful to identify best tDCS responders in future work.

Data availability statement

The raw data supporting the conclusions of this article will be made available by the authors, without undue reservation.

Ethics statement

The studies involving human participants were reviewed and approved by the CIUSSS de la Capitale-Nationale. The patients/participants provided their written informed consent to participate in this study.

Author contributions

SF designed the study. SF and ER collected data. AB led data analysis with the participation of ER. AB led the interpretation of results with the participation of SF. AB wrote the first draft of the manuscript. All authors critically reviewed the manuscript and approved the finalized version.

Funding

This work was supported by the National Sciences and Engineering Research Council of Canada grant (RGPIN-06514-2019) to SF. SF was supported by the Canada Research Chair in Cognitive Neuroplasticity.

Acknowledgments

We thank the participants for their interest in this study.

Conflict of interest

The authors declare that the research was conducted in the absence of any commercial or financial relationships that could be construed as a potential conflict of interest.

Publisher's note

References

Behzadi, Y., Restom, K., Liau, J., and Liu, T. T. (2007). A component based noise correction method (CompCor) for BOLD and perfusion based fMRI. *Neuroimage* 37, 90–101. doi: 10.1016/j.neuroimage.2007.04.042

Bestmann, S., and Walsh, V. (2017). Transcranial electrical stimulation. *Curr. Biol.* 27, R1258–R1262. doi: 10.1016/j.cub.2017.11.001

Birn, R. M., Molloy, E. K., Patriat, R., Parker, T., Meier, T. B., Kirk, G. R., et al. (2013). The effect of scan length on the reliability of resting-state fMRI connectivity estimates. *Neuroimage* 83, 550–558. doi: 10.1016/j.neuroimage.2013.05.099

Boggio, P. S., Liguori, P., Sultani, N., Rezende, L., Fecteau, S., and Fregni, F. (2009). Cumulative priming effects of cortical stimulation on smoking cue-induced craving. *Neurosci. Lett.* 463, 82–86. doi: 10.1016/j.neulet.2009.07.041

Boggio, P. S., Sultani, N., Fecteau, S., Merabet, L., Mecca, T., Pascual-Leone, A., et al. (2008). Prefrontal cortex modulation using transcranial DC stimulation reduces alcohol craving: A double-blind, sham-controlled study. *Drug Alcohol Depend.* 92, 55–60. doi: 10.1016/j.drugalcdep.2007.06.011

Bouchard, A. E., Garofalo, S., Rouillard, C., and Fecteau, S. (2021). "Cognitive functions in substance-related and addictive disorders," in *Transcranial direct current stimulation in neuropsychiatric disorders: Clinical principles and management*, eds A. R. Brunoni, M. A. Nitsche, and C. K. Loo (Cham: Springer International Publishing), 519–531. doi: 10.1007/978-3-030-76136-3_26

Brunelin, J., and Fecteau, S. (2021). Impact of bifrontal transcranial direct current stimulation on decision-making and stress reactivity. A pilot study. *J. Psychiatr. Res.* 135, 15–19. doi: 10.1016/j.jpsychires.2020.12.068

Buckner, R. L., and DiNicola, L. M. (2019). The brain's default network: Updated anatomy, physiology and evolving insights. *Nat. Rev. Neurosci.* 20, 593–608. doi: 10.1038/s41583-019-0212-7

Buckner, R. L., Andrews-Hanna, J. R., and Schacter, D. L. (2008). The brain's default network: Anatomy, function, and relevance to disease. *Ann. N. Y. Acad. Sci.* 1124, 1–38. doi: 10.1196/annals.1440.011

Desikan, R. S., Ségonne, F., Fischl, B., Quinn, B. T., Dickerson, B. C., Blacker, D., et al. (2006). An automated labeling system for subdividing the human cerebral cortex on MRI scans into gyral based regions of interest. *Neuroimage* 31, 968–980. doi: 10.1016/j.neuroimage.2006.01.021

Faul, F., Erdfelder, E., Buchner, A., and Lang, A. G. (2009). Statistical power analyses using G*Power 3.1: Tests for correlation and regression analyses. *Behav. Res. Methods* 41, 1149–1160. doi: 10.3758/BRM.41.4.1149

Faul, F., Erdfelder, E., Lang, A. G., and Buchner, A. (2007). G*Power 3: A flexible statistical power analysis program for the social, behavioral, and biomedical sciences. *Behav. Res. Methods* 39, 175–191. doi: 10.3758/bf03193146

Fecteau, S. (2022). Influencing human behavior with noninvasive brain stimulation: Direct human brain manipulation revisited. *Neuroscientist* 29, 317–331. doi: 10.1177/10738584211067744

Fecteau, S., Fregni, F., Boggio, P. S., Camprodon, J. A., and Pascual-Leone, A. (2010). Neuromodulation of decision-making in the addictive brain. *Subst. Use Misuse* 45, 1766–1786. doi: 10.3109/10826084.2010.482434

Fecteau, S., Pascual-Leone, A., Zald, D. H., Liguori, P., Théoret, H., Boggio, P. S., et al. (2007). Activation of prefrontal cortex by transcranial direct current stimulation reduces appetite for risk during ambiguous decision making. *J. Neurosci.* 27, 6212–6218. doi: 10.1523/JNEUROSCI.0314-07.2007

Fox, M. D., and Raichle, M. E. (2007). Spontaneous fluctuations in brain activity observed with functional magnetic resonance imaging. *Nat. Rev. Neurosci.* 8, 700–711. doi: 10.1038/nrn2201

Fox, M. D., Snyder, A. Z., Vincent, J. L., Corbetta, M., Van Essen, D. C., and Raichle, M. E. (2005). The human brain is intrinsically organized into dynamic, anticorrelated functional networks. *Proc. Natl. Acad. Sci. U.S.A.* 102, 9673–9678. doi: 10.1073/pnas.0504136102

Fregni, F., El-Hagrassy, M. M., Pacheco-Barrios, K., Carvalho, S., Leite, J., Simis, M., et al. (2021). Evidence-based guidelines and secondary meta-analysis for the use of transcranial direct current stimulation in neurological and psychiatric disorders. *Int. J. Neuropsychopharmacol.* 24, 256–313. doi: 10.1093/ijnp/pyaa051

Fregni, F., Orsati, F., Pedrosa, W., Fecteau, S., Tome, F. A., Nitsche, M. A., et al. (2008). Transcranial direct current stimulation of the prefrontal cortex modulates the desire for specific foods. *Appetite* 51, 34–41. doi: 10.1016/j.appet.2007.09.016

Friston, K. J., Worsley, K. J., Frackowiak, R. S., Mazziotta, J. C., and Evans, A. C. (1994). Assessing the significance of focal activations using their spatial extent. *Hum. Brain Mapp.* 1, 210–220. doi: 10.1002/hbm.460010306

Gandiga, P. C., Hummel, F. C., and Cohen, L. G. (2006). Transcranial DC stimulation (tDCS): A tool for double-blind sham-controlled clinical studies in brain stimulation. *Clin. Neurophysiol.* 117, 845–850. doi: 10.1016/j.clinph.2005.12.003

Hallquist, M. N., Hwang, K., and Luna, B. (2013). The nuisance of nuisance regression: Spectral misspecification in a common approach to resting-state fMRI preprocessing reintroduces noise and obscures functional connectivity. *Neuroimage* 82, 208–225. doi: 10.1016/j.neuroimage.2013.05.116

Hampson, M., Driesen, N., Roth, J. K., Gore, J. C., and Constable, R. T. (2010). Functional connectivity between task-positive and task-negative brain areas and its relation to working memory performance. *Magn. Reson. Imaging* 28, 1051–1057. doi: 10.1016/j.mri.2010.03.021

Hone-Blanchet, A., Edden, R. A., and Fecteau, S. (2016). Online effects of transcranial direct current stimulation in real time on human prefrontal and striatal metabolites. *Biol. Psychiatry* 80, 432–438. doi: 10.1016/j.biopsych.2015.11.008

Hutchison, R. M., Womelsdorf, T., Allen, E. A., Bandettini, P. A., Calhoun, V. D., Corbetta, M., et al. (2013). Dynamic functional connectivity: Promise, issues, and interpretations. *Neuroimage* 80, 360–378. doi: 10.1016/j.neuroimage.2013.05.079

Jackson, M. P., Rahman, A., Lafon, B., Kronberg, G., Ling, D., Parra, L. C., et al. (2016). Animal models of transcranial direct current stimulation: Methods and mechanisms. *Clin. Neurophysiol.* 127, 3425–3454. doi: 10.1016/j.clinph.2016.08.016

Kaiser, R. H., Andrews-Hanna, J. R., Wager, T. D., and Pizzagalli, D. A. (2015). Large-scale network dysfunction in major depressive disorder: A meta-analysis of resting-state functional connectivity. *JAMA Psychiatry* 72, 603–611. doi: 10.1001/jamapsychiatry.2015.0071

Keel, J. C., Smith, M. J., and Wassermann, E. M. (2001). A safety screening questionnaire for transcranial magnetic stimulation. *Clin. Neurophysiol.* 112:720.

Keeser, D., Meindl, T., Bor, J., Palm, U., Pogarell, O., Mulert, C., et al. (2011). Prefrontal transcranial direct current stimulation changes connectivity of resting-state networks during fMRI. *J. Neurosci.* 31, 15284–15293. doi: 10.1523/JNEUROSCI.0542-11.2011

Keller, J. B., Hedden, T., Thompson, T. W., Anteraper, S. A., Gabrieli, J. D., and Whitfield-Gabrieli, S. (2015). Resting-state anticorrelations between medial and lateral prefrontal cortex: Association with working memory, aging, and individual differences. *Cortex* 64, 271–280. doi: 10.1016/j.cortex.2014.12.001

Leaver, A. M., Gonzalez, S., Vasavada, M., Kubicki, A., Jog, M., Wang, D. J. J., et al. (2022). Modulation of brain networks during MR-compatible transcranial direct current stimulation. *Neuroimage* 250:118874. doi: 10.1016/j.neuroimage.2022.118874

Lurie, D. J., Kessler, D., Bassett, D. S., Betzel, R. F., Breakspear, M., Kheilholz, S., et al. (2020). Questions and controversies in the study of time-varying functional connectivity in resting fMRI. *Netw. Neurosci.* 4, 30–69. doi: 10.1162/netn_a_00116

Mondino, M., Ghumman, S., Gane, C., Renauld, E., Whittingstall, K., and Fecteau, S. (2020). Effects of transcranial stimulation with direct and alternating current on resting-state functional connectivity: An exploratory study simultaneously combining stimulation and multiband functional magnetic resonance imaging. *Front. Hum. Neurosci.* 13:474. doi: 10.3389/fnhum.2019.00474

Ng, K. K., Lo, J. C., Lim, J. K. W., Chee, M. W. L., and Zhou, J. (2016). Reduced functional segregation between the default mode network and the executive control network in healthy older adults: A longitudinal study. *Neuroimage* 133, 321–330. doi: 10.1016/j.neuroimage.2016.03.029

Nieto-Castanon, A. (2020). *Handbook of functional connectivity magnetic resonance imaging methods in CONN*. New York, NY: Hilbert Press.

Oldfield, R. C. (1971). The assessment and analysis of handedness: The Edinburgh inventory. *Neuropsychologia* 9, 97–113.

Park, C. H., Chang, W. H., Park, J. Y., Shin, Y. I., Kim, S. T., and Kim, Y. H. (2013). Transcranial direct current stimulation increases resting state interhemispheric connectivity. *Neurosci. Lett.* 539, 7–10. doi: 10.1016/j.neulet.2013.01.047

Peña-Gómez, C., Sala-Lonch, R., Junqué, C., Clemente, I. C., Vidal, D., Bargalló, N., et al. (2012). Modulation of large-scale brain networks by transcranial direct current stimulation evidenced by resting-state functional MRI. *Brain Stimul.* 5, 252–263. doi: 10.1016/j.brs.2011.08.006

Preti, M. G., Bolton, T. A., and Van De Ville, D. (2017). The dynamic functional connectome: State-of-the-art and perspectives. *Neuroimage* 160, 41–54. doi: 10.1016/j.neuroimage.2016.12.061

Seeley, W. W., Menon, V., Schatzberg, A. F., Keller, J., Glover, G. H., Kenna, H., et al. (2007). Dissociable intrinsic connectivity networks for salience processing and executive control. *J. Neurosci.* 27, 2349–2356. doi: 10.1523/JNEUROSCI.5587-06.2007

Taebi, A., Becker, B., Klugah-Brown, B., Roecher, E., Biswal, B., Zweerings, J., et al. (2022). Shared network-level functional alterations across substance use disorders: A multi-level kernel density meta-analysis of resting-state functional connectivity studies. *Addict. Biol.* 27:e13200. doi: 10.1111/adb.13200

Tzourio-Mazoyer, N., Landeau, B., Papathanassiou, D., Crivello, F., Etard, O., Delcroix, N., et al. (2002). Automated anatomical labeling of activations in SPM using a macroscopic anatomical parcellation of the MNI MRI single-subject brain. *Neuroimage* 15, 273–289. doi: 10.1006/nimg.2001.0978

Uddin, L. Q., Yeo, B. T. T., and Spreng, R. N. (2019). Towards a universal taxonomy of macro-scale functional human brain networks. *Brain Topogr.* 32, 926–942. doi: 10.1007/s10548-019-00744-6

Vincent, J. L., Kahn, I., Snyder, A. Z., Raichle, M. E., and Buckner, R. L. (2008). Evidence for a frontoparietal control system revealed by intrinsic functional connectivity. *J. Neurophysiol.* 100, 3328–3342. doi: 10.1152/jn.90355.2008

Whitfield-Gabrieli, S., and Ford, J. M. (2012). Default mode network activity and connectivity in psychopathology. *Annu. Rev. Clin. Psychol.* 8, 49–76. doi: 10.1146/annurev-clinpsy-032511-143049

Whitfield-Gabrieli, S., and Nieto-Castanon, A. (2012). Conn: A functional connectivity toolbox for correlated and anticorrelated brain networks. *Brain Connect.* 2, 125–141. doi: 10.1089/brain.2012.0073

frontiers | Frontiers in Neural Circuits

TYPE Methods
PUBLISHED 21 August 2023
DOI 10.3389/fncir.2023.1208930

OPEN ACCESS

EDITED BY
Kevin A. Caulfield,
Medical University of South Carolina,
United States

REVIEWED BY
Christopher Sege,
MUSC Health, United States
Danielle Taylor,
Wayne State University, United States

*CORRESPONDENCE
Brigitte Zrenner
✉ brigitte.zrenner@utoronto.ca

RECEIVED 19 April 2023
ACCEPTED 31 July 2023
PUBLISHED 21 August 2023

CITATION
Zrenner B, Zrenner C, Balderston N, Blumberger DM, Kloiber S, Laposa JM, Tadayonnejad R, Trevizol AP, Zai G and Feusner JD (2023) Toward personalized circuit-based closed-loop brain-interventions in psychiatry: using symptom provocation to extract EEG-markers of brain circuit activity.
Front. Neural Circuits 17:1208930.
doi: 10.3389/fncir.2023.1208930

Toward personalized circuit-based closed-loop brain-interventions in psychiatry: using symptom provocation to extract EEG-markers of brain circuit activity

Brigitte Zrenner[1,2,3,4]*, Christoph Zrenner[1,2,3,5,6], Nicholas Balderston[7], Daniel M. Blumberger[1,2,3], Stefan Kloiber[1,2], Judith M. Laposa[1,2], Reza Tadayonnejad[8,9,10], Alisson Paulino Trevizol[1,2,3], Gwyneth Zai[1,2] and Jamie D. Feusner[1,2,9,10,11]

[1]Campbell Family Mental Health Research Institute, Centre for Addiction and Mental Health, Toronto, ON, Canada, [2]Department of Psychiatry, University of Toronto, Toronto, ON, Canada, [3]Temerty Centre for Therapeutic Brain Intervention, Centre for Addiction and Mental Health, Toronto, ON, Canada, [4]University Psychiatry Hospital, University of Tübingen, Tübingen, Germany, [5]Institute for Biomedical Engineering, University of Toronto, Toronto, ON, Canada, [6]University Neurology Hospital, University of Tübingen, Tübingen, Germany, [7]Center for Neuromodulation in Depression and Stress (CNDS), Department of Psychiatry, Perelman School of Medicine, University of Pennsylvania, Philadelphia, PA, United States, [8]TMS Clinical and Research Service, Neuromodulation Division, Semel Institute for Neuroscience and Human Behavior, University of California, Los Angeles, Los Angeles, CA, United States, [9]Department of Psychiatry and Biobehavioral Sciences, University of California, Los Angeles, Los Angeles, CA, United States, [10]Division of the Humanities and Social Sciences, California Institute of Technology, Pasadena, CA, United States, [11]Department of Women's and Children's Health, Karolinska Institutet, Stockholm, Sweden

Symptom provocation is a well-established component of psychiatric research and therapy. It is hypothesized that specific activation of those brain circuits involved in the symptomatic expression of a brain pathology makes the relevant neural substrate accessible as a target for therapeutic interventions. For example, in the treatment of obsessive-compulsive disorder (OCD), symptom provocation is an important part of psychotherapy and is also performed prior to therapeutic brain stimulation with transcranial magnetic stimulation (TMS). Here, we discuss the potential of symptom provocation to isolate neurophysiological biomarkers reflecting the fluctuating activity of relevant brain networks with the goal of subsequently using these markers as targets to guide therapy. We put forward a general experimental framework based on the rapid switching between psychiatric symptom states. This enable neurophysiological measures to be derived from EEG and/or TMS-evoked EEG measures of brain activity during both states. By subtracting the data recorded during the baseline state from that recorded during the provoked state, the resulting contrast would ideally isolate the specific neural circuits differentially activated during the expression of symptoms. A similar approach enables the design of effective classifiers of brain activity from EEG data in Brain-Computer Interfaces (BCI). To obtain reliable contrast data, psychiatric state switching needs to be achieved multiple times during a continuous recording so that slow changes of brain activity affect both

conditions equally. This is achieved easily for conditions that can be controlled intentionally, such as motor imagery, attention, or memory retention. With regard to psychiatric symptoms, an increase can often be provoked effectively relatively easily, however, it can be difficult to reliably and rapidly return to a baseline state. Here, we review different approaches to return from a provoked state to a baseline state and how these may be applied to different symptoms occurring in different psychiatric disorders.

KEYWORDS

EEG, TMS, symptom provocation, OCD, anxiety

1. Introduction and background

A promising perspective of therapeutic brain stimulation is that it enables the possibility of circuit-based therapies. Unlike pharmacotherapy (where only the dose can be varied), there are a number of configurable parameters in the application of a brain intervention such as transcranial magnetic stimulation (TMS). For example, in addition to intensity, the stimulation can be targeted to specific cortical areas and be applied with specific temporal patterns. Additionally, the synchronization of the timing of stimuli with individual brain oscillations simultaneously recorded in the real-time electroencephalogram (EEG) provides a new avenue for personalizing this therapeutic approach in order to achieve a specific desired therapeutic change in a dysfunctional brain network. However, the vast parameter space of where and how therapeutic TMS is most effective has barely been explored. It is not feasible to perform a 'grid search,' and searching for a protocol that is effective "on average" may not be fruitful since the optimal protocol is likely to vary between patients.

Instead, recent efforts in the neurophysiological domain had been focusing on optimizing personalized therapeutic brain stimulation using concurrent neurophysiological read-outs in the form of concurrent EEG and TMS-evoked EEG (Parmigiani et al., 2023). The motivation is to assess whether the neuroplastic changes induced by TMS are therapeutically effective and optimize the parameters iteratively. Such a TMS-EEG or EEG-derived biomarker that measures the "state" of the circuit on a timescale of minutes is required to implement personalized circuit-based closed-loop brain interventions. However, deriving the state of a specific brain circuit from a few tens of seconds of an EEG signal is not only challenging due to the presence of noise in the EEG (such as ocular and muscle artifacts) but also due to a "curse of dimensionality" (Altman and Krzywinski, 2018) that makes the identification of a reliable mapping from a segment of TMS-EEG data (a matrix consisting of time by channel) to the activity of the circuit of interest at that time (a scalar) difficult.

Reliable EEG state markers of specific neurophysiological processes exist, such as sleep spindles and beta bursts. Different features that can be extracted from the EEG signal with a temporal resolution of seconds (spectral amplitude), fractions of seconds (EEG microstates, coherency-based connectivity states), and even milliseconds (phase of oscillations) are known to reflect underlying neurophysiological processes and have shown promise for personalized therapeutic interventions (Zrenner et al., 2018, 2020; Gordon et al., 2021, 2022). EEG and TMS-EEG signals are also different in wakefulness and sleep and during different pharmacological interventions (Massimini et al., 2005; Sarasso et al., 2014; Ziemann et al., 2015). However, for informing therapy in psychiatric disorders, EEG and TMS-EEG-derived biomarkers from group-level differences between patients and healthy controls (such as frontal alpha power asymmetry) have not translated to a useful method at the individual level. Further, it is unclear whether this is an optimal strategy given the heterogeneity in psychiatric disorders at both the symptom and diagnosis levels.

Whether individual EEG markers of psychiatric symptom severity can be derived using a personalized calibration approach and whether these are more reliable and effective than EEG markers derived from group averages, remains to be tested. We hypothesize that the algorithmic methods used in brain computer interfaces (BCI), where EEG is increasingly effective at decoding brain states with a limited temporal resolution of seconds (e.g., those related to a specific behavior or set of behaviors or circumscribed cognitive phenomena), may also be effective at estimating symptom-related brain states (more broadly involving several, or combinations of, behavioral and cognitive processes) in psychiatric disorders.

Brain computer interfaces methods for the extraction of EEG markers rely on the contrast between cognitive states (e.g., motor imagery), whereby optimized EEG montages (spatial filters) are extracted that optimally differentiate between the two conditions using the difference in the statistical relationships between signals from different brain areas. One such statistical relationship is the covariance matrix, that quantifies the relatedness of the signals measured between every pair of EEG sensors. The resulting contrast in the covariance matrices corresponding to the two conditions can be exploited using the mathematical tool of eigendecomposition in a class of methods termed common spatial patterns (Grosse-Wentrup and Buss, 2008). A combined spatial and temporal decoding approach has also shown promise in the motor system (Metsomaa et al., 2021). By analyzing the difference between the EEG signal extracted during two different cognitive states, the predictive properties of the signal can be determined, while those that are not can be attenuated. In order to avoid a confounding effect of temporal differences (such as change in vigilance and recording properties), it is necessary to switch between the two conditions multiple times to average out slow non-specific

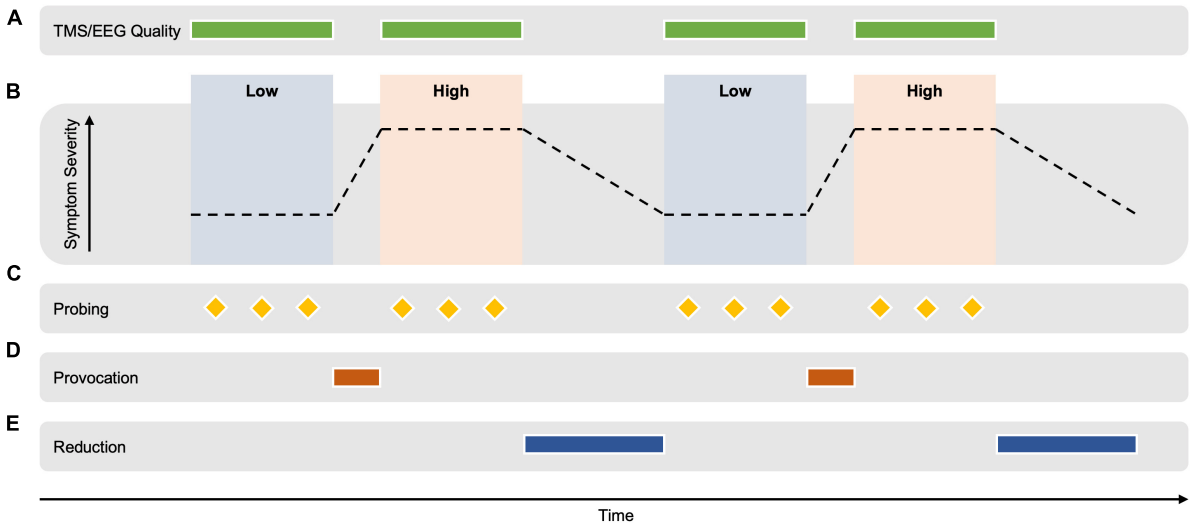

FIGURE 1
Hypothetical example of an experimental design for extracting TMS-EEG-derived biomarkers of brain circuit activity correlating with the expression of psychopathology. **(A)** TMS-EEG signal quality is monitored and optimized during the measurement. **(B)** TMS-EEG/EEG data is acquired during alternating periods of high vs. low symptom severity. TMS-EEG signatures that can distinguish between the two states are computed using the contrast between the TMS-EEG data of both conditions. The emotional/cognitive state should differ only for the degree of symptom severity but otherwise be identical. Psychiatric state switching needs to be achieved multiple times during a continuous recording to distinguish slow changes in the EEG signal that occur with time (e.g., vigilance, presence of artifacts) from differences in the EEG signal due to the emotional/cognitive state. **(C)** Symptom severity is repeatedly assessed during the conditions using physiological markers (e.g., blink reflex, skin conduction, and heart rate) and the participant's report (e.g., visual analog scale). **(D)** A personalized symptom provocation intervention shifts the emotional/cognitive state from a "low" to a "high" symptom severity, e.g., as could occur with the threat of shock paradigm (Grillon et al., 1991; Roemer and Borkovec, 1994; Ameli et al., 2001; Åsli et al., 2009; Balderston et al., 2017a,b; Hur et al., 2020), or with script driven imagery in those with PTSD (Lang, 1979; Liotti et al., 2002) and visual images and/or words in those with OCD (Dehghan et al., 2021) and those with specific phobia (Schienle et al., 2007). The specific provocation method is developed prior to the measurement in a calibration session. **(E)** Similarly, a personalized symptom reduction intervention could potentially return the state to a comparatively "low" symptom severity [e.g., personalized focused distraction (Wegner et al., 1987) or a distracting task (Amir et al., 1997) as has been used in experiments in participants with OCD; or with immediate removal of an aversive stimuli, as demonstrated in participants with OCD (Lutz et al., 2008)]. This transition is expected to take longer than the provocation transition. The measurement should occur in controlled laboratory conditions for less than 90 min, repeated on two separate days to assess the reliability of the derived markers. Note that by TMS-EEG, we mean not only the TMS-evoked EEG potentials, but also TMS-induced oscillations, as well as the ongoing EEG signal between the TMS pulses.

changes (see Figure 1). Note that between the switching steps, the conditions should differ only in the degree of symptom expression, with an otherwise similar cognitive state.

Translating this approach to psychiatry requires EEG data during different levels of symptom severity. Some success has been achieved using long-term recordings of brain data while tracking natural fluctuations in symptoms over several days (Etkin, 2018). To derive EEG markers from a recording under laboratory conditions, it is necessary to switch psychiatric symptoms "on and off" repeatedly for a total of tens of minutes during the recording. Effective approaches for a rapidly controlled provocation of symptoms in different psychiatric disorders have been proposed to "switch on" or "activate" the relevant brain circuits before treatment (e.g., in exposure therapy for phobias or before TMS therapy for obsessive-compulsive disorder OCD) (Carmi et al., 2019).

Symptom provocation can be achieved under controlled conditions to evoke a psychiatric symptom or a neurobiological response via psychopharmacological and/or behavioral stimuli, such as contamination stimuli for OCD and videotapes of combat for patients with posttraumatic stress disorder (PTSD) (D'Souza et al., 1999). Symptom provocation has been applied in the study of most psychiatric disorders, including schizophrenia, major depressive disorder, bipolar disorder, panic disorder, OCD, phobias, PTSD, and substance use disorder (D'Souza et al., 1999).

The ability to "switch off" circuits underlying symptom expression is the goal of psychiatric and behavioral therapy. The issue with computing EEG biomarkers is that established symptom reduction strategies are generally slow compared to symptom provocation. Here, we survey the different approaches for creating such a contrast between "high" and "low" symptom expression from which it may be possible to extract a reliable, individualized EEG-derived biomarker of brain circuit activity. We will summarize symptom provocation methods and discuss possible strategies for achieving fast symptom reduction and switching between both states.

2. Symptom provocation for biomarker identification

The rapid switching between "on" and "off" states is required to identify biomarkers of brain circuit activity, it is clear that not all psychiatric disorders are equally amenable to this approach. Instead of evaluating a specific psychiatric diagnosis, a more promising approach may be considering trans-diagnostic symptoms experienced across different psychiatric disorders. Considering the existing literature, it seems that

symptoms such as anxiety (Holt and Andrews, 1989), phobic fear (Schienle et al., 2007), obsessive thinking and compulsive avoiding behavior (Maia et al., 2022) and craving (Milivojevic et al., 2020) (either for a substance or for food) may be more easily provoked and resolved more rapidly than other symptoms, such as worry, dysphoria/dysthymia and mania/hypomania. We will discuss insights from psychopharmacological interventions for symptom provocation and then focus our discussion on selected symptoms which we consider promising candidates for behavioral interventions for both symptom provocation and symptom reduction and for which physiological models exist that relate the severity of symptom expression to the degree of activity of a specific dysfunctional brain circuit.

2.1. Psychopharmacological interventions for symptoms provocation

There is extensive research on how EEG and TMS-EEG are affected by the neurophysiological changes induced by pharmacological interventions (Ziemann, 2004). However, pharmacological interventions have a long history in psychiatric symptom provocation to yield insights into the biological basis of different disorders. For example, a recent study used isoproterenol to evoke physiological and emotional symptoms of anxiety/fear in patients with anorexia nervosa (Khalsa et al., 2015). When psychopharmacological agents are applied to provoke psychiatric symptoms, bottom-up and top-down approaches are used (D'Souza et al., 1999). An example of the bottom-up approach is the study of MHPG (methoxy-hydroxy-phenylethylene glycol) accumulation and anxiety in response to yohimbine administration. Studies in animal models suggest that α_2 adrenergic antagonists stimulate the brain stem noradrenergic nucleus, the locus coeruleus, increase norepinephrine release and its conversion to MHPG, and produce anxiety-related behaviors (D'Souza et al., 1999). Conversely, in the top-down approach, a psychopharmacological agent is applied to produce a distinctive behavioral response without the underlying neurophysiological mechanism of action being completely understood, e.g., in the induction of panic attacks with sodium lactate (Margraf et al., 1986). The bottom-up approach tests a hypothesis derived from pre-clinical studies, and a top-down approach generates clinically-based hypotheses tested in the laboratory.

Historical examples of the application of psychopharmacological agents for research in psychiatric disorders are the works of Carlsson et al. (1957), Carlsson and Lindqvist (1963), Andén et al. (1970), and Nybäck and Sedvall (1970), which demonstrated the role of dopamine in the pathophysiology of schizophrenia. It was shown that provocation with amphetamines induced stereotypic behaviors in humans (Rylander, 1969), mediated by the dopaminergic system (Randrup, 1970). In subsequent symptom provocation studies, amphetamines enhanced mesolimbic dopamine activity associated with positive symptoms in schizophrenia and reduced mesocortical dopamine activity associated with negative symptoms (Davis et al., 1991). Provocation with psychostimulants in combination with neuroreceptor imaging suggested that patients with schizophrenia respond to provocation with amphetamine with elevated dopamine release compared to controls, highly correlated with an increase in psychotic symptoms (Abi-Dargham et al., 1998). In this case, switching on was achieved with psychostimulants. Switching off is the aim of treatments for positive symptoms in schizophrenia, whether pharmacologically (e.g., primarily DA-D2 antagonists or serotonin and adrenaline receptors targeted by antipsychotic drugs) or through psychotherapy (Keepers et al., 2020). However, neither pharmacotherapy nor psychotherapy rapidly reduce symptoms (on the order of minutes). Furthermore, repeated pharmacological switching (as is possible, for example, for the depth of anesthesia by adjusting the flow rate of intravenous sedatives) seems less applicable for psychiatric symptoms. For example Lorazepam which is often prescribed for short-term relief of anxiety symptoms takes 1–3 min if administered intravenously, but has an elimination half-life of ca. 14 h (Ghiasi et al., 2023) and is therefore not suitable for repeated pharmacological switching. The different concentrations of the medication also have different physiological effects on the EEG and TMS-EEG measures that would be difficult to disentangle from the influence of symptom severity. Behavioral approaches are likely more promising for extracting biomarkers of different endogenous brain states during a relatively short measurement.

2.2. Behavioral interventions for symptom provocation

Symptom provocation by environmental triggers is experienced daily by many psychiatric patients. However, transferring this to a laboratory setting in a reliable and controlled way is not trivial.

2.2.1. Symptom provocation of trauma-related symptoms

One example of behavioral interventions being applied for research purposes is PTSD. In order to provoke symptoms in PTSD, tasks of passive emotion processing are employed. Examples include emotional faces that convey threat [e.g., angry, fearful (Shin et al., 2005)], aversive imagery (e.g., mutilated bodies, images of violence) (Lanius et al., 2007), trauma-specific cues (such as words, noises (Bremner et al., 1999b), pictures), and autobiographical scripts (Bremner et al., 1999a) - the patient's narratives about the traumatic experience that are read to the patient in order to provoke symptoms of PTSD. This script-driven imagery paradigm is based on earlier psychophysiological studies by Lang (1979) and Pitman et al. (1987). Lang demonstrated a significant increase in heart rate and skin conductance measures in phobic subjects during imagery of their phobic objects or situations. Pitman used five individualized scripts portraying actual experiences from the subject's past as well as six standard scripts portraying various hypothetical experiences (two neutral, a combat experience, a positive experience, an action experience and a fear experience) to demonstrate exaggerated physiologic arousal during recollection of traumatic experiences in PTSD.

2.2.2. Symptom provocation in major depressive disorder

There is a significant need to achieve a better understanding of the neurophysiological basis of major depressive disorder (MDD),

and to develop new and more effective therapies, including non-pharmacological therapies. Fluctuations in mood in most cases occur relatively slowly and achieving the rapid switching between high and low degrees of dysphoria that is needed for the approach presented here is likely difficult. Nevertheless, various methods of symptom provocation in MDD have been used successfully to advance this research (Martin, 1990). We summarize some of promising approaches below, which could be adapted to the proposed rapid psychiatric symptom switching framework.

One approach that has been used successfully is the use of a script driven depressive vs. happy autobiographical memory task. This has been used in combination with positron emission tomography to investigate neural pathways mediating transient mood changes in unipolar depression (Liotti et al., 2002). However, in another study it was shown that autonomic markers of symptom severity did not return to baseline after emotional provocations using an autobiographical memory task (Lin et al., 2022). Other studies have used a random number generation task (Shinba, 2014), speech writing and delivery task (Cyranowski et al., 2011), mirror tracing task (Rottenberg et al., 2007) or a video with sad emotional content (Rottenberg et al., 2003). A mood provocation task (combining elements of music associated with sad mood and autobiographical recall presented on a CD player) was also used to investigate the vulnerability of remitted depressed patients to the (re)activation of depressive thinking styles triggered by temporary dysphoric states (Segal et al., 2006). Finally, with regard to behavioral interventions, an emotional non-musical and musical stimuli paradigm was used to investigate the neural processing of emotionally provocative auditory stimuli in MDD (Nummenmaa et al., 2014; Lepping et al., 2016).

In terms of pharmacological intervention to provoke symptoms of MDD, the administration of alpha interferon (IFNa) has been found to cause flu-like symptoms as well as depressive symptoms, including depressed mood, dysphoria, anhedonia, helplessness, mild to severe fatigue, anorexia, and weight loss, hypersomnia, psychomotor retardation, decreased concentration, and confusion (Yirmiya et al., 1999). However, this is likely an unspecific modulation and the pharmacological intervention is difficult to reverse rapidly.

2.2.3. Symptom provocation of specific anxiety

Anxiety is either seen as a symptom of different psychiatric disorders (e.g., generalized anxiety disorder, social anxiety disorder, PTSD, borderline personality disorder) or secondary to other symptoms experienced within a psychiatric disorder–within schizophrenia or caused by intrusive thoughts in OCD or PTSD, for example. Provoking anxiety is easier the more specific the fear is–speaking in front of an audience or solving a difficult task in front of the experimenter in social anxiety disorder, for example. Video-based symptom provocation can also induce anxiety in laboratory settings (Miskovic and Schmidt, 2012; Boehme et al., 2014). In PTSD, anxiety-provoking pictures or sounds containing violence or combat (depending on what caused the trauma) can directly induce anxiety, trigger memories that are anxiety provoking, or a combination of the two. In contrast, worry is a more generalized symptom, and a one size fits all approach will likely not be successful as the cognitive content may differ from person to person. In this case, an individually tailored approach might be more promising.

2.2.4. Symptom provocation of intrusive thoughts

Intrusive thoughts are often provoked by environmental stimuli and are experienced in OCD, PTSD, major depressive disorder, and bipolar disorder. Here we will focus on intrusive thoughts experienced in OCD. Three main conceptualizations of OCD have been described depending on which faculty is taken as central: affective (anxiety/distress), volitional (compulsive), or cognitive (obsessional) (Denys, 2011). In the past, OCD was classified as an anxiety disorder due to the relevance of anxiety in the clinical presentation. However, OCD and the OCD spectrum disorders are grouped under a distinct category in the DSM-5 to take into account that increased anxiety can lead to fearful intrusive obsessive thoughts and volitional (compulsive) behavior but that anxiety can also be secondary to obsessional thoughts and the volitional attempts to regain cognitive control–[it has, however, also been hypothesized that the compulsive behavior itself could be the primary driver of symptoms of OCD (Robbins et al., 2012)]. Subsequently, we will also discuss intrusive thoughts (different from rumination) in the context of OCD, but the approaches also apply to intrusive thoughts as a symptom of other psychiatric disorders.

The state of neural activation in the target region seems important for the efficacy of TMS (Silvanto et al., 2008)–the current TMS treatment protocol for the treatment of OCD that is approved by the U.S. Food and Drug Administration applies symptom provocation before each stimulation session to elicit a moderate level of obsessional distress reported by patients (Food and Drug Administration, 2020). The underlying (although untested) assumption for the application of symptom provocation before treatment is that symptom provocation induces the reconsolidation of fear and distressing memories into long-term memories, which can be disrupted by neural stimulation during this susceptible period (Forcato et al., 2007; Agren et al., 2012; Schiller et al., 2013). Symptom provocation is believed to activate the cortico-striato-thalamo-cortical circuitry, mainly in the right hemisphere, which can be targeted by TMS (Saxena et al., 2001). Stimulating circuits that are functionally activated by symptoms is thought to increase the efficacy and specificity of TMS-induced plasticity as it allows for specific modulation of neural populations most affected by symptoms and stress (Saxena et al., 2001; Silvanto et al., 2008). Notably, whereas symptom provocation, typically as a mechanism for exposure therapy, is an established part of psychotherapy in the treatment of a number of psychiatric conditions, the additional benefit of current therapeutic TMS protocols for OCD is only moderate vs. symptom provocation alone (in the placebo condition, i.e., with sham TMS) (Carmi et al., 2019). In the case of PTSD, recent trials even indicate that TMS can reduce the therapeutic benefit of symptom provocation alone (Isserles et al., 2021). The present challenges of achieving an effective interaction between symptom provocation and therapeutic neuromodulation is part of the motivation for the development of new personalized and biomarker-based brain stimulation protocols.

An individual-tailored symptom provocation hierarchy is designed with the patient prior to treatment with TMS, such as the seven-step process following a provocation hierarchy design proposed by Maia et al. (2022). As described by Tendler et al. (2019), symptom provocation should be administered using an

internal and external hierarchy provocation list to formulate questions that instill obsessive distress until the desired level of self-reported distress is achieved (Maia et al., 2022). The desired level of subjective self-reported distress is defined according to clinical experience with good acceptability and treatment efficacy in clinical trials (Carmi et al., 2019). Symptom provocation aims to achieve a moderate self-reported level of obsessional distress (i.e., "4–7" on a "0–10" Visual Analog Scale) before each stimulation session (Maia et al., 2022). In addition to provocation hierarchy approaches, virtual reality is also emerging as an option to provoke symptoms of OCD (Dehghan et al., 2021). There is evidence that the degree of distress during provocations done immediately prior to TMS for OCD is related to symptom improvement more so than the variability of distress, between-session habituation, and advancing up the hierarchy of symptom provocation hierarchy (Guzick et al., 2022). Challenges in this method include the possibility that patients may engage in compulsions (physical or, more likely, mental compulsions) during the symptom provocation, during TMS stimulation, or after TMS stimulation. These could interfere with the intensity of the symptom provocation, with the efficacy of TMS, or with the overall efficacy of the treatment, respectively.

2.2.5. Symptom provocation of craving

Finally, craving is another symptom that can be provoked in a clinical setting in a relatively straightforward way. Craving is a symptom that occurs in the context of addictions (e.g., to drugs, nicotine, or alcohol) and eating disorders (Mussell et al., 1996; Greeno et al., 2000; Waters et al., 2001; Jarosz et al., 2007; Ng and Davis, 2013), including bulimia nervosa and binge eating disorder. Craving can be cue-induced (for example, presenting a particular smell or picture). It has also been proposed that there are some similarities between OCD and aspects of craving (Modell et al., 1992). In a laboratory setup, administering a cue reactivity task using pictorial pictures of either food or the drug is a possible way to provoke craving. In summary, symptom provocation is a well-established approach for a number of symptoms and psychiatric disorders. However, approaches for rapidly reducing symptoms in an experimental setting are much less studied.

3. Strategies for fast-acting symptom reduction

As discussed above, pharmacological strategies, although a cornerstone of therapy in psychiatry, can only be utilized in exceptional circumstances for the purpose of the approach put forward here. Behavioral therapeutic strategies are likely to be more suitable and psychotherapy is an effective approach to symptom reduction by achieving a behavioral and/or cognitive change. The underlying explanation for different treatment approaches is the widely-used emotion regulation theory by Gross (2015). This theory assumes that emotions are reactions to the world, so to feel differently or experience a reduction of symptoms, one has to try to think or pay attention differently or act differently. However, most established techniques are designed to achieve a lasting change over weeks or months, not minutes. Conversely, methods of achieving rapid symptom reduction are generally only short-lasting and often not helpful (and sometimes harmful), such as eating to reduce cravings. Below, we discuss general approaches that may be suitable for the reduction of the symptoms proposed above, which may occur in different psychiatric disorders, including relaxation techniques, thought suppression, guided attentional distraction, focused distraction, as well as acceptance and the performance of the specific compulsions in a controlled manner.

3.1. Symptom reduction by trigger removal in anxiety disorders

Anxiety is a prevalent symptom in a number of psychiatric disorders as both a primary or secondary symptom. The more specific the anxiety is, the easier it can be modulated by provocation and reduction strategies. One example is specific phobia: When a patient with spider phobia is engaged in a behavioral approach test (BAT) involving a live spider, increased avoidance and subjective distress can be monitored. When the spider is out of sight, subjective distress and avoidance are relatively rapidly reduced. When the spider is presented again, avoidance and subjective distress rise. In this scenario, a quick switch between different states (anxious versus not anxious) can be achieved simply by presenting and removing the trigger. A more general example of this principle is the threat of predictable or unpredictable shock (Davis et al., 2010). Often combined in a single (N)eutral, (P)redictable, and (U)npredictable threat task (Schmitz and Grillon, 2012). Shock threat leads to a rapid increase arousal, which can be measured both physiologically (Hur et al., 2020) and via self-report (Balderston et al., 2017b). When the threat is predictable, this elevated arousal is transient (on the order of seconds) and only present when the cue for the aversive shock is present (Åsli et al., 2009). In contrast, when the threat is unpredictable, the elevated arousal can be sustained (on the order of minutes or longer) and persists during the entire period of elevated threat (Ameli et al., 2001). Typically, elevated arousal is probed via random presentations of a loud white noise, which elicits an acoustic startle reflex (Grillon et al., 1991). This reflex is potentiated during elevated threat (Balderston et al., 2017a).

In social anxiety, symptoms can be reduced by removing the patient from the situation that causes anxiety or stopping the video or other stimulus used for symptom provocation. For investigating specific phobias, removing the anxiety-provoking trigger could be a suitable method to switch behavioral states. Removal of the situation is not a therapeutic approach but a potential experimental behavioral intervention for switching on and off the respective brain circuit to enable the computation of EEG biomarkers. Moreover, it may have ecological validity since avoidance is a common behavioral response to confrontation with anxiety-provoking stimuli naturalistically.

3.2. Symptom reduction by relaxation, suppression, distraction, and acceptance in intrusive thoughts

Here, we consider methods for the fast-acting reduction of intrusive thoughts such as experienced in OCD. Clinical experience

suggests large inter-individual differences regarding the strategies that are likely to be effective. Therefore, developing a practical approach that can rapidly reduce the frequency and intensity of intrusive thoughts in a laboratory setting depends on the individual and the nature of the intrusive thought being targeted. Note that these approaches are designed to develop an EEG-derived biomarker in a laboratory setting. They are not necessarily all suitable in a subsequent therapeutic setting that consists of a combination of symptom provocation with biomarker-guided personalized TMS.

For intrusive thoughts that induce non-specific anxiety, muscle relaxation and diaphragmatic breathing are symptomatic approaches that aim to reduce the physiological symptoms associated with the intrusive thought, which may indirectly reduce the frequency and intensity of intrusive thoughts experienced. The researcher or clinician needs to be familiar with these techniques to effectively guide the patient toward a reduced level of anxiety. Suppression is a more direct mental control technique that can rapidly and effectively manage unwanted thoughts, with several standard thought suppression paradigms available often using various different distractors. As a therapeutic strategy, thought suppression, while it could be effective temporarily (Roemer and Borkovec, 1994), may also exacerbate an existing obsessional state (Wegner, 1994; Grisham and Williams, 2009), and might become a mental compulsion. Nevertheless, thought suppression could be considered a viable approach for symptom modulation in a laboratory setting with the limitation that this approach becomes ineffective quickly and that a potential rebound effect might not coincide with the desired timing of the symptom-provocation phase.

A further approach that is also widely used therapeutically is distraction. A patient's ability to distract themselves from intrusive thoughts, behaviors and accompanying elevated anxiety is essential when compulsions cannot be performed. The extent to which patients can distract themselves varies significantly. Based on Simon et al. (2014), attentional distraction also appears to be effective in OCD patients and thereby distinguishes OCD from other anxiety disorders. It was found that patients with OCD use self-generated distraction less frequently than controls (Amir et al., 1997). As this technique was shown to be effective for reducing clinically relevant intrusive thoughts in the short term (Najmi et al., 2009) (even though not been tested in the long term), guided attentional distraction appears to be a promising candidate approach to switch to a low-symptom state in OCD patients, using, for example, a distracting bar orientation task as in Simon et al. (2014). A similar approach to guided attentional distraction is focused distraction. Instead of performing a task as mentioned above, attention is focused on a specific different thought (Wegner et al., 1987) as opposed to the unfocused distraction strategy employed in thought suppression. One way to apply focused distraction is to ask patients to focus on the thought of a specific weekend with friends they have either enjoyed or hope to enjoy and focus on the details (Najmi et al., 2009).

A further option to achieve a reduction of intrusive thoughts is acceptance. Acceptance is based on increasing the individual's ability to experience distressing thoughts without attempting to alter their content or frequency (Hayes et al., 1999), i.e., without trying to get rid of the thought or accompanying emotions. This strategy aims to reduce reactivity to unwanted thoughts without trying to reduce their frequency (Bach and Hayes, 2002). The underlying idea is that acceptance encourages passive observation of the unwanted thought and discourages the patient from struggling with it. Ultimately, distress typically reduces after practicing this consistently, although that is taught to not be the patient's immediate goal. However, acceptance in most cases is not a rapid strategy compared to distraction that can work instantaneously in most circumstances.

3.3. Symptom reduction by acting on compulsions in OCD

Finally, patients with OCD usually try to cope with anxiety and distress caused by intrusive thoughts, impulses or images by developing repetitive acts or specific rituals. According to the DSM-5, compulsions are defined as repetitive behaviors or mental acts (e.g., praying, counting, and repeating words silently) that the person feels driven to perform. These mental acts and behaviors aim to prevent or reduce distress or prevent some event or situation, but they are either excessive or disconnected with what they are intended to prevent. However, performing the individual ritual might be an effective way to achieve a rapid, short-term reduction in symptom severity, which could be quite suitable for the purpose developed here. This approach may work in a specific subset of anxieties and compulsions. Contamination anxiety and associated hand-washing compulsions are suitable examples for the laboratory setting. Many compulsions will be difficult to perform in the environment of a TMS and EEG recording, either because they only occur in a specific environment (checking doors and locks at home, for example) or because of limitations due to the nature of the intrusive thought and the associated compulsion, such as intrusive thoughts of harming or having harmed others and seeking reassurance.

For most patients, the reassurance may last for some time, and it is difficult to provoke symptoms repeatedly. However, compulsions are not always consistently effective at reducing distress and, in some cases, can cause distress. A further source of reduced reliability is that patients sometimes must repeat compulsions because they were ineffective the first time. It is also important to consider that asking a patient with OCD to act on his or her compulsions might be effective for the proposed EEG-biomarker estimation measurement, but this is not a beneficial therapeutic approach in the long term and can even aggravate the underlying anxiety (Wittgenstein, 1975; de Haan et al., 2013). An alternative experimental symptom provocation model to induce and reduce distress in a relatively controlled manner consists of distress being triggered, e.g., with photographs relevant to their OCD symptom subtype(s), followed by removal of the photographs when the participant pushes a button (Banca et al., 2015). The participant engages in silent counting as a distraction technique between symptom provocations to help reduce distress. This technique mimics the individual symptom-reducing compulsive avoidance behaviors, but does not cause movement or muscle artifacts in the EEG recording and may lead to more homogenous group data, than the use of individual strategies.

3.4. Symptom reduction by consumption in craving

Craving is a prominent symptom of addiction (to drugs, nicotine, or alcohol) or eating disorders. As discussed earlier, craving can be induced relatively easily using a suitable cue, but unlike anxiety (see Section "3.1. Symptom reduction by trigger removal in anxiety disorders" above), cue removal does not by itself reduce craving. There are similarities between OCD and some aspects of craving (Modell et al., 1992), as both are associated with intrusive thoughts that cause significant distress and, in the case of OCD, cause significant anxiety or cause the patient to act on certain compulsions in order to control them or in case of addiction lead to consumption of a substance. Similarly to acting on specific compulsions of OCD, a direct, rapidly acting and controllable approach to reduce craving symptoms could be simply allowing consumption of the substance (or food) craved. Similar limitations apply as in the previous section, and this is not a therapeutically beneficial approach and may worsen the underlying addiction.

3.5. Symptom reduction by mindfulness training

Another approach that has been discussed in the context of addiction is mindfulness training. Mindfulness involves two primary elements: focused attention and open monitoring (Lutz et al., 2008). During focused attention, attention is concentrated on a sensory object (often the sensation of breathing, but interoceptive and proprioceptive body sensations or external visual foci can also be used) while one acknowledges and then disengages from distracting thoughts and emotions. Focused attention practices often precede the practice of open monitoring, in which one observes both the arising of mental contents and the field of awareness in which those contents arise (Garland and Howard, 2018). These techniques have proven beneficial in several different clinical trials in reducing cravings and could be a promising approach to achieve a reduction of cravings in a laboratory setup where the goal is to switch between different brain states within minutes. A downside of this approach may be that it requires a significant amount of prior training and not all study participants are likely able to perform this strategy effectively (Witkiewitz and Bowen, 2010; Garland et al., 2017; Spears et al., 2017).

4. Discussion

4.1. Summary

In this paper, we have considered different approaches that may be applicable to achieve a rapid switching between states of low and high symptom severity in a laboratory setting to extract EEG and TMS-EEG signatures of the fluctuating activity of underlying brain circuits. We have presented anxiety, intrusive thoughts, and craving as exemplary symptoms that may be suitable and relevant to different psychiatric disorders. Symptom provocation (switching "on") is a well-established procedure in psychiatry, and it can be relatively easy to increase symptom severity in a short behavioral intervention. Conversely, rapidly reducing symptoms is generally much more difficult (switching "off").

Strategies that are helpful therapeutically may not be suitable for the experimental paradigm motivating this study. Specifically, strategies requiring ongoing cognitive or behavioral volitional activity throughout the "low symptom severity" period would introduce an additional confounder in brain states. EEG and TMS-EEG-derived biomarkers might then be sensitive to this volitional action, as opposed to the brain circuit activity that underlies the symptom. Similarly, strategies that may be suitable for the experimental approach, where a rapidly induced short-lasting change is required, may not be advisable in certain clinical situations. Specifically, a symptom reduction in OCD may be achieved by executing specific compulsions (such as hand washing) or consuming the object of craving (such as eating food in binge eating behavior, or smoking cigarettes in tobacco use disorder) in a laboratory setting. Alternatively, removing the triggering stimuli, possibly aided by the participant having control over this avoidance-like behavior, may also be effective and perhaps more controllable.

Whereas the "threat of shock paradigm" presented above is an example for the effective experimental induction of anxiety, this paradigm cannot easily be adapted to other symptoms. The use of script driven imagery on the other hand seems to be a promising generalizable approach to realize the goal of rapid psychiatric symptom switching, when combined with intermittent recovery periods to reverse the provocation. Pitman et al. (1987) played a relaxation instruction tape prior to starting the experiment, using the approach of guided attentional distraction. Data from Lang (1979) demonstrates that imaging of relevant phobic content prompts a specific increase in the amplitude of physiological arousal. This suggests that intrusive thoughts caused by pathologic emotional networks can be instigated in the laboratory through various means, including imagery, and that the activation of these networks is reflected not only in subjective reports but also in specific patterns in the EEG and TMS-EEG response.

The desired experimental paradigm of rapid switching between two states that differ only in symptom severity, and that can be achieved during a TMS/EEG measurement in a laboratory setting, will likely not be feasible for all types of symptoms and in all patient populations. However, we hope that this approach will yield new insights in specific cases. A specific proof-of-concept personalized therapeutic brain intervention based on EEG markers of circuit activity would be an important milestone in developing future closed-loop EEG and TMS treatment approaches. We suggest anxiety, intrusive thoughts and craving as possible candidates for such an initial proof-of-concept study. Below, we discuss practical considerations regarding the design of the experimental paradigm motivating this investigation.

4.2. Design considerations

Although it is exciting to consider how much can be learned from the symptom provocation possibilities described above, it is important to consider the implementation of these possibilities within the context of good experimental design and rigorous

electrophysiological data collection techniques. Accordingly, the following section will serve as a practical guide for how to properly conduct well-controlled EEG and TMS/EEG measurements while provoking psychiatric symptoms.

First, for the EEG-biomarker extraction, the cognitive-behavioral state between the two conditions should be similar. In an ideal scenario, the patient is in an otherwise neutral state in both conditions that enables the acquisition of TMS and EEG data without excessive signal artifacts (awake, seated in a chair, with relaxed scalp muscles, eyes open, fixating a visual target) and the behavioral intervention is short and limited to a few minutes between the conditions (see **Figure 1**). If it is necessary to use a mental task to achieve a change in symptom severity (such as visual stimuli, mental imagery or mental verbalization), similar tasks should be used during both conditions (e.g., observation of critical faces in one condition and observation of neutral faces in the other condition; or a less effective version of a focused distraction task, that is otherwise similar).

Second, symptom severity should be measured repeatedly during each condition to assess whether the intervention is effective. Physiological markers (skin conductance, heart rate, blink reflex, pupillometry) should be considered where available such that assessment of the effectiveness of an induced state could be corroborated by objective measurements. In the case of anxiety and craving, a visual analog scale can also be used. In the case of discrete symptoms that are either there or not, such as intrusive thoughts, the study participant can press a button to indicate when the intrusive thought occurred. This could be complemented with a visual analog scale for distress, since it is possible for one to have an intrusive thought without distress, e.g., during the symptom reduction phase of the experiment.

Third, the task should be practiced, and the measurement procedures should be demonstrated during a preparatory experimental session to reduce novelty, salience, and training effects during the recording. This could potentially also have another beneficial effect as practicing ahead of time might produce an experimentally-advantageous expectancy or priming effect, such that the person anticipates that the provocation will induce distress and the technique following it would reduce distress.

Regarding the neurophysiological measures, signal quality should be monitored during the measurement so that excessive artifacts (e.g., due to scalp muscle activity, eye blinks and eye movements) can be addressed. Obtaining high-quality concurrent TMS and EEG recordings is not trivial; recommendations for data acquisition and analysis have recently been summarized elsewhere (Hernandez-Pavon et al., 2023), and this is an active area of research. It is also not obvious to decide the target location and intensity of the TMS. It may be necessary to investigate different candidate stimulation parameters in a calibration session to determine the optimal location to probe the reactivity of the circuit under investigation at an intensity that achieves an optimal trade-off between maximizing cortical responses and minimizing TMS-related EEG artifacts.

4.3. Limitations

An important inherent limitation in the proposed approach is that only a small subset of symptoms and psychiatric conditions are likely suitable for the rapid, controlled modulation of symptom severity (such as a small number of specific phobias, other anxiety conditions with specific triggers, and OCD). While resulting TMS/EEG-derived biomarkers could yield relevant insights into those specific pathologies, it is currently unclear whether the findings are likely to generalize. This limitation could be further exacerbated if highly individualized provocation and reduction strategies are required, increasing the variability between participants, as the EEG measurement will be affected by the specific strategy employed to achieve the symptom modulation.

When evaluating strategies that could lead to a short-term symptom reduction but are not consistent with therapeutic approaches (such as smoking to reduce craving or execution of rituals to reduce compulsions), the potential negative short- and long-term effects on the study participant needs to be evaluated, and a clear ethical justification of any such strategies is required.

Another limitation concerns the neurophysiological measures: EEG is much more sensitive to the activity of superficially located brain regions than deep brain regions (and dipoles oriented orthogonally to the scalp surface instead of parallel). Even if an effective strategy to modulate symptom severity can be found, it may not be possible to derive reliable EEG markers for that symptom. Similar constraints affect the TMS-EEG data; TMS is thought to primarily activate neurons in the superficial parts of the cortical sulcal walls and the gyral crowns. It may be difficult to achieve the goal of using TMS to probe the circuits underlying the specific psychopathology under investigation if none of the nodes of the circuit are accessible to TMS stimulation. In these cases, indirect circuit stimulation through a connected superficial (accessible) area can be considered.

Note that the proposed approach depends on the assumption that changes in the EEG reflect changes in the expression of symptoms with a congruent timeline. Furthermore, because increased pathological network activity will likely coincide with involuntarily simultaneously increased activity in compensatory networks, it may be difficult to disentangle the respective EEG-signatures. Finally, even if a suitable EEG-derived biomarker can be identified, this does not automatically mean that the target circuit can be effectively modulated with a given TMS protocol.

In conclusion, it is important to match the timescale of fluctuations in circuit activity with the timescale of the neurophysiological measures. EEG data needs to be acquired over several minutes to compute reliable spectral estimates; at least dozens of TMS-EEG trials are required to extract evoked potentials and induced oscillations. For symptoms such as anxiety and craving, a stable high vs. low symptom severity condition may be achievable for tens of minutes. However, for transient symptoms, such as intrusive thoughts, symptoms may fluctuate on a much faster timescale and the underlying short-lasting physiological changes might not be accessible with the same neurophysiological measures. Lastly, different synchronization and analysis approaches may be required to identify discrete EEG events instead of slow variations.

5. Outlook

We believe that the current lack of reliable biomarkers that index the fluctuating activity of brain circuit activity with a

temporal resolution of tens of seconds is a critical barrier in the development of a next generation of personalized therapeutic brain stimulation protocols. We hope that the approach put forward in this work may help determine such EEG-derived biomarkers and that this will lead to more effective brain intervention therapies for patients suffering from neuropsychiatric disorders.

Data availability statement

The original contributions presented in this study are included in this article/supplementary material, further inquiries can be directed to the corresponding author.

Author contributions

BZ, CZ, DB, and JF contributed to the conception and design of the work. BZ and JF wrote the first draft of the manuscript. CZ, NB, DB, SK, JL, RT, AT, and GZ wrote sections of the manuscript. All authors contributed to the manuscript revision and read and approved the submitted version.

Funding

DB receives research support from the Canadian Institutes of Health Research (CIHR), NIH, Brain Canada, and the Temerty Family through the CAMH Foundation. SK reports grants from the Labatt Family Innovation Fund in Brain Health (Department of Psychiatry, University of Toronto), the Max Bell Foundation, the Canadian Centre on Substance Use and Addiction, the Ontario Ministry of Health and Long-Term Care (MOHLTC), and CIHR. JF receives research support from the NIH, the Klarman Family Foundation, and the CAMH Discovery Fund. BZ receives research support from CIHR. CZ receives research support from CIHR and the Brain Canada Foundation.

Conflict of interest

BZ and CZ are shareholders in sync2brain GmbH (Tübingen, Germany) a University of Tübingen spin-off start-up company developing technology for personalized therapeutic TMS. BZ reports part-time salary support from sync2brain GmbH, unrelated to this work. DB received research support and in-kind equipment support for an investigator-initiated study from Brainsway Ltd. and has been the site principal investigator for three sponsor-initiated studies for Brainsway Ltd. DB also received in-kind equipment support from MagVenture for 3 investigator-initiated studies. DB received medication supplies for an investigator-initiated trial from Indivior. DB has participated in one Scientific Advisory Board Meeting for Janssen and one meeting for Welcony Inc. SK has received honorarium for past consultation for EmpowerPharm.

The remaining authors declare that the research was conducted in the absence of any commercial or financial relationships that could be construed as a potential conflict of interest.

Publisher's note

References

Abi-Dargham, A., Gil, R., Krystal, J., Baldwin, R. M., Seibyl, J. P., Bowers, M., et al. (1998). Increased striatal dopamine transmission in schizophrenia: Confirmation in a second cohort. *Am. J. Psychiatry* 155, 761–767. doi: 10.1176/ajp.155.6.761

Agren, T., Engman, J., Frick, A., Björkstrand, J., Larsson, E. M., Furmark, T., et al. (2012). Disruption of reconsolidation erases a fear memory trace in the human amygdala. *Science* 337, 1550–1552. doi: 10.1126/science.1223006

Altman, N., and Krzywinski, M. (2018). The curse(s) of dimensionality. *Nat. Methods* 15, 399–400. doi: 10.1038/s41592-018-0019-x

Ameli, R., Ip, C., and Grillon, C. (2001). Contextual fear-potentiated startle conditioning in humans: Replication and extension. *Psychophysiology* 38, 383–390. doi: 10.1111/1469-8986.3830383

Amir, N., Cashman, L., and Foa, E. B. (1997). Strategies of thought control in obsessive-compulsive disorder. *Behav. Res. Ther.* 35, 775–777. doi: 10.1016/S0005-7967(97)00030-2

Andén, N.-E., Butcher, S. G., Corrodi, H., Fuxe, K., and Ungerstedt, U. (1970). Receptor activity and turnover of dopamine and noradrenaline after neuroleptics. *Eur. J. Pharmacol.* 11, 303–314. doi: 10.1016/0014-2999(70)90006-3

Åsli, O., Kulvedrøsten, S., Solbakken, L. E., and Flaten, M. A. (2009). Fear potentiated startle at short intervals following conditioned stimulus onset during delay but not trace conditioning. *Psychophysiology* 46, 880–888. doi: 10.1111/j.1469-8986.2009.00809.x

Bach, P., and Hayes, S. C. (2002). The use of acceptance and commitment therapy to prevent the rehospitalization of psychotic patients: A randomized controlled trial. *J. Consult. Clin. Psychol.* 70, 1129–1139. doi: 10.1037/0022-006X.70.5.1129

Balderston, N. L., Liu, J., Roberson-Nay, R., Ernst, M., and Grillon, C. (2017b). The relationship between dlPFC activity during unpredictable threat and CO2-induced panic symptoms. *Transl. Psychiatry* 7:1266. doi: 10.1038/s41398-017-0006-5

Balderston, N. L., Hale, E., Hsiung, A., Torrisi, S., Holroyd, T., Carver, F. W., et al. (2017a). Threat of shock increases excitability and connectivity of the intraparietal sulcus. *ELife* 6:e23608. doi: 10.7554/eLife.23608

Banca, P., Voon, V., Vestergaard, M. D., Philipiak, G., Almeida, I., Pocinho, F., et al. (2015). Imbalance in habitual versus goal directed neural systems during symptom provocation in obsessive-compulsive disorder. *Brain* 138(Pt 3), 798–811. doi: 10.1093/brain/awu379

Boehme, S., Mohr, A., Becker, M. P., Miltner, W. H., and Straube, T. (2014). Area-dependent time courses of brain activation during video-induced symptom provocation in social anxiety disorder. *Biol. Mood Anxiety Disord.* 4:6. doi: 10.1186/2045-5380-4-6

Bremner, J. D., Staib, L. H., Kaloupek, D., Southwick, S. M., Soufer, R., and Charney, D. S. (1999b). Neural correlates of exposure to traumatic pictures and sound in Vietnam combat veterans with and without posttraumatic stress disorder: A positron emission tomography study. *Biol. Psychiatry* 45, 806–816. doi: 10.1016/s0006-3223(98)00297-2

Bremner, J. D., Narayan, M., Staib, L. H., Southwick, S. M., McGlashan, T., and Charney, D. S. (1999a). Neural correlates of memories of childhood sexual abuse

in women with and without posttraumatic stress disorder. *Am. J. Psychiatry* 156, 1787–1795. doi: 10.1176/ajp.156.11.1787

Carlsson, A., and Lindqvist, M. (1963). Effect of chlorpromazine or haloperidol on formation of 3-methoxytyramine and normetanephrine in mouse brain. *Acta Pharmacol. Toxicol.* 20, 140–144. doi: 10.1111/j.1600-0773.1963.tb01730.x

Carlsson, A., Lindqvist, M., and Magnusson, T. (1957). 3,4-dihydroxyphenylalanine and 5-hydroxytryptophan as reserpine antagonists. *Nature* 180:1200. doi: 10.1038/1801200a0

Carmi, L., Tendler, A., Bystritsky, A., Hollander, E., Blumberger, D. M., Daskalakis, J., et al. (2019). Efficacy and safety of deep transcranial magnetic stimulation for obsessive-compulsive disorder: A prospective multicenter randomized double-blind placebo-controlled trial. *Am. J. Psychiatry* 176, 931–938. doi: 10.1176/appi.ajp.2019.18101180

Cyranowski, J. M., Hofkens, T. L., Swartz, H. A., Salomon, K., and Gianaros, P. J. (2011). Cardiac vagal control in nonmedicated depressed women and nondepressed controls: Impact of depression status, lifetime trauma history, and respiratory factors. *Psychosom. Med.* 73, 336–343. doi: 10.1097/PSY.0b013e318213925d

Davis, K. L., Kahn, R. S., Ko, G., and Davidson, M. (1991). Dopamine in schizophrenia: A review and reconceptualization. *Am. J. Psychiatry* 148, 1474–1486. doi: 10.1176/ajp.148.11.1474

Davis, M., Walker, D. L., Miles, L., and Grillon, C. (2010). Phasic vs sustained fear in rats and humans: Role of the extended amygdala in fear vs anxiety. *Neuropsychopharmacology* 35, 105–135. doi: 10.1038/npp.2009.109

de Haan, S., Rietveld, E., and Denys, D. (2013). On the nature of obsessions and compulsions. *Mod. Trends Pharmacopsychiatry* 29, 1–15. doi: 10.1159/000351929

Dehghan, B., Saeidimehr, S., Sayyah, M., and Rahim, F. (2021). The Effect of virtual reality on emotional response and symptoms provocation in patients with OCD: A systematic review and meta-analysis. *Front. Psychiatry* 12:733584. doi: 10.3389/fpsyt.2021.733584

Denys, D. (2011). Obsessionality & compulsivity: A phenomenology of obsessive-compulsive disorder. *Philos. Ethics Humanit. Med.* 6:3. doi: 10.1186/1747-5341-6-3

D'Souza, D. C., Berman, R. M., Krystal, J. H., and Charney, D. S. (1999). Symptom provocation studies in psychiatric disorders: Scientific value, risks, and future. *Biol. Psychiatry* 46, 1060–1080. doi: 10.1016/S0006-3223(99)00209-7

Etkin, A. (2018). Decoding mood. *Nat. Biotechnol.* 36, 932–933. doi: 10.1038/nbt.4258

Food and Drug Administration (2020). *FDA permits marketing of transcranial magnetic stimulation for treatment of obsessive compulsive disorder*. FDA. Available online at: https://www.fda.gov/news-events/press-announcements/fda-permits-marketing-transcranial-magnetic-stimulation-treatment-obsessive-compulsive-disorder (accessed August 23, 2021).

Forcato, C., Burgos, V. L., Argibay, P. F., Molina, V. A., Pedreira, M. E., and Maldonado, H. (2007). Reconsolidation of declarative memory in humans. *Learn. Mem.* 14, 295–303. doi: 10.1101/lm.486107

Garland, E. L., and Howard, M. O. (2018). Mindfulness-based treatment of addiction: Current state of the field and envisioning the next wave of research. *Addict. Sci. Clin. Pract.* 13:14. doi: 10.1186/s13722-018-0115-3

Garland, E. L., Baker, A. K., and Howard, M. O. (2017). Mindfulness-oriented recovery enhancement reduces opioid attentional bias among prescription opioid-treated chronic pain patients. *J. Soc. Soc. Work Res.* 8, 493–509. doi: 10.1086/694324

Ghiasi, N., Bhansali, R. K., and Marwaha, R. (2023). *Lorazepam. StatPearls*. Treasure Island, FL: StatPearls Publishing.

Gordon, P. C., Belardinelli, P., Stenroos, M., Ziemann, U., and Zrenner, C. (2022). Prefrontal theta phase-dependent rTMS-induced plasticity of cortical and behavioral responses in human cortex. *Brain Stimul.* 15, 391–402. doi: 10.1016/j.brs.2022.02.006

Gordon, P. C., Dörre, S., Belardinelli, P., Stenroos, M., Zrenner, B., Ziemann, U., et al. (2021). Prefrontal theta-phase synchronized brain stimulation with real-time EEG-triggered TMS. *Front. Hum. Neurosci.* 15:691821. doi: 10.3389/fnhum.2021.691821

Greeno, C. G., Wing, R. R., and Shiffman, S. (2000). Binge antecedents in obese women with and without binge eating disorder. *J. Consult. Clin. Psychol.* 68, 95–102. doi: 10.1037/0022-006X.68.1.95

Grillon, C., Ameli, R., Woods, S. W., Merikangas, K., and Davis, M. (1991). Fear-potentiated startle in humans: Effects of anticipatory anxiety on the acoustic blink reflex. *Psychophysiology* 28, 588–595. doi: 10.1111/j.1469-8986.1991.tb01999.x

Grisham, J. R., and Williams, A. D. (2009). Cognitive control of obsessional thoughts. *Behav. Res. Ther.* 47, 395–402. doi: 10.1016/j.brat.2009.01.014

Gross, J. J. (2015). Emotion regulation: Current status and future prospects. *Psychol. Inq.* 26, 1–26. doi: 10.1254/fpj.151.21

Grosse-Wentrup, M., and Buss, M. (2008). Multiclass common spatial patterns and information theoretic feature extraction. *IEEE Trans. Biomed. Eng.* 55, 1991–2000. doi: 10.1109/TBME.2008.921154

Guzick, A. G., Schweissing, E., Tendler, A., Sheth, S. A., Goodman, W. K., and Storch, E. A. (2022). Do exposure therapy processes impact the efficacy of deep TMS for obsessive-compulsive disorder? *J. Obsessive Compuls. Relat. Disord.* 35:100756. doi: 10.1016/j.jocrd.2022.100756

Hayes, S. C., Strosahl, K. D., and Wilson, K. G. (1999). *Acceptance and commitment therapy*. New York, NY: Guilford press.

Hernandez-Pavon, J. C., Veniero, D., Bergmann, T. O., Belardinelli, P., Bortoletto, M., Casarotto, S., et al. (2023). TMS combined with EEG: Recommendations and open issues for data collection and analysis. *Brain Stimul.* 16, 567–593. doi: 10.1016/j.brs.2023.02.009

Holt, P. E., and Andrews, G. (1989). Provocation of panic: Three elements of the panic reaction in four anxiety disorders. *Behav. Res. Ther.* 27, 253–261. doi: 10.1016/0005-7967(89)90044-2

Hur, J., Smith, J. F., DeYoung, K. A., Anderson, A. S., Kuang, J., Kim, H. C., et al. (2020). Anxiety and the neurobiology of temporally uncertain threat anticipation. *J. Neurosci.* 40, 7949–7964. doi: 10.1523/JNEUROSCI.0704-20.2020

Isserles, M., Tendler, A., Roth, Y., Bystritsky, A., Blumberger, D. M., Ward, H., et al. (2021). Deep transcranial magnetic stimulation combined with brief exposure for posttraumatic stress disorder: A prospective multisite randomized trial. *Biol. Psychiatry* 90, 721–728. doi: 10.1016/j.biopsych.2021.04.019

Jarosz, P. A., Dobal, M. T., Wilson, F. L., and Schram, C. A. (2007). Disordered eating and food cravings among urban obese African American women. *Eat. Behav.* 8, 374–381. doi: 10.1016/j.eatbeh.2006.11.014

Keepers, G. A., Fochtmann, L. J., Anzia, J. M., Benjamin, S., Lyness, J. M., Mojtabai, R., et al. (2020). The American psychiatric association practice guideline for the treatment of patients with schizophrenia. *Am. J. Psychiatry* 177, 868–872. doi: 10.1176/appi.ajp.2020.177901

Khalsa, S. S., Craske, M. G., Li, W., Vangala, S., Strober, M., and Feusner, J. D. (2015). Altered interoceptive awareness in anorexia nervosa: Effects of meal anticipation, consumption and bodily arousal. *Int. J. Eat. Disord.* 48, 889–897. doi: 10.1002/eat.22387

Lang, P. J. (1979). Presidential address, 1978. A bio-informational theory of emotional imagery. *Psychophysiology* 16, 495–512. doi: 10.1111/j.1469-8986.1979.tb01511.x

Lanius, R. A., Frewen, P. A., Girotti, M., Neufeld, R. W., Stevens, T. K., and Densmore, M. (2007). Neural correlates of trauma script-imagery in posttraumatic stress disorder with and without comorbid major depression: A functional MRI investigation. *Psychiatry Res.* 155, 45–56. doi: 10.1016/j.pscychresns.2006.11.006

Lepping, R. J., Atchley, R. A., Chrysikou, E., Martin, L. E., Clair, A. A., Ingram, R. E., et al. (2016). Neural processing of emotional musical and nonmusical stimuli in depression. *PLoS One* 11:e0156859. doi: 10.1371/journal.pone.0156859

Lin, I. M., Wu, Y. C., Su, W. S., Ke, C. K., Lin, P. Y., Huang, M. F., et al. (2022). Cardiac autonomic and cardiac vagal control during and after depressive and happiness autobiographical memories in patients with major depressive disorder. *Front. Psychiatry* 13:878285. doi: 10.3389/fpsyt.2022.878285

Liotti, M., Mayberg, H. S., McGinnis, S., Brannan, S. L., and Jerabek, P. (2002). Unmasking disease-specific cerebral blood flow abnormalities: Mood challenge in patients with remitted unipolar depression. *Am. J. Psychiatry* 159, 1830–1840. doi: 10.1176/appi.ajp.159.11.1830

Lutz, A., Slagter, H. A., Dunne, J. D., and Davidson, R. J. (2008). Attention regulation and monitoring in meditation. *Trends Cogn. Sci.* 12, 163–169. doi: 10.1016/j.tics.2008.01.005

Maia, A., Almeida, S., Cotovio, G., Rodrigues da Silva, D., Viana, F. F., Grácio, J., et al. (2022). Symptom provocation for treatment of obsessive-compulsive disorder using transcranial magnetic stimulation: A step-by-step guide for professional training. *Front. Psychiatry* 13:924370. doi: 10.3389/fpsyt.2022.924370

Margraf, J., Ehlers, A., and Roth, W. T. (1986). Sodium lactate infusions and panic attacks: A review and critique. *Psychosom. Med.* 48, 23–51. doi: 10.1097/00006842-198601000-00002

Martin, M. (1990). On the induction of mood. *Clin. Psychol. Rev.* 10, 669–697. doi: 10.1016/0272-7358(90)90075-L

Massimini, M., Ferrarelli, F., Huber, R., Esser, S. K., Singh, H., and Tononi, G. (2005). Breakdown of cortical effective connectivity during sleep. *Science* 309, 2228–2232. doi: 10.1126/science.1117256

Metsomaa, J., Belardinelli, P., Ermolova, M., Ziemann, U., and Zrenner, C. (2021). Causal decoding of individual cortical excitability states. *Neuroimage* 245:118652. doi: 10.1016/j.neuroimage.2021.118652

Milivojevic, V., Angarita, G. A., Hermes, G., Sinha, R., and Fox, H. C. (2020). Effects of Prazosin on provoked alcohol craving and autonomic and neuroendocrine response to stress in alcohol use disorder. *Alcohol. Clin. Exp. Res.* 44, 1488–1496. doi: 10.1111/acer.14378

Miskovic, V., and Schmidt, L. A. (2012). Social fearfulness in the human brain. *Neurosci. Biobehav. Rev.* 36, 459–478. doi: 10.1016/j.neubiorev.2011.08.002

Modell, J. G., Glaser, F. B., Cyr, L., and Mountz, J. M. (1992). Obsessive and compulsive characteristics of craving for alcohol in alcohol abuse and dependence. *Alcohol. Clin. Exp. Res.* 16, 272–274. doi: 10.1111/j.1530-0277.1992.tb01375.x

Mussell, M. P., Mitchell, J. E., de Zwaan, M., Crosby, R. D., Seim, H. C., and Crow, S. J. (1996). Clinical characteristics associated with binge eating in obese females: A descriptive study. *Int. J. Obes. Relat. Metab. Disord.* 20, 324–331.

Najmi, S., Riemann, B. C., and Wegner, D. M. (2009). Managing unwanted intrusive thoughts in obsessive-compulsive disorder: Relative effectiveness of suppression, focused distraction, and acceptance. *Behav. Res. Ther.* 47, 494–503. doi: 10.1016/j.brat.2009.02.015

Ng, L., and Davis, C. (2013). Cravings and food consumption in Binge Eating Disorder. *Eat. Behav.* 14, 472–475. doi: 10.1016/j.eatbeh.2013.08.011

Nummenmaa, L., Saarimäki, H., Glerean, E., Gotsopoulos, A., Jääskeläinen, I., Hari, R., et al. (2014). Emotional speech synchronizes brains across listeners and engages large-scale dynamic brain networks. *Neuroimage* 102, 498–509.

Nybäck, H., and Sedvall, G. (1970). Further studies on the accumulation and disappearance of catecholamines formed from tyrosine-14C in mouse brain. Effect of some phenothiazine analogues. *Eur. J. Pharmacol.* 10, 193–205. doi: 10.1016/0014-2999(70)90273-6

Parmigiani, S., Ross, J. M., Cline, C. C., Minasi, C. B., Gogulski, J., and Keller, C. J. (2023). Reliability and validity of transcranial magnetic stimulation-electroencephalography biomarkers. *Biol. Psychiatry Cogn. Neurosci. Neuroimaging* 8, 805–814. doi: 10.1016/j.bpsc.2022.12.005

Pitman, R. K., Orr, S. P., Forgue, D. F., de Jong, J. B., and Claiborn, J. M. (1987). Psychophysiologic assessment of posttraumatic stress disorder imagery in Vietnam combat veterans. *Arch. Gen. Psychiatry* 44, 970–975. doi: 10.1001/archpsyc.1987.01800230050009

Randrup, A. (1970). "Biochemical, anatomical and psychological investigations of stereotyped behavior induced by amphetamines," in *Amphetamine and related compounds*, eds E. Costa and S. Garattini (New York, NY: Raven Press), 695–713.

Robbins, T. W., Gillan, C. M., Smith, D. G., de Wit, S., and Ersche, K. D. (2012). Neurocognitive endophenotypes of impulsivity and compulsivity: Towards dimensional psychiatry. *Trends Cogn. Sci.* 16, 81–91. doi: 10.1016/j.tics.2011.11.009

Roemer, L., and Borkovec, T. D. (1994). Effects of suppressing thoughts about emotional material. *J. Abnorm. Psychol.* 103, 467–474. doi: 10.1037/0021-843X.103.3.467

Rottenberg, J., Clift, A., Bolden, S., and Salomon, K. (2007). RSA fluctuation in major depressive disorder. *Psychophysiology* 44, 450–458. doi: 10.1111/j.1469-8986.2007.00509.x

Rottenberg, J., Wilhelm, F. H., Gross, J. J., and Gotlib, I. H. (2003). Vagal rebound during resolution of tearful crying among depressed and nondepressed individuals. *Psychophysiology* 40, 1–6. doi: 10.1111/1469-8986.00001

Rylander, G. (1969). "Clinical and medico-criminological aspects of addiction to central stimulating drugs," in *Abuse of central stimulants*, eds F. Sjoquist and M. Tottie (Stockholm: Almqvist and Wiksell), 251–273.

Sarasso, S., Rosanova, M., Casali, A. G., Casarotto, S., Fecchio, M., Boly, M., et al. (2014). Quantifying cortical EEG responses to TMS in (un)consciousness. *Clin. EEG Neurosci.* 45, 40–49. doi: 10.1177/1550059413513723

Saxena, S., Bota, R. G., and Brody, A. L. (2001). Brain-behavior relationships in obsessive-compulsive disorder. *Semin. Clin. Neuropsychiatry* 6, 82–101. doi: 10.1053/scnp.2001.21833

Schienle, A., Schäfer, A., Hermann, A., Rohrmann, S., and Vaitl, D. (2007). Symptom provocation and reduction in patients suffering from spider phobia: An fMRI study on exposure therapy. *Eur. Arch. Psychiatry Clin. Neurosci.* 257, 486–493. doi: 10.1007/s00406-007-0754-y

Schiller, D., Kanen, J. W., LeDoux, J. E., Monfils, M. H., and Phelps, E. A. (2013). Extinction during reconsolidation of threat memory diminishes prefrontal cortex involvement. *Proc. Natl. Acad. Sci. U.S.A.* 110, 20040–20045. doi: 10.1073/pnas.1320322110

Schmitz, A., and Grillon, C. (2012). Assessing fear and anxiety in humans using the threat of predictable and unpredictable aversive events (the NPU-threat test). *Nat. Protoc.* 7, 527–532. doi: 10.1038/nprot.2012.001

Segal, Z. V., Kennedy, S., Gemar, M., Hood, K., Pedersen, R., and Buis, T. (2006). Cognitive reactivity to sad mood provocation and the prediction of depressive relapse. *Arch. Gen. Psychiatry* 63, 749–755. doi: 10.1001/archpsyc.63.7.749

Shin, L. M., Wright, C. I., Cannistraro, P. A., Wedig, M. M., McMullin, K., Martis, B., et al. (2005). A functional magnetic resonance imaging study of amygdala and medial prefrontal cortex responses to overtly presented fearful faces in posttraumatic stress disorder. *Arch. Gen. Psychiatry* 62, 273–281. doi: 10.1001/archpsyc.62.3.273

Shinba, T. (2014). Altered autonomic activity and reactivity in depression revealed by heart-rate variability measurement during rest and task conditions. *Psychiatry Clin. Neurosci.* 68, 225–233. doi: 10.1111/pcn.12123

Silvanto, J., Muggleton, N., and Walsh, V. (2008). State-dependency in brain stimulation studies of perception and cognition. *Trends Cogn. Sci.* 12, 447–454. doi: 10.1016/j.tics.2008.09.004

Simon, D., Adler, N., Kaufmann, C., and Kathmann, N. (2014). Amygdala hyperactivation during symptom provocation in obsessive-compulsive disorder and its modulation by distraction. *Neuroimage Clin.* 4, 549–557. doi: 10.1016/j.nicl.2014.03.011

Spears, C. A., Hedeker, D., Li, L., Wu, C., Anderson, N. K., Houchins, S. C., et al. (2017). Mechanisms underlying mindfulness-based addiction treatment versus cognitive behavioral therapy and usual care for smoking cessation. *J. Consult. Clin. Psychol.* 85, 1029–1040. doi: 10.1037/ccp0000229

Tendler, A., Sisko, E., Barnea-Ygael, N., Zangen, A., and Storch, E. A. (2019). A method to provoke obsessive compulsive symptoms for basic research and clinical interventions. *Front. Psychiatry.* 10:814. doi: 10.3389/fpsyt.2019.00814

Waters, A., Hill, A., and Waller, G. (2001). Bulimics' responses to food cravings: Is binge-eating a product of hunger or emotional state? *Behav. Res. Ther.* 39, 877–886. doi: 10.1016/S0005-7967(00)00059-0

Wegner, D. M. (1994). Ironic processes of mental control. *Psychol. Rev.* 101, 34–52. doi: 10.1037/0033-295X.101.1.34

Wegner, D. M., Schneider, D. J., Carter, S. R., and White, T. L. (1987). Paradoxical effects of thought suppression. *J. Pers. Soc. Psychol.* 53, 5–13. doi: 10.1037/0022-3514.53.1.5

Witkiewitz, K., and Bowen, S. (2010). Depression, craving, and substance use following a randomized trial of mindfulness-based relapse prevention. *J. Consult. Clin. Psychol.* 78, 362–374. doi: 10.1037/a0019172

Wittgenstein, L. (1975). *On certainty*. Oxford: Blackwell.

Yirmiya, R., Weidenfeld, J., Pollak, Y., Morag, M., Morag, A., Avitsur, R., et al. (1999). Cytokines, "depression due to a general medical condition," and antidepressant drugs. *Adv. Exp. Med. Biol.* 461, 283–316. doi: 10.1007/978-0-585-37970-8_16

Ziemann, U. (2004). TMS and drugs. *Clin. Neurophysiol.* 115, 1717–1729. doi: 10.1016/j.clinph.2004.03.006

Ziemann, U., Reis, J., Schwenkreis, P., Rosanova, M., Strafella, A., Badawy, R., et al. (2015). TMS and drugs revisited 2014. *Clin. Neurophysiol.* 126, 1847–1868. doi: 10.1016/j.clinph.2014.08.028

Zrenner, B., Zrenner, C., Gordon, P. C., Belardinelli, P., McDermott, E. J., Soekadar, S. R., et al. (2020). Brain oscillation-synchronized stimulation of the left dorsolateral prefrontal cortex in depression using real-time EEG-triggered TMS. *Brain Stimul.* 13, 197–205. doi: 10.1016/j.brs.2019.10.007

Zrenner, C., Desideri, D., Belardinelli, P., and Ziemann, U. (2018). Real-time EEG-defined excitability states determine efficacy of TMS-induced plasticity in human motor cortex. *Brain Stimul.* 11, 374–389. doi: 10.1016/j.brs.2017.11.016

frontiers | Frontiers in Neural Circuits

TYPE Original Research
PUBLISHED 05 September 2023
DOI 10.3389/fncir.2023.1202671

OPEN ACCESS

EDITED BY
Kevin A. Caulfield,
Medical University of South Carolina,
United States

REVIEWED BY
Panpan Hu,
Anhui Medical University, China
Masafumi Yoshimura,
Faculty of Rehabilitation Kansai Medical University, Japan

*CORRESPONDENCE
Min Zhang
✉ zhang_min_3464@126.com
Tian Tian
✉ tongjitiantian@163.com

RECEIVED 11 April 2023
ACCEPTED 08 August 2023
PUBLISHED 05 September 2023

CITATION
Qin Y, Ba L, Zhang F, Jian S, Tian T, Zhang M and Zhu W (2023) Multisite rTMS combined with cognitive training modulates effective connectivity in patients with Alzheimer's disease. *Front. Neural Circuits* 17:1202671. doi: 10.3389/fncir.2023.1202671

Multisite rTMS combined with cognitive training modulates effective connectivity in patients with Alzheimer's disease

Yuanyuan Qin[1], Li Ba[2], Fengxia Zhang[3], Si Jian[1], Tian Tian[1]*, Min Zhang[2]* and Wenzhen Zhu[1]

[1]Department of Radiology, Tongji Hospital, Tongji Medical College, Huazhong University of Science and Technology, Wuhan, Hubei, China, [2]Department of Neurology, Tongji Hospital, Tongji Medical College, Huazhong University of Science and Technology, Wuhan, Hubei, China, [3]Department of Rehabilitation, RenMin Hospital of Wuhan University, Wuhan, Hubei, China

Purpose: To investigate the effective connectivity (EC) changes after multisite repetitive transcranial magnetic stimulation (rTMS) combined with cognitive training (COG).

Method: We selected 51 patients with mild or moderate Alzheimer's disease (AD) and delivered 10 Hz rTMS over the left dorsal lateral prefrontal cortex (DLPFC) and the lateral temporal lobe (LTL) combined with COG or sham stimulation for 4 weeks. The selected AD patients were divided into real (real rTMS+COG, $n = 11$) or sham (sham rTMS+COG, $n = 8$) groups to undergo neuropsychological assessment, resting-state fMRI, and 3D brain structural imaging before (T0), immediately at the end of treatment (T4), and 4 weeks after treatment (T8). A 2 × 3 factorial design with "time" as the within-subjects factor (three levels: T0, T4, and T8) and "group" as the between-subjects factor (two levels: real and sham) was used to investigate the EC changes related to the stimulation targets in the rest of the brain, as well as the causal interactions among seven resting-state networks based on Granger causality analysis (GCA).

Results: At the voxel level, the EC changes from the left DLPFC out to the left inferior parietal lobe and the left superior frontal gyrus, as well as from the left LTL out to the left orbital frontal cortex, had a significant group × time interaction effect. At the network level, a significant interaction effect was identified in the increase in EC from the limbic network out to the default mode network. The decrease in EC at the voxel level and the increase in EC at the network level were both associated with the improved ability to perform activities of daily living and cognitive function.

Conclusion: Multisite rTMS combined with cognitive training can modulate effective connectivity in patients with AD, resulting in improved ability to perform activities of daily living and cognitive function.

KEYWORDS

repetitive transcranial magnetic stimulation, cognitive training, Alzheimer's disease, resting-state fMRI, effective connectivity

Highlights

- Multisite rTMS combined with cognitive training has been shown to be potentially effective in patients with early-stage Alzheimer's disease.
- The effective connectivity changes associated with this new non-drug adjuvant intervention were investigated.
- The decrease in effective connectivity at the voxel level and the increase at the network level were both associated with improved ability to perform activities of daily living and cognitive function.

Introduction

Alzheimer's disease (AD) is an irreversible neurodegenerative disorder with recent understanding as a disconnection syndrome. The functional connectivity of large-scale networks is progressively disrupted during disease progression (Gomez-Ramirez and Wu, 2014). As pharmacotherapy for AD is currently limited, attention has been paid to non-drug adjuvant interventions such as repetitive transcranial magnetic stimulation (rTMS). Using a pulsed magnetic field to create a current in the human brain, rTMS can produce a persistent effect on the cortical synapse function after stimulation (Huang et al., 2017). The frequency of pulse applications during rTMS and the stimulation target are two prominent parameters for evaluating the after-effects of rTMS. Traditionally, a high frequency induces an excitation effect while a low frequency induces the opposite (Riedel et al., 2019). High-frequency rTMS delivered at 10 Hz significantly improved the cognitive function in AD patients but low-frequency rTMS delivered at 1 Hz did not (Ahmed et al., 2012). For the stimulation target, single-site rTMS on the left dorsal lateral prefrontal cortex (DLPFC) was shown to be potentially effective in patients with AD (Level C of evidence) (Di Lazzaro et al., 2021).

Recently, multisite rTMS combined with cognitive training, also called "rTMS-COG therapy," has been shown to be potentially effective in AD patients at the early stage (Level B of evidence) (Di Lazzaro et al., 2021). Using the NeuroAD system, 6-site (left and right DLPFCs, left and right parietal cortices, Broca's area, and Wernicke's area) rTMS combined with cognitive training improved apathy and cognitive functions, including memory and language, in AD (Lee et al., 2016; Suarez Moreno et al., 2022). However, upon directly comparing a single site (only left DLPFC) and multisite (the same as the aforementioned 6-site approach) rTMS procedure, both approaches performed similarly within a short treatment period (Alcala-Lozano et al., 2018). The discrepancy is presumably due to the use of rTMS alone. Another double-site (right middle frontal gyrus and right inferior parietal lobule) rTMS procedure that did not combine cognitive training failed to validate the multi-target focused rTMS hypothesis in young healthy participants (Feng et al., 2021). A possible explanation would be that coupling multisite stimulation with cognitive training enhances the treatment effect (Nguyen et al., 2018). The combination of multi-target stimulation and cognitive training has shown to be a promising clinical application prospect. However, the neurobiological effects of rTMS-COG therapy need to be further expounded.

Resting-state functional magnetic resonance imaging (rs-fMRI) is an appropriate tool for evaluating the neurobiological effects of neurostimulation. rTMS has been approved for its ability to modulate local activity in a remote area that is functionally connected to cortical stimulation targets (Aceves-Serrano et al., 2022; Qin et al., 2022). However, the causal interactions between the stimulation targets and other brain regions have yet to be explored. To our knowledge, functional connectivity (FC) is defined as the temporal correlation between two remote areas that are computationally efficient but undirected; effective connectivity (EC) further provides direction information about these associations (Deshpande and Hu, 2012). Granger causality analysis (GCA) determines whether the activity in brain region X engages in directed interaction with the activity in region Y, or vice versa (de Graaf et al., 2009). GCA on rs-fMRI data enabled us to investigate EC based on multiple linear regression (Deshpande and Hu, 2012) and determine the positive or negative influences of the stimulation targets on the rest of the brain after rTMS stimulation.

Besides the commonly known dysfunction of the default mode network (DMN) (Greicius et al., 2004), AD is also affected by other large-scale functional brain networks, such as the executive control network (ECN) and frontoparietal network (FPN) (Liu et al., 2012; Zhao et al., 2018). The DLPFC, associated with working memory and attention, is an important node of the ECN and the FPN, and the lateral temporal lobe (LTL) nearest to the hippocampal formation (HF) is an important node of the DMN. In this study, we chose the left DLPFC and left LTL as double-site stimulation targets, combined with six types of cognitive training tasks (Zhang et al., 2019; Qin et al., 2022). The study aimed to investigate the EC changes associated with stimulation targets on the rest of the brain, as well as the causal interactions among resting-state networks (RSNs) after multisite rTMS-COG therapy.

Materials and methods

The study was approved by the Ethics Committee of Tongji Hospital (Wuhan, China; Chinese Clinical Trail Registry Registration number: ChiCTR-INR-16009227). Written informed consent was obtained from all participants before enrollment according to the Declaration of Helsinki.

Participants, study design, and intervention

Patients with AD were recruited in this study based on the National Institute of Neurological Disorders and Stroke-Alzheimer Disease and Related Disorders (NINCDS-ADRDA) criteria (Dubois et al., 2007). None of the participants had any history of head injury, stroke, depression, or tumor. All the patients had taken medicine such as acetylcholinesterase inhibitors (Donepezil) or N-Methyl-D-aspartate receptor antagonists (memantine) for at least 3 months at a stable dosage. In total, 51 participants with mild or moderate AD (clinical dementia rating ≤ 2) were recruited and randomly assigned into a real rTMS with cognitive training ($n = 26$) group or a sham group (only receiving cognitive training, $n = 25$) using a web-based randomization generator (http://www.jerrydallal.com/random/randomize.htm).

Before treatment, all patients underwent neuropsychological assessment and MRI scanning (T0). Then, the real rTMS or sham stimulation was repeated five times from Monday to Friday for

4 weeks. Another MRI scan and neuropsychological assessment were performed on Saturday morning at the end of the 4-week treatment (T4). To evaluate the long-time effect, an MRI scan and neuropsychological assessment were followed up 4 weeks after the end of treatment (T8). All neuropsychological measures before and after the treatment were assessed by a specialist with over 20 years of experience who was blinded to the allotment.

In the real group, rTMS was conducted in combination with cognitive training for up to 1 h each day. A butterfly coil (MCF-B65) with an inner diameter of 35 mm was used for the rTMS treatment, and the treatment was guided by an optical navigation system (Magventure, Germany). High-frequency rTMS pulses were delivered separately to the stimulation target first in the left DLPFC (Talairach coordinates: X = −35, Y = 24, Z = 48) and then in the left LTL (Talairach coordinates: X = −60, Y = −15, Z = −15). The following parameters were used: 20 trains (5 s duration at 10 Hz with an inter-train interval of 25 s), 100% resting motor threshold (RMT), 1,000 pulses, and 10 min in total for each target, and there were no maintenance sessions. The protocol in the sham condition was the same as that in the real condition, except that the coil was positioned with the lateral edge of one wing touching the scalp at 90°(Pascual-Leone et al., 1996). All participants were asked if they had any symptoms of discomfort after the stimulation.

The cognitive training was completed on an iPad tablet (version 9.1; Apple, USA) with several cognitive tasks selected by an experienced cognitive therapist. The memory tasks were completed during rTMS stimulation, while the other tasks, including attention tasks, mathematical calculations, agility drills, language tasks, and logic thinking tasks, were practiced after the stimulation ended (Zhang et al., 2019). Please refer to our previous article for detailed information.

MRI data acquisition

The MRI data were acquired using a 3T scanner (Discovery 750, GE Healthcare) using a 32-channel head coil. To minimize head motion and reduce scanner noise, tight but comfortable foam padding and earplugs were used. During the resting-state fMRI scan, participants were instructed to close their eyes, not fall asleep, and not think of anything in particular. Gradient-echo echo-planar imaging (EPI) sequence was used to acquire fMRI images with the following parameters: repetition time/echo time (TR/TE) = 2000/30 ms, flip angle = 90°, matrix = 64 × 64, field of view = 240, slice thickness = 4 mm, interleaved acquisition, 29 axial slices in total, and 240 timepoints. A sagittal T1-weighted structure image was also acquired using a 3D brain-volume (3D-BRAVO) sequence with the following parameters: TR/TE = 8.2/3.2 ms, TI = 450 ms, slice gap = 1 mm, matrix = 256 × 256, flip angle = 8°, and voxel size = 1 × 1 mm.

MR data preprocessing

The resting-state fMRI data were preprocessed using SPM8 (http://www.fil.ion.ucl.ac.uk/spm/). The first 10 timepoints of the rs-fMRI data were discarded, leaving the remaining 230 timepoints for slice timing and motion correction (threshold: translational or rotational motion parameters lower than 2 mm or 2°). The normalization included the following steps: (1) structural images were linearly coregistered to the mean functional image; (2) the transformed structural images were segmented, and then the gray matter was non-linearly coregistered to the Montreal Neurological Institute (MNI) space; and (3) the motion-corrected functional volumes were normalized to the MNI space using the parameters estimated during the non-linear coregistration. The functional images were resampled into a voxel size of 3 × 3 × 3 mm^3 and then smoothed using a Gaussian kernel of 8 × 8 × 8 mm^3 full width at half-maximum (FWHM). Finally, functional images were band-pass-filtered with a frequency from 0.01 to 0.1 Hz, and several nuisance covariates (24 head motion parameters, averaged signal from white matter, cerebrospinal fluid, and global signal) were regressed out by performing multiple linear regression analysis.

A 6 mm radius sphere centered on stimulation targets, that is, the left DLPFC and the left LTL, was used as the seed region. The coordinates were the same as those used for the rTMS treatment. Bivariate first-order coefficient-based voxel-wise GCA was performed to explore the influence of the stimulation target on the rest of the brain using the REST toolbox (http://www.restfmri.net).

Resting-state fMRI networks were identified by using the Group ICA program of the fMRI toolbox (http://www.nitrc.org/projects/cogicat/). Seven classic networks, including a visual network, a sensorimotor network, a dorsal attention network, a salience/ventral attention network, a limbic network, a control network, and a default mode network (DMN), were used as the networks of interest, which were obtained by a clustering approach across the cerebral cortex using resting-state functional connectivity MRI from 1,000 healthy subjects (Yeo et al., 2011). The generated network components were exported to calculate the inter-network effective connectivity.

Statistics

The normal distribution of the data was determined by performing the Kolmogorov–Smirnov test. The χ^2 test or Fisher's exact test was performed to compare the categorical variables. An independent t-test or the Mann–Whitney test was performed for the quantitative parameters. EC changes at the voxel and network level were analyzed using a flexible factorial design installed in SPM12. We considered a 2 × 3 factorial design with "time" as the within-subjects factor (three levels: T0, T4, and T8) and "group" as the between-subjects factor (two levels: real rTMS + COG and sham rTMS + COG). If the group × time interaction was significant, *post-hoc* analysis was performed to explore the simple effects of time and group with the least significant difference (LSD) correction. All behavioral measures were analyzed using the IBM Statistical Package for the Social Sciences (SPSS) version 25, and graphs were made in GraphPad Prism 8. The relationship between EC changes and behavioral changes before and after the intervention was explored by performing a partial correlation analysis. Sex, age, education level, CDR, and disease duration were set as covariates in all tests.

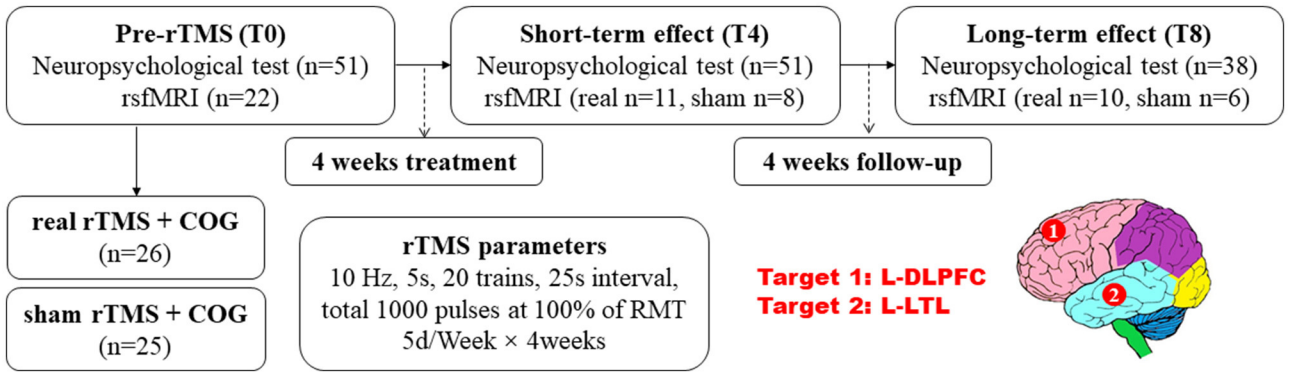

FIGURE 1
Experiment design: the evaluation of neuropsychological test scores and resting-state functional MRI before and after rTMS application, as well as the rTMS parameters and targets. rTMS, repetitive transcranial magnetic stimulation; COG, cognitive training; DLPFC, dorsal lateral prefrontal cortex, and LTL, lateral temporal lobe; L, left.

Results

All the 51 patients enrolled received pre- and post-neuropsychological tests, with 26 allocated to the real rTMS + COG group and 25 to the sham rTMS + COG group, in which only 22 of them underwent pre-treatment MRI scan because the family members of the others refused. At the end of 4 weeks' treatment (T4), three patients in real group missed the MRI scan, with 11 patients in real group and 8 patients in sham group. At timepoint T8, one patient in real group refused to be scanned again. Two patients in sham group missed the scan time because of damage to the MRI instrument on the day of the scheduled. Figure 1 shows the flow diagram of this study and the detailed rTMS parameters.

Before treatment, there were no significant differences in sex, age, education level, course of the disease, and clinical dementia rating (CDR) between the real and sham groups ($p > 0.05$). Table 1 shows the detailed demographic characteristics. As for the alteration of neuropsychological scores, the MMSE score increment at T4 in the real group significantly differed from that of the sham group ($p = 0.04$). The activities of daily living (ADL) score decrease in the real group significantly differed from that in the sham group at T4 ($p = 0.01$) and T8 ($p = 0.02$). As for the Montreal Cognitive Assessment (MoCA), Alzheimer's Disease Assessment Scale-Cognitive Subscale (ADAS-cog), and the auditory verbal learning test (AVLT) changes, there were no significant differences between the real and sham groups at either T4 or T8 ($p > 0.05$).

TABLE 1 Demographic characteristics of the real and sham groups.

		real rTMS + COG	sham rTMS + COG	t/Z/χ^2	P
Sex (male/female, *n*)		2/9	3/5	0.26	0.61
Age (yrs.)		67.36 ± 6.98	66.25 ± 8.07	0.32	0.75
Education (yrs.)		12.27 ± 1.79	11.50 ± 2.83	0.73	0.48
Course of disease (yrs.)		3.64 ± 1.96	3.63 ± 1.51	0.01	0.99
CDR (0.5/1/2)		3/4/4	0/5/3	2.85	0.24
MMSE	T4-T0	3.00 ± 1.55	1.38 ± 1.51	−2.06	**0.04**
	T8-T0	2.40 ± 1.58	1.50 ± 3.02	−1.16	0.25
MoCA	T4-T0	2.64 ± 2.58	2.13 ± 2.36	−0.17	0.87
	T8-T0	2.40 ± 2.27	2.00 ± 3.85	−0.55	0.59
ADAS-cog	T4-T0	−3.79 ± 3.50	−0.96 ± 2.59	−1.78	0.08
	T8-T0	−4.13 ± 2.26	−1.80 ± 4.14	−1.12	0.26
AVLT	T4-T0	4.13 ± 3.80	1.45 ± 4.63	−0.71	0.48
	T8-T0	8.75 ± 11.30	−2.86 ± 8.57	−1.70	0.09
ADL	T4-T0	−2.73 ± 1.62	−0.88 ± 0.83	−2.59	**0.01**
	T8-T0	−2.89 ± 2.20	1.00 ± 2.76	−2.26	**0.02**

rTMS, repetitive transcranial magnetic stimulation; COG, cognitive training; CDR, Clinical Dementia Rating; MMSE, Mini-Mental State Examination; MoCA, Montreal Cognitive Assessment; ADAS-cog, Alzheimer's Disease Assessment Scale-Cognitive Subscale; AVLT, auditory verbal learning test–HuaShan version; ADL, activities of daily living.

EC changes at the voxel level

In general, the left DLPFC seed from the GCA analysis showed significant causal outflow to five clusters ($p < 0.05$, FWE corrected), that is, the left inferior parietal lobe (IPL), the left superior frontal gyrus (SFG), the left postcentral gyrus (PoCG), the left thalamus, and the right parahippocampus (Figure 2A). However, the reverse influence after rTMS-COG treatment was not significant ($p > 0.05$).

Specifically, a significant group × time interaction effect ($F = 14.057$, $p = 0.000$) was observed for EC changes from the left DLPFC to the left IPL. *Post-hoc* analysis indicated that, compared with the baseline, high-frequency rTMS + COG produced a significant reduction in EC at timepoints T4 ($p = 0.010$) and T8 ($p = 0.001$), while sham rTMS + COG produced a significant increase in EC at timepoint T8 ($p = 0.024$) (Figure 2B, line chart). The EC changes differed significantly between the real and sham groups at T8 ($p = 0.001$) but not at T4 ($p = 0.115$) (Figure 2B, bar chart).

In terms of EC changes from the left DLPFC to the left SFG, a significant time × group effect was also identified (F = 10.766, $p = 0.001$). Compared with the baseline, high-frequency rTMS + COG produced a significant reduction in EC at timepoints T4 ($p = 0.000$) and T8 ($p = 0.000$) (Figure 2C, line chart). The EC changes differed significantly between the real and sham groups at both T4 ($p = 0.003$) and T8 ($p = 0.002$) (Figure 2C, bar chart).

For EC changes from the left DLPFC to the left PoCG, only the time main effect was significant (F = 4.053, $p = 0.035$). High-frequency rTMS + COG produced a significant reduction in EC at timepoint T8 ($p = 0.013$) but not at timepoint T4 ($p = 0.164$) (Figure 2D, line chart). The EC changes differed significantly between the real and sham groups at T8 ($p = 0.013$) but not at T4 ($p = 0.285$) (Figure 2D, bar chart).

The EC changes from the left DLPFC to the left thalamus also showed a significant time main effect (F = 3.579, $p = 0.049$). The real rTMS + COG produced a significant reduction in EC at timepoints T4 ($p = 0.001$) and T8 ($p = 0.024$) (Figure 2E, line chart). The EC changes differed significantly between the real and sham groups at both T4 ($p = 0.046$) and T8 ($p = 0.025$) (Figure 2E, bar chart).

The EC changes from the left DLPFC to the right parahippocampus also showed a time main effect (F = 5.704, $p = 0.012$). Compared with the baseline, the high-frequency rTMS + COG produced a significant reduction in EC at timepoints T4 ($p = 0.017$) and T8 ($p = 0.047$), while the results of the sham group were not significant at either T4 or T8 (Figure 2F, line chart). The EC changes between the real and sham groups also showed no difference at either T4 ($p = 0.247$) or T8 ($p = 0.140$) (Figure 2F, bar chart).

The left LTL seed from the GCA analysis revealed two clusters with significant causal outflow ($p < 0.05$, FWE corrected), that is, the left orbital frontal cortex (OFC) and the right superior temporal gyrus (STG) (Figure 3A), with no significant reverse influence ($p > 0.05$). The EC changes from the left LTL out to the left OFC showed significant time × group interaction (F = 4.198, $p = 0.032$). Compared with the baseline, the high-frequency rTMS + COG produced a significant reduction in EC at timepoints T4 ($p = 0.030$) and T8 ($p = 0.037$). The sham group showed no significant difference at T4 ($p = 0.072$), but it produced a significant increase in EC at T8 ($p = 0.024$) (Figure 3B, line chart). The EC changes between the real and sham groups differed significantly at T8 ($p = 0.008$) but not at T4 ($p = 0.491$) (Figure 3B, bar chart).

In terms of the EC changes from the left LTL to the right STG, the time main effect was significant (F = 7.442, $p = 0.016$). The real rTMS + COG produced a significant reduction in EC at timepoint T4 ($p = 0.004$), but it showed no significant changes at T8 ($p = 0.232$). The sham group showed no significant changes at either T4 ($p = 0.155$) or T8 ($p = 0.159$) (Figure 3C, line chart). The EC changes between the real and sham groups showed no significant difference at either T4 ($p = 0.138$) or T8 ($p = 0.121$) (Figure 3C, line chart). Table 2 summarizes the voxel-level results of EC changes for directional influence to and from the left DLPFC and left LTL seeds.

EC changes at the network level

For pairwise EC changes of the seven networks, a significant time × group interaction was only observed from the limbic network out to the default mode network (DMN) (F = 7.070, $p = 0.005$, Figure 4A). Compared with the baseline, the high-frequency rTMS + COG induced no significant EC changes at T4 ($p = 0.231$), but it produced a significant increase at T8 ($p = 0.034$). The sham group showed no significant EC changes at T4 ($p = 0.381$), but it showed a significant decrease at T8 ($p = 0.014$) (Figure 4B). The EC changes between the real and sham groups showed significant differences at T8 ($p = 0.005$) but not at T4 ($p = 0.255$) (Figure 4C).

Partial correlation analysis

For voxel-level EC changes, partial correlation analysis showed that the EC changes from the left DLPFC out to the left IPL, left SFG, left PoCG, left thalamus, and right parahippocampus were all positively correlated with ADL changes at T4 or T8 ($P < 0.05$), indicating that the reduction in EC induced by the real rTMS intervention improved the ability to perform activities of daily living. In particular, the decrease in EC from the left DLPFC out to the right parahippocampus was associated with a decrease in ADAS-cog score 4 weeks after the end of the treatment (T8), indicating that the reduction in EC from the left DLPFC out to the right parahippocampus was associated with improved cognitive function in patients with mild to moderate AD in the long term. For the network-level EC changes, the increase in EC from the limbic network out to the DMN at T8 was correlated with an increase in MoCA score after rTMS-COG treatment. Table 3 shows the partial correlation analysis results.

Discussion

Using the left DLPFC and the left LTL as the stimulation targets, we explored the EC alterations after multisite rTMS-COG therapy and obtained three main results: first, at the voxel level, EC changes from the left DLPFC out to the left IPL and left SFG, as well as from the left LTL out to the left OFC had a significant group × time interaction effect. Second, at the network level, a significant interaction was identified on the EC increment from the limbic network out to the DMN. Third, the decrease in EC at the voxel level and the increase in EC at the network level were associated with improved ability to perform activities of daily living and cognition.

rTMS-COG therapy-induced effective connectivity decrease from stimulation targets out to several brain regions at the voxel level

In our study, rTMS-COG therapy induced a decrease in EC from the left DLPFC out to the left IPL and from the left LTL out to the left OFC, while cognitive training alone (sham condition) induced a significant increase in EC in the long term (T8). rTMS stimulation on the left DLPFC has been observed to have definite benefits for patients with mild AD (Di Lazzaro et al., 2021). As an important node of the ECN and the FPN (Vincent et al., 2008), the left DLPFC has been mostly used and has

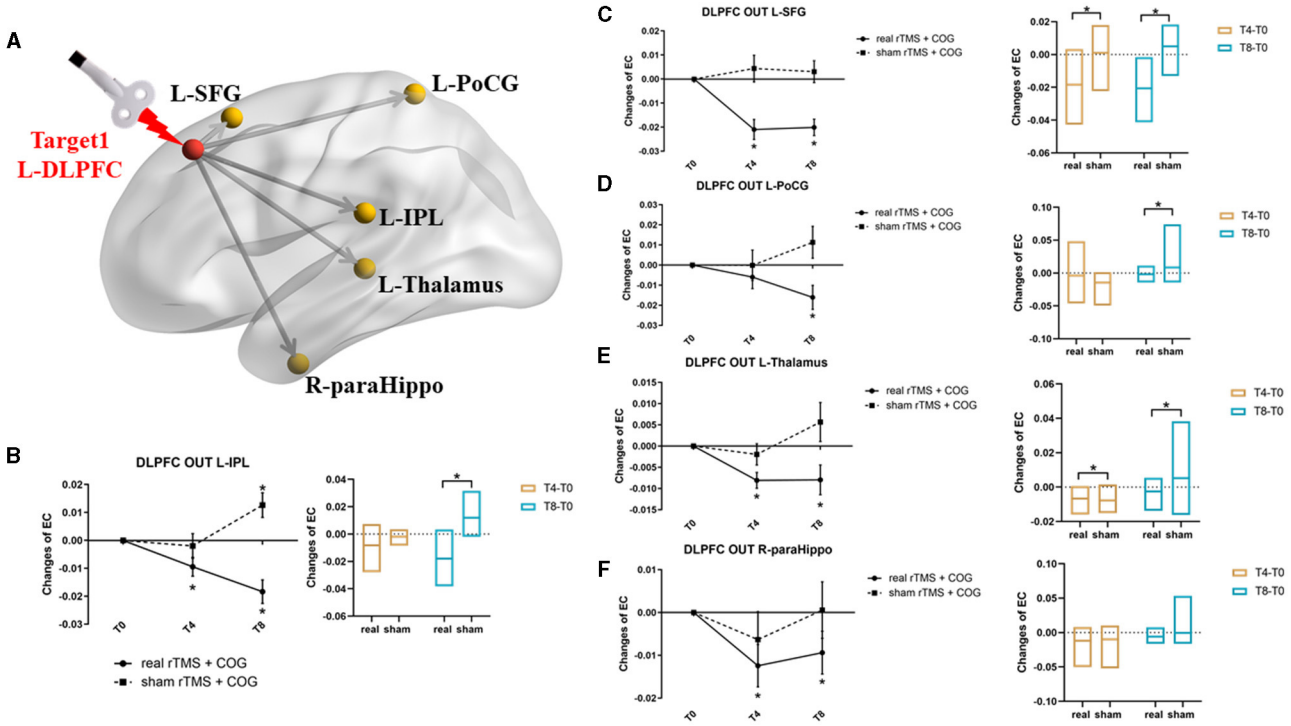

FIGURE 2
Results of EC changes from the left DLPFC out to the rest of whole brain at voxel level. **(A)** The pattern diagram showing the stimulation site (left DLPFC) and the five brain regions with significant EC changes. **(B–F)** Line and bar charts showing the *post-hoc* analysis results from left DLPFC out to left IPL **(B)**, left SFG **(C)**, left PoCG **(D)**, left thalamus **(E)**, and right parahippocampus **(F)**. *Indicates $p < 0.05$, FWE corrected. L, left; R, right; DLPFC, dorsal lateral prefrontal cortex; IPL, inferior parietal lobe; SFG, superior frontal gyrus; PoCG, postcentral gyrus; paraHippo, parahippocampus, EC, effective connectivity.

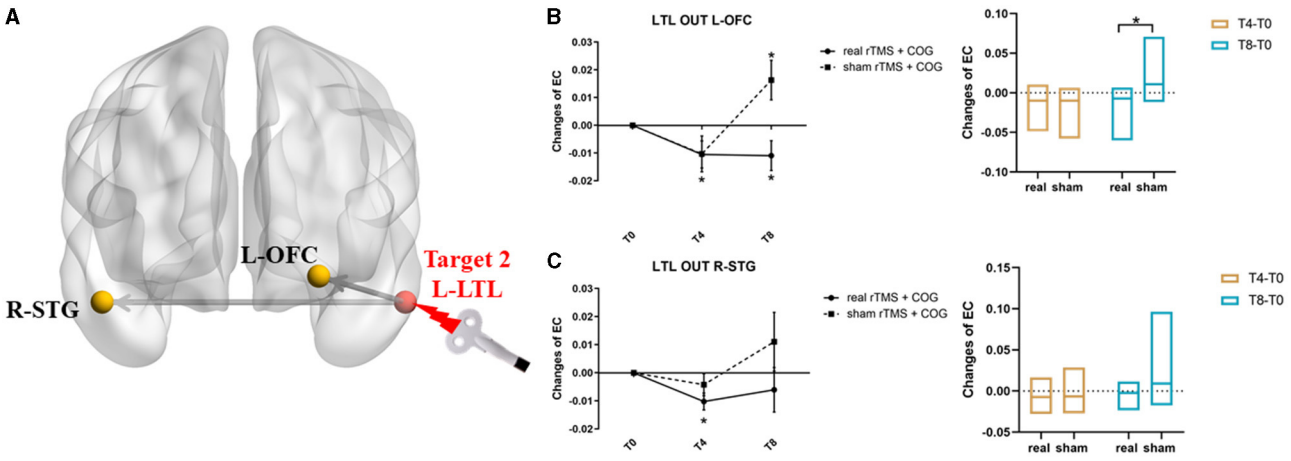

FIGURE 3
Results of EC changes from the left LTL out to the rest of whole brain at voxel level. **(A)** The pattern diagram showing the stimulation site (left LTL) and the two brain regions with significant EC changes. **(B, C)** Line and bar charts showing the *post-hoc* analysis results from left LTL out to left lOFC **(B)** and right STG **(C)**. *Indicates $p < 0.05$, FWE corrected. L, left; R, right; LTL, lateral temporal lobe; OFC, orbital frontal cortex; STG, superior temporal gyrus; EC, effective connectivity.

been proven to be a beneficial stimulation target for AD (Cotelli et al., 2008, 2011; Ahmed et al., 2012). The IPL related to bottom-up attention and episodic memory is an important node of the ECN (Xiao et al., 2022). Information flow from the IPL to the anterior DMN subsystem has been reported, along with extensive connections between the parietal cortex and the frontal cortex (the parieto-frontal circuit) (Buckner et al., 2009; Luo et al., 2019). Our study found a significant decrease in EC from the left DLPFC to the ipsilateral IPL, associated with improved ADL score both in the short and long term (T4 and T8). This is also in line with previous observations that the TMS of the left DLPFC could selectively modulate functional connectivity both within and between the

TABLE 2 2 × 3 flexible factorial design results of effective connectivity changes.

	Cluster size	Peak MNI coordinate		Peak intensity	
DLPFC → L-IPL (group × time)	10	−60	−30	21	22.4392
DLPFC → L-SFG (group × time)	12	−24	18	57	25.8903
DLPFC → L-PoCG (time main effect)	5	−21	−48	6	21.094
DLPFC → L-Thalamus (time main effect)	6	−9	−30	0	27.6886
DLPFC → R-parahippocampus (time main effect)	14	24	−6	−36	30.9024
LTL → L-OFC (group × time)	40	−27	60	−12	33.3441
LTL → R-STG (time main effect)	38	48	12	−21	58.5413

L, left; R, right; DLPFC, dorsal lateral prefrontal cortex; IPL, inferior parietal lobe; SFG, superior frontal gyrus; PoCG, postcentral gyrus; LTL, lateral temporal lobe; OFC, orbital frontal cortex; STG, superior temporal gyrus.

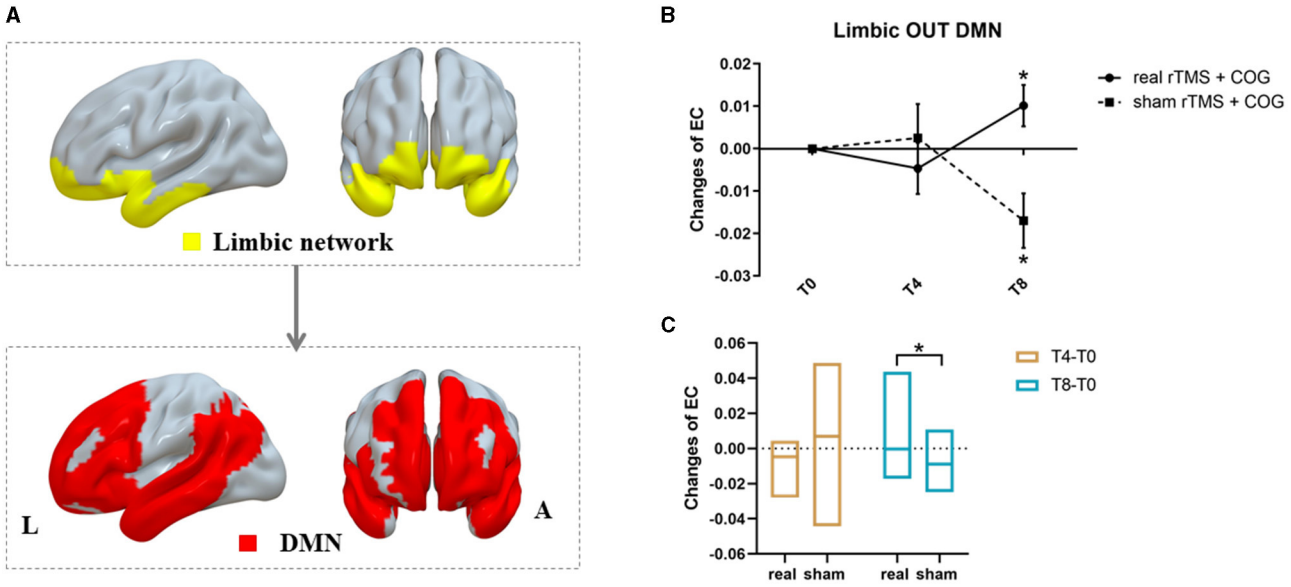

FIGURE 4
Results of inter-network EC changes among seven classic resting-state networks. **(A)** The pattern diagram showing significant pairwise EC changes from limbic network out to DMN. **(B, C)** Line and bar charts showing the *post-hoc* analysis results. *Indicates $p < 0.05$, FWE corrected. L, left; R, right; DMN, default mode network.

ECN and DMN in patients with depression (Liston et al., 2014). rTMS over DLPFC modulated the coupling between the ECN and the DMN in healthy people and in heroin-dependent individuals (van der Werf, 2010; Chen et al., 2013; Jin et al., 2022). Stimulation of the left LTL with transcranial direct current stimulation (tDCS) improved recognition memory in AD patients (Ferrucci et al., 2008). Similarly, in our study, a decrease in EC from the left LTL out to the ipsilateral OFC improved episodic memory in the short term (T4) and the ability to perform activities of daily living in the long term (T8).

For EC changes from the left DLPFC out to the left SFG, rTMS-COG therapy induced a significant decrease in EC in both the short and long terms, with no significant changes for cognitive training (sham condition). Causal interactions between the frontoparietal central executive and the DMN were well identified in a TMS/fMRI study (Chen et al., 2013). Since the FPN covers several frontoparietal areas, including the SFG (Vincent et al., 2008), our study showed that rTMS targeted on the left DLPFC also induces information flow within the FPN, resulting in benefits for ADL in both the short and long terms.

rTMS-COG therapy-induced EC increase at the network level

rTMS is effective for increasing and decreasing (low-frequency: decrease, high-frequency: increase) functional coherence within the prefrontal-limbic network (Riedel et al., 2019). rTMS reportedly induces hypoconnectivity within the DMN in patients with amnestic mild cognitive impairment (aMCI)(Cui et al., 2019). However, the inter-network causal effect after multisite rTMS-COG treatment has yet to be expounded. In our study, compared with the cognitive training group (the sham condition), high-frequency rTMS-COG treatment induced a significant increase in EC from the limbic network out to the DMN at the 4-week follow-up after treatment (T8), indicating that multisite TMS-COG therapy had a long-term effect at the network level. Furthermore,

TABLE 3 Partial correlation analysis of effective connectivity changes and neuropsychological score changes.

EC changes	Neuropsychological score changes		PCC	*p*
DLPFC → L-IPL	ADL	T4-T0	0.725	0.027
	ADL	T8-T0	0.916	0.004
DLPFC → L-SFG	ADL	T4-T0	0.687	0.041
	ADL	T8-T0	0.939	0.002
DLPFC → L-PoCG	ADL	T8-T0	0.940	0.002
DLPFC → L-Thalamus	ADL	T4-T0	0.858	0.003
	ADL	T8-T0	0.971	0.000
DLPFC → R-parahippocampus	ADAS-cog	T8-T0	0.822	0.023
	ADL	T8-T0	0.762	0.047
LTL → L-OFC	AVLT	T4-T0	−0.712	0.032
	ADL	T8-T0	0.817	0.025
LTL → R-STG	ADL	T8-T0	0.871	0.011
Limbic network → DMN	MOCA	T8-T0	0.770	0.043

EC, effective connectivity; PCC, partial correlation coefficient; L, left; R, right; DLPFC, dorsal lateral prefrontal cortex; IPL, inferior parietal lobe; SFG, superior frontal gyrus; PoCG, postcentral gyrus; LTL, lateral temporal lobe; OFC, orbital frontal cortex; STG, superior temporal gyrus; ADL, activities of daily living; ADAS-cog, Alzheimer's Disease Assessment Scale-Cognitive Subscale; AVLT, auditory verbal learning test–HuaShan version; MoCA, Montreal Cognitive Assessment.

the inter-network increase in EC was associated with cognition improvement (MoCA score increase).

It is particularly noteworthy that, although the cognitive training tasks were the same in the real rTMS and sham groups in our study, we could not ascribe the improvement in clinical outcomes in the real group to rTMS itself. It has been reported that TMS may have a synergistic effect with cognitive training (Rabey et al., 2013). Interlaced with cognitive training, rTMS has additional beneficial effects (Bentwich et al., 2011). Our results may aid the understanding of the neurobiological effects of rTMS-COG therapy on a macro-scale.

Limitations

Our study has several limitations. First, due to the longitudinal design, the sample size and statistical efficiency were limited. Therefore, we cannot rule out the possibility that some of the changes we observed after rTMS-COG were not causally related to the treatment. Second, AD patients were recruited based on the NINCDS-ADRDA criteria instead of the amyloid/tau/neurodegenaration (ATN) diagnostic framework. These criteria were chosen because the cerebral spinal fluid (CSF) biomarker and molecular neuroimaging with positron emission tomography (PET) are usually unavailable in clinical practice due to their "invasive" characteristics. The heterogeneity across participants may have influenced the results, so our findings could be considered exploratory. When interpreting the findings of the present study, a great deal of caution is needed. A multi-center cohort study is needed to validate our pilot study.

Conclusions

In summary, at the voxel level, multisite rTMS-COG therapy changed the EC from the stimulation targets out to several brain regions, covering important networks, especially the DMN, ECN, and FPC. At the network level, rTMS-COG increased the EC from the DMN out to the limbic network. All the alterations were accompanied by better outcomes related to the ability to perform activities of daily living and cognition function in the short or long terms or both. This study provides a novel explanation for the neurobiological mechanisms of multisite rTMS-COG therapy in AD patients and further sheds light on the direction of targeted brain network modulation in the future.

Data availability statement

The raw data supporting the conclusions of this article will be made available by the authors, without undue reservation.

Ethics statement

The study was approved by the Ethics Committee of Tongji Hospital (Wuhan, China). Written informed consent of all participants were obtained according to the declaration of Helsinki before enrollment. The patients/participants provided their written informed consent to participate in this study.

Author contributions

YQ: conceptualization and writing. LB: data curation. FZ: visualization and investigation. SJ: software. TT: methodology, statistics, and software. MZ: supervision and validation. WZ: writing, reviewing, and editing. All authors contributed to the article and approved the submitted version.

Funding

This study was supported by the National Key Research and Development Project (No. 2018YFE0118900)

and the National Natural Science Foundation of China (No. 81873890).

Conflict of interest

The authors declare that the research was conducted in the absence of any commercial or financial relationships that could be construed as a potential conflict of interest.

Publisher's note

References

Aceves-Serrano, L., Neva, J. L., and Doudet, D. J. (2022). Insight into the effects of clinical repetitive transcranial magnetic stimulation on the brain from positron emission tomography and magnetic resonance imaging studies: a narrative review. *Front. Neurosci.* 16, 787403. doi: 10.3389/fnins.2022.787403

Ahmed, M. A., Darwish, E. S., Khedr, E. M., El Serogy, Y. M., and Ali, A. M. (2012). Effects of low versus high frequencies of repetitive transcranial magnetic stimulation on cognitive function and cortical excitability in Alzheimer's dementia. *J. Neurol.* 259, 83–92. doi: 10.1007/s00415-011-6128-4

Alcala-Lozano, R., Morelos-Santana, E., Cortes-Sotres, J. F., Garza-Villarreal, E. A., Sosa-Ortiz, A. L., and Gonzalez-Olvera, J. J. (2018). Similar clinical improvement and maintenance after rTMS at 5 Hz using a simple vs. complex protocol in Alzheimer's disease. *Brain Stimul.* 11, 625–627. doi: 10.1016/j.brs.2017.12.011

Bentwich, J., Dobronevsky, E., Aichenbaum, S., Shorer, R., Peretz, R., Khaigrekht, M., et al. (2011). Beneficial effect of repetitive transcranial magnetic stimulation combined with cognitive training for the treatment of Alzheimer's disease: a proof of concept study. *J. Neural Transm. (Vienna).* 118, 463–471. doi: 10.1007/s00702-010-0578-1

Buckner, R. L., Sepulcre, J., Talukdar, T., Krienen, F. M., Liu, H., Hedden, T., et al. (2009). Cortical hubs revealed by intrinsic functional connectivity: mapping, assessment of stability, and relation to Alzheimer's disease. *J. Neurosci.* 29, 1860–1873. doi: 10.1523/JNEUROSCI.5062-08.2009

Chen, A. C., Oathes, D. J., Chang, C., Bradley, T., Zhou, Z. W., Williams, L. M., et al. (2013). Causal interactions between fronto-parietal central executive and default-mode networks in humans. *Proc. Natl. Acad. Sci. U S A.* 110, 19944–19949. doi: 10.1073/pnas.1311772110

Cotelli, M., Calabria, M., Manenti, R., Rosini, S., Zanetti, O., Cappa, S. F., et al. (2011). Improved language performance in Alzheimer disease following brain stimulation. *J. Neurol. Neurosurg. Psychiatr.* 82, 794–797. doi: 10.1136/jnnp.2009.197848

Cotelli, M., Manenti, R., Cappa, S. F., Zanetti, O., and Miniussi, C. (2008). Transcranial magnetic stimulation improves naming in Alzheimer disease patients at different stages of cognitive decline. *Eur. J. Neurol.* 15, 1286–1292. doi: 10.1111/j.1468-1331.2008.02202.x

Cui, H., Ren, R., Lin, G., Zou, Y., Jiang, L., Wei, Z., et al. (2019). Repetitive transcranial magnetic stimulation induced hypoconnectivity within the default mode network yields cognitive improvements in amnestic mild cognitive impairment: a randomized controlled study. *J. Alzheimers Dis.* 69, 1137–1151. doi: 10.3233/JAD-181296

de Graaf, T. A., Jacobs, C., Roebroeck, A., and Sack, A. T. (2009). FMRI effective connectivity and TMS chronometry: complementary accounts of causality in the visuospatial judgment network. *PLoS One.* 4, e8307. doi: 10.1371/journal.pone.0008307

Deshpande, G., and Hu, X. (2012). Investigating effective brain connectivity from fMRI data: past findings and current issues with reference to Granger causality analysis. *Brain Connect.* 2, 235–245. doi: 10.1089/brain.2012.0091

Di Lazzaro, V., Bella, R., Benussi, A., Bologna, M., Borroni, B., Capone, F., et al. (2021). Diagnostic contribution and therapeutic perspectives of transcranial magnetic stimulation in dementia. *Clin. Neurophysiol.* 132, 2568–2607. doi: 10.1016/j.clinph.2021.05.035

Dubois, B., Feldman, H. H., Jacova, C., Dekosky, S. T., Barberger-Gateau, P., Cummings, J., et al. (2007). Research criteria for the diagnosis of Alzheimer's disease: revising the NINCDS-ADRDA criteria. *Lancet Neurol.* 6, 734–746. doi: 10.1016/S1474-4422(07)70178-3

Feng, Z. J., Deng, X. P., Zhao, N., Jin, J., Yue, J., Hu, Y. S., et al. (2021). Resting-State fMRI functional connectivity strength predicts local activity change in the dorsal cingulate cortex: a multi-target focused rTMS study. *Cereb Cortex.* 10, 380. doi: 10.1093/cercor/bhab380

Ferrucci, R., Mameli, F., Guidi, I., Mrakic-Sposta, S., Vergari, M., Marceglia, S., et al. (2008). Transcranial direct current stimulation improves recognition memory in Alzheimer disease. *Neurology.* 71, 493–498. doi: 10.1212/01.wnl.0000317060.43722.a3

Gomez-Ramirez, J., and Wu, J. (2014). Network-based biomarkers in Alzheimer's disease: review and future directions. *Front. Aging Neurosci.* 6, 12. doi: 10.3389/fnagi.2014.00012

Greicius, M. D., Srivastava, G., Reiss, A. L., and Menon, V. (2004). Default-mode network activity distinguishes Alzheimer's disease from healthy aging: evidence from functional MRI. *Proc. Natl. Acad. Sci. U SA.* 101, 4637–4642. doi: 10.1073/pnas.0308627101

Huang, Y. Z., Lu, M. K., Antal, A., Classen, J., Nitsche, M., Ziemann, U., et al. (2017). Plasticity induced by non-invasive transcranial brain stimulation: a position paper. *Clin Neurophysiol.* 128, 2318–2329. doi: 10.1016/j.clinph.2017.09.007

Jin, L., Yuan, M., Zhang, W., Su, H., Wang, F., Zhu, J., et al. (2022). Repetitive transcranial magnetic stimulation modulates coupling among large-scale brain networks in heroin-dependent individuals: A randomized resting-state functional magnetic resonance imaging study. *Addict Biol.* 27(2):e13121. doi: 10.1111/adb.13121

Lee, J., Choi, B. H., Oh, E., Sohn, E. H., and Lee, A. Y. (2016). Treatment of Alzheimer's disease with repetitive transcranial magnetic stimulation combined with cognitive training: a prospective, randomized, double-blind, placebo-controlled study. *J. Clin. Neurol.* 12, 57–64. doi: 10.3988/jcn.2016.12.1.57

Liston, C., Chen, A. C., Zebley, B. D., Drysdale, A. T., Gordon, R., Leuchter, B., et al. (2014). Default mode network mechanisms of transcranial magnetic stimulation in depression. *Biol Psychiatry.* 76, 517–526. doi: 10.1016/j.biopsych.2014.01.023

Liu, Z., Zhang, Y., Bai, L., Yan, H., Dai, R., Zhong, C., et al. (2012). Investigation of the effective connectivity of resting state networks in Alzheimer's disease: a functional MRI study combining independent components analysis and multivariate Granger causality analysis. *NMR Biomed.* 25, 1311–1320. doi: 10.1002/nbm.2803

Luo, X., Li, K., Jia, Y. L., Zeng, Q., Jiaerken, Y., Qiu, T., et al. (2019). Altered effective connectivity anchored in the posterior cingulate cortex and the medial prefrontal cortex in cognitively intact elderly APOE epsilon4 carriers: a preliminary study. *Brain Imaging Behav.* 13, 270–282. doi: 10.1007/s11682-018-9857-5

Nguyen, J. P., Suarez, A., Le Saout, E., Meignier, M., Nizard, J., and Lefaucheur, J. P. (2018). Combining cognitive training and multi-site rTMS to improve cognitive functions in Alzheimer's disease. *Brain Stimul.* 11, 651–652. doi: 10.1016/j.brs.2018.02.013

Pascual-Leone, A., Rubio, B., Pallardo, F., and Catala, M. D. (1996). Rapid-rate transcranial magnetic stimulation of left dorsolateral prefrontal cortex in drug-resistant depression. *Lancet.* 348, 233–237. doi: 10.1016/S0140-6736(96)01219-6

Qin, Y., Zhang, F., Zhang, M., and Zhu, W. (2022). Effects of repetitive transcranial magnetic stimulation combined with cognitive training on resting-state brain activity in Alzheimer's disease. *Neuroradiol J.* 35, 566–572. doi: 10.1177/19714009211067409

Rabey, J. M., Dobronevsky, E., Aichenbaum, S., Gonen, O., Marton, R. G., and Khaigrekht, M. (2013). Repetitive transcranial magnetic stimulation combined with cognitive training is a safe and effective modality for the treatment of Alzheimer's disease: a randomized, double-blind study. *J. Neura.l Transm (Vienna).* 120, 813–819. doi: 10.1007/s00702-012-0902-z

Riedel, P., Heil, M., Bender, S., Dippel, G., Korb, F. M., Smolka, M. N., et al. (2019). Modulating functional connectivity between medial frontopolar cortex and amygdala by inhibitory and excitatory transcranial magnetic stimulation. *Hum. Brain Mapp.* 40, 4301–4315. doi: 10.1002/hbm.24703

Suarez Moreno, A., Nguyen, J. P., Calmelet, A., Le Saout, E., Damier, P., de Decker, L., et al. (2022). Multi-site rTMS with cognitive training improves apathy in the long term in Alzheimer's disease: A 4-year chart review. *Clin. Neurophysiol.* 137, 75–83. doi: 10.1016/j.clinph.2022.02.017

van der Werf, YD, Sanz-Arigita, EJ, Menning, S, and van den Heuvel, OA. (2010). Modulating spontaneous brain activity using repetitive transcranial magnetic stimulation. *BMC Neurosci*. 11, 145. doi: 10.1186/1471-2202-11-145

Vincent, J. L., Kahn, I., Snyder, A. Z., Raichle, M. E., and Buckner, R. L. (2008). Evidence for a frontoparietal control system revealed by intrinsic functional connectivity. *J. Neurophysiol*. 100, 3328–3342. doi: 10.1152/jn.90355.2008

Xiao, G., Wu, Y., Yan, Y., Gao, L., Geng, Z., Qiu, B., et al. (2022). Optimized magnetic stimulation induced hypoconnectivity within the executive control network yields cognition improvements in Alzheimer's patients. *Front. Aging Neurosci*. 14, 847223. doi: 10.3389/fnagi.2022.847223

Yeo, B. T., Krienen, F. M., Sepulcre, J., Sabuncu, M. R., Lashkari, D., Hollinshead, M., et al. (2011). The organization of the human cerebral cortex estimated by intrinsic functional connectivity. *J. Neurophysiol*. 106, 1125–1165. doi: 10.1152/jn.00338.2011

Zhang, F., Qin, Y., Xie, L., Zheng, C., Huang, X., and Zhang, M. (2019). High-frequency repetitive transcranial magnetic stimulation combined with cognitive training improves cognitive function and cortical metabolic ratios in Alzheimer's disease. *J. Neural Transm (Vienna)*. 126, 1081–1094. doi: 10.1007/s00702-019-02022-y

Zhao, Q., Lu, H., Metmer, H., Li, W. X. Y., and Lu, J. (2018). Evaluating functional connectivity of executive control network and frontoparietal network in Alzheimer's disease. *Brain Res*. 1678, 262–272. doi: 10.1016/j.brainres.2017.10.025

frontiers | Frontiers in Neural Circuits

TYPE Brief Research Report
PUBLISHED 06 September 2023
DOI 10.3389/fncir.2023.1214959

OPEN ACCESS

EDITED BY
Rachel M. Sherrard,
Sorbonne-Université, France

REVIEWED BY
Jennifer Rodger,
University of Western Australia, Australia
Abhishek Datta,
Soterix Medical Inc., United States

*CORRESPONDENCE
Kevin A. Caulfield
✉ caulfiel@musc.edu

RECEIVED 30 April 2023
ACCEPTED 09 August 2023
PUBLISHED 06 September 2023

CITATION
Cho JY, Van Hoornweder S, Sege CT, Antonucci MU, McTeague LM and Caulfield KA (2023) Template MRI scans reliably approximate individual and group-level tES and TMS electric fields induced in motor and prefrontal circuits.
Front. Neural Circuits 17:1214959.
doi: 10.3389/fncir.2023.1214959

Template MRI scans reliably approximate individual and group-level tES and TMS electric fields induced in motor and prefrontal circuits

Jennifer Y. Cho[1], Sybren Van Hoornweder[2], Christopher T. Sege[3], Michael U. Antonucci[4], Lisa M. McTeague[3,5] and Kevin A. Caulfield[1,3]*

[1]Department of Neuroscience, Medical University of South Carolina, Charleston, SC, United States, [2]Faculty of Rehabilitation Sciences, REVAL–Rehabilitation Research Center, Hasselt University, Diepenbeek, Belgium, [3]Department of Psychiatry, Medical University of South Carolina, Charleston, SC, United States, [4]Department of Radiology and Radiological Science, Medical University of South Carolina, Charleston, SC, United States, [5]Ralph H. Johnson VA Medical Center, Charleston, SC, United States

Background: Electric field (E-field) modeling is a valuable method of elucidating the cortical target engagement from transcranial magnetic stimulation (TMS) and transcranial electrical stimulation (tES), but it is typically dependent on individual MRI scans. In this study, we systematically tested whether E-field models in template MNI-152 and Ernie scans can reliably approximate group-level E-fields induced in N = 195 individuals across 5 diagnoses (healthy, alcohol use disorder, tobacco use disorder, anxiety, depression).

Methods: We computed 788 E-field models using the CHARM–SimNIBS 4.0.0 pipeline with 4 E-field models per participant (motor and prefrontal targets for TMS and tES). We additionally calculated permutation analyses to determine the point of stability of E-fields to assess whether the 152 brains represented in the MNI-152 template is sufficient.

Results: Group-level E-fields did not significantly differ between the individual vs. MNI-152 template and Ernie scans for any stimulation modality or location ($p > 0.05$). However, TMS-induced E-field magnitudes significantly varied by diagnosis; individuals with generalized anxiety had significantly higher prefrontal and motor E-field magnitudes than healthy controls and those with alcohol use disorder and depression ($p < 0.001$). The point of stability for group-level E-field magnitudes ranged from 42 (motor tES) to 52 participants (prefrontal TMS).

Conclusion: MNI-152 and Ernie models reliably estimate group-average TMS and tES-induced E-fields transdiagnostically. The MNI-152 template includes sufficient scans to control for interindividual anatomical differences (i.e., above the point of stability). Taken together, using the MNI-152 and Ernie brains to approximate group-level E-fields is a valid and reliable approach.

KEYWORDS

TMS, tES, tDCS, non-invasive brain stimulation, electric field (E-field) modeling, finite element method (FEM), MNI-152, template MRI scan

Introduction

Transcranial magnetic stimulation (TMS) and transcranial electrical stimulation (tES) are two methods of non-invasively stimulating the human brain (Barker et al., 1985; Nitsche and Paulus, 2000; Dayan et al., 2013). Using electromagnetic (i.e., TMS) or direct electrical energy (i.e., tES), non-invasive brain stimulation can excite or inhibit the different brain regions via long-term potentiation (LTP) or long-term depression (LTD)-like effects (Chervyakov et al., 2015; Kronberg et al., 2017). Researchers have utilized TMS and tES to stimulate various neural circuits to understand how exciting or inhibiting different brain regions within networks causally affects brain activity (Sack, 2006; Hobot et al., 2021; Grover et al., 2022). In addition, both TMS and tES have been used clinically for treating multiple neurological and psychiatric diagnoses. Most notably, TMS is US FDA-approved to treat depression (O'Reardon et al., 2007; George et al., 2010), depression with anxiety, obsessive compulsive disorder (OCD) (Carmi et al., 2019), migraine headaches, and tobacco use disorder (Zangen et al., 2021). However, while TMS is FDA-approved to treat these four diagnoses, it is not consistently effective for every patient. For instance, once daily TMS for depression has response rates in a naturalistic setting of approximately 50–70% (Carpenter et al., 2012, 2021). While impressive, there is still room for improvement. In addition, tES studies have reported varying results (Horvath et al., 2015), with multiple well-designed clinical trials reporting mixed findings in the treatment of depression (Brunoni et al., 2017; Loo et al., 2018) and in other domains such as working memory (Brunoni and Vanderhasselt, 2014; Papazova et al., 2018; Westwood and Romani, 2018). Thus, there is an ongoing need to further understand and develop more effective TMS and tES treatments for multiple diagnoses. A key consideration to improve TMS and tES efficacy is determining whether a therapeutic level of stimulation engages the cortical target and neural circuit of interest (Zmeykina et al., 2020; Turi et al., 2021). A tool that can elucidate the amount of target and circuit engagement, and potentially improve clinical responses via personalized dosing, is electric field (E-field) modeling.

E-field modeling is a method of accurately estimating how much non-invasive brain stimulation applied at the scalp reaches the cortical level using magnetic resonance imaging (MRI) scans, tissue segmentations/meshing, and tissue conductivity values (Huang et al., 2017; Saturnino et al., 2019). As the magnitude of the E-field affects brain activity in a specific region or network, variability in the induced E-field can subsequently impact clinical response (Suen et al., 2020; Caulfield et al., 2022b; Zhang et al., 2022; Deng et al., 2023). Seminal studies in clinical TMS described how older individuals with larger scalp-to-cortex distances did not respond to treatments suggesting that the induced E-field magnitude is key to maximizing therapeutic response (Kozel et al., 2000; Nahas et al., 2004). Regarding tES, researchers have reported varying effects at differing scalp stimulation intensities in 0.5 mA increments (Moliadze et al., 2012; Batsikadze et al., 2013), highlighting the need for dose standardization and more advanced understanding of tES-induced E-fields at the cortical level. E-field modeling can elucidate dose-response relationships between E-field magnitude and therapeutic response and has broad applications including prospective dosing to ensure patients receive similar E-field intensities at specific brain regions (Caulfield et al., 2020, 2021; Saturnino et al., 2021; Dannhauer et al., 2022). However, most clinical brain stimulation providers do not implement E-field modeling for a variety of reasons, including the difficulty of obtaining structural MRI scans, lack of E-field modeling expertise, and need for advanced equipment such as neuronavigation (Caulfield et al., 2022a).

A possible proxy for using individual MRI scans that has not yet been systematically investigated is whether using a template MRI scan would be a suitable method of approximating group-average E-field values. While a group-level E-field model is incapable of explaining interindividual variability, it is highly informative in the search for what E-field intensities are clinically meaningful, in which populations and setting. As many researchers also retrospectively report the induced E-fields in template or standard brains included in E-field modeling packages (e.g., Konakanchi et al., 2020; Cobb et al., 2021), we sought to assess the accuracy of utilizing template brains to estimate group-level E-field averages. Moreover, utilizing template MRI scans could be useful for exploring general, non-patient specific properties of non-invasive brain stimulation such as the effects of novel tES electrode placements, coil architecture or angle, or estimating group-level effects such as in grant applications or to demonstrate the feasibility of tES or TMS in particular populations.

In this study, our goal was to assess whether using the MNI-152 brain or Ernie brain included in E-field modeling software packages would produce similar E-field values to $N = 195$ TMS participants with T1w MRI scans. If template scan and group-average E-field values were similar, researchers and clinical providers without access to individual MRI scans could still inform and approximate E-field modeling derived values with greater certainty than would be afforded in the absence of computational approaches.

Materials and methods

Participants

In total, we included the MRI scans of 195 participants in this E-field modeling study from an initial dataset of $N = 197$; two participants were deemed to have poor segmentation integrity and were excluded from further analysis. Each participant was treated with TMS in six Medical University of South Carolina IRB-approved protocols and provided written informed consent. The 195 participants were comprised of 106 men and 89 women, with an average age = 39.3 ± 14.0 years old and age range = 20–69 years old. Participants had the following five diagnoses: healthy controls ($N = 31$), alcohol use disorder ($N = 87$), tobacco use disorder ($N = 31$), generalized anxiety ($N = 25$), and depression ($N = 21$).

In addition, we utilized the MRI scans of the MNI-152 template brain (Fonov et al., 2011) and Ernie, an MRI scan and head model included in the SimNIBS software package that is commonly used to approximate E-fields. The MNI-152 template is an averaged structural MRI template based on 152 people, including 86 male/66 female brains with an average age = 25.02 ± 4.90 and age range = 18–44 years old. While the demographical information of the Ernie dataset has not been previously published due to PHI

considerations, this head model has been used in several E-field modeling studies (e.g., Kalloch et al., 2020; Gomez et al., 2021).

Motor threshold acquisition procedure

Using a MagVenture MagPro R30 or X100 machine and Cool-B65 TMS coil, TMS operators acquired resting motor threshold (rMT) values for each of the 195 participants using a visual approach. We defined the motor threshold as 5/10 visible anterior pollicis brevis (APB) muscle twitches. The rMT values were an average of 50.46 ± 8.91% (range = 31–78%) of maximal machine output. Therefore, the average 120% rMT stimulation intensity was 60.55 ± 10.70% of maximal machine output. Both TMS machines have a maximal dI/dt stimulator-coil output of 150e6 A/s, ensuring that each participant was stimulated with the same intensity across machines.

As rMTs were not acquired for the MNI-152 and Ernie brains, we simulated TMS using 120% of the group average rMT from the $N = 195$ experimentally determined values to the closest percentage point. This equated to 61% of machine output on the MagVenture MagPro systems with Cool-B65 TMS coil.

MRI scan parameters

Individual MRI scans were acquired at MUSC on a Siemens PRISMA 3T scanner and 32-channel head coil. Each participant underwent an MPRAGE structural T1w MRI scan with 0.9 mm × 0.9 mm × 0.9 mm isotropic voxels, image size: 256 × 256 × 256 voxels, TR: 2,300 ms, TE: 2.32 ms, TI: 900 ms, acceleration factor PE: 2, 192 slices, fat suppression off. The MNI-152 template brain is an open access composite brain comprised of 152 individuals with 1 mm × 1 mm × 1 mm voxels and image size: 182 × 238 × 282 voxels (Fonov et al., 2011). The Ernie T1w scan was acquired with 1 mm × 1 mm × 1 mm voxels with image size 182 × 238 × 282 voxels.

E-field modeling overview

We utilized SimNIBS 4.0.0 (Saturnino et al., 2019) and the CHARM segmentation and meshing pipeline (Puonti et al., 2020) for E-field modeling based on individual MRI scans acquired in each participant and the MNI-152 and Ernie scans (**Figure 1**). In total, we created $N = 195$ individual head models and one head model each for the MNI-152 brain and the Ernie brain. CHARM segments and meshes MRI scans into anatomically accurate tetrahedral head models comprised of 9 tissue layers: scalp, compact bone, spongy bone, cerebrospinal fluid (CSF), gray matter, white matter, eyeballs, blood vessels, and muscle. We assigned standard tissue conductivity values (Wagner et al., 2004; Opitz et al., 2015; Saturnino et al., 2015) to each tissue type (Scalp: 0.465 S/m, compact bone: 0.008 S/m, spongy bone: 0.025 S/m, CSF: 1.654 S/m, gray matter: 0.275 S/m, white matter: 0.126 S/m, eyeballs: 0.5 S/m, blood vessels: 0.6 S/m, and muscle: 0.16 S/m). As each tissue is assigned a different conductivity value, E-field modeling can accurately estimate the magnitude of stimulation that reaches the cortex in both TMS and tES. We visually inspected each head model to ensure the accuracy of segmentation and meshing. Due to this process, the head models for two individuals from an initial 197 scans were excluded due to noticeable intersections between tissue layers.

TMS E-field modeling

Using the 10-10_UI_Jurak_2007 EEG coordinate file output in SimNIBS (Jurcak et al., 2007), we centered the simulated MagVenture_Cool-B65 coil model over C3 (motor) and F3 (prefrontal) (Beam et al., 2009) stimulation targets in two E-field models (**Figures 1**, **2**). For stimulation intensity, we calculated the dI/dt value in A/s, with a maximum stimulator-coil output of 150e6 A/s. Using the motor threshold values, we calculated the 120% motor threshold stimulator output and multiplied this value by the maximum stimulator output (e.g., 50% stimulator output = 75e6 A/s). Custom MATLAB scripts ensured that the coil angle was oriented exactly 45° relative to the sagittal plane in each model.

tES E-field modeling

For tES simulations, we bilaterally centered electrodes over the motor (C3 and C4) or prefrontal (F3 and F4) cortices using the same 10-10_UI_Jurak_2007 EEG coordinate file (**Figures 1**, **2**). We used conventional 7 cm × 5 cm pad electrodes with the longer electrode axis oriented left/right on each participant's scalp. tES was simulated using 2 mA electrical current with the anodal electrode placed over the left hemisphere (C3 and F3) and the cathodal electrode placed over the right hemisphere (C4 and F4). While there are other commonly used electrode placements such as C3-supraorbital (SO) and F3-SO, we chose bilateral placements as they are commonly used and previous reports have found no significant differences in large-scale modeling between bilateral C3-C4 and C3-SO placements with 7 cm × 5 cm pad electrodes (Caulfield and George, 2022).

E-field magnitude outcome measure

To examine the E-field at the cortical target, we utilized two region of interest (ROI) analyses for both the TMS and tES models. Both ROIs extracted the average E-field within a spherical volume with a radius of 10 mm with a gray matter mask, as has been previously reported in the literature (e.g., Caulfield et al., 2022a; Caulfield and George, 2022). At a post-processing step, the CHARM segmentation pipeline fits the MNI template brain to the individual scan enabling researchers to perform analyses using standardized MNI coordinates across participants. Notably, this MNI template fitting does not affect the segmentation and meshing process as CHARM was trained on $N = 20$ individual head models.

For each person, the ROIs were centered over the stimulation target in the left hemisphere at motor MNI coordinate: −52.2, −16.4, 57.8 and prefrontal MNI coordinate at −35.5, 49.4, 32.4, based on publications reporting the locations of the cortical projections from scalp locations C3 (motor cortex) and F3

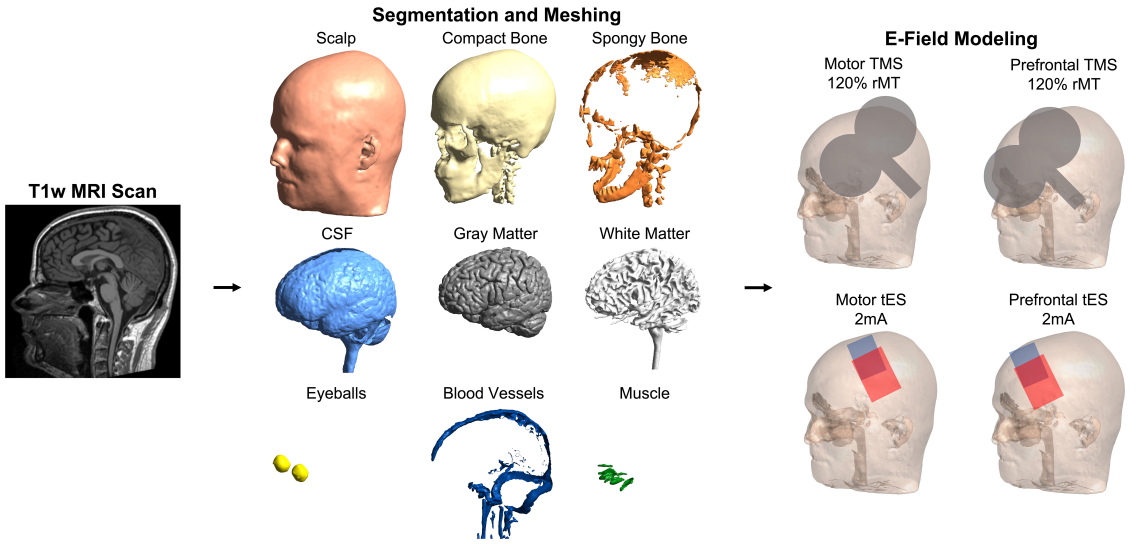

FIGURE 1
Electric field modeling pipeline. We created 195 individual head models and head models for the MNI-152 template brain and Ernie, an included mesh in the SimNIBS example folder. For each person, we computed four E-field models to simulate the effects of stimulation over the motor and prefrontal cortices with TMS and tES. This figure shows the pipeline in a representative participant.

(prefrontal cortex) (Okamoto et al., 2004; Okamoto and Dan, 2005).

Statistical measures

We conducted two types of statistical analyses to assess the suitability of utilizing the MNI-152 and Ernie scans and head models in lieu of having individual MRI scans. First, we used four one-way ANOVAs to assess the group-level differences between individual MRI scan E-field models and the MNI-152 and Ernie E-field models (four ANOVAs; one ANOVA each for motor TMS, prefrontal TMS, motor tES, and prefrontal tES). In addition, we computed additional one-way ANOVAs measuring the effects of diagnosis or sex on E-field results and differences between individual, MNI-152, and Ernie scans (eight total ANOVAs; one set of four ANOVAs for diagnosis and one set of four ANOVAs for sex). For sex, we accounted for conditions of men in the N = 195 sample, women in the N = 195 sample, the MNI-152 template, and Ernie. We chose to not examine the effects age on E-field magnitudes due to the collinearity of age and increased scalp-to-cortex distances already inherently being accounted for in E-field models and the unknown age of Ernie. All ANOVAs were calculated using SPSS 27.0 (IBM Corp., Armonk, NY, USA). For all statistical measures, the significance level was set to $\alpha = 0.05$ (two-tailed).

Second, to determine the minimum number of E-field models on individual scans to obtain a stable E-field value, we performed four permutation statistical analyses on the 195 individual E-field models in MATLAB R2022b (The Mathworks Inc., Natick, MA, USA). Our approach was based on the work of Van Hoornweder et al. (2022a). In the sample of N = 195 E-field models for each stimulation paradigm (i.e., motor TMS, prefrontal TMS, motor tES, and prefrontal tES), we randomly selected subsamples with increasing size from N = 1 to N = 195, repeating the procedure 10,000 times per subsample (i.e., 1,950,000 subsamples for each permutation). We chose to combine the heterogenous populations to maximize the likelihood of determining a corridor of stability since each individual diagnostic population had only N = 21 to N = 87 participants. We defined a corridor of stability between the 5 and 95th percentile range of the entire sample. In line with prior methodology, we calculated the "point of stability" which we defined as the point where the mean of the randomly selected subsample enters the corridor of stability and does not leave it at increasing subsample sizes. Our primary goal in determining the point of stability was to assess how many individual scans and subsequent E-field models would be needed to produce stable E-field values on the group level; if this number were larger than 152, it would suggest that a template brain with more scans than the MNI-152 composite scan would be necessary to accurately estimate group-level E-field models. All data are reported as mean ± standard deviation (SD).

Results

TMS electric field magnitudes

For both motor and prefrontal TMS-induced E-fields, the 195 individual MRI scans did not significantly differ from the MNI-152 and Ernie brains (**Figures 3A, B**). TMS-induced motor E-fields did not significantly differ amongst the individual brains (85.3 ± 15.5 V/m), MNI-152 template (78.2 V/m), and Ernie brain (81.5 V/m), $F(2, 194) = 0.13$, $p = 0.88$, $\eta_p^2 = 0.001$ (**Figure 3A** and **Table 1**). Similarly, TMS-induced prefrontal E-fields did not significantly differ between individual brains (80.3 ± 14.9 V/m), the MNI-152 template (80.1 V/m), and Ernie brain (72.6 V/m), $F(2, 194) = 0.14$, $p = 0.87$, $\eta_p^2 = 0.001$ (**Figure 3B**).

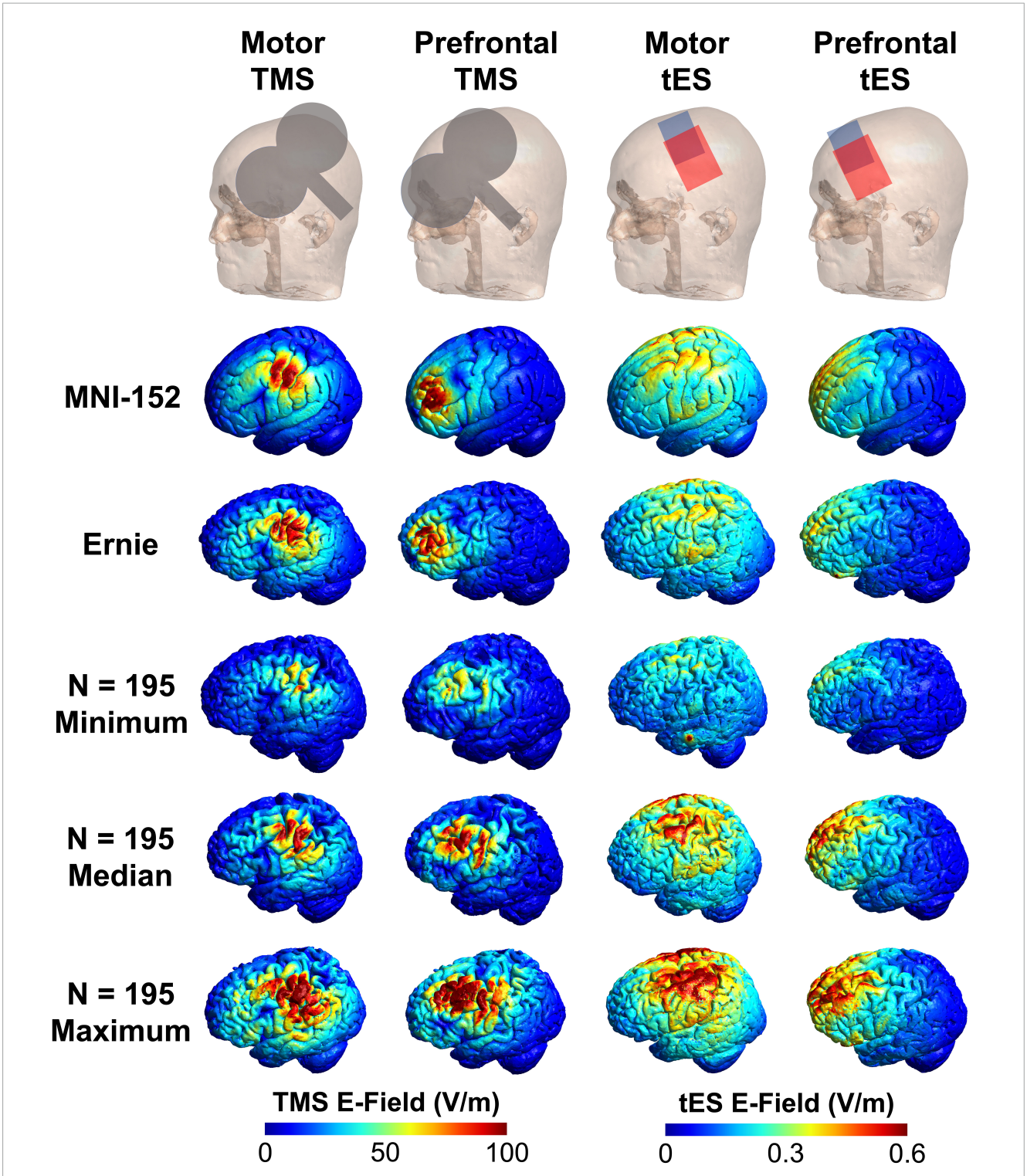

FIGURE 2
Visual comparison of the MNI-152, Ernie, and *N* = 195 individual E-field models. Here, we show the TMS coil and tES electrode placements, and E-field models in the MNI-152 and Ernie brains, as well as the E-field models in the *N* = 195 participants with the minimum, median, and maximum E-fields. Qualitatively, the MNI-152 and Ernie brains produce similar E-field magnitudes as the median models for each of the four stimulation types.

We additionally measured the differences in TMS-induced E-fields by diagnosis, finding that there were significant effects of diagnosis on E-field magnitude in both motor [$F(4, 190) = 6.09$, $p < 0.001$, $\eta_p^2 = 0.114$] and prefrontal TMS [$F(4, 190) = 5.96$, $p < 0.001$, $\eta_p^2 = 0.111$]. See Table 1 for detailed E-field magnitudes reported by diagnosis. For motor TMS, *post hoc* Tukey-corrected analyses revealed significant differences between generalized anxiety (95.8 ± 15.9 V/m) compared to healthy controls (84.2 ± 14.5 V/m), alcohol use disorder (81.6 ± 13.7 V/m), and depression (81.1 ± 17.2 V/m). We found additional

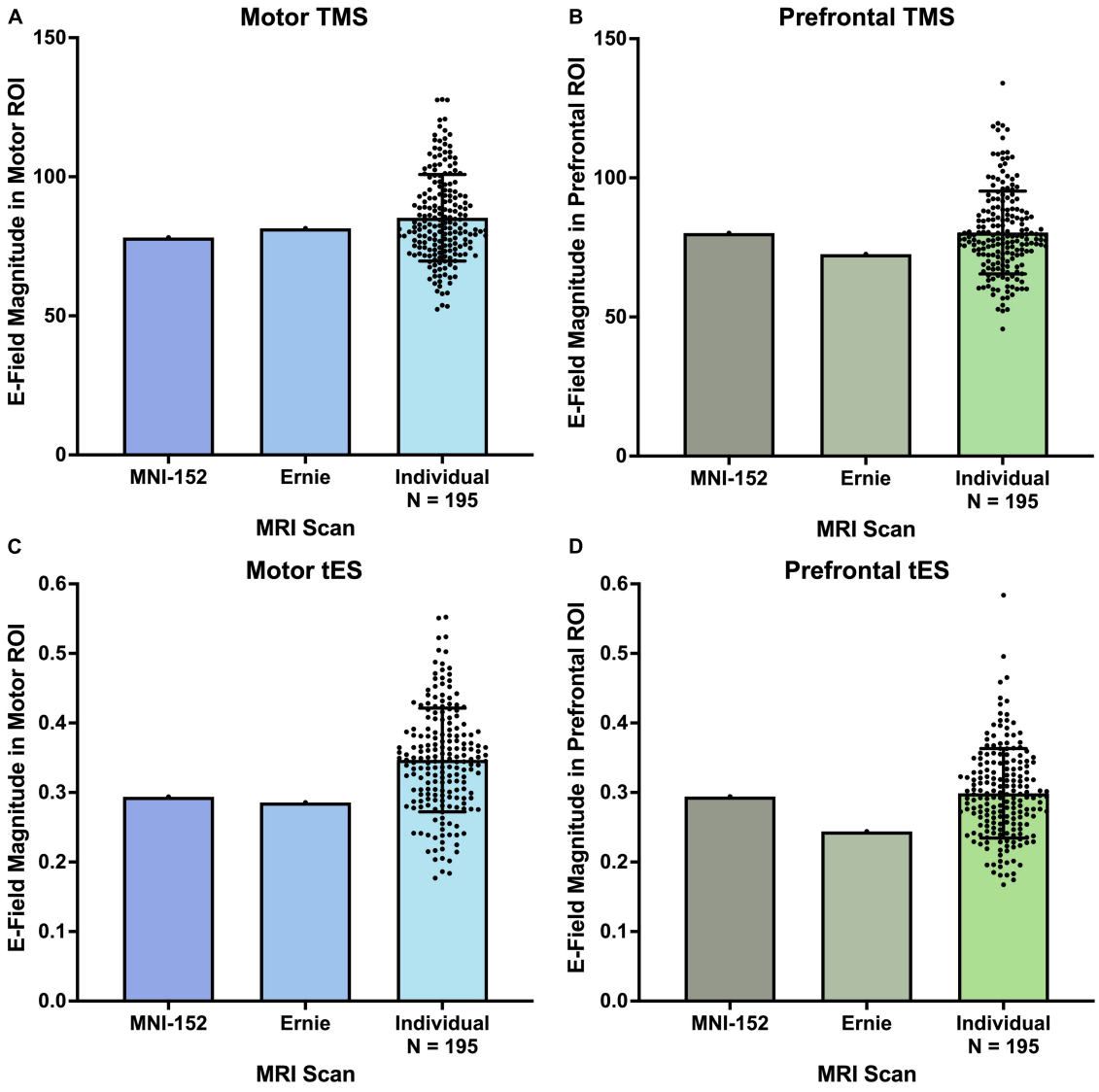

FIGURE 3
E-field magnitudes produced from the MNI-152, Ernie, and *N* = 195 individual head models. There were no significant differences between the E-field magnitudes produced at motor and prefrontal ROIs between the MNI-152, Ernie, and *N* = 195 individual models, suggesting that template brains can reliably approximate the E-fields produced on a group level. Error bars denote ± standard deviation.

TABLE 1 Electric field means and standard deviations (in parentheses) of MNI-152, Ernie, transdiagnostic, and individual diagnostic populations.

	Motor TMS (V/m)	Prefrontal TMS (V/m)	Motor tES (V/m)	Prefrontal tES (V/m)
MNI-152	81.46	80.14	0.293	0.294
Ernie	78.16	72.58	0.286	0.244
Transdiagnostic (*N* = 195)	85.26 (15.54)	80.35 (14.88)	0.347 (0.075)	0.299 (0.064)
Anxiety (*N* = 25)	95.76 (15.90)	88.75 (13.44)	0.350 (0.082)	0.289 (0.062)
Tobacco use disorder (*N* = 31)	90.96 (15.52)	87.30 (17.74)	0.376 (0.098)	0.318 (0.087)
Healthy controls (*N* = 31)	84.20 (14.48)	79.23 (13.11)	0.343 (0.059)	0.310 (0.052)
Alcohol use disorder (*N* = 87)	81.60 (13.66)	76.35 (12.43)	0.341 (0.064)	0.291 (0.057)
Depression (*N* = 21)	81.11 (17.17)	78.30 (17.25)	0.327 (0.080)	0.299 (0.070)

differences between the motor E-field magnitudes produced in tobacco use disorder (91.0 ± 15.5 V/m) and alcohol use disorder. For prefrontal TMS, participants with generalized anxiety (88.8 ± 13.4 V/m) and tobacco use disorder (87.3 ± 17.7 V/m) had significantly higher E-fields than those with alcohol use disorder (76.3 ± 12.4 V/m).

Regarding the effects of sex on TMS-induced E-fields, we found no significant differences between E-field magnitudes for men, women, the MNI-152, or Ernie brains. For motor TMS models, women (87.7 ± 15.5 V/m), men (83.2 ± 15.4 V/m), the MNI-152 template (78.2 V/m), and Ernie (81.5 V/m) did not significantly differ in E-field magnitude, $F(3, 193) = 0.89$, $p = 0.45$, $\eta_p^2 = 0.014$, $F(3, 193) = 1.42$, $p = 0.24$, $\eta_p^2 = 0.022$. Similarly, for prefrontal TMS models did not significantly differ between populations of women (82.1 ± 14.8 V/m), men (78.8 ± 14.8 V/m), the MNI-152 template (80.1 V/m), and Ernie (72.6 V/m), $F(3, 193) = 0.89$, $p = 0.45$, $\eta_p^2 = 0.014$.

tES electric field magnitudes

Likewise, both the motor and prefrontal tES E-fields were similar between the $N = 195$ individual scans, the MNI-152 template, and Ernie brains (Figures 3C, D). Motor tES E-fields did not significantly differ between the individual brains (0.35 ± 0.075 V/m), MNI-152 template (0.29 V/m), and Ernie brain (0.29 V/m), $F(2, 194) = 0.58$, $p = 0.56$, $\eta_p^2 = 0.006$ (Figure 3C). Furthermore, prefrontal tES E-fields did not significantly vary between individual brains (0.30 ± 0.06 V/m), the MNI-152 template (0.29 V/m), and Ernie brain (0.24 V/m), $F(2, 194) = 0.36$, $p = 0.70$, $\eta_p^2 = 0.004$ (Figure 3D).

In contrast to the TMS-induced E-fields, tES E-fields did not differ by diagnosis for both motor [$F(4, 190) = 1.76$, $p = 0.14$, $\eta_p^2 = 0.036$] and prefrontal tES [$F(4, 190) = 1.42$, $p = 0.23$, $\eta_p^2 = 0.029$]. See Table 1 for specific E-field magnitudes by diagnosis.

With regards to the effects of sex on tES-induced E-fields, we found no significant differences between E-field magnitudes for men, women, the MNI-152, or Ernie brains. For motor tES, there were no significant differences between women (0.36 ± 0.082 V/m), men (0.33 ± 0.066 V/m), the MNI-152 template (0.29 V/m), and Ernie brains (0.29 V/m), $F(3, 193) = 2.52$, $p = 0.06$, $\eta_p^2 = 0.038$. Likewise, for prefrontal tES, there were no significant differences between women (0.30 ± 0.069 V/m), men (0.30 ± 0.061 V/m), MNI-152 template (0.29 V/m), and Ernie brains (0.24 V/m), $F(3, 193) = 0.42$, $p = 0.74$, $\eta_p^2 = 0.006$.

Sample size stability analyses

Using four permutation analyses, we determined the minimum number of participants and E-field models needed to produce stable group-level E-field values in this heterogenous $N = 195$ group (Figure 4). For motor TMS, the stable E-field value was achieved at $N = 48$ participants compared to $N = 52$ for prefrontal TMS (Figures 4A, B). Regarding motor tES, $N = 42$ participants were needed to achieve stability, versus $N = 51$ for prefrontal tES (Figures 4C, D).

Discussion

In this study, we assessed the utility of calculating TMS and tES E-field models in the template MNI-152 scan and Ernie brain compared to $N = 195$ participants with 5 diagnoses (i.e., healthy controls, alcohol use disorder, tobacco use disorder, generalized anxiety, and depression). We simulated four common non-invasive brain stimulation protocols (i.e., motor and prefrontal TMS and tES) per participant for 788 total E-field models. We found that there were no significant group-level differences of the E-field magnitudes induced from motor and prefrontal TMS and tES from individual scans vs. MNI-152 and Ernie brains. For TMS, the MNI-152 template produced 8.3 and 0.3% lower E-fields for the motor and prefrontal cortices, respectively, while the Ernie brain had 4.5 and 9.7% lower E-fields than the group average motor and prefrontal E-fields from the $N = 195$ participants (Figure 3 and Table 1). There were more pronounced, albeit still non-significant differences for tES, with the MNI-152 template producing 16.3 and 1.6% lower E-fields and the Ernie brain having 17.7 and 18.4% lower E-fields in the motor and prefrontal cortices, respectively, than the $N = 195$ individual models. Thus, while there were no significant overall E-field magnitude differences, it appears that the MNI-152 and Ernie brains are most accurate at estimating the group-level regions and neural circuits simulated by TMS, compared to tES. In conjunction with prior reports (Minjoli et al., 2017; Tzirini et al., 2022), MNI-152 and Ernie brains may be most accurate at estimating TMS-induced E-fields due to TMS being less affected by individual tissue composition due to the electromagnetic stimulation approach compared to the direct electrical stimulation method utilized in tES, which is more heavily governed by the underlying tissue composition.

It is also important to consider the effects of diagnosis on E-field magnitude. Here, we reported that TMS-induced E-fields differ as a product of diagnosis, such that individuals with generalized anxiety and tobacco use disorder had significantly higher motor and prefrontal E-fields than those with alcohol use disorder. In addition, individuals with generalized anxiety had significantly higher motor E-fields than healthy controls and people with depression. Interestingly, these nuanced relationships between E-field magnitude and diagnosis only existed for TMS and not tES, as all tES-induced E-fields did not differ by diagnosis (Table 1). This may be in part due to uniform tES applying the same stimulation intensity of 2 mA across models whereas our TMS models used the experimentally-determined dI/dt values based on individual motor thresholds determined for each person. Since a uniform stimulation intensity was applied across each person, fixed dose 2 mA tES may have reduced the amount of variation between individuals that individualized motor threshold values provide. These data point at the utility of personalized dosing for tES as certain diagnoses likely require a higher individualized dosage for appropriate target engagement of cortical targets and neural circuits. Moreover, since we found no group-level differences combining across diagnoses between $N = 195$ TMS and tES E-fields and template MNI-152 and Ernie brains, this relationship may change depending on the different diagnoses considered. Therefore, future research should consider further investigating the appropriateness of using template MNI-152 and Ernie brains to estimate group-level E-fields in different populations. Likely, these TMS-induced E-field data indicate differing neurophysiology and the up- or down-regulation of neural circuits across diagnostic populations. In comparison, similar tES-induced E-fields across diagnoses might indicate that the scalp-to-cortex distance and tissue compositions may be relatively similar

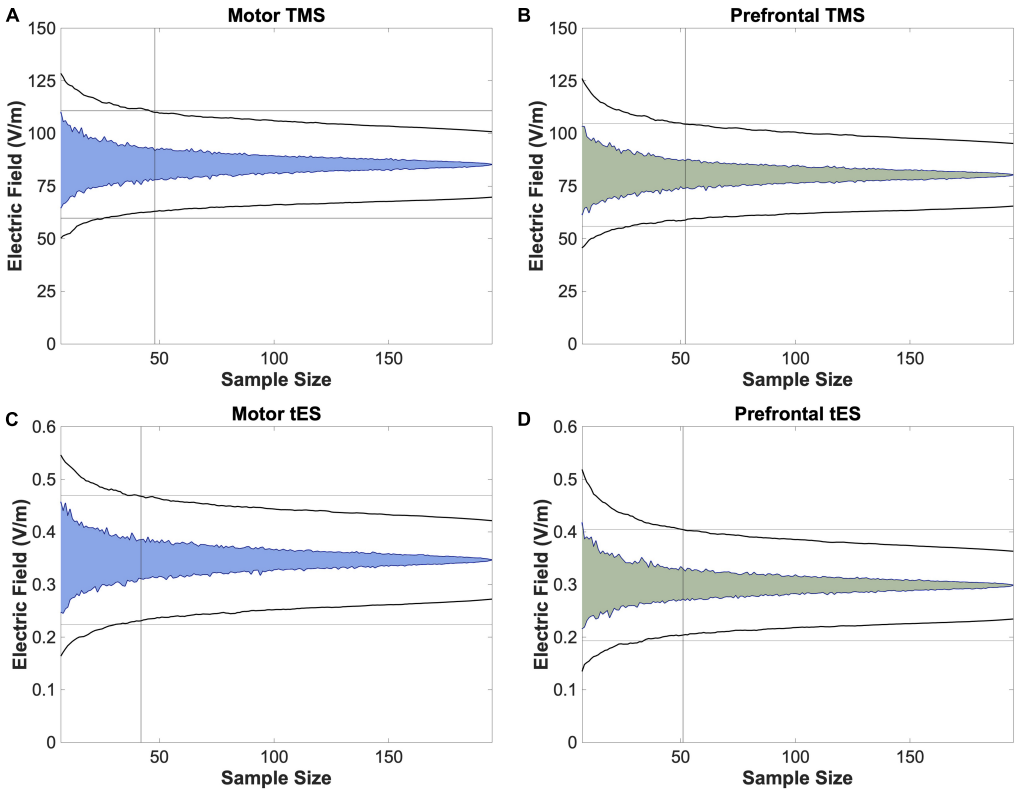

FIGURE 4
Permutation analyses to determine stable sample sizes in *N* = 195 participants. To further analyze whether utilizing a template scan is an appropriate method of approximating group-level E-field magnitudes of different stimulation paradigms, we performed bootstrapping analyses to determine the stable sample size at which the E-fields produced remained within the 95% confidence interval, as denoted with a vertical line. We found that this number ranged from 42 (motor tES) to 52 (prefrontal TMS). As 52 participants is lower than the 152 scans included in the MNI-152 template, these data suggest that utilizing template scans may be a method of estimating stable group-level E-field magnitudes.

across populations, as reflected by the similar tES-induced E-field magnitude values. Future research could further elucidate the modality-specific findings and interactions with diagnoses that we reported here.

In a second series of analyses, we used a permutation approach to compute the point of stability at which the group average E-field value did not increase in variance with additional E-field models (i.e., the point of stability). The point of stability differed slightly by stimulation modality and location, with a range of 42 to 52. Notably, the point of stability across stimulation modalities was always well short of the 152 scans included in the MNI-152 brain, further validating the composite brain as having a high enough number of scans that the interindividual variation is likely appropriately represented. Taken together, these data validate the strategy of using a template MNI-152 brain scan to approximate group-level E-field results as it takes many scans into consideration that average across neuroanatomical idiosyncrasies.

There are numerous implications of this research and how template MRI scans could be utilized to estimate how much stimulation reaches the cortex. First, while the utility of using template brains for E-field modeling is question-dependent, it appears that template brains can reliably estimate group-level effects, even in a clinically heterogenous group. We report that the group-level E-field values from individual MRI scans do not significantly differ from the E-field values produced from MNI-152 and Ernie brains, validating the use of template scans to estimate group-level E-field values. Using template scans for E-field modeling could have multiple uses. For instance, using template scans for E-field modeling could inform the effects of more sophisticated and optimized electrode positioning, sizes, and inter-electrode distances such as through high definition tES (HD-tES) or anterior posterior pad surround tES (APPS-tES), as has been done in prior publications (Datta et al., 2009; Deng et al., 2013; Saturnino et al., 2015; Laakso et al., 2016; Caulfield and George, 2022). As many tES studies do not acquire MRI scans, particularly with the increasing use of at-home tES (André et al., 2016; Riggs et al., 2018; Pilloni et al., 2022), using a template MRI scan to plan more optimized tES electrode positioning and intensity for a specific goal may help to ensure that a therapeutic cortical intensity is induced at the right target on the group level.

It is also interesting to compare our findings to prior efforts looking at datasets of 60 or more individual E-field models such as the study by Laakso et al. (2016). Similar to our results, these researchers reported more variable frontal tES-induced E-fields than motor E-fields, substantiating our finding that prefrontal tES-induced E-fields required a greater number of participants to obtain a point of stability (**Figure 4**). This is notable as Laakso et al. (2016) included 64 healthy younger adults whereas we collapsed across 5 transdiagnostic groups, suggesting that our results might hold

true in individual populations. It is also important to note other potential differences between our study and the one by Laakso et al. (2016), including different E-field measures (ROI magnitude vs. whole brain normal component). Further research with larger sample sizes per diagnostic condition is needed.

Furthermore, tES has widespread clinical potential but there have been mixed results to date, possibly in part to different amounts of stimulation reaching the cortex with uniform 2 mA dosing. Personalized E-field dosing is an approach that could standardize the stimulation intensity at the cortical target based on varying the dose at the scalp (Caulfield et al., 2020). While personalized E-field dosing is not possible using a template scan, our hope is that we have validated the approach of modeling on the MNI-152 or Ernie brains to provide reliable general estimations for how much stimulation is reaching the cortex in an average person. In turn, the information obtained from quantifying how much stimulation is reaching the cortex on average will surely benefit the ongoing search for the optimal E-field magnitude to maximize non-invasive brain stimulation effects within specific clinical populations and settings (Wischnewski et al., 2021; Alekseichuk et al., 2022; Caulfield et al., 2022b).

Moreover, it is now a common practice to include E-field models in brain stimulation publications and grant applications to substantiate experimental choices of where to position the TMS coil or tES electrodes and which stimulation intensity to choose. As such, including E-field models are informative and allow peers to assess whether an appropriate amount of stimulation reaches the cortex and adequately stimulates the neural circuit of interest. In lieu of having already acquired MRI scans, many researchers perform these E-field models on the MNI-152 template brain (Konakanchi et al., 2020; Cobb et al., 2021), or on the Ernie brain (Kalloch et al., 2020; Gomez et al., 2021) included in the SimNIBS software package. Our study validates the strategy of performing E-field modeling on these MNI-152 and Ernie head models as they can reliably approximate group-level E-field effects of how much and where in different brain regions and neural circuits the stimulation reaches the cortex. Furthermore, it was previously unclear whether the use of the MNI-152 template brain, comprised of healthy adults, would adequately estimate the stimulation intensity in clinical populations. While our scope was limited to diagnoses of mental health and healthy participants, our finding that the group-level E-fields induced from motor and prefrontal tES and TMS did not differ from the template brain suggests that template brain models produce roughly the same E-field magnitudes transdiagnostically. This work should be further evaluated in other diagnoses as particular populations (e.g., stroke) could have greater E-field differences compared to template scan E-fields, especially based on lesion location (Minjoli et al., 2017; Mantell et al., 2021).

While the specific research question dictates the most suitable E-field modeling approach, these data suggest an upper sample size limit of what researchers might consider for future group-level E-field modeling studies. Since it is relatively simple to scale up the number of models and participants in modeling approaches, some researchers have included hundreds of participants with the goal of obtaining stable E-field values that were not significantly impacted by outliers (e.g., Caulfield and George, 2022). Our bootstrapping data suggest that for research questions about the group-level effects of E-field modeling, there is no additional increase in the variation of modeling results above 52 individuals for any stimulation modality. Thus, if the experimenter includes more participants with the objective of reducing the variation of group-level E-field estimates, there are diminishing returns above the point of stability. However, it is important to note that prior findings suggesting that the point of stability is higher than $N = 52$ were likely biased by larger sample sizes (Van Hoornweder et al., 2022a), as is the case in any permutation approach. Future research might also consider performing permutation analyses that separate participants by diagnosis to investigate whether there are differences in the point of stability by condition.

Finally, while we primarily considered how E-field modeling in a template brain might be able to inform group-level analyses, it is important to substantiate how an individually selected E-field value would compare to the MNI template brain estimate (see **Figure 2** for minimum, median, and maximum E-fields in the $N = 195$ sample compared to the MNI-152 template and Ernie brain). We reported the following averages and ranges of E-field magnitudes produced from TMS and tES: motor TMS: 85.3 $\pm$ 15.5 V/m; prefrontal TMS: 80.3 $\pm$ 14.9 V/m; motor tES: 0.35 $\pm$ 0.07 V/m; prefrontal tES: 0.30 $\pm$ 15.5 V/m. While examining individual E-fields in retrospective or prospective study designs necessitates having individual MRI scans, considering these averages $\pm$ 2 SD provides a 95% confidence interval for E-field magnitudes in these TMS and tES protocols. Using these ranges, there were between 7 and 10 individuals falling outside of 2 SD in each stimulation protocol. That the MNI-152 template and Ernie head models produced similar E-field values as the group average values suggests that they are suitable proxy head models for estimating group-average E-fields and that most people (i.e., approximately 95% of people) do not significantly differ on an individual-by-individual basis from the E-fields produced in the MNI-152 brain.

Limitations and future directions

Briefly, it is important to consider the limitations of this study. We used the MNI-152 brain as a commonly utilized template, but there may be closer matching composite MRI scans depending on the population of interest. For instance, if a researcher wanted to investigate the group-level E-fields in an aging population could consider using more specific age-matched (Fillmore et al., 2015) or diagnosis-matched (Dadar et al., 2022) templates for potentially more accurate simulations. While we used bilateral electrode placements (i.e., C3-C4 and F3-F4) instead of other common electrode placements (e.g., C3-SO and F3-SO), prior large-scale findings have shown that there are no significant differences in E-field magnitudes between C3-C4 and C3-SO (Caulfield and George, 2022). This prior results leads us to believe that the MNI template and Ernie scan would be similarly suitable to accurately estimate E-field magnitudes at other similar electrode placements. In addition, we only utilized a T1w MRI scan for E-field modeling in our naturalistic sample, based on the MRI scans acquired across the parent studies. However, prior reports have described how the inclusion of both T1w and T2w MRI scans improves segmentation accuracy at the skull-CSF border (Nielsen et al., 2018; Van Hoornweder et al., 2022b) and how this can affect E-field modeling values in a regionally-specific

fashion (Van Hoornweder et al., 2022). Furthermore, we chose a spherical ROI as our outcome measure, but this may not have encapsulated the peak E-fields induced from tES. Prior results have reported that the maximal E-field is not always located underneath the center of tES electrodes (Caulfield and George, 2022) in the conventional bilateral electrode placement. Forthcoming research has also highlighted the importance of considering the focality of stimulation and recommended reporting both ROI and percentile-based outcome measures (Van Hoornweder et al., 2023), which we did not do here. Thus, extending these data to report percentile-based E-fields could more broadly inform future studies and grant applications utilizing the template scan approach. With larger sample sizes, future analyses could extend the point of stability analyses to specific diagnoses (e.g., healthy controls or participants with anxiety). This method could help to inform the needed number of participants to achieve stable E-field values in these diagnoses as opposed to the transdiagnostic approach that we took here. Finally, we focused on superficial brain targets in this study due to these regions being the primary targets in TMS and tES. In addition, it is more difficult to standardize the tissue compositions between participants at deeper targets due to varying levels of gray vs. white matter. Future research could consider examining deeper targets in more depth, but this was beyond the scope of the current study.

Conclusion

Utilizing the MNI-152 template scan and Ernie brain produce similar group-level estimations of TMS and tES-induced E-field magnitudes over the motor and prefrontal cortices. Using the MNI-152 brain to approximate group-level E-field effects can provide valuable insight into the amount of stimulation reaching different cortical regions and neural circuits in lieu of individual MRI scans. While preliminary, TMS-induced E-field magnitudes, but not tES-induced E-field magnitudes differed in some diagnoses, including higher motor and prefrontal E-fields in participants with generalized anxiety than alcohol use disorder, healthy controls, and those with depression. Further research is needed to further elucidate the relationships between different diagnoses and E-fields, and whether these impact response to TMS and tES treatments.

Data availability statement

The datasets presented in this article are not readily available because these data are part of ongoing studies but will be made available upon reasonable request. Requests to access the datasets should be directed to KC, caulfiel@musc.edu.

Ethics statement

The studies involving humans were approved by Medical University of South Carolina IRB. The studies were conducted in accordance with the local legislation and institutional requirements. The participants provided their written informed consent to participate in this study.

Author contributions

All authors significantly contributed to the study conceptualization, data analysis, figures creation, writing the original document, editing the document prior to submission, and approved the submitted version.

Funding

This work was supported by an NINDS F31 grant (NIH F31NS126019) to KC, a Research Foundation Flanders grant (G1129923N) to SV, the COBRE for Stroke Recovery (NIH P20GM109040; LM) National Center of Neuromodulation for Rehabilitation (NC NM4R; NIH P2CHD086844; LM), a VA Small Projects in Rehabilitation Research (SPiRE) Pilot grant (LM), and the National Alliance for Research on Schizophrenia and Depression (NARSAD; LM).

Conflict of interest

The authors declare that the research was conducted in the absence of any commercial or financial relationships that could be construed as a potential conflict of interest.

Publisher's note

All claims expressed in this article are solely those of the authors and do not necessarily represent those of their affiliated organizations, or those of the publisher, the editors and the reviewers. Any product that may be evaluated in this article, or claim that may be made by its manufacturer, is not guaranteed or endorsed by the publisher.

References

Alekseichuk, I., Wischnewski, M., and Opitz, A. (2022). A minimum effective dose for (transcranial) alternating current stimulation. *Brain Stimul.* 15, 1221–1222.

André, S., Heinrich, S., Kayser, F., Menzler, K., Kesselring, J., Khader, P. H., et al. (2016). At-home tDCS of the left dorsolateral prefrontal cortex improves visual short-term memory in mild vascular dementia. *J. Neurol. Sci.* 369, 185–190.

Barker, A. T., Jalinous, R., and Freeston, I. L. (1985). Non-invasive magnetic stimulation of human motor cortex. *Lancet* 325, 1106–1107.

Batsikadze, G., Moliadze, V., Paulus, W., Kuo, M. F., and Nitsche, M. (2013). Partially non-linear stimulation intensity-dependent effects of direct current stimulation on motor cortex excitability in humans. *J. Physiol.* 591, 1987–2000.

Beam, W., Borckardt, J. J., Reeves, S. T., and George, M. S. (2009). An efficient and accurate new method for locating the F3 position for prefrontal TMS applications. *Brain Stimul.* 2, 50–54. doi: 10.1016/j.brs.2008.09.006

Brunoni, A. R., and Vanderhasselt, M. A. (2014). Working memory improvement with non-invasive brain stimulation of the dorsolateral prefrontal cortex: A systematic review and meta-analysis. *Brain Cogn.* 86, 1–9.

Brunoni, A. R., Moffa, A. H., Sampaio-Junior, B., Borrione, L., Moreno, M. L., Fernandes, R. A., et al. (2017). Trial of electrical direct-current therapy versus escitalopram for depression. *N. Engl. J. Med.* 376, 2523–2533.

Carmi, L., Tendler, A., Bystritsky, A., Hollander, E., Blumberger, D. M., Daskalakis, J., et al. (2019). Efficacy and safety of deep transcranial magnetic stimulation for obsessive-compulsive disorder: A prospective multicenter randomized double-blind placebo-controlled trial. *Am. J. Psychiatry* 176, 931–938.

Carpenter, L. L., Janicak, P. G., Aaronson, S. T., Boyadjis, T., Brock, D. G., Cook, I. A., et al. (2012). Transcranial magnetic stimulation (TMS) for major depression: A multisite, naturalistic, observational study of acute treatment outcomes in clinical practice. *Depress Anxiety.* 29, 587–596.

Carpenter, L., Aaronson, S., Hutton, T. M., Mina, M., Pages, K., Verdoliva, S., et al. (2021). Comparison of clinical outcomes with two Transcranial Magnetic Stimulation treatment protocols for major depressive disorder. *Brain Stimul.* 14, 173–180.

Caulfield, K. A., and George, M. S. (2022). Optimized APPS-tDCS electrode position, size, and distance doubles the on-target stimulation magnitude in 3000 electric field models. *Sci. Rep.* 12:20116. doi: 10.1038/s41598-022-24618-3

Caulfield, K. A., Badran, B. W., DeVries, W. H., Summers, P. M., Kofmehl, E., Li, X., et al. (2020). Transcranial electrical stimulation motor threshold can estimate individualized tDCS dosage from reverse-calculation electric-field modeling. *Brain Stimul.* 13, 961–969. doi: 10.1016/j.brs.2020.04.007

Caulfield, K. A., Fleischmann, H. H., Cox, C. E., Wolf, J. P., George, M. S., and McTeague, L. M. (2022a). Neuronavigation maximizes accuracy and precision in TMS positioning: Evidence from 11,230 distance, angle, and electric field modeling measurements. *Brain Stimul.* 15, 1192–1205. doi: 10.1016/j.brs.2022.08.013

Caulfield, K. A., Indahlastari, A., Nissim, N. R., Lopez, J. W., Fleischmann, H. H., Woods, A. J., et al. (2022b). Electric field strength from prefrontal transcranial direct current stimulation determines degree of working memory response: A potential application of reverse-calculation modeling? *Neuromodulation* 25, 578–587. doi: 10.1111/ner.13342

Caulfield, K. A., Li, X., and George, M. S. (2021). Four electric field modeling methods of dosing prefrontal Transcranial Magnetic Stimulation (TMS): Introducing APEX MT dosimetry. *Brain Stimul.* 14, 1032–1034. doi: 10.1016/j.brs.2021.06.012

Chervyakov, A. V., Chernyavsky, A. Y., Sinitsyn, D. O., and Piradov, M. A. (2015). Possible mechanisms underlying the therapeutic effects of transcranial magnetic stimulation. *Front. Hum. Neurosci.* 9:303. doi: 10.3389/fnhum.2015.00303

Cobb, A. R., O'Connor, P., Zaizar, E., Caulfield, K., Gonzalez-Lima, F., and Telch, M. J. (2021). tDCS-Augmented in vivo exposure therapy for specific fears: A randomized clinical trial. *J. Anxiety Disord.* 78:102344. doi: 10.1016/j.janxdis.2020.102344

Dadar, M., Camicioli, R., and Duchesne, S. (2022). Multi sequence average templates for aging and neurodegenerative disease populations. *Sci. Data* 9:238. doi: 10.1038/s41597-022-01341-2

Dannhauer, M., Huang, Z., Beynel, L., Wood, E., Bukhari-Parlakturk, N., and Peterchev, A. V. (2022). TAP: Targeting and analysis pipeline for optimization and verification of coil placement in transcranial magnetic stimulation. *J. Neural Eng.* 19, 026050. doi: 10.1088/1741-2552/ac63a4

Datta, A., Bansal, V., Diaz, J., Patel, J., Reato, D., and Bikson, M. (2009). Gyri-precise head model of transcranial direct current stimulation: Improved spatial focality using a ring electrode versus conventional rectangular pad. *Brain Stim.* 2, 201–207.e1. doi: 10.1016/j.brs.2009.03.005

Dayan, E., Censor, N., Buch, E. R., Sandrini, M., and Cohen, L. G. (2013). Noninvasive brain stimulation: From physiology to network dynamics and back. *Nat. Neurosci.* 16, 838–844.

Deng, Z.-D., Lisanby, S. H., and Peterchev, A. V. (2013). Controlling stimulation strength and focality in electroconvulsive therapy via current amplitude and electrode size and spacing: Comparison with magnetic seizure therapy. *J. ECT* 29:325. doi: 10.1097/YCT.10.1097/YCT.0b013e3182a4b4a7

Deng, Z.-D., Robins, P. L., Dannhauer, M., Haugen, L. M., Port, J. D., and Croarkin, P. E. (2023). Comparison of coil placement approaches targeting dorsolateral prefrontal cortex in depressed adolescents receiving repetitive transcranial magnetic stimulation: An electric field modeling study. *medRxiv [Preprint]*. doi: 10.1101/2023.02.06.23285526

Fillmore, P. T., Phillips-Meek, M. C., and Richards, J. E. (2015). Age-specific MRI brain and head templates for healthy adults from 20 through 89 years of age. *Front. Aging Neurosci.* 7:44. doi: 10.3389/fnagi.2015.00044

Fonov, V., Evans, A. C., Botteron, K., Almli, C. R., McKinstry, R. C., and Collins, D. L. (2011). Unbiased average age-appropriate atlases for pediatric studies. *Neuroimage* 54, 313–327. doi: 10.1016/j.neuroimage.2010.07.033

George, M. S., Lisanby, S. H., Avery, D., McDonald, W. M., Durkalski, V., Pavlicova, M., et al. (2010). Daily left prefrontal transcranial magnetic stimulation therapy for major depressive disorder: A sham-controlled randomized trial. *Arch. Gen. Psychiatry* 67, 507–516.

Gomez, L. J., Dannhauer, M., and Peterchev, A. V. (2021). Fast computational optimization of TMS coil placement for individualized electric field targeting. *Neuroimage* 228:117696. doi: 10.1016/j.neuroimage.2020.117696

Grover, S., Wen, W., Viswanathan, V., Gill, C. T., and Reinhart, R. M. G. (2022). Long-lasting, dissociable improvements in working memory and long-term memory in older adults with repetitive neuromodulation. *Nat. Neurosci.* 25, 1237–1246. doi: 10.1038/s41593-022-01132-3

Hobot, J., Klincewicz, M., Sandberg, K., and Wierzchoń, M. (2021). Causal inferences in repetitive transcranial magnetic stimulation research: Challenges and perspectives. *Front. Hum. Neurosci.* 14:586448. doi: 10.3389/fnhum.2020.586448

Horvath, J. C., Forte, J. D., and Carter, O. (2015). Evidence that transcranial direct current stimulation (tDCS) generates little-to-no reliable neurophysiologic effect beyond MEP amplitude modulation in healthy human subjects: A systematic review. *Neuropsychologia* 66, 213–236.

Huang, Y., Liu, A. A., Lafon, B., Friedman, D., Dayan, M., Wang, X., et al. (2017). Measurements and models of electric fields in the in vivo human brain during transcranial electric stimulation. *eLife* 6:e18834.

Jurcak, V., Tsuzuki, D., and Dan, I. (2007). 10/20, 10/10, and 10/5 systems revisited: Their validity as relative head-surface-based positioning systems. *Neuroimage* 34, 1600–1611. doi: 10.1016/j.neuroimage.2006.09.024

Kalloch, B., Bazin, P.-L., Villringer, A., Sehm, B., and Hlawitschka, M. (2020). A flexible workflow for simulating transcranial electric stimulation in healthy and lesioned brains. *PLoS One* 15:e0228119. doi: 10.1371/journal.pone.0228119

Konakanchi, D., de Jongh Curry, A. L., Waters, R. S., and Narayana, S. (2020). Focality of the induced E-field is a contributing factor in the choice of TMS parameters: Evidence from a 3D computational model of the human brain. *Brain Sci.* 10:1010. doi: 10.3390/brainsci10121010

Kozel, F., Nahas, Z., DeBrux, C., Molloy, M., Lorberbaum, J., Bohning, D., et al. (2000). How the distance from coil to cortex relates to age, motor threshold and possibly the antidepressant response to repetitive transcranial magnetic stimulation. *J. Neuropsychiatry Clin. Neurosci.* 12, 376–384. doi: 10.1176/jnp.12.3.376

Kronberg, G., Bridi, M., Abel, T., Bikson, M., and Parra, L. C. (2017). Direct current stimulation modulates LTP and LTD: Activity dependence and dendritic effects. *Brain Stimul.* 10, 51–58. doi: 10.1016/j.brs.2016.10.001

Laakso, I., Tanaka, S., Mikkonen, M., Koyama, S., Sadato, N., and Hirata, A. (2016). Electric fields of motor and frontal tDCS in a standard brain space: A computer simulation study. *Neuroimage* 137, 140–151. doi: 10.1016/j.neuroimage.2016.05.032

Loo, C. K., Husain, M. M., McDonald, W. M., Aaronson, S., O'Reardon, J. P., Alonzo, A., et al. (2018). International randomized-controlled trial of transcranial direct current stimulation in depression. *Brain Stimul.* 11, 125–133.

Mantell, K. E., Sutter, E. N., Shirinpour, S., Nemanich, S. T., Lench, D. H., Gillick, B. T., et al. (2021). Evaluating transcranial magnetic stimulation (TMS) induced electric fields in pediatric stroke. *Neuroimage Clin.* 29:102563. doi: 10.1016/j.nicl.2021.102563

Minjoli, S., Saturnino, G. B., Blicher, J. U., Stagg, C. J., Siebner, H. R., Antunes, A., et al. (2017). The impact of large structural brain changes in chronic stroke patients on the electric field caused by transcranial brain stimulation. *Neuroimage Clin.* 15, 106–117. doi: 10.1016/j.nicl.2017.04.014

Moliadze, V., Atalay, D., Antal, A., and Paulus, W. (2012). Close to threshold transcranial electrical stimulation preferentially activates inhibitory networks before switching to excitation with higher intensities. *Brain Stim.* 5, 505–511. doi: 10.1016/j.brs.2011.11.004

Nahas, Z., Li, X., Kozel, F. A., Mirzki, D., Memon, M., Miller, K., et al. (2004). Safety and benefits of distance-adjusted prefrontal transcranial magnetic stimulation in depressed patients 55-75 years of age: A pilot study. *Depress Anxiety.* 19, 249–256. doi: 10.1002/da.20015

Nielsen, J. D., Madsen, K. H., Puonti, O., Siebner, H. R., Bauer, C., Madsen, C. G., et al. (2018). Automatic skull segmentation from MR images for realistic volume conductor models of the head: Assessment of the state-of-the-art. *Neuroimage* 174, 587–598. doi: 10.1016/j.neuroimage.2018.03.001

Nitsche, M. A., and Paulus, W. (2000). Excitability changes induced in the human motor cortex by weak transcranial direct current stimulation. *J. Physiol.* 527, 633–639.

O'Reardon, J. P., Solvason, H. B., Janicak, P. G., Sampson, S., Isenberg, K. E., Nahas, Z., et al. (2007). Efficacy and safety of transcranial magnetic stimulation in the acute treatment of major depression: A multisite randomized controlled trial. *Biol. Psychiatry* 62, 1208–1216.

Okamoto, M., and Dan, I. (2005). Automated cortical projection of head-surface locations for transcranial functional brain mapping. *Neuroimage* 26, 18–28. doi: 10.1016/j.neuroimage.2005.01.018

Okamoto, M., Dan, H., Sakamoto, K., Takeo, K., Shimizu, K., Kohno, S., et al. (2004). Three-dimensional probabilistic anatomical cranio-cerebral correlation via

the international 10–20 system oriented for transcranial functional brain mapping. *Neuroimage* 21, 99–111. doi: 10.1016/j.neuroimage.2003.08.026

Opitz, A., Paulus, W., Will, S., Antunes, A., and Thielscher, A. (2015). Determinants of the electric field during transcranial direct current stimulation. *Neuroimage* 109, 140–150.

Papazova, I., Strube, W., Becker, B., Henning, B., Schwippel, T., Fallgatter, A. J., et al. (2018). Improving working memory in schizophrenia: Effects of 1mA and 2mA transcranial direct current stimulation to the left DLPFC. *Schizophrenia Res.* 202, 203–209. doi: 10.1016/j.schres.2018.06.032

Pilloni, G., Vogel-Eyny, A., Lustberg, M., Best, P., Malik, M., Walton-Masters, L., et al. (2022). Tolerability and feasibility of at-home remotely supervised transcranial direct current stimulation (RS-tDCS): Single-center evidence from 6,779 sessions. *Brain Stim.* 15, 707–716. doi: 10.1016/j.brs.2022.04.014

Puonti, O., Van Leemput, K., Saturnino, G. B., Siebner, H. R., Madsen, K. H., and Thielscher, A. (2020). Accurate and robust whole-head segmentation from magnetic resonance images for individualized head modeling. *Neuroimage* 219:117044.

Riggs, A., Patel, V., Paneri, B., Portenoy, R. K., Bikson, M., and Knotkova, H. (2018). At-home Transcranial Direct Current Stimulation (tDCS) With telehealth support for symptom control in chronically-Ill patients with multiple symptoms. *Front. Behav. Neurosci.* 12:93. doi: 10.3389/fnbeh.2018.00093

Sack, A. T. (2006). Transcranial magnetic stimulation, causal structure–function mapping and networks of functional relevance. *Curr. Opin. Neurobiol.* 16, 593–599. doi: 10.1016/j.conb.2006.06.016

Saturnino, G. B., Antunes, A., and Thielscher, A. (2015). On the importance of electrode parameters for shaping electric field patterns generated by tDCS. *Neuroimage* 120, 25–35. doi: 10.1016/j.neuroimage.2015.06.067

Saturnino, G. B., Madsen, K. H., and Thielscher, A. (2021). Optimizing the electric field strength in multiple targets for multichannel transcranial electric stimulation. *J. Neural Eng.* 18:014001. doi: 10.1088/1741-2552/abca15

Saturnino, G. B., Puonti, O., Nielsen, J. D., Antonenko, D., Madsen, K. H., and Thielscher, A. (2019). "SimNIBS 2.1: A comprehensive pipeline for individualized electric field modelling for transcranial brain stimulation," in *Brain and hum bod model 2018*, eds S. Makarov, M. Horner, and G. Noetscher (Cham: Springer), 3–25. doi: 10.1007/978-3-030-21293-3_1

Suen, P. J. C., Doll, S., Batistuzzo, M. C., Busatto, G., Razza, L. B., Padberg, F., et al. (2020). Association between tDCS computational modeling and clinical outcomes in depression: Data from the ELECT-TDCS trial. *Eur. Arch. Psychiatry Clin. Neurosci.* 271, 101–110. doi: 10.1007/s00406-020-01127-w

Turi, Z., Normann, C., Domschke, K., and Vlachos, A. (2021). Transcranial magnetic stimulation in psychiatry: Is there a need for electric field standardization? *Front. Hum. Neurosci.* 15:639640. doi: 10.3389/fnhum.2021.639640

Tzirini, M., Chatzikyriakou, E., Kouskouras, K., Foroglou, N., Samaras, T., and Kimiskidis, V. K. (2022). Electric Field distribution induced by TMS: Differences due to anatomical variation. *Appl. Sci.* 12:4509.

Van Hoornweder, S., Caulfield, K. A., Nitsche, M., Thielscher, A., and L J Meesen, R. (2022a). Addressing transcranial electrical stimulation variability through prospective individualized dosing of electric field strength in 300 participants across two samples: The 2-SPED approach. *J. Neural Eng.* 19:056045. doi: 10.1088/1741-2552/ac9a78

Van Hoornweder, S., Meesen, R. L. J., and Caulfield, K. A. (2022). Accurate tissue segmentation from including both T1-weighted and T2-weighted MRI scans significantly affect electric field simulations of prefrontal but not motor TMS. *Brain Stim.* 15, 942–945. doi: 10.1016/j.brs.2022.06.008

Van Hoornweder, S., Meesen, R., and Caulfield, K. A. (2022b). On the importance of using both T1-weighted and T2-weighted structural magnetic resonance imaging scans to model electric fields induced by non-invasive brain stimulation in SimNIBS. *Brain Stimul.* 15, 641–644. doi: 10.1016/j.brs.2022.04.010

Van Hoornweder, S., Nuyts, M., Frieske, J., Verstraelen, S., Meesen, R. L. J., and Caulfield, K. A. (2023). A systematic review and large-scale tES and TMS electric field modeling study reveals how outcome measure selection alters results in a person- and montage-specific manner. *bioRxiv [Preprint]*. doi: 10.1101/2023.02.22.529540

Wagner, T. A., Zahn, M., Grodzinsky, A. J., and Pascual-Leone, A. (2004). Three-dimensional head model simulation of transcranial magnetic stimulation. *IEEE Trans. Biomed. Eng.* 51, 1586–1598.

Westwood, S. J., and Romani, C. (2018). Null effects on working memory and verbal fluency tasks when applying anodal tDCS to the inferior frontal gyrus of healthy participants. *Front. Neurosci.* 12:166. doi: 10.3389/fnins.2018.00166

Wischnewski, M., Mantell, K. E., and Opitz, A. (2021). Identifying regions in prefrontal cortex related to working memory improvement: A novel meta-analytic method using electric field modeling. *Neurosci. Biobehav. Rev.* 130, 147–161. doi: 10.1016/j.neubiorev.2021.08.017

Zangen, A., Moshe, H., Martinez, D., Barnea-Ygael, N., Vapnik, T., Bystritsky, A., et al. (2021). Repetitive transcranial magnetic stimulation for smoking cessation: A pivotal multicenter double-blind randomized controlled trial. *World Psychiatry* 20, 397–404. doi: 10.1002/wps.20905

Zhang, B. B. B., Stöhrmann, P., Godbersen, G. M., Unterholzner, J., Kasper, S., Kranz, G. S., et al. (2022). Normal component of TMS-induced electric field is correlated with depressive symptom relief in treatment-resistant depression. *Brain Stim.* 15, 1318–1320. doi: 10.1016/j.brs.2022.09.006

Zmeykina, E., Mittner, M., Paulus, W., and Turi, Z. (2020). Weak rTMS-induced electric fields produce neural entrainment in humans. *Sci. Rep.* 10:11994. doi: 10.1038/s41598-020-68687-8

Frontiers in
Neural Circuits

Explores the emergent properties of neural circuits - the brain's elementary modules

Part of the most cited neuroscience journal series, focuses on the anatomy, physiology, development and function of neural circuitry, exploring how plasticity shapes the architecture of the brain's elementary modules.

Discover the latest Research Topics

See more →

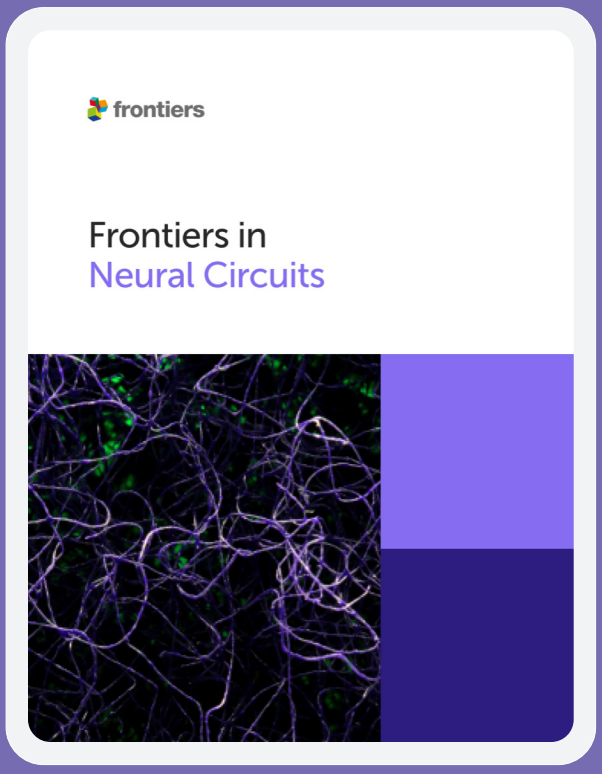

Frontiers

Avenue du Tribunal-Fédéral 34
1005 Lausanne, Switzerland
frontiersin.org

Contact us

+41 (0)21 510 17 00
frontiersin.org/about/contact